High-pressure Reactions as a Method for the Synthesis of New Materials

Wysokociśnieniowe reakcje jako metoda syntezy nowych materiałów

Szymon Sobczak

A thesis submitted to
the Adam Mickiewicz University, Poznań, Faculty of Chemistry,
in fulfilment of requirements for the degree of
Doctor of Philosophy in Chemistry
supervised by Prof. Dr Hab. Andrzej Katrusiak
and co-supervised by Dr Michał Andrzejewski

Poznań, 2021

Acknowledgements

First, I would like to express my sincere gratitude to my advisor Prof. Andrzej Katrusiak for the numerus discussions and continuous support during my research, for his patience, motivation, and immense knowledge. I could not have imagined having a better advisor and mentor during these past years. His excellent guidance showed me way for understanding matter not only under extremes.

Besides my advisor, I would like to thank Dr Michał Andrzejewski for teaching me all the high-pressure experimental skills and for his fruitful suggestions to my work. Now, from the perspective of this several years I cannot imagine better way to start the adventure with science.

Words fail me to express my appreciation to my friend, Aleksandra. Thank you doesn't seem sufficient but it is said with appreciation and love for your support and friendship.

My sincere thanks also goes to my fellow labmates, current and the past ones, for the stimulating discussions, for the atmosphere in the group, and for all the fun we have had. Without your precious support it would not be possible to conduct this research. I am particularly grateful to Paulina Ratajczyk; it was a pleasure to work with you.

Also I thank all my friends and collaborators at the McGill University. Especially, I am immensely grateful to Dr Tomislav Friščić who provided me an opportunity to join his team and for hundreds of discussions, as well as the countless e-mails and ideas that I received.

I would like to take this opportunity and genuinely thank to all my collaborators Prof. Artur R. Stefankiewicz, Prof. Adam Huczyński and Prof. Stefan Lis from Department of Chemistry, Adam Mickiewicz University Poznań; Prof. Mirosław Mączka from Institute of Low Temperature and Structure Research, Polish Academy of Sciences as well as Prof. Giulio I. Lampronti and Prof. Ana M. Belenguer from Department of Chemistry, University of Cambridge; Prof. Leonard J. Barbour from Department of Chemistry and Polymer Science, University of Stellenbosch; Prof. Tapas Kumar Maji from School of Advanced Materials, Jawaharlal Nehru Centre for Advanced Scientific Research; and Prof. Nandini Garg from Department of Condensed Matter Physics and Materials Science, Tata Institute of Fundamental Research. I truly believe that our collaboration led to highly valuable results.

And most of all, I would like to share this moment of happiness with a person who's love, support, encourage, was the source of my life energy resides. Dominika I thank you for being unselfishly helping me throughout the happy and hard moments. You were always beside me to push me and motivate me.

Last but not the least, I would like to thank my family: my mother and my sister for supporting me throughout all these years.

Finally, I am grateful to the Polish National Science Centre for fanatical support in grant Preludium 2017/27/N/ST5/00693 and OPUS 2015/19/B/ST5/00262 as well as European Social Fund, Operational Program Knowledge Education Development, for Grant POWR.03.02.00-00-I023/17. Part of this research was supported by PLGrid Infrastructure.

"Science is what scientists do,
and there are as many scientific methods as there are individual scientists"

Percy Williams Bridgman

CONTENTS

1

Introduction

Of the common experimental variables, pressure is by far the least used for investigating the properties of condensed phases, such as solutions, melts, solids and their interphases. For most scientists, the fact that we are born, live and die at approximately one atmosphere suffices to concentrate their attention on other variables such as composition, temperature, electric potential, *etc.* which often does not require an expensive apparatus for many years associated with high-pressure studies. However, they are scientists concerned with the systems below the sea level, in ocean seabed, in deep geological deposits or the outer space, who must necessarily expand their research to the thermodynamic dimension of pressure.

For centuries, the enormous potential of high-pressure could not be exploited due to the lack of adequate experiments. Most of the principles of modern high-pressure equipment can be traced directly to P.W. Bridgman in the first half of 20th century. The later progress has been, in a sense, evolutionary. The attainable high pressure, and thus the range of possible transformations and methods expanded dramatically through the ingenious use of diamonds. That moment, almost 60 years ago, when Jamieson's group at the University of Chicago[1] and Weir's group at the National Bureau of Standards[2] independently designed a diamond-anvil cell (DAC), was beginning of more frequent reports on high-pressure phenomena. The simple construction of the DAC, which was gradually perfected,[3] opened the way to spectacular benchmark experiments. Today's high-pressure research is a fusion of many disciplines from geology through chemistry and physics to biochemistry and molecular biology. The number of reports on high-pressure phenomena appearing in the literature makes it difficult to summarize them in

a brief form. Thus, I will emphasize topics of interest to chemists with brief excursions into relevant aspects of statistical physics and thermodynamics.

1.1 High-pressure chemistry

The investigation of chemical equilibria and chemical reaction rates in solution is one of the most thoroughly established inputs of high-pressure research into modern chemistry. It was known long ago that the equilibrium position in chemical reactions may be shifted by the application of external pressure, both in the liquid and gaseous phase. This redistribution in the physical and chemical balance of a given system is an application of *Le Chatelier's* principle, which will result in an overall smaller volume. This effect can be simply summarized by[4]

$$\left(\frac{\partial \ln K}{\partial p}\right)_T = -\left(\frac{\Delta V}{RT}\right), \tag{1.1}$$

where ΔV is a volume of reaction, defined by

$$\Delta V = \sum V_{products} - \sum V_{substrates} \tag{1.2}$$

(*In equations 1.1 and 1.2 the pressures in MPa, the temperature in K, and R = 8.314 cm³ MPa K⁻¹ mol⁻¹, and so ΔV has units of cm³mol⁻¹*)

The volume of the reaction may be measured either by determining how the pressure affects the reaction equilibrium or by determining the individual partial molar volumes of used reagents and products.[5,6] In analogy, the reaction rates in solution may be similarly affected by the pressure according to whether the formation of transition state leads to an increase or decrease of the activation volume $\Delta V^{\neq}$.

Equilibrium and kinetic parameters can be then combined in diagrams illustrating the Gibbs free energy (G), enthalpy (H) and volume (V) changes in proceeding in the sequence:

Substrates → Transition State →Products

also including intermediates when they are formed (Figure 1).

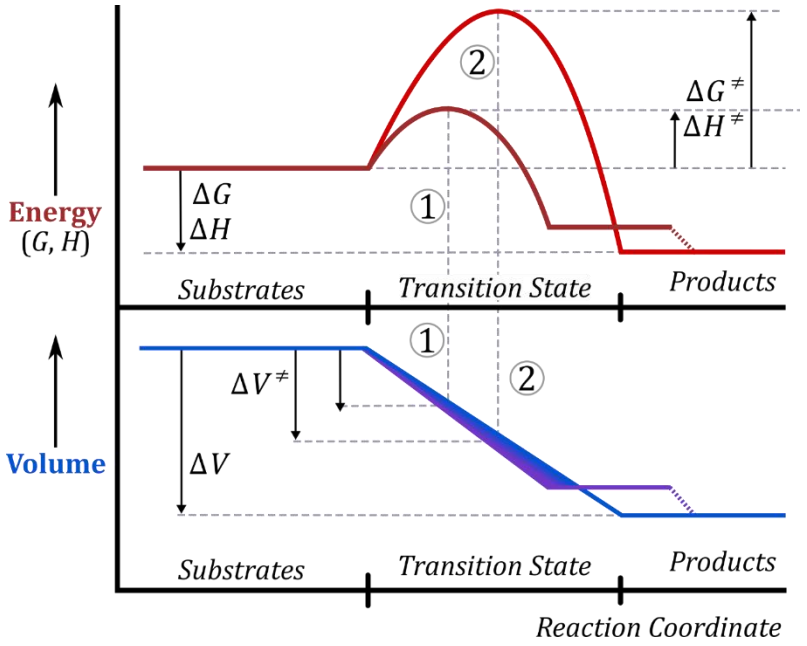

Figure 1. Schematic comparison of energy and volume profiles. The number (1) indicates an 'early' transition state, possible to achieve in fast reactions under kinetic control, and (2) 'late' transition state of long equilibrated reactions.

When substrates A and B form product AB and no intermediates are produced, *i.e.* there is a single-step reaction, the volume of activation, $\Delta V^{\neq}$, is such that the transition state is almost halfway between reactant and product states. However, reactions are often not following this simple reaction route, and yields in several products, where one is the major product, which is either a more stable product, or is formed at a faster reaction rate. Then two factors need to be taken into consideration: *thermodynamic* (a formation of the stable product is favorable) and *kinetic* (a product which forms faster is preferred). If there is enough energy to overcome all the reaction barriers for products, and the reaction is in equilibrium with the most stable product, the reaction is thermodynamic-controlled. On the other hand, if the reaction tends to produce a less stable product as a major product, and the activation energy for this reaction pathway is smaller corresponding to an 'early' transition state, the reaction can be considered as kinetically

controlled. The ratio of products depends on the relative difference between their activation energies.

These general assumptions indicate a simple and lucid way of describing a reaction system under high-pressure in gaseous or liquid state, but with an exemption, that reaction mechanism is simple and leads mainly to intrinsic changes.[7] Consequently, a reaction with a negative volume of activation is strongly accelerated by pressure, while the positive volume of activation is hampered.[8–11] When a chemical bond is formed, the distance between two atoms decreases from their original van der Waals distance to the bonding distance. This process usually decreases the volume by about 10-20 cm^3 in 1 mole of a substance. Even the formation of interactions as weak as the hydrogen bond can reduce volume by approximately 5 cm^3/mole.[9–11] On the other hand, a homolytic bond cleavage has the opposite effect, of modestly increasing volume (typically 5-10 cm^3/mole).[9–11] Significant contributions to volume originate from steric features of molecules and thus, *o*-substituted benzenes occupy 3-5 cm^3/mole less space than their *m* or *p* isomers and thus the reaction where the *o*-substituted derivative is produced, are more favored.[9–11] The situation becomes more complex, when charged species are produced or consumed during a reaction. The presence of ions or drastic polarity changes of reactants strongly affect the volume occupied by the solvent molecules surrounding the reacting system and increasing or decreasing in the solvation layer. This phenomenon, known as electrostriction,[12] in most cases leads to a strong reduction in ΔV but the quantitative evaluation of its contribution is difficult. Electrostriction depends on the solvent environment, and is especially large in relatively non-polar solvents, where the range of coulombic forces is larger, and the compressibilities increase.[12]

The solvent effect is not only limited to electrostriction. The compressed liquid changes its physical properties: the boiling point is increased, as well as the density and viscosity. The electric permittivity and electric conductivity change, too. Moreover, increased pressure leads to the elimination of all empty spaces and thus the distances between isolated molecules decrease and the space necessary for thermally-induced motion and collisions become more tight.[13,14]

1.2 Application of high-pressure in organic synthesis

There are numerus examples of pressure-induced reactions conducted in compressed liquid environment. The Menshutkin reaction[15,16] (Figure 2a) is an example of a reaction occurring mainly because of high-pressure, in short time and with a high yield.[17] During this coupling reaction, a tertiary amine is converted into a quaternary ammonium salt by an alkyl halide. In the case of highly nucleophilic tertiary amines, like 1,4-diazabicyclooctane (DABCO), the substitution reaction with dichloromethane at room temperature and normal pressure takes several hours when heated at reflux (336-337 K),[18] and pyridines does not readily react at all. However, these reactions are greatly accelerated when compressed. The reason can be found in the exceptionally large ΔV, estimated as -50 cm^3 mol^{-1}. This results from the formation of a new bond and charge-pair generation, which leads to the electrostriction.[17] To this point, several examples of this reaction at high-pressure were shown.[19–21]

Interestingly, the application of high-pressure seems to be especially useful for highly substituted reactants. A perfect example is the oximation of di-*t*-butylketone, not observed at ambient pressure because of a steric hindrance.[22] The Robinson annulation[23] (Figure 2b) at ambient pressure fails when the terminal methylene group is highly substituted, but is easly achieved under high-pressure conditions.[22] The similar effect of enhanced yield for sterically crowded substrates is observed during Michael [24] and Mannich additions.[25] In Michael addition (Figure 2c) nitromethane can be attached even to unsaturated ketone of a steroid.[26,27] In Mannich reaction (Figure 2d), normally limited to formaldehyde, methylene chloride[28] or bis(dimethyamino)methane can be successfully used instead.[29] Application of high-pressure in Henry reaction,[30] during which nitroalkanes are converted to nitroalcohols in a presence of ketones, also leads to higher yields, on the contrary to ambient pressure, where they could be only obtained in a limited number of special cases. One of the most spectacular demonstrations of

pressure-promoted reaction was presented by Jurczak, in the synthesis of a 3-dimensional covalent frameworks.[31–33]

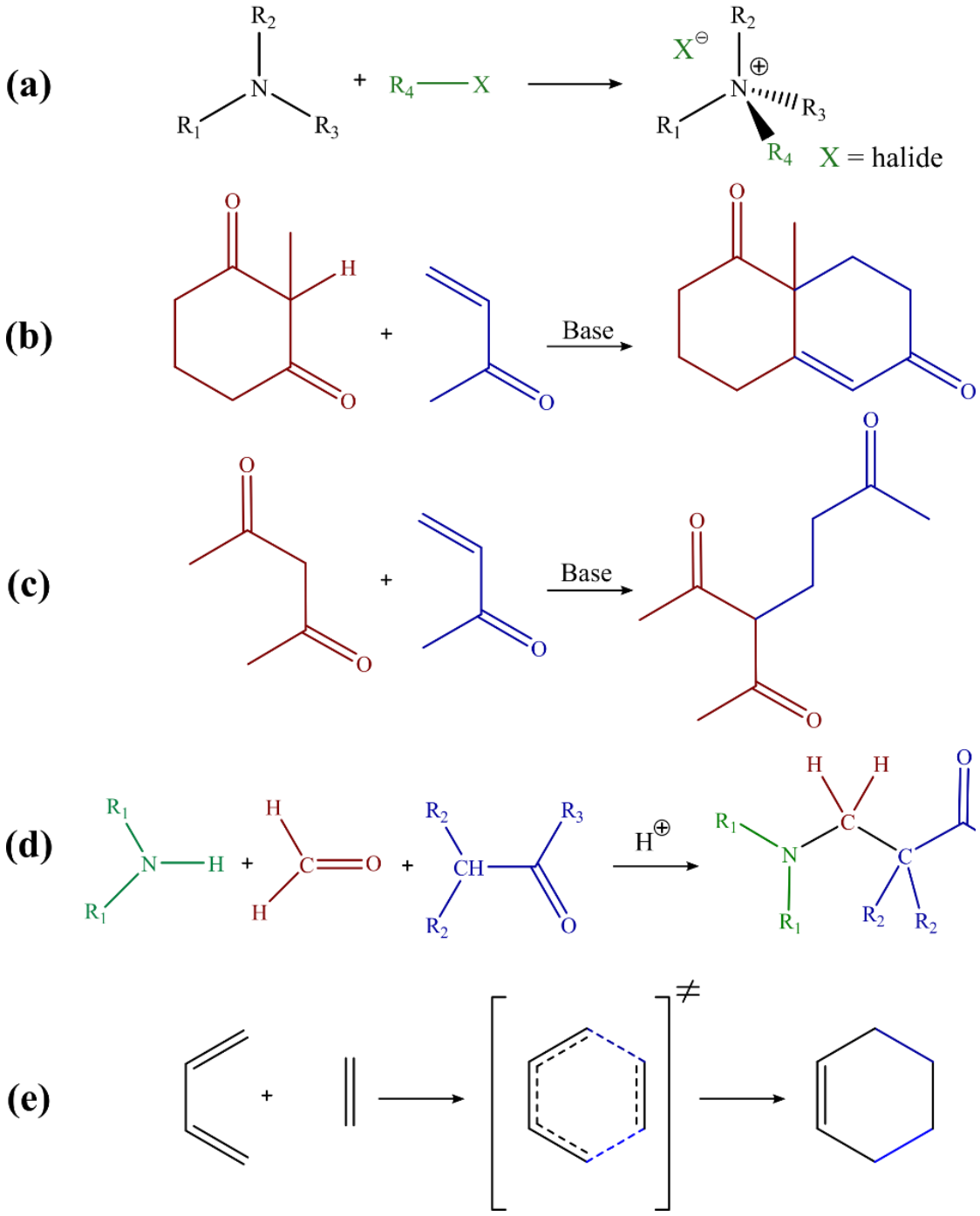

Figure 2. Schematically represented examples of (a) Menshutkin reaction; (b) Robinson annulation; (c) Michael and (d) Mannich additions; and (e) Diels-Alder reaction.

One of the most prominent types of reaction accelerated at elevated pressure is the Diels-Alder reaction (Figure 2e). First described by Otto Diels and Kurt Alder in 1928, quickly proved to be a powerful and widely applicable method in the synthesis of pharmaceutical products and new materials. Starting in the nineteen-thirties,[34] numerous applications of high-pressure for the Diels-Alder reaction were found.[35–40] The initial controversies around the reaction mechanism, according to which this highly exothermic reaction should be hampered at high pressure were quickly dispelled. [41,42] On the example of the reaction between a conjugated diene and a substituted alkene,[43–46] it was shown that because of the simultaneous formation of two new C-C bonds, the ΔV can be significantly reduced in the range between -25 to -50 $cm^3\ mol^{-1}$, which is responsible for observed acceleration at high pressure.[47] Similar mechanistic reasoning was applied in the understanding of cyclic reorganization of σ and π bonds, such as cheletropic reactions and pericyclic rearrangements.[7,48,49] Despite the fact, both these reactions are associated with much smaller ΔV than in regular Diels-Alders reaction, they are also strongly favored by high-pressure conditions. This can be explained by the reduction of space required for the thermally-induced motion and collision of molecules which leads to the total restriction of the rotational degrees of freedom. A good example of such reaction is the trimerization of acetonitrile to 2,4,6-trimethyl-1,3,5-triazine highly accelerated by the pressure.[50–52]

Free-radical reactions are an intriguing example of pressure-promoted reactions. As it was already pointed out, the volume expansion should be always expected for homolytic bond dissociations, which is also necessary for the formation of a free radical. Several reports on the homolytic bond cleavages showed that this process requires volume expansion of nearly $\Delta V^{\neq}$ = +10 $cm^3\ mol^{-1}$,[6,53,54] which clearly contradicts the possible promotion by the high-pressure conditions. However it was confirmed that numerous free radical reactions are pressure-sensitive. The explanation can be found in a non-straightforward mechanism,[55–57] strongly dependent on the arrangement of the interacting molecules in the liquid state.[58] Many of radical reactions promoted by the use of light or ultrasounds generate a significant number of free radicals. This obviously can not be expected at high-pressure. More likely, the radical reactions which are accelerated

by pressure, occur during a self-amplifying chain of events, which progress in short-cycles (of initiation, propagation and termination) overall leading to reduction of ΔV.

1.3 Application of high-pressure in inorganic chemistry

Pressure can be also successfully applied in the inorganic chemistry. One of the most famous pressure-promoted reaction, without any doubt, is the Haber–Bosch process.[59] This process named after its inventors, German chemists Fritz Haber and Carl Bosch, implemented in the first decade of the 20th century, is the main industrial procedure for the production of ammonia today.[60] However, this is not the only example of pressure-accelerated synthesis of the inorganic materials. The application of high-pressure significantly simplified the production of metallic nitrides[61–70] and hydrides.[71–80] At the high-pressure, these compounds can be formed by the heating of a pure metal in a chosen gaseous atmosphere. These findings provided not only valuable information about the physical characteristics of those materials but also have extended our understanding of the thermodynamics and dynamics of the process.[81–83]

The reactivity and direction of a chemical reaction at high-pressure mostly depend on an electron configuration of metal cations. In the context of atomic orbitals, a general division into open and closed-shell electron configuration can be made. The closed-shell configuration, with a filled valence shell, is very stable and thus it can be expected that high-pressure would induce a substitution reaction. According to the best known classification, a substitution mechanism can be either of the dissociative (D), interchange (I) or associative (A) type (Figure 3). During the D process an intermediate of a lower coordination number is formed, while A involves a formation of a transition state of higher ligancy. In the I mechanism, the bond formation and bond cleavage occur simultaneously, however more associative (I_a) or more dissociative (I_d) nature of a process can be distinguished. Obviously, high-pressure conditions will accelerate the process decreasing the molar volume of reactants, in contrast to a dissociatively activated

process of positive $\Delta V^{\neq}$. It is also possible to observe a ligands-exchange reaction. In this case, as the bond breakage and formation occur at the same time, only a small effect in $\Delta V^{\neq}$ can be expected (slightly negative $\Delta V^{\neq}$ for I_a and a slightly positive $\Delta V^{\neq}$ for I_d). It has to be emphasized, that this interpretation is solely based on the consideration of intrinsic volume contributions, like changes in bond lengths or bond angles, and corresponds mainly to symmetric chemical reactions, such as solvent exchange. For asymmetric substitution reactions, this process is frequently accompanied by major changes in charge distribution, dipole moment and dipole-dipole interactions, so that the volume changes are mainly due to electrostriction effects.[4]

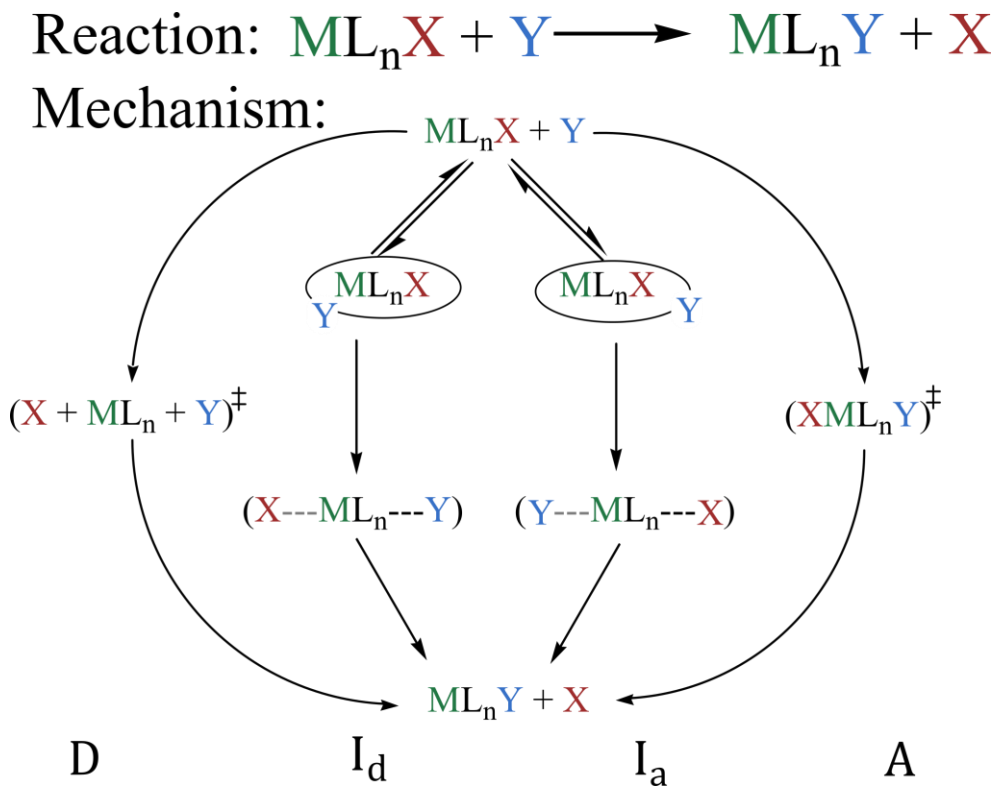

Figure 3. Schematic diagram of possible mechanisms for the ligand (Y) substitution reaction for the complex of metal (M), substituted with a number *n* of ligands (L) and interchanging group (X). For the dissociative (D) and associative (A) mechanisms the transition states indicate the degree of bond breakage or formation, respectively. For the associative (I_a) and dissociative (I_d) interchange reactions a precursor complex in pre-equilibrium process is formed before the interchange of X takes place.

On the other hand, metal ions of the open-shell configuration at high-pressure are prone to the spin-state changes or even to transfers of electrons between ions due to instabilities and switching between partly filled valence electronic states. Such transformations can be triggered by high-pressure effect of increasing the overlap between adjacent electronic orbitals, leading to redox reactions.

1.4 Solid-State reactions at high pressure

In general, solid-state chemistry is the field that includes a synthesis, structure, and the determination of properties, all focused on solid materials, particularly on molecular crystals. Hence the scope of topochemistry strongly overlaps with solid-state physics, mineralogy, crystallography, ceramics, metallurgy, thermodynamics, materials science, and electronics, with a focus on the synthesis of novel materials and their characterization. One of the most effective methods for the synthesis of materials in a solid form is mechanosynthesis. The term 'mechanochemistry' following the IUPAC definition is a chemical reaction induced by mechanical energy and is mostly used in the contexts of the solid-state processes and reactions initiated by any type of mechanical treatment or involving reagents, which were preliminarily activated mechanically.[84] The mechanical energy can be also applied in a form of continuous and hydrostatically applied pressure.[85] The mechanical treatment improves diffusion, generates strains and introduces structural, electronic and ionic defects in crystals.[86] Moreover, if the heat of reaction is small and a considerable difference exists between the summed specific heats of reactants and products, is possible to reach a reaction equilibrium at some fixed temperature and pressure, which can lead to completely new products above or under these conditions.[87]

Besides the molecules themselves are strongly affected by high-pressure. The increased overlap between electronic orbitals can eventually result in delocalization of electrons,[88] broadening of the allowed energy bands and a decrease in magnitude of the gaps of forbidden energy between bands,[89–91] leading to large changes in the outer

electron shells under high-pressure.[92] Moreover, since the orbitals with different quantum numbers differ in shape, size and thus in their compliance to distortions, the compression can lead to the displacement of orbitals. This effect has consequences in a shift of energy from the empty π^* orbital to the occupied π orbital, a change in relative energy of *d* orbitals in transition metal complexes as well as in a change of interaction energy between electron donor and acceptor (either in a molecular, or in a transition metal complex). This transformation in the solid phase at high pressure was summarized and connected to the Ehrenfest's classification of phase transitions by Drickamer in 1972.[93]

Table 1. Dirickamer's classification of high-pressure phenomena in solid-state.[93]

Class I	Class II	Class III	Class IV
First order transition	First order transition	electronic transition	electronic transition
Electronic component negligible	Electronic component significant	Significant change in volume and/or structure	Continues with increasing pressure
fcc → *sc* KCl, KBr, KI	*bcc* → *hcp* Iron *(ferro to paramagnetic transformation)*	*s* → *d* Cesium, Rubidium and *s* → *d* Cerium and other rare earth metals	Spin changes in open shell metals Solid-state redox Reactions Fe^{3+} to Fe^{2+}
fcc → *hcp* Lead	Diamond → white tin Silicon, Germanium, InSb, GaAs etc. *(semiconductor to metal transformation)*	disproportionation and decomposition reactions	Reactive ground states of hydrocarbons electron donor-acceptor complexes Rare earth salts

According to this classification, Class I covers all events with atoms, ions, or molecular rearrangements, however with no electronic implications to their structures. Class II refers to all phenomena associated with polymorphism leading to a drastic change in electrical or magnetic properties. Transformations of Classes I and II are of the most common phenomena at extremely high pressure.[93–96] Among them high-pressure spin transitions attract a lot of attention, due to their wide spectrum of applications.[97–102] An example, well illustrating the features of Class II transformation can be found in a nonphotomagnetic cyano-bridged Fe^{2+}–Nb^{4+} coordination polymer $Fe^{2+}(pyrazole)_4]_2[Nb^{4+}(CN)_8]\cdot 4H_2O$, which under compression becomes a pressure-induced spin-crossover photomagnet.[97]

Class III consists mainly of electronic transitions, which occur discontinuously and are accompanied by a volume discontinuity. Typical earth metals such as Ca and Sr of *fcc* structure at ambient conditions, transform under compression (to 20 GPa for Ca and 3.5 GPa for Sr) to the *bcc* structure, surprisingly reducing their coordination number.[88] It was explained however, that due to pressure-induced mixing of 3*d* and 4*s* orbitals, Ca and Sr acquire the character of transition metals. Decomposition and solid-state redox reactions are less frequently reported.[103] The compression above 1 GPa of H_3BO_3 was sufficient to induce a phase transition, followed by a chemical decomposition into cubic HBO_2 and ice-VI (transformed into ice-VII at 2 GPa). The large drop of volume and strong structural changes in the layered triclinic structure of H_3BO_3, accompanying the decomposition, suggests that due to the high activation energy a phase composition is highly dependent on the specific pressure–time path followed by the sample[104] A pressure-induced solid-state disproportionation was found also in α-$DmaFe^{2+}Fe^{3+}For_6$ (Dma = $(CH_3)_2NH_2^+$, For = $HCOO^-$) compressed in methanol or ethanol.[105]

Class IV contains new ground states established over a range of pressures, co-operative phenomena, or events involving a continuous change in the degree of configuration interaction. To this class, also some pressure-induced reactions in solids can be included. The examples of dimerization and polymerization are often found in the literature, as the tendency of the unsaturated molecules to form more saturated polymers with extended structure, and higher density can be expected.[106–111]

An exceptional example of the Class IV transformation, shedding a new light on the behavior of aromatics compounds, was recently reported.[112] A gradual compression of *syn*-1,6:8,13-biscarbonyl[14]annulene leads to stabilization of the one of resonant mesomers.[112] Another example is carbon disulfide, where compression to 8 GPa leads to a strong anisotropic structural distortion and increasion of the intermolecular S···S and C···S interactions energy which results in the polymerization.[113] An organic polyiodide salt when compressed above 10 GPa, initially adds iodines to triiodide anion till discrete heptaiodide units are formed, which on the further compression leads topolymerized into a 3D polyanionic network.[114] Numerous examples of izomerisation[115–118] or substitution[119–129] can also be found in the literature.[103] The reduction of oxidation state in iron ions has been evidenced in pressure-induced reaction leading to a series of oxides Fe_2O_3, Fe_3O_4, Fe_4O_5 and FeO presently regarded as the engine of chemical transformation in the crust of our planet.[130] Interestingly, Prussian Blue, ferric ferrocyanide, along with increasing pressure is capable for the electron transfer between iron atoms of two oxidation states.[102,131,132] This complicated process consists of several steps, where the first one is a reduction of high spin Fe(III) by the electron transfer from the ligand, which is followed by a transfer of an electron from the low spin Fe(II) ion to high spin Fe(III) through the cyanide bridge. This results in an increase of high spin Fe(II) content at the site coordinated to the nitrogen and leads to the production of low spin Fe(III) at the site coordinated to the carbon.[131,133] Similar effect was observed in $Cs_2[PdX_4]\cdot I_2$ (X = Cl, Br, or I),[134] where $Cs_2[Pd^{2+}I_4]\cdot I_2$ reacts to $Cs_2[Pd^{4+}I_6]$ at 2.5 GPa[134] and α-$DmaFe^{2+}Fe^{3+}For_6$ (Dma = $(CH_3)_2NH_2^+$, For = $HCOO^-$) compressed in glycerol.[105]

1.5 Purpose and goals

According to the concepts of '*green'* chemistry, modern science is focused on improving existing, and exploring new techniques leading to sustainable synthesis of chemical compounds.[135–137] Traditionally, new materials are produced by solvothermal and solution-based methods. However, both these approaches require considerable amounts of energy and generates a lot of wastes. Some of these problems can be overcome by taking the inspiration from nature. Mankind has always dependent on mineral resources, many of which were formed in the unique high-pressure and high-temperature environment in Earth's crust. What is more, the energy required for compressing a sample to a considerable pressure of about 500 MPa (5 times higher than that at the bottom of the Mariana Trench) is a small fraction, about an order of magnitude less, compared to the energy needed for heating the sample by about 70 K. The high-pressure technologies clearly paved their way in the food industry, where pressure up to nearly 1000 MPa is routinely used for preserving the products, without loss of the edibles qualities. Thus, in my work, I was interested in mimicking such extreme conditions, in order to synthesize novel materials.

The results of the research performed within my PhD have been published in a series of 18 papers; seven of them have been chosen for describing my main achievements. These 7 articles, labeled **R1**-**R7**, are listed below and their copies are included in Appendix B. Several types of transformations described in this thesis are schematically presented on Figure 4. Some of these reactions (2, 4, 5, and 6) require the dissolution of substrates, while reactions 1 and 3 are solid-solid transformations. I have studied the reactivity of different systems, such as inorganic, reactions 4 and 5, the reactions of hybrid inorganic-organic materials (1, 2, and 3), as well as the exchange reaction of the disulfide bond (6). In my thesis, I was focused on the general description of the subject, I have avoided repeating the material of articles **R1**-**R7** and I have referred to their figures, tables, and sections.

Articles described within this thesis:

(**R1**) Półrolniczak, A.; Sobczak, S.; Katrusiak, A. Solid-State Associative Reactions and the Coordination Compression Mechanism. *Inorg. Chem.* **2018**, *57* (15), 8942–8950

(**R2**) Sobczak, S.; Katrusiak, A. Environment-Controlled Postsynthetic Modifications of Iron Formate Frameworks. *Inorg. Chem.* **2019**, *58* (17), 11773–11781

(**R3**) Sobczak, S.; Fidelli, A.; Do, J.-L. Demopoulos, G.; Moores, A.; Friščić, T.; Katrusiak A. Toward elusive iodoplumbic acid 'HPbI$_3$': first observation of hydronium salts of the PbI$_3^-$ anion through high-energy isochoric synthesis at elevated temperature and pressure. *ChemRxiv - archived.* **2021.**

(**R4**) Sobczak, S.; Drożdż, W.; Lampronti, G. I.; Belenguer, A. M. A.; Katrusiak, A.; Stefankiewicz, A. R. Dynamic Covalent Chemistry under High-Pressure: A New Route to Disulfide Metathesis. *Chem. - A Eur. J.* **2018**, *24* (35), 8769–8773

(**R5**) Sobczak, S.; Ratajczyk, P.; Katrusiak, A.; Squeezing out the catalysts: the disulphide bond exchange in aryl disulphides at high hydrostatic pressure. *ChemRxiv - archived.* **2020**, doi.org/10.26434/chemrxiv.13160996.v2

(**R6**) Sobczak, S.; Katrusiak, A. Colossal Strain Release by Conformational Energy Up-Conversion in a Compressed Molecular Crystal. *J. Phys. Chem. C* **2017**, 121 (5), 2539–2545

(**R7**) Sobczak, S.; Ratajczyk, P.; Katrusiak, A.; High-pressure nucleation of low-density polymorphs. *Chem. – A Eur. J*. **2021**, 10.1002/chem.202005121

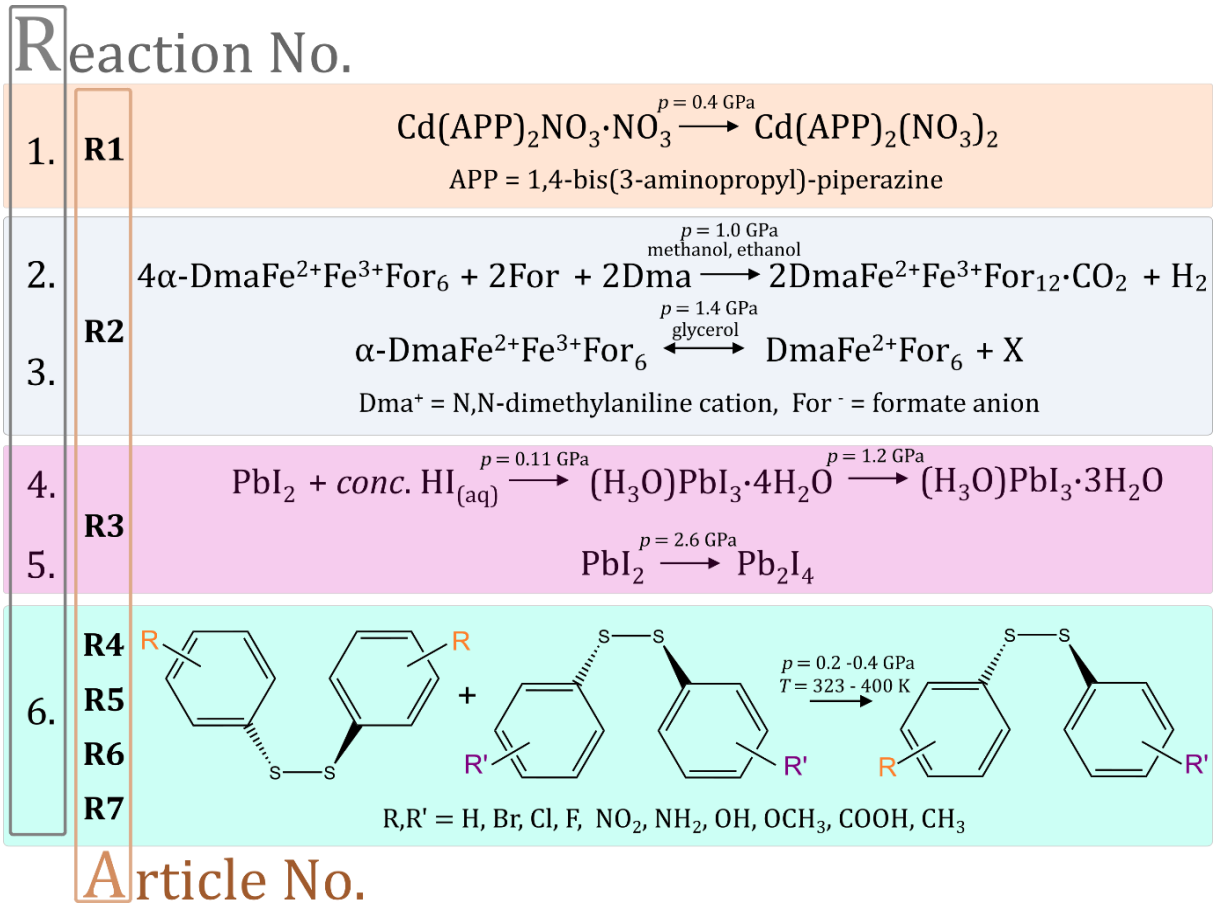

Figure 4. Main types of chemical reactions performed within this thesis.

2

Methods

Each of my articles describes in detail the experimental and theoretical methods applied in my research. Thus, in the following sections I will only briefly summarize the experiments and calculations.

2.1 High-pressure apparatus

Although the diamond anvil-cell (DAC) was invented over 60 years ago, this simple device remains to be the most efficient for generating high static pressure. Numerous different DAC designs have been used since then.[138–141] In my work I applied mainly a Merrill-Bassett DAC,[3] modified by supporting the diamonds directly on the steel discs with conical windows. Owing to the large spectral transparency of the diamond and low absorption of X-ray and neutrons, the DAC can be used for *in-situ* direct observations of a sample and for investigation of its structure by diffraction methods as well as by complementary UV-VIS, IR or Raman spectroscopy.[142] There is a vast literature dedicated to the DAC designs and their applications and this ingenious device has been described only briefly in my thesis.

The simplest construction of the DAC consists of (Figure 5);

- Force-generating component — screws or an externally controlled gas membrane;
- Two opposed diamond anvils (D) supported on discs (DS);
- A steel gasket (G).

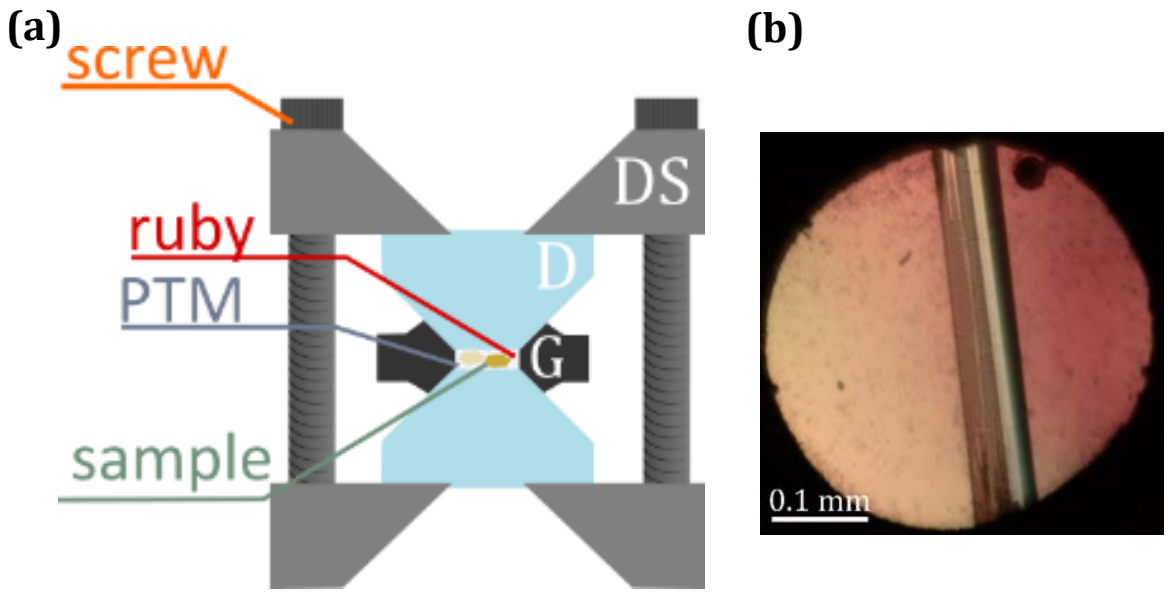

Figure 5. (a) A cross-section of the DAC with a solid sample, a ruby and a pressure-transmitting medium (PTM) inside a metal gasket (G). The force on diamonds (D), directly mounted in supporting discs (DS), is generated by tightening the screws; and (b) single crystal of $(H_3O)PbI_3 \cdot 4H_2O$ crystallized at 0.11 GPa, a ruby sphere for pressure calibration lie by the upper edge of the gasket.

The preparation of a high-pressure experiment starts with mounting a solid sample, together with a pressure calibrant, inside a spark-eroded hole in a metal gasket, placed between two diamonds. The gasket used for my experiments was made of a thin stainless steel foil or tungsten, 0.3 mm thick, with a hole of 0.45 mm in diameter. The remaining volume filled by a liquid, allows for transferring uniformly force generated by diamonds and also, when it was needed, acts as a solvent. Pressure was calibrated by the ruby-fluorescence method, which is based on the redshift of the two narrow bands (692.8 and 694.2 nm at ambient conditions) of ruby fluorescence, occurring due to the presence of Cr^{3+} ions.[143,144] The fluorescence of the ruby chip excited with a laser of $\lambda = 532$ nm, was measured with an enhanced-resolution Photon Control spectrometer. For high-pressure studies at elevated temperatures, an internal DAC heater was used. Due to the mounting the heater directly on the diamonds, the temperature was transferred to the studied sample with negligible heat losses.

For experiments in compressed liquid phase, a high-pressure piston-and-cylinder device was used, where pressure is generated by using a manually operated hydraulic press. The experimental chamber was enclosed in a cylindrical steel vessel supported mechanically by two outer steel shells and closed from below by a stopper supported on a detachable bottom. To ensure the constant starting volume of 9.80 ml, the pressure vessel was equipped with a neck with an overflow outlet. Both the piston and the stopper were sealed by wedge-type brass seals and rubber or Teflon O-rings.[145] All this piston-and-cylinder experimental setup was produced at the Institute of Physical Chemistry of the Polish Academy of Sciences in Warsaw.

2.2 *"Lab in a DAC"*

The DAC is a versatile multi-purpose apparatus adaptable for various types of experiments.[85] However, to use it as a high-pressure reactor I had to develop a procedure, according to which I could operate on reactants in micromolar scale.

First, each of substrate's single-crystals, of $V_{si}\, d_i \,/\, M_{si}$ (V_{si}, d_i and M_{si} are the grain volume, density and molecular weight of substrate, respectively) was precisely measured under the microscope and selected to obtain the required molarity (Figure 6). Next, crystals were loaded into the DAC together with a small ruby sphere, filled with a solvent and sealed. The solvent volume (V_{sol}) was calculated as follows:

$$V_{sol} = V_{DAC} - [(V_{\mathrm{si}} + V_{\mathrm{sii}}) + V_r],$$

were V_{DAC} is the DAC chamber volume, and V_r is the volume of the ruby sphere, and the molar concertation (c_{i}) of substrate No. *i* is:

$$c_i = (V_{\mathrm{si}} \times d_{si}/M_{si})/V_{\mathrm{sol}}.$$

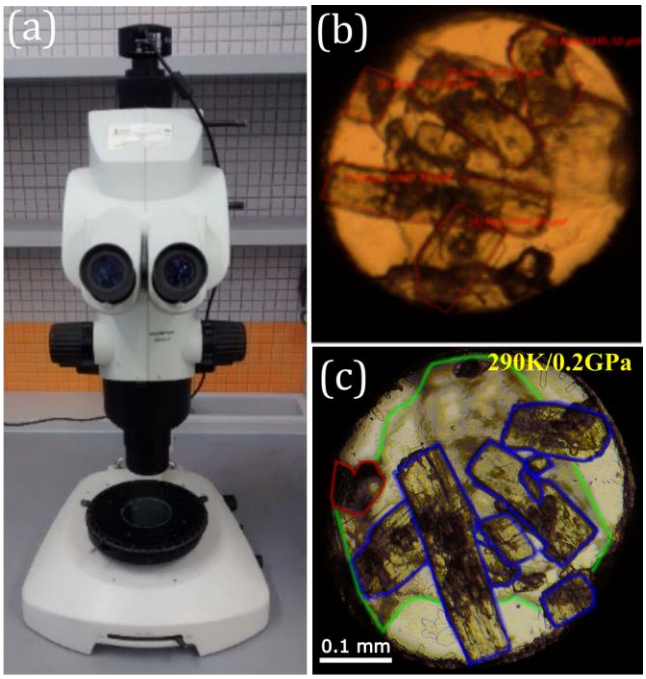

Figure 6. (a) Olympus MVX10 microscope used for substrates measurements before they were loaded into the DAC; and (b-c) single-crystals of homodimeric disulphides.

The chemical and physical properties of the used solvent, are an important element for obtaining reproducible results under the hydrostatic pressure in a DAC. The PTM can greatly affect the reaction mechanism and thus change its outcome. Many of common solvents, such as benzene, *t*-butanol, dimethyl sulfoxide or cyclohexane, quickly solidify at elevated pressure at room temperature, as the pressure tends to increase their melting points of about 15-20°C per 1 kbar.[4] The viscosity of liquid also increases approximately twice every kilobar, which can strongly affects the reaction. Moreover, the polarity of the solvent has an enormous influence on the electrostriction volume. For example, in the non-polar solvents, during the reactions with ionic species, the electrostriction effect is usually magnified. On the other hand, in the polar solvents, usually denser than non-polar ones because of the interactions between the molecules themselves, this effect cannot lead to a significant decrease of ΔV.[7]

Particularly important is the temperature control over during the high-pressure reactions. In my experiments, the solid substrates, loaded into the DAC chamber, were dissolved by increasing the temperature by an internal DAC heater. This device,

developed in our group, can be mounted directly on the diamond allowing for an accurate (up to 0.2°C) control over the temperature inside the chamber.

The optimization of the reaction conditions, due to the quick analysis of the crude solid recovered from DAC, was possible by the application of a mass spectrometer using the direct injection probe (described in section **2.4**). The reaction conditions were optimized by repeating the reaction several times for different concentrations, solvents, pressures and temperatures.

2.3 Structural studies

X-Ray diffraction experiments at high pressure were carried out on a 4-circle KUMA KM4 and Oxford Diffraction Xcalibur Eos diffractometers with graphite-monochromated MoKα (λ = 0.71073 Å) radiation and a CCD detector. The DAC was aligned with a gasket-shadow centering procedure.[146] The reflection intensities were corrected for the DAC absorption and gasket shadowing, and the diamond-anvils reflections were eliminated.[147,148]

The ambient-pressure structural experiments were performed on SuperNova CCD diffractometer equipped with X-ray micro-source (Cu Kα=1.54178 Å).

Low-temperature structural studies were performed on Xcalibur EOS CCD diffractometer with a CryoStream attachment cooling a sample with the stream of gaseous nitrogen down to 100 K.

For the collection and reduction of data program CrysAlisPro was used.[149] The structures were solved by using direct methods in program SHELXS and refined by full-matrix least-squares with SHELXL[150] implemented in the OLEX2 interface.[151]

Powder X-ray diffraction (XRD) measurements were performed on a Bruker AXS D8 Advance diffractometer equipped with a Johansson monochromator (CuKα1 = 1.54060 Å) and a silicon-stripe LynxEye detector.

2.4 Complementary characterization method

DSC measurements were performed on a Mettler-Toledo DSC823 module in sealed aluminum crucibles (40 μL), heated in flowing nitrogen (150 mL min^{-1}) at a rate of 10°C min^{-1}. TG measurements were performed on a Mettler-Toledo TGA/SDTA 851 module in sealed aluminum crucibles (40 μL), heated at a rate of 10°C min^{-1}.

Mass spectra were recorded with a Bruker 320-MS tandem triple quadrupole mass spectrometer using the direct injection probe (DIP-MS) method. This technique is based on the introduction of a sample directly into the ionization chamber, followed by their vaporization and eventual ionization by the electronic impact. Because it is often mentioned as a fast alternative for samples that do not require gas chromatographic separation,[152] this technique has been applied as an alternative method of analyzing crude solids directly recovered from the DAC.

The ^{13}C NMR spectra were collected on Varian VC NMR-S 400 MHz spectrometer. Spectra were corrected accordingly to the used solvent and processed in the MestReNova program.

2.5 Quantum mechanical calculations

The quantum-mechanical calculations have been carried out in order to investigate the thermodynamic behavior of the molecules, interplay between molecular conformation and intra- or intermolecular interaction on the potential energy. The calculations on molecular systems were performed using Gaussian software.[153] This widely used program, utilizes fundamental laws of quantum mechanics to predict energies, molecular structures and spectroscopic data (NMR, IR, UV, *etc*). It has the ability to use DFT, semi-empirical, perturbation and many other methods.

3

Results

My research was aimed at understanding and applying the high-pressure transformations in various materials, to modify their structure and properties. I investigated both, inorganic and organic systems, either in the compressed solid and in the liquid state. I chose the materials that represent the abovementioned fundamental classes and were mainly studied at normal conditions, in order to describe their behavior and possible reactivity under high-pressure, and to find and describe the mechanisms of their responses. Accordingly, in my thesis the reactions occurring in the solid-state, such as in closed-shell hybrid metal–organic coordination polymer: $Cd(APP)_2NO_3{\cdot}NO_3$ [APP = 1,4-bis(3-aminopropyl)piperazine], described in Półrolniczak, A.; Sobczak, S.; Katrusiak, A. Solid-State Associative Reactions and the Coordination Compression Mechanism. *Inorg. Chem.* **2018**, *57* (15), 8942–8950 (hereafter referred as **R1**) are discussed along the reactions in an open-shell compound α-$DmaFe^{2+}Fe^{3+}For_6$ (Dma = $(CH_3)_2NH_2^+$, For = $HCOO^-$). The discussion is further explored by the liquid-mediated redox reaction α-$DmaFe^{2+}Fe^{3+}For_6$ leading to the precipitation of $Dma_3Fe^{2+}{}_3Fe^{3+}For_{12}{\cdot}CO_2$ crystals, stable at the ambient conditions, published as Sobczak, S.; Katrusiak, A. Environment-Controlled Postsynthetic Modifications of Iron Formate Frameworks. *Inorg. Chem.* **2019**, *58* (17), 11773–11781 (**R2**). The topic of high-pressure reactions in compressed liquid environment has been extended by the reactions in compressed saturated solution of PbI_2 in concentrated HI. Was included in Sobczak, S.; Fidelli, A.; Do, J.-L. Demopoulos, G.; Moores, A.; Friščić, T.; Katrusiak A. Toward elusive iodoplumbic acid '$HPbI_3$': first observation of hydronium salts of the PbI_3^- anion through high-energy isochoric synthesis at elevated temperature and pressure. *ChemRxiv – archived* **2021** (**R3**). Next, the aryl disulfide exchange reactions at high-pressure, have been investigated and

described in two articles: Sobczak, S.; Drożdż, W.; Lampronti, G. I.; Belenguer, A. M. A.; Katrusiak, A.; Stefankiewicz, A. R. Dynamic Covalent Chemistry under High-Pressure: A New Route to Disulfide Metathesis. *Chem. - A Eur. J.* **2018**, *24* (35), 8769–8773 (**R4**); and Sobczak, S.; Ratajczyk, P.; Katrusiak, A.; Squeezing out the catalysts: the disulfide bond exchange in aryl disulfides at high hydrostatic pressure *ChemRxiv - archived* **2020**, doi.org/10.26434/chemrxiv.13160996.v2 (**R5**). The explanation of the high-pressure phenomena accompanying the disulfide exchange reaction, has been described in two articles: Sobczak, S.; Katrusiak, A. Colossal Strain Release by Conformational Energy Up-Conversion in a Compressed Molecular Crystal. *J. Phys. Chem. C* **2017**, 121 (5), 2539–2545 (**R6**) as well as Sobczak, S.; Ratajczyk, P.; Katrusiak, A.; High-pressure nucleation of low-density polymorphs *Chem. – A Eur. J*. **2021**, 10.1002/chem.202005121 (**R7**). The series of publications **R1-R7,** constituting this thesis, are enclosed in Appendix B.

3.1 Pressure-induced reactions of solids

As stressed in Introduction, the behavior of the metal-containing compounds at high-pressure strongly depends on electron configuration of the valence shell. The substitution reactions of complexes, frequently observed and described for a liquid environment, were also reported in the solid state.[61,133,154] However mechanism of such pressure-induced reactions was not fully understood. From many experimental and theoretical studies, a clear perspective emerges on the factors determining the transformations in response to the squeezing of an ambient-pressure molecular solid. The first set of reliable rules, allowing to predict the possible reactions in compressed solid, were constructed by Prewitt and Downs.[155] Their original concept of 9 rules of thumb, was further broaden by Grochala et al.[156] This huge and thorough background provided us with valuable information we applied in the search of the underlying mechanism of complexes reactions at high-pressure**.**

Article **R1** describes $Cd(APP)_2NO_3{\cdot}NO_3$, a closed-shell metal-based coordination polymer with a guest counter-balancing the charge of the framework. Its structure

possesses all structural features according to which the increase of coordination number can be predicted: (i) the presence of a potential ligand in the close vicinity of (ii) a closed-shell metal cation; which is (iii) coordinately unsaturated and capable of increasing its coordination number. The synthetic procedure for $Cd(APP)_2NO_3{\cdot}NO_3$ as well as the crystal structure with its topological features have been described in details in article **R1**. Figure 2 in **R1** shows the anomalous change in the unit-cell parameters in $Cd(APP)_2NO_3{\cdot}NO_3$ as a function of pressure. During the isothermal compression to 0.4 GPa a significant drop in the unit-cell volume of 80 $Å^3$ (Table 1 in **R1**) was observed. The structural determinations revealed a transformation between the low-pressure phase $Cd(APP)_2NO_3{\cdot}NO_3$ and high-pressure phase $Cd(APP)_2(NO_3)_2$. The strong strain caused by the significantly reduced distance between Cd^{2+} and NO_3^- resulted in fragmentation of the crystal sample. The formation of a new bond increases the Cd-coordination number from 6 to 7, which is connected with systematic changes of the coordination polyhedron: the six original Cd–N and Cd–O bonds become somewhat longer and angles between them decrease in order to accommodate the seventh bond (Figures 3a and b in **R1**). The formation of additional Cd–O coordination bond can be classified as associative type of substitution mechanism.

My detailed survey of the Cambridge Structural Database[157] revealed numerous other examples of similar reactions leading to the increased coordination number under high pressure in the solid-state. The analogous transformations occur also at low-temperature, which is consistent with the rule of inverse pressure and temperature effects[158] (Figures 4 and 5 in **R1**). Moreover, all these transformations consistently indicated a common reaction mechanism, which could be associated to the radius−ratio rule of Gustav F. Huttig, often attributed to Goldschmidt or Pauling.[159] In the structural model the metal cation and its ligands, anions or atoms, are treated as sphere with characteristic radii. The compression affects the system by reducing atomic radii, however, the anions are more compressed than the cation at the center, because electrons in anions are further away from the nucleus due to the excess of negative charge, while the electrons in cations are strongly affected by the nucleus. Moreover, the another sphere of the anions protects the central cation from the effect of pressure. The

different compression of cation and anions reduces the ratio of anionic-to-cationic radii which explains the high-pressure tendency for association reactions coupled to an increase of a coordination number. The reduced ratio at some point of compression favors the increased coordination number achieved by associative substitution.

A different behavior at high-pressure was expected for the open-shell metal cations like Fe^{2+} and Fe^{3+} in α-$DmaFe^{2+}Fe^{3+}For_6$. Its high-pressure study has been reported in article **R2**. Due to the presence of a short linker capable to mediate electron transfers between two Fe-atoms of different oxidation states, this compound revealed several possible transformations (Figure 1 in **R2**). We have found that α-$DmaFe^{2+}Fe^{3+}For_6$ does not dissolve in Daphne Oil 7474, 2-propanol and glycerol, which are the pressure transmitting media (PTM) frequently used in high-pressure research due to their high hydrostatic limits.[160–162] In all these three media α-$DmaFe^{2+}Fe^{3+}For_6$ can be compressed up to 1.40 GPa without inducing anomalous changes in the crystal structure, as illustrated in Figure 3 of **R2**. Above this pressure point, two different transitions occur, depending on the applied PTM. In Daphne Oil 7474 and in 2-propanol, the α-$DmaFe^{2+}Fe^{3+}For_6$ crystal transforms, above 1.40 GPa, to a new high-pressure phase γ. The full description of the α to γ phase transition has been described in detailes in the section "***Compression in Oil and in Isopropanol***" of article **R2**. It must be stressed that this transition has a dual nature, of reconstructive and order−disorder types. The pressure-induced bond isomerization occurs due to the change in configuration of every sixth formate anion from *anti*−*anti* to *anti*−*syn* (Figure 5 in article **R2**). This reduces volume of the voids and stops the rotations of Dma counter-cations in phase γ.

The compression of α-$DmaFe^{2+}Fe^{3+}For_6$ in glycerol, above 1.40 GPa, in a reversible process induces the reduction of all Fe^{3+} cations, and below the critical pressure the crystal transforms back to phase α. The transformation can be observed visually, as the black crystals become transparent, starting from the crystal edges, and this change is progressing toward the center of the compressed crystal (Figure 7 in **R2**). Simultaneously, in the diffraction pattern new reflections appear, and the solution of this new structure revealed compound hp-$DmaFe^{2+}For_3$ of the trigonal space group $R\bar{3}c$ (a detailed description can be found in the Supporting Information to article **R2** as well as

in the section "***Squeezing Dma off α-DmaFe^{2+}Fe^{3+}For$_6$ in Glycerol***" in **R2**). The occurrence of the reduction reaction is corroborated by the charged balance between Dma^+ cations, for anions and Fe atoms, as well as by the length of Fe^{2+}–O bonds (Figure 2 in **R2**). Remarkably, this high-pressure phase of DmaFe^{2+}For$_3$ is identical, in all terms of chemical, structural and physical features, with that obtained at ambient conditions (Figure 3 in article **R2**). It appears that different stability regions of these phases determined in different experiments are due to different crystal environment, e.g. the PTM in the high-pressure experiment. The mechanism for this reversible reduction was rationalized by the "breathing-like behavior" associated to a partial "zone-collapse"[163] of the α-DmaFe^{2+}Fe^{3+}For$_6$ structure, as no new Bragg reflections other than those from hp-DmaFe^{2+}For$_3$ could be found in the recorded diffraction images (Figure S1 in the Supporting Information of **R2**). The more profound understanding of the reaction reversibility requires additional data and investigations with complementary high-pressure techniques.

3.2 Pressure-induced reactions in solutions

Some structural analogies between α-DmaFe^{2+}Fe^{3+}For$_6$ and Prussian Blue[164] justify the assumption that the dissolution of this material can change the Fe oxidation states. At ambient conditions, α-DmaFe^{2+}Fe^{3+}For$_6$ hardly dissolves in simple alcohols, like methanol or ethanol. Although the solubility of most substances decreases at the high pressure,[165] we found that single crystals of α-DmaFe^{2+}Fe^{3+}For$_6$ can be compressed in both these alcohols only to 1.10 GPa, above which the dissolution starts. The dissolution process is followed by the precipitation of small green cubic crystals (Figure 8 in **R2**). These new *in situ* grown crystals survived the pressure release and could be recovered to the ambient conditions. The structural analysis by the X-ray diffraction revealed the formation of $Dma_3Fe^{2+}{}_3Fe^{3+}For_{12}\cdot CO_2$, analogous to Mn^{3+}, Fe^{3+}, Al^{3+}, Ga^{3+} and In^{3+} formates, synthesized previously at ambient conditions (Figure 8 in **R2**). Their crystal structure is similar, however there are several significant chemical differences. Most

apparent is different oxidation state of the metal center. In $Dma_3Fe^{2+}3Fe^{3+}For_{12}\cdot CO_2$, Fe^{2+} and Fe^{3+} cations are in the 3:1 ratio. In the compounds reported before,[166] all metals are at the (III) oxidation state. The mixed oxidation state of cations in $Dma_3Fe^{2+}{}_3Fe^{3+}For_{12}\cdot CO_2$, similarly as it was done for hp-$DmaFe^{2+}For_3$, has been established according to the charge balance of the whole network as well as to the Fe–O bond lengths, directly corresponding to the weighted average distance of [3Fe(II)+Fe(III)]/4···O (Figure 2 in **R2**). Another difference is the contents of voids. In $Dma_3Fe^{2+}{}_3Fe^{3+}For_{12}\cdot CO_2$ the neutral CO_2 molecules and Dma cations are trapped in the framework, while in the M^{3+} analogues their voids are occupied by molecules HCOOH, H_2O and CO_2. The presence of CO_2 in $Dma_3Fe^{2+}{}_3Fe^{3+}For_{12}\cdot CO_2$ molecules is consistent with the voids volume and with the number of electrons (e^-) located inside and determined by the SQUEEZE algorithm implemented in Platon.[167] It should be stressed that the reaction took place in the sealed DAC chamber, which is a closed system and no other elements than C, N, O, H and Fe can be found inside. The linear conformation and molecular dimensions of the refined CO_2 molecule perfectly match the peaks in the electron-density map. The determined C=O bonds, as well as the O=C=O angle, agree with those in the CO_2 molecule and at the same time the observed dimensions are inconsistent with those in the formate anion or the formic acid molecule. The results observed for α-$DmaFe^{2+}Fe^{3+}For_6$ clearly indicated that the liquid-mediated high-pressure reactions can provide means to access the new forms of the materials which are unattainable by the conventional methods.

The recent development of the solar-cell devices has inspired the extensive studies on the existence of iodoplumbic(II) acid. It was attempted in multiple investigations to prove its existence, however to this point the acid composition and stability remained controversial.[168,169]

Goldschmidt's classical Tolerance Factor (defined as $TF = r_A + r_X / \sqrt{2}(r_M + r_X)$, where r_A , r_M and r_X represent the radii of cation, metal and halide ions, respectively) is often used to predict the dimensionality of either hybrid or inorganic halide perovskites system.[170] The *TF* values between $0.8 \leq TF \leq 1$ favor the stable 3-dimensional (3D) AMX_3 perovskite structures, while those out of this range promote structures of lower

dimensionalities: 2D, 1D or 0D.[171–173] As it is highly unlikely to observe a free form of proton in the aqueous solution (H^+) due to its extremely high charge density (≈ $2 \cdot 10^{10}$ times that of Na^+), the probable structure of iodoplumbic(II) acid can be supported only by the hydronium cation H_3O^+. The TF factor estimated for that iodoplumbic(II) acid, assuming the effective ionic radius of hydronium cation as 100 pm,[174] equals 0.667. That suggests that at ambient conditions that material, supported by the hydronium cation, will be rather unstable.

Thus, we have focused our investigations on the effect of the ball milling and high-pressure, both using the mechanical energy, on the reaction system of PbI_2 dissolved in concentrated aqueous HI, hoping that the energy introduced to the system in this way will result in the formation of the desired product. As the result of the milling experiments, we have obtained crystalline compound $(H_3O)_2Pb_3I_8 \cdot 6H_2O$ (Figure 1 in article **R3**). This material was reported before, yielding of the gas phase reaction of HI with PbI_2.[175] The structure of $(H_3O)_2Pb_3I_8 \cdot 6H_2O$ consists of trimeric chains of $[Pb_3I_8]^{2-}$ with water molecules between these chains. Nevertheless, the compression to 0.11 GPa of this same starting system, of PbI_2 in concentrated $HI_{(aq)}$, resulted in the formation of a new $(H_3O)PbI_3 \cdot 4H_2O$ salt (Figure 1 in article **R3**). The structure of $(H_3O)PbI_3 \cdot 4H_2O$ is built of the polyanionic PbI_3^- tapes extending in one dimension, in the form of dimeric, edge-sharing chains and of intercalated H_2O and H_3O^+ molecules. The structure of $(H_3O)PbI_3 \cdot 4H_2O$ represents the NH_4CdCl_3-type double-chains topology, isostructural to other one-dimensional iodoplumbate structures incorporating for example ammonium, cesium and rubidium cations (NH_4PbI_3, $CsPbI_3$ and $RbPbI_3$).[176–178] However, in $(H_3O)PbI_3 \cdot 4H_2O$ the negative charge of the framework is counterbalanced by hydronium cations. Although the presence of heavy atoms in the structure hinders the precise location of hydrogen atoms and makes it difficult to distinguish water molecules from H_3O^+ cations, it is reasonable to assume that the H_3O^+ cations form the shortest contacts to the iodine anions (Figure 2b in article **R3**). When the pressure is increased above 1.20 GPa, a new hydronium salt, $(H_3O)PbI_3 \cdot 3H_2O$, crystallizes (Figure 1 in article **R3**). This new compound is based on identical polymeric anions with the edge-sharing PbI_6-octahedra,

like those in $(H_3O)PbI_3 \cdot 4H_2O$, but with a lower content of water between the anionic sheets (Figure 2c in article **R3**).

Interestingly, the stability region favoring the existence of the hydronium salts is clearly distinguishable (Figure 5 in article **R3**). Above 1.2 GPa and at temperature above 420 K, a pink-colored crystalline material (Figure 4 in article **R3**), different from the colorless crystals of $(H_3O)PbI_3 \cdot 4H_2O$ and $(H_3O)PbI_3 \cdot 3H_2O$ is formed. The X-ray diffraction measurements for this crystal at 2.05 GPa and above 320 K, revealed a new polymorph of PbI_2, hereafter denoted as the polymorph β. The high-pressure β-PbI_2, unlike the well-known 2D layered PbI_2 structure (α- PbI_2), assumes a three-dimensional (3D) framework of alternating six- and seven-coordinated lead cations. The opposite side of the hydronium salts stability region is revealed by a single-crystal-to-single-crystal transformation from $(H_3O)PbI_3 \cdot 4H_2O$ to $[H_3O]_{2x}[Pb_{1-x}I_2] \cdot (2-2x)H_2O$ (Figure 3 in article **R3**), while the pressure is released to 0.1 MPa.

The successful pressure-induced reactions in the hybrid, as well as in the purely inorganic systems, encouraged us to attempt on triggering the organic reaction. Our interest focused on disulfide exchange reactions, which are intensely studied due to their potential applications. However, these reactions require long equilibration times, often combined with the use of a strong base or a reductor to induce an attack of a free thiolate at the disulfide bond.[179] Only recently some progress towards more environmental-friendly methods has been achieved.[180,181] Improved methods of green chemistry require the exploration of new paths leading to reactions of high conversion rates, decreased amount of used energy and minimal amounts of necessary reactants.[135–137] Our first attempt to induce an exchange reaction was undertaken on the two homodimeric aryl disulfides: bis(4-chlorophenyl)disulfide and bis(2-nitrophenyl)disulfide, described in article **R4**. At ambient conditions in order to obtain high yield, this reaction needs to be conducted under mechanical grinding with a base catalyst 1,8-diazabicycloundec-7-ene (DBU). On the contrary, the solution-based methods for this process, result in almost perfect equilibrium between substrates and products (Figure 1 and Supporting Information in article **R4**), accelerating after application of the reducing agent combined with an excess of heat. For the high-pressure reactions, an equimolar amount of both

homodimers were used and by strictly following the same reaction procedure we have conducted 21 reactions in various conditions of pressure, temperature and different solvents environments (for molarity calculations and reaction procedure see Supporting Information in **R4** and "***Reaction procedure and optimization***" section in **R5**). We found that by changing the molar concentration of substrates we were able not only to obtain almost 100% conversion to the heterodimeric product, subsequently grown in the form of single-crystals (Figure 2 in **R4**), but also by modifying the solvent chemical character (from polar protic to polar aprotic), we could control the polymorphic form of the product.

In order to fully understand the mechanism of exchange reactions at high-pressure, we have extended our original investigation to another 15 different homodimeric aryl disulfides described in article **R5**. The variety of substrates, differing in the types, positions, and chemical character of substituents (Figure 1 in **R5**) were combined together to produce an overview of high-pressure reactivity, illustrated in Figure 2 in article **R5**. The obtained 21 different heterodimeric products provided the basis for understanding the pressure-induced disulfide bond exchange mechanism. Contrary to the previously postulated mechanism of [2+2] metathesis, our high-pressure results confirm that this reaction occurs according to the radical-mediated mechanism.[182] In this model the high-pressure conditions allow to overcome the energetic barrier needed to the cleavage of a disulfide bond and formation of two sulfur-centered radicals (Scheme 1 in **R5**). Of course, the homolytic disulfide bond dissociation is a process connected with the volume expansion and undoubtedly it is a rate-determining step.

Our previous studies on one of the most basic representatives of aromatic disulfides, di-*p*-tolyl disulfide described in article **R6**, has shown that at high-pressure disulfides can absorb a significant amount of energy due to conformational changes. The isothermal compression of the ambient-pressure phase α di-*p*-tolyl disulfide induces a first-order transition to phase β at 1.60 GPa, which differentiates the conformers of molecules. On the other hand, the isochoric recrystallization already at 0.45 GPa results in the formation of a new polymorph γ (Table 1 and Figure 3 in article **R6**). In the

structure of polymorph γ, all shortest intermolecular contacts S···H and C···C (Figure 7 in **R6**) are longer compared to those in phases α and β. This expansion of all the shortest contacts results from the strong conformational conversion, after which the molecular shape is better suited for closely packing in the crystal. However, this conformational conversion requires the energy, provided when the compound is dissolved at high-pressure. These results show, that even high-energetic barriers of conformers can be overcome by the high-pressure treatment. It suggests that the higher potential energy (E_p) conformers can be regarded as steps reducing the distance to the next E_p barrier required to dissociate the disulfide bond, which is necessary for the reaction to occur.[183,184]

In order to investigate if the disulfide-exchange reactions at high-pressure occur under thermodynamic or kinetic control, we performed a series of experiments on compressed solutions, where several homodimeric systems (corresponding to the successfully performed reactions in the DAC) were well mixed, and in the next stage, compressed in the piston-cylinder press (details are described in the Supporting Information in **R5**). The amounts of heterodimeric products traced by ^{13}C-NMR, before and just after the sample was compressed (all related spectra can be found also in the Supporting Information in **R5**), showed that while four systems equilibrated already at ambient conditions, in seven others the product was not formed. Moreover, the compression accelerated the conversion to heterodimers in only one of the attempted reactions. That result, somewhat surprising, contrasts with the calculated reaction volume diagrams (Figure 3 in **R5**). According to the van der Waals volume calculations (for details see the Supporting Information in **R5**), in most reactions the product is smaller than at least one of the starting substrates. It seems reasonable to assume that the volume reduction of -8.26 Å^3, calculated between the substrate and product molecule, is not enough to compensate the reaction volume (ΔV^o) gain, associated with the formation of radicals.

For explaining the nature of this phenomenon, we have focused our attention on the reactions conducted in the DAC, with a special concern for the solid form of obtained products. Using the example of bis-3-nitrophenyl disulfide described in article **R7**, we

have investigated the process of high-pressure crystallization (described within this thesis in section 2.2 as well as in the "***Experimental***" section in **R7** and "***Reaction procedure and optimization*****"** in **R5**). Following the same protocol as it was applied for the crystallization of reaction products, we obtained two new polymorphs β and γ of bis-3-nitrophenyl disulfide (Figure 1 and Table 1 in **R7**). Both these new polymorphs display characteristic features of kinetic polymorphs, such as: (i) lower symmetry; (ii) lower density and (iii) higher number *Z*' of symmetry-independent molecules; as well as (iv) higher potential energy of the conformers, compared to those obtained under dynamic-regime. Interestingly, polymorph A, the product obtained in a high-pressure reaction in isopropanol described in the article **R4,** also displays all characteristic features (i-iv) of the kinetic polymorph. That led us to the conclusion that the nucleation occurring under high-pressure/high-temperature conditions, is the crucial point for initiating a high-conversion rate of the disulfide exchange reactions. As described in section "***Control by the Entropy*****"** of article **R5**, the full conversion to heterodimeric disulfide originates from an entropy-driven kinetic process (Figure 4 in **R5**). The system maximizes its entropy at high-pressure and high-temperature, which is achieved when the dissolved and conformationally differentiates substrates start to dissociate into the sulfenyl radicals. Then the reaction follows to minimize the reaction volume, which leads to the formation of the product. By reducing the temperature, the kinetic regime of precipitation is imposed. The nucleation takes place in the extreme conditions for the highly excited molecules, which can be described as the high-entropy environment, hence the high-entropy nucleation (**R4**). Naturally, for equilibrium reactions, there must be some systematic factor favoring the desired product. In this case of disulfide exchange reactions, this is the increased dipole moments of the heterodimers, compared to the dipoles of homodimeric substrates, that favors the nucleation of the products due to the stronger electrostatic attraction. Once the nuclei of heterodimeric products are more likely to be formed, the reaction equilibrium is shifted and the conversion rate increases. This stokes up on the kinetic crystallization that preserves in the crystals the high-entropy features and high-E_p conformers nucleated at extreme conditions of high-temperature and high-pressure environment. Moreover, due to the increased viscosity of the solution under high-pressure, the time scale required for the kinetic crystallization

expands compared to normal conditions. The described process provides the molecular-level illustration of Ostwald's rule of stages. The process of the entropy-driven equilibrium redistribution has been described in section "***Control by the Entropy***" in article **R6** and nucleation leading to kinetic polymorphs in section "***Discussion***" of article **R7**.

4

Conclusions

In the series of 7 publications, I have shown how the high pressure can be used for inducing a chemical reaction, leading to new materials. The described examples illustrate that high pressure is an efficient stimulus activating reactions of organic, inorganic and hybrid organic-inorganic systems, to the point that the catalysts, indispensable at ambient conditions, are no longer needed. The detailed investigations of several reaction systems in the solid and liquid states, by combining several analytic methods, allowed me to better understand the observed processes and to apply this understanding in practice. Some of the most significant results of this thesis are summarized below.

The structural changes and chemical reactions in the closed-shell metal coordination complexes can be predicted based on the pressure dependence of the radii of metal cation and ligands, according to the radius−ratio rule, with consideration of the arrangement of ligands around the central cation, and the presence of other potential ligands in the vicinity of a metal cation. High-pressure can increase the coordination number of cations in those systems, without changing their oxidation state.

One of the unexpected results of my research was the observation of the effects of the pressure-transmitting media on the solid-state transformations, so far connected with the sample material only. The introduction of an open-shell metal cation coordinated by ligands capable to mediate an electron transfer can lead to a variety of pressure-induced transformations, depending on the liquid environment. The compression of α-$DmaFe^{2+}Fe^{3+}For_6$ resulted in three different types of transformations: (i) order−disorder and displacive reversible phase transition (between phases α and γ);

(ii) reversible chemical reaction involving the reduction of Fe^{3+} cations (yielding $DmaFe^{2+}For_3$); and (iii) irreversible redox reaction with reduction of organic ligands, leading to single-crystalline $Dma_3Fe^{2+}{}_3Fe^{3+}For_{12}{\cdot}CO_2$. While the reactions involving the closed-shell metals lead to increased coordination number and can be conducted in the solid-state or *via* the liquid state, as observed for $Cd(APP)_2NO_3{\cdot}NO_3$ and PbI_2 dissolved in concentrated $HI_{(aq)}$, respectively, the high-pressure redox reactions depend on physical and chemical properties of the liquid environment.

The example of a system extremely sensitive to the external stimuli, depending not only on the acidity, iodine and water contents as well as the pressure and temperature, was found in the series of structurally closely related lead halide PbI_2 polymorphs α and β, as well as their hydronium salts. All these structures consist of the PbI_6 octahedra shearing edges in common polymeric sheets (2D) and ribbons (1D) Pb–I bonded motives, consisting of the scaffolds for all of those structures. The weakest of the cohesion forces occur between the polyanions. In all these related structures the close positions and short contacts of the electronegative iodine atoms lead to the high susceptibility of the interanionic regions to the compressed environment. We have shown that the compensation of these electrostatically unfavored close locations of iodine atoms can be achieved by the intercalation, either by water molecules and/or by hydronium cations that form $OH{\cdots}I^-$ and $OH^+{\cdots}I^-$ hydrogen bonds. In this way, the sort I···I contacts between polyanions are eliminated.

In the disulfide exchange reaction, we have successfully applied a novel approach, where the effect of pressure was used instead of catalytic or reducing agents. We have presented the explanation for the radical-mediated mechanism of this reaction at high-pressure, by connecting it to the effects of increased entropy of the system. In this project we have used advantages of the DAC used as a high-pressure reactor for carrying out the synthesis, compared to the large-volume piston-cylinder press.

We have also connected high-pressure behavior of aryl disulfides, capable of absorbing the mechanical energy of compression by exciting higher states of these molecules. In the case study on di-*p*-tolyl disulfide, it was shown that disulfide molecules

can absorb the stress energy, of about 6 $kJmol^{-1}$ by conformational conversion in the compressed liquid environment.

Finally, we have explained how the reaction equilibrium in aryl disulfide exchange reaction is shifted toward the heterodimeric products, by the process of high-entropy nucleation. The closed system of the DAC allowed us to investigate the high-pressure and high-temperature recrystallization of homodimeric bis-3-nitrophenyl disulfide. As a result, we crystallized polymorphs β and γ of bis-3-nitrophenyl disulfide, which were obtained under high pressure but were less dense than polymorph α obtained at ambient conditions. At first glance, these results seemed to contradict one of the main paradigms of thermodynamics. Generally, the high-pressure crystallizations and syntheses lead to high-density polymorphs and products. In fact, the high-pressure techniques are aimed at obtaining hard, high-density materials. However, such processes are performed slowly under the dynamic regime, allowing the system to equilibrate. We found, that the high-pressure conditions can be effectively used to expand the thermodynamic space of temperature and concertation, where the kinetic polymorphs can be formed. At the high-pressure, viscosity of the system is significantly increased, which affects the molecular conformations and leaves no sufficient time for the molecules to reorient or change the positions of their substituents, thus directing the crystallization to kinetic polymorphs. This observation provides a rational explanation for the puzzling density relation of polymorphs A and B of 4-chlorophenyl-2'-nitrophenyl-disulfide, from which form A was the less-dense polymorph obtained in the pressure-induced disulfide exchange reaction. Owing to the confined reaction space, the entropy of the system can be increased in a controlled manner to a stage when the substrates are dissolved and the molecules are excited into high energy conformers and rota-vibrational states leading to the dissociation of the S–S bond. Then, by lowering the temperature, the high-entropy nucleation and subsequent kinetic crystallization can offset the thermodynamic equilibrium, resulting in high yields of exchanged disulfides for catalyst-free, high-pressure reactions.

This result shows that most of the common technological difficulties and their dangerous consequences for the environment, like purification of the products,

considerable large heat-energy consumption, wasting the solvents, the troublesome processes of dissolution and evaporation of solvents, often damaging the environment *etc*. can be circumvented by performing reactions under high pressure in confined space. Importantly, the pressure-induced exchange of the disulfide bond meets 7 out of 12 green chemistry principles,[185] in particular:

- The process uses less solvent, which results in a cleaner reaction profile and less waste left after the synthesis process;
- Our reaction is designed to account for every atom because the catalyst is eliminated, while the conversion rates and selectivity reaches 100%;
- Contact with all chemical catalysts used before to accelerate the disulfide exchange is highly hazardous for the living organisms. Just to mention DBU (1,8-diazabicycloundec-7-ene), which is carcinogenic and corrosive or phosphine compounds that may cause, nausea, vomits, stomach pain, thirst, muscle pain, difficulty breathing, *etc.*;
- The high-pressure method not only requires less solvent but in contrary to the ultrasound-accelerated disulfide exchange, does not require $CHCl_3$ or $CHBr_3$ and can proceed in simple alcohols, like methanol or isopropanol;
- We have significantly shortened the long reaction time required for the exchange reactions at normal pressure, even when intensive heating is applied;
- We have shown how to apply analytical methodologies for the real-time and ongoing high-pressure process monitoring and control;
- The closed vessel can prevent releasing any toxic gases.

Undoubtedly, reactions under elevated pressure are interesting, but they still remain an unexplored area requiring more investigation. The few examples of different reactions presented in this thesis illustrate some potential of pressure-induced reactions. It has been demonstrated that new chemical compounds and new forms of materials can be obtained by using high-pressure techniques. They can overcome some of the problems of the traditional synthetic methods, like the generation of waste or the consumption of

considerable amounts of energy. It appears that the new aspects of high-pressure technique can be attractive to the industry, as these methods offer high reaction yields and provide a more environmentally responsible manner for obtaining new materials, frequently attained in a form of single-crystal, and thus not requiring any additional purification. It should be stressed that the environment protection and following the principles of green chemistry are increasingly urgent in the modern world. Undoubtedly, the cost of energy and waste disposal can be considerably reduced by applying high-pressure methods. Also, a smaller number of reaction steps and shorter processes, ascribed for the pressure-induced reactions, are important for the environment. Therefore, the high-pressure methods can provide means to achieving more efficient, safer and more environmentally friendly chemical reactions and transformations of various materials.

5

Bibliography

(1) Jamieson, J. C.; Lawson, A. W.; Nachtrieb, N. D. New Device for Obtaining X-Ray Diffraction Patterns from Substances Exposed to High Pressure. *Rev. Sci. Instrum.* **1959**, *30* (11), 1016–1019. https://doi.org/10.1063/1.1716408.

(2) Weir, C. E.; Lippincott, E. R.; Van Valkenburg, A.; Bunting, E. N. Infrared Studies in the 1- to 15-Micron Region to 30,000 Atmospheres. *J. Res. Natl. Bur. Stand. Sect. A Phys. Chem.* **1959**. https://doi.org/10.6028/jres.063a.003.

(3) Merrill, L.; Bassett, W. A. Miniature Diamond Anvil Pressure Cell for Single Crystal X-Ray Diffraction Studies. *Rev. Sci. Instrum.* **1974**, *45* (2), 290–294. https://doi.org/10.1063/1.1686607.

(4) van Eldik, R.; Jonas, J. *High Pressure Chemistry and Biochemistry*; Eldik, R., Jonas, J., Eds.; Springer Science & Business Media: Dordrecht, 1987. https://doi.org/10.1007/978-94-009-3827-4.

(5) van Eldik, R.; Hubbard, C. D. Effect of Pressure on Inorganic Reactions: Introduction and Mechanistic Applications. In *High Pressure Chemistry: Synthetic, Mechanistic, and Supercritical Applications*; 2007. https://doi.org/10.1002/9783527612628.ch01.

(6) Wurche, F.; Klärner, F. G. The Effect of Pressure on Organic Reactions: Basic Principles and Mechanistic Applications. *High Press. Chem. Synth. Mech. Supercrit. Appl.* **2007**, 41–96. https://doi.org/10.1002/9783527612628.ch02.

(7) Noble, W. J. Organic Synthesis at High Pressure. In *High Pressure Chemistry and Biochemistry*; 1987. https://doi.org/10.1007/978-94-009-3827-4_12.

(8) Van Eldik, R.; Asano, T.; Le Noble, W. J. Activation and Reaction Volumes in Solution. 2. *Chem. Rev.* **1989**, *89* (3), 549–688. https://doi.org/10.1021/cr00093a005.

(9) Van Eldik, R.; Asano, T.; Le Noble, W. J. Activation and Reaction Volumes in Solution. 2 [Erratum to Document Cited in CA110(24):219738v]. *Chem. Rev.* **1989**, *89* (8), 1981–1981. https://doi.org/10.1021/cr00098a015.

(10) Drljaca, A.; Hubbard, C. D.; van Eldik, R.; Asano, T.; Basilevsky, M. V.; le Noble, W. J. Activation and Reaction Volumes in Solution. 3. *Chem. Rev.* **1998**, *98* (6), 2167–2290. https://doi.org/10.1021/cr970461b.

(11) Asano, T.; Noble, W. J. L. Activation and Reaction Volumes in Solution. *Chem. Rev.* **1978**, *78* (4), 407–489. https://doi.org/10.1021/cr60314a004.

(12) Hamann, S. D. The Role of Electrostriction in High Pressure Chemistry. *Rev. Phys. Chem. Japan* **1980**, *50*, 147-168.

(13) Hills, G. The Physics and Chemistry of High Pressures. *Symp. Soc. Exp. Biol.* **1972**, *26*, 1–26.

(14) Demazeau, G. rard. High Pressure in Solid-State Chemistry. *J. Phys. Condens. Matter* **2002**, *14* (44), 11031–11035. https://doi.org/10.1088/0953-8984/14/44/422.

(15) Menschutkin, N. Über Die Affinitätskoeffizienten Der Alkylhaloide Und Der Amine. *Zeitschrift für Phys. Chemie* **1890**, *6* (1). https://doi.org/10.1515/zpch-1890-0107.

(16) Menschutkin, N. Beiträge Zur Kenntnis Der Affinitätskoeffizienten Der Alkylhaloide Und Der Organischen Amine. *Zeitschrift für Phys. Chemie* **1890**, *5U* (1). https://doi.org/10.1515/zpch-1890-0546.

(17) Okamoto, Y.; Shimagawa, Y. On the Synthesis and Properties of 1-Methyl 2,6-Di-t-Butyl Pyridinium Iodine. *Tetrahedron Lett.* **1966**. https://doi.org/10.1016/S0040-4039(01)99653-4.

(18) Banks, R. E.; Mohialdin-Khaffaf, S. N.; Lal, G. S.; Sharif, I.; Syvret, R. G. 1-Alkyl-4-Fluoro-1,4-Diazoniabicyclo[2.2.2]Octane Salts: A Novel Family of Electrophilic Fluorinating Agents. In *Journal of the Chemical Society, Chemical Communications*; **1992,** 595-596. https://doi.org/10.1039/C39920000595.

(19) Olejniczak, A.; Katrusiak, A. Pressure Induced Transformations of 1,4-Diazabicyclo[2.2.2]Octane (Dabco) Hydroiodide: Diprotonation of Dabco, Its N-Methylation and Co-Crystallization with Methanol. *CrystEngComm* **2010**, *12* (9), 2528. https://doi.org/10.1039/c001379j.

(20) Andrzejewski, M.; Olejniczak, A.; Katrusiak, A. Remote Halogen Switch of Amine Hydrophilicity. *CrystEngComm* **2012**, *14* (20), 6374–6376. https://doi.org/10.1039/c2ce25401h.

(21) Anioła, M.; Katrusiak, A. Pressure-Preferred Symmetric Reactions of 4,4′-Bipyridine Hydrobromide. *CrystEngComm* **2016**, *18* (18), 3223–3228. https://doi.org/10.1039/c6ce00356g.

(22) Jones, W. H.; Tristram, E. W.; Benning, W. F. High Pressure Studies: Oximes of Hindered Ketones. *J. Am. Chem. Soc.* **1959**, *81* (9), 2151–2154. https://doi.org/10.1021/ja01518a034.

(23) Rapson, W. S.; Robinson, R. 307. Experiments on the Synthesis of Substances Related to the Sterols. Part II. A New General Method for the Synthesis of Substituted Cyclohexenones. *J. Chem. Soc.* **1935**, *37* (2), 1285. https://doi.org/10.1039/jr9350001285.

(24) Little, R. D.; Masjedizadeh, M. R.; Wallquist, O.; Mcloughlin, J. I. The Intramolecular Michael Reaction. In *Organic Reactions*; John Wiley & Sons, Inc.: Hoboken, NJ, USA, **1995**; pp 315–552. https://doi.org/10.1002/0471264180.or047.02.

(25) Mannich, C.; Krösche, W. Ueber Ein Kondensationsprodukt Aus Formaldehyd, Ammoniak Und Antipyrin. *Arch. Pharm. (Weinheim).* **1912**, *250* (1), 647–667. https://doi.org/10.1002/ardp.19122500151.

(26) Matsumoto, K. Synthesis under High Pressure: Michael Addition. *Angew. Chemie Int. Ed. English* **1980**, *19* (12), 1013–1014. https://doi.org/10.1002/anie.198010131.

(27) Matsumoto, K. High Pressure Michael Addition Catalyzed by Fluoride Ions. *Angew. Chemie Int. Ed. English* **1981**, *20* (9), 770–771. https://doi.org/10.1002/anie.198107701.

(28) Matsumoto, K. Synthesis under High Pressure: Mannich Reaction of Ketones and Esters with Dichloromethane and Secondary Amines. *Angew. Chemie Int. Ed. English* **1982**, *21* (12), 922–922. https://doi.org/10.1002/anie.198209221.

(29) Barker, J. M.; Huddleston & Michael, P. R.; Wood, L. L. Synthetic Communications An International Journal for Rapid Communication of Synthetic Organic Chemistry Mannich Reactions of Methoxythiophens. *Mannich React. Methoxythiophens, Synth. Commun.* **1975**, *5* (1), 59–64.

(30) Henry, L. Formation Synthétique d'alcools Nitrés. *CR Hebd Acad Sci* **1895**, *120*, 1265–1268.

(31) Jurczak, J. Application of High Pressure in Organic Synthesis. *Phys. B+C* **1986**, *139–140* (C), 709–

716. https://doi.org/10.1016/0378-4363(86)90683-2.

(32) Jurczak, J.; Ostaszewski, R.; Pietraszkiewicz, M.; Salański, P. High Pressure Approach to the Synthesis of Cryptands and Related Compounds. *J. Incl. Phenom.* **1987**, *5* (5), 553–561. https://doi.org/10.1007/BF00662994.

(33) Jurczak, J.; Kasprzyk, S.; Sałański, P.; Stankiewicz, T. High-Pressure Approach to the Synthesis of Macrocyclic Diamides. *High Press. Res.* **1993**, *11* (1–3), 139–143. https://doi.org/10.1080/08957959208201699.

(34) Fawcett, E. W.; Gibson, R. O. 90. The Influence of Pressure on a Number of Organic Reactions in the Liquid Phase. *J. Chem. Soc.* **1934**, No. 386, 386. https://doi.org/10.1039/jr9340000386.

(35) Jurczak, J.; KawczyńSki, A. L.; KoźLuk, T. Stability of Cycloadducts Obtained by High-Pressure Diels-Alder Reaction between 3,4-Dimethoxyfuran and 1,4-Benzoquinones: Kinetic Studies of Retro-Diels-Alder Reaction. *J. Org. Chem.* **1985**, *50* (7), 1106–1107. https://doi.org/10.1021/jo00207a035.

(36) Dauben, W. G.; Kessel, C. R.; Takemura, K. H. Simple, Efficient Total Synthesis of Cantharidin via a High-Pressure Diels-Alder Reaction. *J. Am. Chem. Soc.* **1980**, *102* (22), 6893–6894. https://doi.org/10.1021/ja00542a060.

(37) Trân-Huu-Dâu, M. E.; Wartchow, R.; Winterfeldt, E.; Wong, Y. S. New Cyclohexadienone Derivatives: Preparation and Chiral Discrimination in High-Pressure Diels - Alder Cycloadditions. *Chem. - A Eur. J.* **2001**, *7* (11), 2349–2369. https://doi.org/10.1002/1521-3765(20010601)7:11<2349::AID-CHEM23490>3.0.CO;2-C.

(38) Pandey, S. K.; Orellana, A.; Greene, A. E.; Poisson, J. F. High-Pressure Diels-Alder Approach to Natural Kainic Acid. *Org. Lett.* **2006**, *8* (24), 5665–5668. https://doi.org/10.1021/ol062419l.

(39) Minuti, L.; Taticchi, A.; Gacs-Baitz, E.; Marrocchi, A. High Pressure Diels-Alder Reactions of 2-Vinyl-3,4-Dihydronaphthalene. Synthesis of Cyclopenta[c]- and Indeno[c]Phenanthrenones. *Tetrahedron* **1995**, *51* (32), 8953–8958. https://doi.org/10.1016/0040-4020(95)00504-2.

(40) Kotsuki, H.; Hondo, A.; Nishizawa, H.; Ochi, M.; Matsuoka, K. High-Pressure Diels-Alder Reactions of Vinylfurans. *J. Org. Chem.* **1981**, *46* (26), 5454–5455. https://doi.org/10.1021/jo00339a055.

(41) Walling, C.; Peisach, J. Organic Reactions Under High Pressure. IV. The Dimerization of Isoprene. *J. Am. Chem. Soc.* **1958**, *80* (21), 5819–5824. https://doi.org/10.1021/ja01554a058.

(42) Benson, S. W.; Berson, J. A. The Effect of Pressure on the Rate and Equilibrium Constants of Chemical Reactions. The Calculation of Activation Volumes by Application of the Tait Equation. *J. Am. Chem. Soc.* **1962**, *84* (2), 152–158. https://doi.org/10.1021/ja00861a005.

(43) Grieger, R. A.; Eckert, C. A. Mechanistic Evidence for the Diels–Alder Reaction from High-Pressure Kinetics. *J. Am. Chem. Soc.* **1970**, *92* (24), 7149–7153. https://doi.org/10.1021/ja00727a021.

(44) Stewart, C. A. Dimerization of Chloroprene and Related Dienes. *J. Am. Chem. Soc.* **1971**, *93* (19), 4815–4821. https://doi.org/10.1021/ja00748a025.

(45) Stewart, C. A. Competing Diradical and Electrocyclic Reactions. Difference in Activation Volumes. *J. Am. Chem. Soc.* **1972**, *94* (2), 635–637. https://doi.org/10.1021/ja00757a055.

(46) Jurczak, J.; Tkacz, M. Stereochemistry of Diels-Alder Reactions at High Pressure. 4. Asymmetric Induction in High-Pressure Cycloadditions of (R)-(-)-Menthyl Glyoxylate and Symmetric 1,3-Dienes. *J. Org. Chem.* **1979**, *44* (19), 3347–3352. https://doi.org/10.1021/jo01333a016.

(47) van Eldik, R.; Klärner, F. G. *High Pressure Chemistry: Synthetic, Mechanistic, and Supercritical Applications*; van Eldik, R., Klärner, F., Eds.; Wiley, **2007**. https://doi.org/10.1002/9783527612628.

(48) Hamann, S. D. *High Pressure Chemistry*; van Eldik, R., Klärner, F., Eds.; Wiley, **2003**; Vol. 15. https://doi.org/10.1146/annurev.pc.15.100164.002025.

(49) Isaacs, N. S. *High Pressure Food Science, Bioscience and Chemistry*; **1998**. https://doi.org/10.1533/9781845698379.

(50) Zhulin, V. M.; Volchek, S. I. High-Pressure Trimerization of Acetonitrile to 2,4,6-Trimethyl-l,3,5-Triazine. *Bull. Acad. Sci. USSR Div. Chem. Sci.* **1977**, *26* (6), 1192–1196. https://doi.org/10.1007/BF01143899.

(51) Cairns, T. L.; Larchar, A. W.; McKusick, B. C. The Trimerization of Nitriles at High Pressures. *J. Am. Chem. Soc.* **1952**, *74* (22), 5633–5636. https://doi.org/10.1021/ja01142a028.

(52) Olejniczak, A.; Katrusiak, A. Supramolecular Reaction between Pressure-Frozen Acetonitrile Phases α and β. *J. Phys. Chem. B* **2008**, *112* (24), 7183–7190. https://doi.org/10.1021/jp800753n.

(53) Buback, M.; Lendle, H. Die Kinetik Des Zerfalls von Tert. Butylperoxypivalat Bei Hohen Drücken Und Temperaturen. *Zeitschrift fur Naturforsch. - Sect. A J. Phys. Sci.* **1981**, *36* (12), 1371–1377. https://doi.org/10.1515/zna-1981-1219.

(54) Kimura, Y.; Yoshimura, Y.; Nakahara, M. Chemical Reactions in the Medium Density Fluid. Anomaly in the Volume Profile of the Dimerization Reaction of 2-Methyl-2-Nitrosopropane in Carbon Dioxide. *Chem. Lett.* **1987**, *16* (4), 617–620. https://doi.org/10.1246/cl.1987.617.

(55) Klärner, F.-G.; Wurche, F. The Effect of Pressure on Organic Reactions. *J. für Prakt. Chemie* **2000**, *342* (7), 609–636. https://doi.org/10.1002/1521-3897(200009)342:7<609::AID-PRAC609>3.0.CO;2-Z.

(56) Conant, J. B.; Peterson, W. R. Polymerization Reactions under High Pressure. II. The Mechanism of the Reaction. *J. Am. Chem. Soc.* **1932**, *54* (2), 628–635. https://doi.org/10.1021/ja01341a028.

(57) Walling, C.; Augurt, T. A. Organic Reactions under High Pressure. X. The Mechanism of Aldehyde Polymerization at High Pressures. *J. Am. Chem. Soc.* **1966**, *88* (18), 4163–4167. https://doi.org/10.1021/ja00970a009.

(58) Stoiljkovich, D.; Jovanovich, S.; Jovanovićch, S. Mechanism of the High-Pressure Free Radical Polymerization of Ethylene. *J. Polym. Sci. A1.* **1981**, *19* (3), 741–747. https://doi.org/10.1002/pol.1981.170190313.

(59) Appl, M. Ammonia, 2. Production Processes. In *Ullmann's Encyclopedia of Industrial Chemistry*; **2011**. https://doi.org/10.1002/14356007.o02_o11.

(60) Appl, M. Ammonia 1. *Ullmann's Encycl. Ind. Chem.* **2012**. https://doi.org/10.1002/14356007.a02_143.pub3

(61) Badding, J. V. High-Pressure Synthesis, Characterization, and Tuning of Solid State Materials. *Annu. Rev. Mater. Sci.* **1998**, *28* (1), 631–658. https://doi.org/10.1146/annurev.matsci.28.1.631.

(62) Bykov, M.; Chariton, S.; Fei, H.; Fedotenko, T.; Aprilis, G.; Ponomareva, A. V.; Tasnádi, F.; Abrikosov, I. A.; Merle, B.; Feldner, P.; et al. High-Pressure Synthesis of Ultraincompressible Hard Rhenium Nitride Pernitride Re2(N2)(N)2 Stable at Ambient Conditions. *Nat. Commun.* **2019**, *10* (1), 6–13. https://doi.org/10.1038/s41467-019-10995-3.

(63) Niwa, K.; Dzivenko, D.; Suzuki, K.; Riedel, R.; Troyan, I.; Eremets, M.; Hasegawa, M. High Pressure Synthesis of Marcasite-Type Rhodium Pernitride. *Inorg. Chem.* **2014**. https://doi.org/10.1021/ic402885k.

(64) Niwa, K.; Suzuki, K.; Muto, S.; Tatsumi, K.; Soda, K.; Kikegawa, T.; Hasegawa, M. Discovery of the Last Remaining Binary Platinum-Group Pernitride RuN2. *Chem. - A Eur. J.* **2014**. https://doi.org/10.1002/chem.201404165.

(65) Niwa, K.; Terabe, T.; Kato, D.; Takayama, S.; Kato, M.; Soda, K.; Hasegawa, M. Highly Coordinated Iron and Cobalt Nitrides Synthesized at High Pressures and High Temperatures. *Inorg. Chem.* **2017**. https://doi.org/10.1021/acs.inorgchem.7b00516.

(66) Bykov, M.; Bykova, E.; Aprilis, G.; Glazyrin, K.; Koemets, E.; Chuvashova, I.; Kupenko, I.; McCammon, C.; Mezouar, M.; Prakapenka, V.; et al. Fe-N System at High Pressure Reveals a Compound Featuring Polymeric Nitrogen Chains. *Nat. Commun.* **2018**. https://doi.org/10.1038/s41467-018-05143-2.

(67) Bhadram, V. S.; Kim, D. Y.; Strobel, T. A. High-Pressure Synthesis and Characterization of Incompressible Titanium Pernitride. *Chem. Mater.* **2016**. https://doi.org/10.1021/acs.chemmater.6b00042.

(68) Young, A. F.; Sanloup, C.; Gregoryanz, E.; Scandolo, S.; Hemley, R. J.; Mao, H. K. Synthesis of Novel Transition Metal Nitrides IrN2 and OsN2. *Phys. Rev. Lett.* **2006**. https://doi.org/10.1103/PhysRevLett.96.155501.

(69) Crowhurst, J. C.; Goncharov, A. F.; Sadigh, B.; Evans, C. L.; Morrall, P. G.; Ferreira, J. L.; Nelson, A. J. Synthesis and Characterization of the Nitrides of Platinum and Iridium. *Science (80-.).* **2006**. https://doi.org/10.1126/science.1121813.

(70) Crowhurst, J. C.; Goncharov, A. F.; Sadigh, B.; Zaug, J. M.; Aberg, D.; Meng, Y.; Prakapenka, V. B. Synthesis and Characterization of Nitrides of Iridium and Palladium. In *Journal of Materials Research*; **2008**. https://doi.org/10.1557/jmr.2008.0027.

(71) Zhou, D.; Semenok, D. V.; Xie, H.; Huang, X.; Duan, D.; Aperis, A.; Oppeneer, P. M.; Galasso, M.; Kartsev, A. I.; Kvashnin, A. G.; et al. High-Pressure Synthesis of Magnetic Neodymium Polyhydrides. *J. Am. Chem. Soc.* **2020**, *142* (6), 2803–2811. https://doi.org/10.1021/jacs.9b10439.

(72) Howie, R. T.; Narygina, O.; Guillaume, C. L.; Evans, S.; Gregoryanz, E. High-Pressure Synthesis of Lithium Hydride. *Phys. Rev. B - Condens. Matter Mater. Phys.* **2012**, *86* (6), 1–4. https://doi.org/10.1103/PhysRevB.86.064108.

(73) Kamegawa, A.; Goto, Y.; Kataoka, R.; Takamura, H.; Okada, M. High-Pressure Synthesis of Novel Compounds in an Mg-Ni System. *Renew. Energy* **2008**, *33* (2), 221–225. https://doi.org/10.1016/j.renene.2007.05.008.

(74) Degtyareva, O.; Proctor, J. E.; Guillaume, C. L.; Gregoryanz, E.; Hanfland, M. Formation of Transition Metal Hydrides at High Pressures. *Solid State Commun.* **2009**, *149* (39–40), 1583–1586. https://doi.org/10.1016/j.ssc.2009.07.022.

(75) Scheler, T.; Degtyareva, O.; Marqués, M.; Guillaume, C. L.; Proctor, J. E.; Evans, S.; Gregoryanz, E. Synthesis and Properties of Platinum Hydride. *Phys. Rev. B - Condens. Matter Mater. Phys.* **2011**, *83* (21), 1–5. https://doi.org/10.1103/PhysRevB.83.214106.

(76) Kuzovnikov, M. A.; Tkacz, M.; Meng, H.; Kapustin, D. I.; Kulakov, V. I. High-Pressure Synthesis of Tantalum Dihydride. *Phys. Rev. B* **2017**, *96* (13), 2–7. https://doi.org/10.1103/PhysRevB.96.134120.

(77) Kuzovnikov, M. A.; Tkacz, M. Synthesis of Ruthenium Hydride. *Phys. Rev. B* **2016**, *93* (6), 1–5. https://doi.org/10.1103/PhysRevB.93.064103.

(78) Scheler, T.; Marqués, M.; Konôpková, Z.; Guillaume, C. L.; Howie, R. T.; Gregoryanz, E. High-Pressure Synthesis and Characterization of Iridium Trihydride. *Phys. Rev. Lett.* **2013**, *111* (21), 1–5. https://doi.org/10.1103/PhysRevLett.111.215503.

(79) Burtovyy, R.; Tkacz, M. High-Pressure Synthesis of a New Copper Hydride from Elements. *Solid State Commun.* **2004**, *131* (3–4), 169–173. https://doi.org/10.1016/j.ssc.2004.05.014.

(80) Donnerer, C.; Scheler, T.; Gregoryanz, E. High-Pressure Synthesis of Noble Metal Hydrides. *J. Chem. Phys.* **2013**, *138* (13). https://doi.org/10.1063/1.4798640.

(81) Tkacz, M. Thermodynamics of the Metal-Hydrogen Systems in DAC. *Defect Diffus. Forum* **2002**, *208–209*, 107–116. https://doi.org/10.4028/www.scientific.net/ddf.208-209.107.

(82) Tkacz, M. Thermodynamic Properties of Iron Hydride. *J. Alloys Compd.* **2002**, *330–332*, 25–28. https://doi.org/10.1016/S0925-8388(01)01487-6.

(83) Baranowski, B.; Tkacz, M. The Equilibrium Between Solid Aluminium Hydride and Gaseous Hydrogen. *Zeitschrift für Phys. Chemie* **1983**, *135* (135), 27–38. https://doi.org/10.1524/zpch.1983.135.135.027.

(84) Gaffet, E.; Bernard, F.; Niepce, J. C.; Charlot, F.; Gras, C.; Caër, G. Le; Guichard, J. L.; Delcroix, P.; Mocellin, A.; Tillement, O. Some Recent Developments in Mechanical Activation and Mechanosynthesis. In *Journal of Materials Chemistry*; **1999**. https://doi.org/10.1039/a804645j.

(85) Katrusiak, A. Lab in a DAC - High-Pressure Crystal Chemistry in a Diamond-Anvil Cell. *Acta Crystallogr. Sect. B Struct. Sci. Cryst. Eng. Mater.* **2019**, *75*, 918–926. https://doi.org/10.1107/S2052520619013246.

(86) Boldyreva, E. Mechanochemistry of Inorganic and Organic Systems: What Is Similar, What Is Different? *Chem. Soc. Rev.* **2013**, *42* (18), 7719. https://doi.org/10.1039/c3cs60052a.

(87) Welech, J. E. Solid-Solid Reactions. In *Chemistry of the solid state*; Garner, W. E., Ed.; Butterworths Scientific Publications: London, **1955**.

(88) Liu, L. G.; Bassett, W. A. *High-Pressure Phases with Implications for the Earth's Interior, Clarendon*; Oxford University Press: New York, **1986**. https://doi.org/https://doi.org/10.1029/88EO01157.

(89) Seitz, F.; Johnson, R. P. Modern Theory of Solids. II. *J. Appl. Phys.* **1937**, *8* (3), 186–199. https://doi.org/10.1063/1.1710281.

(90) Seitz, F.; Johnson, R. P. Modern Theory of Solids. II. *J. Appl. Phys.* **1937**, *8* (3), 84–97. https://doi.org/10.1063/1.1710281.

(91) Seitz, F.; Johnson, R. P. Modern Theory of Solids. I. *J. Appl. Phys.* **1937**, *8* (2), 84–97. https://doi.org/10.1063/1.1710273.

(92) Mc Millan, P. F. Chemistry at High Pressure. *Chem. Soc. Rev.* **2006**, *35* (10), 855–857. https://doi.org/10.1039/b610410j.

(93) Drickamer, H. G.; Frank, C. W. *Electronic Structure, Electronic Transitions, and the High Pressure Chemistry and Physics of Solids*; **1972**; Vol. 23. https://doi.org/doi:10.1146/annurev.pc.23.100172.000351.

(94) Edwards, D. M. *Electronic Transitions and the High Pressure Chemistry and Physics of Solids*; Springer Netherlands: Dordrecht, **2015**; Vol. 24. https://doi.org/10.1088/0031-9112/24/11/034.

(95) Katrusiak, A. High-Pressure X-ray Diffraction Studies on Organic Crystals. *Cryst. Res. Technol.* **1991**, *26* (5), 523–531. https://doi.org/10.1002/crat.2170260502.

(96) Katrusiak, A. High-Pressure Crystallography. *Acta Crystallogr. Sect. A Found. Crystallogr.* **2008**, *64* (1), 135–148. https://doi.org/10.1107/S0108767307061181.

(97) Pinkowicz, D.; Rams, M.; Mišek, M.; Kamenev, K. V.; Tomkowiak, H.; Katrusiak, A.; Sieklucka, B. Enforcing Multifunctionality: A Pressure-Induced Spin-Crossover Photomagnet. *J. Am. Chem. Soc.* **2015**, *137* (27), 8795–8802. https://doi.org/10.1021/jacs.5b04303.

(98) O'Neal, K. R.; Brinzari, T. V.; Wright, J. B.; Ma, C.; Giri, S.; Schlueter, J. A.; Wang, Q.; Jena, P.; Liu, Z.; Musfeldt, J. L. Pressure-Induced Magnetic Crossover Driven by Hydrogen Bonding in CuF 2(H2O)2 (3-Chloropyridine). *Sci. Rep.* **2014**, *4*, 1–6. https://doi.org/10.1038/srep06054.

(99) Prescimone, A.; Morien, C.; Allan, D.; Schlueter, J. A.; Tozer, S. W.; Manson, J. L.; Parsons, S.; Brechin, E. K.; Hill, S. Pressure-Driven Orbital Reorientations and Coordination-Sphere Reconstructions in [CuF 2(H 2O) 2(Pyz)]. *Angew. Chemie - Int. Ed.* **2012**, *51* (30), 7490–7494. https://doi.org/10.1002/anie.201202367.

(100) Parois, P.; Moggach, S. A.; Sanchez-Benitez, J.; Kamenev, K. V.; Lennie, A. R.; Warren, J. E.; Brechin, E. K.; Parsons, S.; Murrie, M. Pressure-Induced Jahn-Teller Switching in a Mn12 Nanomagnet. *Chem. Commun.* **2010**, *46* (11), 1881–1883. https://doi.org/10.1039/b923962f.

(101) Prescimone, A.; Milios, C. J.; Moggach, S.; Warren, J. E.; Lennie, A. R.; Sanchez-Benitez, J.; Kamenev, K.; Bircher, R.; Murrie, M.; Parsons, S.; et al. [Mn6] under Pressure: A Combined Crystallographic and Magnetic Study. *Angew. Chemie - Int. Ed.* **2008**, *47* (15), 2828–2831. https://doi.org/10.1002/anie.200705819.

(102) Drickamer, H. G.; Frank, C. W. *Electronic Transitions and the High Pressure Chemistry and Physics of Solids*; Springer Netherlands: Dordrecht, **1973**; Vol. 23. https://doi.org/10.1007/978-94-011-6896-0.

(103) Boldyreva, E. V. High-Pressure Diffraction Studies of Molecular Organic Solids. A Personal View. *Acta Crystallogr. Sect. A Found. Crystallogr.* **2008**, *64* (1), 218–231. https://doi.org/10.1107/S0108767307065786.

(104) Kuznetsov, A. Y.; Pereira, A. S.; Shiryaev, A. A.; Haines, J.; Dubrovinsky, L.; Dmitriev, V.; Pattison, P.; Guignot, N. Pressure-Induced Chemical Decomposition and Structural Changes of Boric Acid. *J. Phys. Chem. B* **2006**, *110* (28), 13858–13865. https://doi.org/10.1021/jp061650d.

(105) Sobczak, S.; Katrusiak, A. Environment-Controlled Postsynthetic Modifications of Iron Formate Frameworks. *Inorg. Chem.* **2019**, *58* (17), 11773–11781. https://doi.org/10.1021/acs.inorgchem.9b01817.

(106) Ciabini, L.; Bini, R.; Ceppatelli, M.; Citroni, M.; Schettino, V. Chemical Reactions at Very High Pressure. In *Advances in Chemical Physics*; Wiley-Blackwell, **2005**; Vol. 131, pp 105–242. https://doi.org/10.1002/0471739464.ch4.

(107) Chelazzi, D.; Ceppatelli, M.; Santoro, M.; Bini, R.; Schettino, V. Pressure-Induced Polymerization in Solid Ethylene. *J. Phys. Chem. B* **2005**, *109* (46), 21658–21663. https://doi.org/10.1021/jp0536495.

(108) Schettino, V.; Bini, R. Molecules under Extreme Conditions: Chemical Reactions at High Pressure. *Phys. Chem. Chem. Phys.* **2003**, *5* (10), 1951–1965. https://doi.org/10.1039/b301381b.

(109) Trout, C. C.; Badding, J. V. Solid State Polymerization of Acetylene at High Pressure and Low Temperature. *J. Phys. Chem. A* **2000**, *104* (34), 8142–8145. https://doi.org/10.1021/jp000198+.

(110) Li, K.; Zheng, H.; Hattori, T.; Sano-Furukawa, A.; Tulk, C. A.; Molaison, J.; Feygenson, M.; Ivanov, I. N.; Yang, W.; Mao, H. K. Synthesis, Structure, and Pressure-Induced Polymerization of Li3Fe(CN)6 Accompanied with Enhanced Conductivity. *Inorg. Chem.* **2015**, *54* (23), 11276–11282. https://doi.org/10.1021/acs.inorgchem.5b01851.

(111) Wang, Y.; Li, K.; Sano-Furukawa, A.; Hong, F.; Zheng, H.; Katrusiak, A.; Liao, F.; Andrzejewski, M.; Hattori, T.; Wang, L.; et al. Phase Transitions and Polymerization of C 6 H 6 –C 6 F 6 Cocrystal under Extreme Conditions . *J. Phys. Chem. C* **2016**, *120* (51), 29510–29519. https://doi.org/10.1021/acs.jpcc.6b11245.

(112) Casati, N.; Kleppe, A.; Jephcoat, A. P.; Macchi, P. Putting Pressure on Aromaticity along with in Situ Experimental Electron Density of a Molecular Crystal. *Nat. Commun.* **2016**, *7*, 1–8. https://doi.org/10.1038/ncomms10901.

(113) Dziubek, K. F.; Katrusiak, A. Compression of Intermolecular Interactions in CS 2 Crystal. *J. Phys.*

Chem. B **2004**, *108* (50), 19089–19092. https://doi.org/10.1021/jp0458250.

(114) Poręba, T.; Ernst, M.; Zimmer, D.; Macchi, P.; Casati, N. Pressure-Induced Polymerization and Electrical Conductivity of a Polyiodide. *Angew. Chemie - Int. Ed.* **2019**, *58* (20), 6625–6629. https://doi.org/10.1002/anie.201901178.

(115) Kiran, M. S. R. N.; Ross, N. L.; Ramamurty, U.; Li, W.; Cheetham, A. K.; Spencer, E. C. Pressure-Induced Bond Rearrangement and Reversible Phase Transformation in a Metal-Organic Framework. *Angew. Chemie Int. Ed.* **2014**, *53* (22), 5583–5586. https://doi.org/10.1002/anie.201310276.

(116) Casati, N.; Macchi, P.; Sironi, A. Staggered to Eclipsed Conformational Rearrangement of [Co 2(CO)6(PPh3)2] in the Solid State: An X-Ray Diffraction Study at High Pressure and Low Temperature. *Angew. Chemie - Int. Ed.* **2005**, *44* (47), 7736–7739. https://doi.org/10.1002/anie.200502241.

(117) Chupakhin, A. P.; Sidel'nikov, A. A.; Boldyrev, V. V. Control of the Reactivity of Solids by Changing Their Mechanical Properties. *React. Solids* **1987**, *3* (1–2), 1–19. https://doi.org/10.1016/0168-7336(87)80013-X.

(118) Zakharov, B. A.; Boldyreva, E. V. High Pressure: A Complementary Tool for Probing Solid-State Processes. *CrystEngComm* **2019**, *21* (1), 10–22. https://doi.org/10.1039/c8ce01391h.

(119) Cai, W.; Gładysiak, A.; Anioła, M.; Smith, V. J.; Barbour, L. J.; Katrusiak, A. Giant Negative Area Compressibility Tunable in a Soft Porous Framework Material. *J. Am. Chem. Soc.* **2015**, *137* (29), 9296–9301. https://doi.org/10.1021/jacs.5b03280.

(120) Andrzejewski, M.; Katrusiak, A. Piezochromic Topology Switch in a Coordination Polymer. *J. Phys. Chem. Lett.* **2017**, *8* (5), 929–935. https://doi.org/10.1021/acs.jpclett.7b00019.

(121) Lanza, A.; Germann, L. S.; Fisch, M.; Casati, N.; Macchi, P. Solid-State Reversible Nucleophilic Addition in a Highly Flexible MOF. *J. Am. Chem. Soc.* **2015**, *137* (40), 13072–13078. https://doi.org/10.1021/jacs.5b09231.

(122) Kurmoo, M.; Wang, B.; Liu, B.; Gao, S.; Li, M.; Wang, Z. Erbium-Formate Frameworks Templated by Diammonium Cations: Syntheses, Structures, Structural Transition and Magnetic Properties. *Dalt. Trans.* **2011**, *40* (22), 6038. https://doi.org/10.1039/c1dt10241a.

(123) McKellar, S. C.; Graham, A. J.; Allan, D. R.; Mohideen, M. I. H.; Morris, R. E.; Moggach, S. A. The Effect of Pressure on the Post-Synthetic Modification of a Nanoporous Metal-Organic Framework. *Nanoscale* **2014**, *6* (8), 4163–4173. https://doi.org/10.1039/c3nr04161a.

(124) Allan, D. R.; Blake, A. J.; Huang, D.; Prior, T. J.; Schröder, M. High Pressure Co-Ordination Chemistry of a Palladium Thioether Complex: Pressure versus Electrons. *Chem. Commun.* **2006**, *2* (39), 4081–4083. https://doi.org/10.1039/b606736k.

(125) Warren, J. E.; Murrie, M.; Moggach, S. A.; Parois, P.; Lennie, A. R.; Rowantree, N.; Parsons, S.; Brechin, E. K.; Galloway, K. W. Polymerisation of a Cu(II) Dimer into 1D Chains Using High Pressure. *CrystEngComm* **2009**, *11* (12), 2601. https://doi.org/10.1039/b912707k.

(126) Gould, J. A.; Rosseinsky, M. J.; Moggach, S. A. Tuning the Coordination Chemistry of a Cu(Ii) Complex at High-Pressure. *Dalt. Trans.* **2012**, *41* (18), 5464–5467. https://doi.org/10.1039/c2dt12302a.

(127) Tidey, J. P.; Wong, H. L. S.; McMaster, J.; Schröder, M.; Blake, A. J. High-Pressure Studies of Three Polymorphs of a Palladium(II) Oxathioether Macrocyclic Complex. *Acta Crystallogr. Sect. B Struct. Sci. Cryst. Eng. Mater.* **2016**, *72* (3), 357–371. https://doi.org/10.1107/S2052520616007435.

(128) Bujak, M.; Angel, R. J. High-Pressure- and Low-Temperature-Induced Changes in [(CH 3)3NH(CH3)3NH3][SbCl 5]. *J. Phys. Chem. B* **2006**, *110* (21), 10322–10331. https://doi.org/10.1021/jp060652v.

(129) Prescimone, A.; Sanchez-Benitez, J.; Kamenev, K. K.; Moggach, S. A.; Warren, J. E.; Lennie, A. R.; Murrie, M.; Parsons, S.; Brechin, E. K. High Pressure Studies of Hydroxo-Bridged Cu(II) Dimers. *Dalt. Trans.* **2010**, *39* (1), 113–123. https://doi.org/10.1039/b918287j.

(130) Mao, H. K.; Hu, Q.; Yang, L.; Liu, J.; Kim, D. Y.; Meng, Y.; Zhang, L.; Prakapenka, V. B.; Yang, W.; Mao, W. L. When Water Meets Iron at Earth's Core-Mantle Boundary. *Natl. Sci. Rev.* **2017**, *4* (6), 870–878. https://doi.org/10.1093/nsr/nwx109.

(131) Drickamer, H. G.; Bastron, V. C.; Fisher, D. C.; Grenoble, D. C. The High-Pressure Chemistry of Iron. *J. Solid State Chem.* **1970**, *2* (1), 94–104. https://doi.org/10.1016/0022-4596(70)90038-1.

(132) Slichter, C. P.; Drickamer, H. G. Pressure-Induced Electronic Changes in Compounds of Iron. *J. Chem. Phys.* **2004**, *56* (5), 2142–2160. https://doi.org/10.1063/1.1677511.

(133) Bastron, V. C.; Drickamer, H. G. Solid State Reactions in Organic Crystals at Very High Pressure. *J. Solid State Chem.* **1971**, *3* (4), 550–563. https://doi.org/10.1016/0022-4596(71)90101-0.

(134) Armbrüster, M.; Tse, J.; Heines, P.; Schwarz, U.; Keller, H.-L. Pressure-Induced Internal Redox Reaction of Cs 2 [PdI 4]·I 2 , Cs 2 [PdBr 4]·I 2 , and Cs 2 [PdCl 4]·I 2 . *Inorg. Chem.* **2006**, *45* (24), 9818–9825. https://doi.org/10.1021/ic0601945.

(135) Poliakoff, M.; Licence, P. Green Chemistry. *Nature* **2007**, *450* (7171), 810–812. https://doi.org/10.1038/450810a.

(136) Cernansky, R. Chemistry: Green Refill. *Nature* **2015**, *519* (7543), 379–380. https://doi.org/10.1038/nj7543-379a.

(137) Sanderson, K. Chemistry: It's Not Easy Being Green. *Nature* **2011**, *469* (7328), 18–20. https://doi.org/10.1038/469018a.

(138) Chervin, J. C.; Canny, B.; Besson, J. M.; Pruzan, P. A Diamond Anvil Cell for IR Microspectroscopy. *Rev. Sci. Instrum.* **1995**, *66* (3), 2595–2598. https://doi.org/10.1063/1.1145594.

(139) Hazen, R. M.; Finger, L. W. High-Temperature Diamond-Anvil Pressure Cell for Single-Crystal Studies. *Rev. Sci. Instrum.* **1981**, *52* (1), 75–79. https://doi.org/10.1063/1.1136450.

(140) Jayaraman, A. Diamond Anvil Cell and High-Pressure Physical Investigations. *Rev. Mod. Phys.* **1983**. https://doi.org/10.1103/RevModPhys.55.65.

(141) Bassett, W. A. High Pressure Research : An Diamond Anvil Cell , 50th Birthday. *High Press. Res.* **2009**, *29* (2), 163–186.

(142) Katrusiak, A. High-Pressure x-Ray Diffraction Studies of Organic Crystals. *High Press. Res.* **1990**, *4* (1–6), 496–498. https://doi.org/10.1080/08957959008246167.

(143) Piermarini, G. J.; Block, S.; Barnett, J. D.; Forman, R. A. Calibration of the Pressure Dependence of the R1ruby Fluorescence Line to 195 Kbar. *J. Appl. Phys.* **1975**, *46* (6), 2774–2780. https://doi.org/10.1063/1.321957.

(144) Mao, H. K.; Xu, J.; Bell, P. M. Calibration of the Ruby Pressure Gauge to 800 Kbar under Quasi-Hydrostatic Conditions. *Journal of Geophysical Research*. **1986**, pp 4673–4676. https://doi.org/10.1029/jb091ib05p04673.

(145) Dziubek, K. F.; Katrusiak, A. Complementing Diffraction Data with Volumetric Measurements. *Zeitschrift fur Krist.* **2014**, *229* (2), 129–134. https://doi.org/10.1515/zkri-2013-1677.

(146) Budzianowski, A.; Katrusiak, A. High-Pressure Crystallographic Experiments with a CCD-Detector. In *High-Pressure Crystallography*; Springer Netherlands: Dordrecht, **2004**; Vol. 140, pp 101–112. https://doi.org/10.1007/978-1-4020-2102-2_7.

(147) Dziubek, K.; Katrusiak, A. Structural Refinements on Restricted Intensity Data Collected in High-Pressure Diffraction Experiments. *Defect Diffus. Forum* **2002**, *208–209*, 319–0. https://doi.org/10.4028/www.scientific.net/DDF.208-209.319.

(148) Katrusiak, A. Absorption Correction for Crystal-Environment Attachments from Direction Cosines. *Zeitschrift für Krist. - Cryst. Mater.* **2001**, *216* (12), 646–647. https://doi.org/10.1524/zkri.216.12.646.22488.

(149) Rigaku Corporation. CrysAlis(Pro) Software System, Version 1.171.37.31. *Technol. UK Ltd, Yarnton, Oxford, UK* **2014**, *44* (0).

(150) Sheldrick, G. M. Crystal Structure Refinement with SHELXL. *Acta Crystallogr. Sect. C Struct. Chem.* **2015**, *71* (1), 3–8. https://doi.org/10.1107/S2053229614024218.

(151) Dolomanov, O. V.; Bourhis, L. J.; Gildea, R. J.; Howard, J. A. K.; Puschmann, H. OLEX2: A Complete Structure Solution, Refinement and Analysis Program. *J. Appl. Crystallogr.* **2009**, *42* (2), 339–341. https://doi.org/10.1107/S0021889808042726.

(152) Flego, C.; Zannoni, C. Direct Insertion Probe-Mass Spectrometry (DIP-MS) Maps and Multivariate Analysis in the Characterization of Crude Oils. *Energy and Fuels* **2013**, *27* (1), 46–55. https://doi.org/10.1021/ef301124s.

(153) Frisch, M. J., Trucks, G. W., Schlegel, H. B., Scuseria, G. E., Robb, M. A., Cheeseman, J. R., Scalmani, G., Barone, V., Petersson, G. A. Gaussian 16, Rev. C.01. *Gaussian, Inc.* 2016.

(154) Grochala, W.; Hoffmann, R.; Feng, J.; Ashcroft, N. W. The Chemical Imagination at Work in Very Tight Places. *Angew. Chemie - Int. Ed.* **2007**, *46* (20), 3620–3642. https://doi.org/10.1002/anie.200602485.

(155) Prewitt, C. T.; Downs, R. T. High-Pressure Crystal Chemistry. *Ultrah. Press. Mineral. Phys. Chem. Earth's Deep Inter.* **2019**, 283–318.

(156) Grochala, W.; Hoffmann, R.; Feng, J.; Ashcroft, N. W. The Chemical Imagination at Work in Very Tight Places. *Angew. Chemie - Int. Ed.* **2007**, *46* (20), 3620–3642. https://doi.org/10.1002/anie.200602485.

(157) Groom, C. R.; Bruno, I. J.; Lightfoot, M. P.; Ward, S. C. The Cambridge Structural Database. *Acta Crystallogr. Sect. B Struct. Sci. Cryst. Eng. Mater.* **2016**, *72* (2), 171–179. https://doi.org/10.1107/S2052520616003954.

(158) Hazen, R. M.; Finger, L. W. Comparative Crystal Chemistry: Temperature, Pressure, Composition and the Variation of Crystal Structure. *Comp. Cryst. Chem. Temp. Press. Compos. Var. Cryst. Struct.* **1982**.

(159) Jensen, W. B. The Origin of the Ionic-Radius Ratio Rules. *J. Chem. Educ.* **2010**, *87* (6), 587–588. https://doi.org/10.1021/ed100258f.

(160) Klotz, S.; Chervin, J. C.; Munsch, P.; Le Marchand, G. Hydrostatic Limits of 11 Pressure Transmitting Media. *J. Phys. D. Appl. Phys.* **2009**, *42* (7). https://doi.org/10.1088/0022-3727/42/7/075413.

(161) Osakabe, T.; Kakurai, K. Feasibility Tests on Pressure-Transmitting Media for Single-Crystal Magnetic Neutron Diffraction under High Pressure. *Japanese J. Appl. Physics, Part 1 Regul. Pap. Short Notes Rev. Pap.* **2008**, *47* (8 PART 1), 6544–6547. https://doi.org/10.1143/JJAP.47.6544.

(162) Angel, R. J.; Bujak, M.; Zhao, J.; Gatta, G. D.; Jacobsen, S. D. Effective Hydrostatic Limits of Pressure Media for High-Pressure Crystallographic Studies. *J. Appl. Crystallogr.* **2007**, *40* (1), 26–32. https://doi.org/10.1107/S0021889806045523.

(163) Sobczak, S.; Katrusiak, A. Zone-Collapse Amorphization Mimicking the Negative Compressibility of a Porous Compound. *Cryst. Growth Des.* **2018**, *18* (2), 1082–1089.

https://doi.org/10.1021/acs.cgd.7b01535.

(164) Hagen, K. S.; Naik, S. G.; Boi, H. H.; Masello, A.; Christou, G. Intensely Colored Mixed-Valence Iron(II) Iron(III) Formate Analogue of Prussian Blue Exhibits Néel N-Type Ferrimagnetism. *J. Am. Chem. Soc.* **2009**, *131* (22), 7516–7517. https://doi.org/10.1021/ja901093b.

(165) Patyk-Kaźmierczak, E.; Warren, M. R.; Allan, D. R.; Katrusiak, A. Pressure Inverse Solubility and Polymorphism of an Edible γ-Cyclodextrin-Based Metal-Organic Framework. *Phys. Chem. Chem. Phys.* **2017**, *19* (13), 9086–9091. https://doi.org/10.1039/c7cp00593h.

(166) Tian, Y.-Q.; Zhao, Y.-M.; Xu, H.-J.; Chi, C.-Y. CO_2 Template Synthesis of Metal Formates with a ReO_3 Net. *Inorg. Chem.* **2007**, *46* (5), 1612–1616. https://doi.org/10.1021/ic0617240.

(167) Spek, A. L. PLATON SQUEEZE: A Tool for the Calculation of the Disordered Solvent Contribution to the Calculated Structure Factors. *Acta Crystallogr. Sect. C Struct. Chem.* **2015**, *71*, 9–18. https://doi.org/10.1107/S2053229614024929.

(168) Ke, W.; Spanopoulos, I.; Stoumpos, C. C.; Kanatzidis, M. G. Myths and Reality of HPbI3 in Halide Perovskite Solar Cells. *Nat. Commun.* **2018**, *9* (1). https://doi.org/10.1038/s41467-018-07204-y.

(169) Wang, F.; Yu, H.; Xu, H.; Zhao, N. HPbI3: A New Precursor Compound for Highly Efficient Solution-Processed Perovskite Solar Cells. *Adv. Funct. Mater.* **2015**, *25* (7), 1120–1126. https://doi.org/https://doi.org/10.1002/adfm.201404007.

(170) Sato, T.; Takagi, S.; Deledda, S.; Hauback, B. C.; Orimo, S. Extending the Applicability of the Goldschmidt Tolerance Factor to Arbitrary Ionic Compounds. *Sci. Rep.* **2016**, *6* (1), 23592. https://doi.org/10.1038/srep23592.

(171) Bradley, A. J.; Jay, A. H.; So, M. The Lattice Spacings of Iron- Aluminium Alloys. *The Journal of the Iron and Steel Institute*. 1932, pp 339–357.

(172) Burger, S.; Ehrenreich, M. G.; Kieslich, G. Tolerance Factors of Hybrid Organic-Inorganic Perovskites: Recent Improvements and Current State of Research. *J. Mater. Chem. A* **2018**, *6* (44), 21785–21793. https://doi.org/10.1039/C8TA05794J.

(173) Goldschmidt, V. M. Die Gesetze Der Krystallochemie. *Naturwissenschaften* **1926**, *14* (21), 477–485. https://doi.org/10.1007/BF01507527.

(174) Marcus, Y. Volumes of Aqueous Hydrogen and Hydroxide Ions at 0 to 200 °C. *J. Chem. Phys.* **2012**, *137* (15), 154501. https://doi.org/10.1063/1.4758071.

(175) Daub, M.; Hillebrecht, H. On the Demystification of "HPbI3" and the Peculiarities of the Non-Innocent Solvents H2O and DMF. *Zeitschrift für Anorg. und Allg. Chemie* **2018**, *644* (22), 1393–1400. https://doi.org/https://doi.org/10.1002/zaac.201800267.

(176) Bedlivy, D.; Mereiter, K. The Structures of Potassium Lead Triiodide Dihydrate and Ammonium Lead Triiodide Dihydrate. *Acta Crystallogr. Sect. B Struct. Crystallogr. Cryst. Chem.* **1980**, *36* (4), 782–785. https://doi.org/10.1107/S0567740880004529.

(177) MØLLER, C. K. Crystal Structure and Photoconductivity of Cæsium Plumbohalides. *Nature* **1958**, *182* (4647), 1436–1436. https://doi.org/10.1038/1821436a0.

(178) Trots, D. M.; Myagkota, S. V. High-Temperature Structural Evolution of Caesium and Rubidium Triiodoplumbates. *J. Phys. Chem. Solids* **2008**, *69* (10), 2520–2526. https://doi.org/10.1016/j.jpcs.2008.05.007.

(179) Black, S. P.; Sanders, J. K. M.; Stefankiewicz, A. R. Disulfide Exchange: Exposing Supramolecular Reactivity through Dynamic Covalent Chemistry. *Chem. Soc. Rev.* **2014**, *43* (6), 1861–1872. https://doi.org/10.1039/c3cs60326a.

(180) Belenguer, A. M.; Friščić, T.; Day, G. M.; Sanders, J. K. M. M. Solid-State Dynamic Combinatorial Chemistry: Reversibility and Thermodynamic Product Selection in Covalent Mechanosynthesis. *Chem. Sci.* **2011**, *2* (4), 696. https://doi.org/10.1039/c0sc00533a.

(181) Fritze, U. F.; von Delius, M. Dynamic Disulfide Metathesis Induced by Ultrasound. *Chem. Commun.* **2016**, *52* (38), 6363–6366. https://doi.org/10.1039/C6CC02034H.

(182) Nevejans, S.; Ballard, N.; Miranda, J. I.; Reck, B.; Asua, J. M. The Underlying Mechanisms for Self-Healing of Poly(Disulfide)S. *Phys. Chem. Chem. Phys.* **2016**, *18* (39), 27577–27583. https://doi.org/10.1039/c6cp04028d.

(183) Dopieralski, P.; Ribas-Arino, J.; Anjukandi, P.; Krupicka, M.; Kiss, J.; Marx, D. The Janus-Faced Role of External Forces in Mechanochemical Disulfide Bond Cleavage. *Nat. Chem.* **2013**, *5* (8), 685–691. https://doi.org/10.1038/nchem.1676.

(184) Dopieralski, P.; Ribas-Arino, J.; Anjukandi, P.; Krupicka, M.; Marx, D. Unexpected Mechanochemical Complexity in the Mechanistic Scenarios of Disulfide Bond Reduction in Alkaline Solution. *Nat. Chem.* **2017**, *9* (2), 164–170. https://doi.org/10.1038/NCHEM.2632.

(185) De La Guardia, M.; Armenta, S. *Green Analytical Chemistry: Theory and Practice*; Elsevier, 2010.

Appendix A: Streszczenie

W serii siedmiu publikacji pokazałem, w jaki sposób wysokie ciśnienie można wykorzystać do indukowania i akcelerowania reakcji chemicznych, prowadzących do powstania nowych materiałów. Opisane przykłady ilustrują, iż ciśnienie może z powodzeniem zostać zastosowane do przeprowadzania reakcji w układach organicznych, nieorganicznych, a także w hybrydowych układach organiczno-nieorganicznych. Co więcej, moje badania pokazują, iż reakcje prowadzone w warunkach wysokiego ciśnienia mogą być efektywne do tego stopnia, że niewymagany jest w nich katalizator. Dzięki zastosowaniu wielu metod analitycznych określiłem mechanizmy reakcji przebiegających w ciele stałym oraz w fazie ciekłej, co pozwoliło na szczegółowe i dogłębne zrozumienie obserwowanych procesów. Poniżej podsumowałem niektóre z najważniejszych wyników opisanych w ramach mojej rozprawy doktorskiej.

Zmiany w strukturze związków oraz powiązane z nimi reakcje chemiczne w kompleksach koordynacyjnych metali o zamkniętej powłoce walencyjnej dążą do wzrostu liczby koordynacyjnej jonu metalu centralnego. Opierając się o regułę Goldschmidta i Paulinga możliwe staje się zatem zaprojektowanie materiału zdolnego do takich przemian, co zostało opisane w artykule **R1**. Wykazałem, że zmieniający się wraz ze wzrostem ciśnienia stosunek promieni kationów metali i ligandów, przy odpowiednim rozmieszczeniu ligandów wokół atomu centralnego oraz kationie metalu, który ma możliwość zwiększenia swojej liczby koordynacyjnej, z dużym prawdopodobieństwem doprowadzi do reakcji asocjacji dodatkowego liganda.

Natomiast w materiałach w których obecne są centra metaliczne o otwartej powłoce walencyjnej, wraz z ligandami zdolnymi do pośredniczenia w transporcie elektronów, wzrost ciśnienia może doprowadzić do znacznie bardziej skomplikowanych przekształceń, będących tematem artykułu **R2**. W zależności od ciekłego środowiska w którym analog błękitu pruskiego α-$DmaFe^{2+}Fe^{3+}For_6$ zostaje poddany działaniu wysokiego cisnienia, mogą zostać wywołane trzy odmienne procesy prowadzące do:

odwracalnego przejścia fazowego (między fazami α i γ), odwracalnej redukcji wszystkich jonów Fe^{3+}, a także do nieodwracalnej reakcji redoks, związanej z redukcją ligandów mrówczanowych.

Podobną wrażliwość na warunki środowiskowe opisałem dla układu PbI_2 rozpuszczonego w stężonym kwasie HI poddanemu wpływowi wysokiego ciśnienia i temperatury. Opisane w artykule **R3** przemiany wskazują, iż zależnie od kwasowości układu, zawartości jodu i wody, a także od panującego ciśnienia i temperatury, możliwe jest otrzymanie szeregu ściśle powiązanych strukturalnie polimorfów α-PbI_2 i β-PbI_2 oraz ich soli hydroniowych.

W reakcjach wymiany dwusiarczków arylowych z powodzeniem zastosowałem nowatorskie podejście, w którym zamiast czynników katalityczno-redukujących wykorzystany został efekt wysokiego ciśnienia. Badania wstępne zamieszczone w artykule **R4**, zostały następnie rozwinięte i szczegółowo opisane w artykule **R5.** Prace te, pozwoliły poznać mechanizm indukowanej wysokim ciśnieniem reakcji wymiany między dwusiarczkami arylowymi. W ramach prac wykazałem niewątpliwe korzyści z prowadzenia badań naukowych przy zastosowaniu komory diamentowej jako reaktora wysokociśnieniowego, w porównaniu z prasą tłok-cylinder, tradycyjnie wykorzystywaną do prowadzenia reakcji w warunkach wysokiego ciśnienienia.

W pracy **R6** połączyłem zmiany strukturalne zachodzące w dwusiarczkach arylowych poddanych działaniu wysokiego ciśnienienia, z ich aplikacyjnym wykorzystaniem jako składników zmniejszających tarcie w smarach i olejach. Na przykładzie disiarczku di-*p*-tolylu wykazałem, że cząsteczki te mogą absorbować energię około 6 $kJmol^{-1}$, poprzez konformacyjną konwersję w środowisku sprężonej cieczy.

Na przykładzie polimorfów β i γ disiarczku bis-3-nitrofenylu opisanych w artykule **R7**, wyjaśniłem w jaki sposób warunki wysokiego ciśnienia można skutecznie wykorzystać do tworzenia polimorfów kinetycznych. Polimorfy te posiadają niższą gęstość niż te otrzymane w warunkach niskiego ciśnienia. Początkowo, zdawało się to przeczyć podstawom termodynamiki, ale w efekcie pozwoliło na opisanie nukleacji wysokoentropowej i następującej krystalizacji kinetycznej. Co więcej, powiązanie

obserwacji związanych z procesem nukleacji w warunkach wysokiego ciśnienia i wysokiej temperatury, z dwoma formami polimorficznych produktów otrzymanych w artykule **R4**, pozwoliło wyjaśnić jak w procesie wysokociśnieniowego zarodkowania krystalitów równowaga reakcji przesuwa się na stronę produktów.

Reakcje przebiegające z zastosowaniem wysokiego ciśnienia, choć są niezwykle interesujące i wykazują spory potencjał, nadal pozostają w dużej części niezbadanym obszarem wymagającym wielu dalszych badań. Jednakże, przedstawione w tej rozprawie przykłady różnych układów reakcyjnych udowadniają, że zastosowanie wysokiego ciśnienia pozwala przezwyciężyć niektóre z najczęstszych problemów tradycyjnych metod syntezy, takich jak powstawanie produktów ubocznych i szkodliwych oparów, zużywanie znacznych ilości energii i rozpuszczalników, czy stosowania katalizatorów, których usunięcie z produktów często przewyższa koszty samej reakcji. Ponadto, dodatkowymi zaletami płynącymi ze stosowania tej metody są wysoka wydajność oraz możliwość otrzymania monokrystalicznych form produktów, które nie wymagają dodatkowego oczyszczania.

Appendix B: Scientific articles

(R1) Półrolniczak, A.; Sobczak, S.; Katrusiak, A. Solid-State Associative Reactions and the Coordination Compression Mechanism. *Inorg. Chem.* **2018**, 57 (15), 8942–8950

Inorganic Chemistry
Cite This: Inorg. Chem. 2018, 57, 8942−8950
Article
pubs.acs.org/IC

Solid-State Associative Reactions and the Coordination Compression Mechanism

Aleksandra Półrolniczak,[†] Szymon Sobczak,[†] and Andrzej Katrusiak*

Department of Materials Chemistry, Faculty of Chemistry, Adam Mickiewicz University, Umultowska 89b, 61-614 Poznan, Poland

Supporting Information

ABSTRACT: Coordination polymers and metal−organic frameworks can be modified by high pressure, according to its effects on the radii of central and ligand atoms. The pressure reduces the ligands' radii, and the coordination number is usually increased. Such transformations of the coordination quite generally conform to the inverse rule of pressure and temperature effects, although the temperature-induced transformations are much less frequently observed. The two-dimensional coordination polymer $Cd(APP)_2NO_3{\cdot}NO_3$ [APP = 1,4-bis(3-aminopropyl)-piperazine] undergoes a pressure-induced isostructural phase transition triggered by a topochemical reaction, yielding $Cd(APP)_2(NO_3)_2$. The transition retains the symmetry of both phases, and their structures have been determined by X-ray diffraction for the single crystals compressed in a diamond-anvil cell. The reaction increases the Cd coordination, from 6-fold in phase I to 7-fold in phase II, where the new Cd−O bond involves an additional nitrate anion in the Cd coordination sphere.

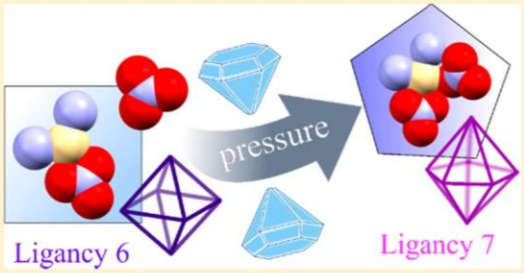

INTRODUCTION

High pressure has become an established highly efficient tool for inducing strong structural transformations in various types of chemical compounds.[1−3] In their structures, the parameters most susceptible to pressure are intermolecular contacts and soft conformational rotations. Unsaturated compounds exposed to the pressure exceeding 10 GPa often polymerize randomly and yield amorphous phases, difficult for structural characterization.[4−13] Therefore, invaluable are pressure-induced reactions retaining the crystalline products,[14−24] suitable for determining the atomic positions by X-ray diffraction at subsequent stages of the reaction. Such transformations of a coordination polymer (CP)[25−27] can also fine-tune its properties and induce new functionalities, leading to their practical applications.

It was shown recently that the postsynthetic modification (PSM) of porous coordination polymers (PCPs)[28] is an efficient way for obtaining new modified materials. To date, the PSM was performed in several ways, but the categories of pressure-enforced and mechanochemical modifications belong to the most efficient methods. Two types of pressure-induced PSMs can be distinguished: ligand-exchange and bond-rearrangement reactions. This transformation often involves the breaking[29−32] and formation[19,20,22−24,29,33,34] of new bonds with metallic centers. Such nonoxidative and oxidative reactions usually change the coordination number, and in some cases, coordination complexes polymerize into CPs.[14,15,17] However, no systematic analysis generalizing these pressure effects has been performed.

Presently, we report a pressure-controlled reaction of a CP, where NO_3 anions "detached" in the voids at 0.1 MPa, above 0.4 GPa forms a coordination bond to the Cd cation. As a result, the coordination number of this CP is increased. To our knowledge, this is the first pressure-induced topochemical reaction of a CP, where the metal cation becomes coordinated by an NO_3^- anion unbonded in nearby voids at ambient conditions. This unprecedented pressure-catalyzed associative reaction has been rationalized by the compression of ionic radii of ligands coordinating Cd^{2+} and those in its vicinity.

RESULTS AND DISCUSSION

At 0.4 GPa, complex $Cd(APP)_2NO_3{\cdot}NO_3$ [APP = 1,4-bis(3-aminopropyl)piperazine] undergoes an associative reaction, leading to the product $Cd(APP)_2(NO_3)_2$, as shown in Scheme 1. In this reaction, a new coordination bond is formed and the coordination number increases from 6 to 7. This reaction proceeds around the central cation, while the strain in its more distant crystalline environment is absorbed by flexible APP linkers and their displacements. Therefore, this reaction can be classified as a solid-state phase transition, as described below.

Crystal Strain. At ambient conditions, the crystal of hydrated $Cd(APP)_2NO_3{\cdot}NO_3$ is built of polymeric sheets extending along the crystal plane $(10\bar{2})$, separated by water molecules (Figures 1 and S1). In this two-dimensional polymer, cation Cd^{2+} is 6-fold-coordinated by four amine N atoms of four APP molecules and two O atoms of one nitrate group. The voids between the APP struts accommodate another NO_3^- anion and two water molecules per formula unit. The structure and properties of the $Cd(APP)_2NO_3{\cdot}NO_3$

Received: April 4, 2018
Published: July 6, 2018

DOI: 10.1021/acs.inorgchem.8b00913
Inorg. Chem. 2018, 57, 8942−8950

Scheme 1. Solid–Solid Reaction of $Cd(APP)_2NO_3{\cdot}NO_3$ at 0.4 GPa, Leading to 7-Fold-Coordinated Cd^{2+} in $Cd(APP)_2(NO_3)_2$

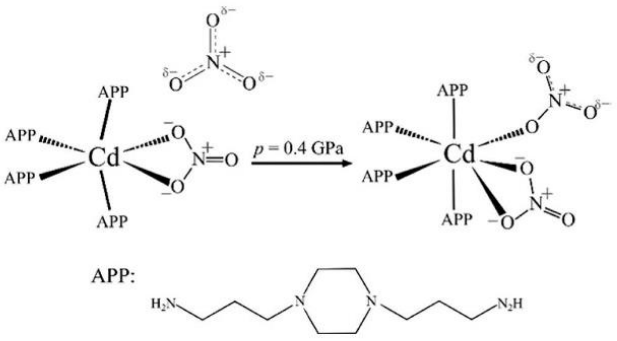

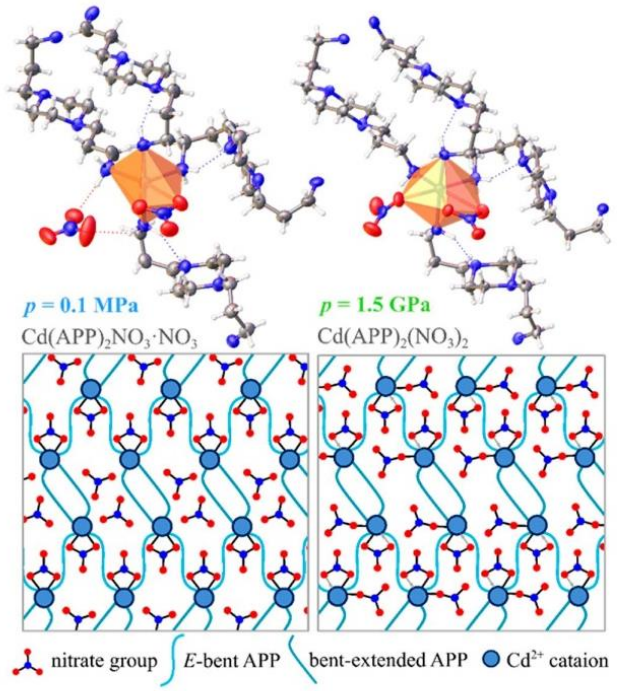

Figure 1. (Left) Cation Cd^{2+} 6-fold-coordinated by four APP molecules and one bidentate nitrate anion in $Cd(APP)_2NO_3{\cdot}NO_3$. (Right) 7-Fold coordination in $Cd(APP)_2(NO_3)_2$ after the reaction. Schemes of the corresponding polymeric layers are shown in the bottom; note two APP conformers. *E*-bent and bent-extended, discriminated in the legend (cf. Figure S3).

crystal strongly depend on the conformation of amine APP struts. The shapes of two independent APP linkers are very similar in their central parts. This central part consists of a piperazine ring, which is relatively rigid in the chair conformation. However, the flexible N-substituted equatorial 3-aminopropyl chains can be considerably bent or extended.

The typical structural effects of compression, i.e., shortened intermolecular contacts, reduced voids, and distorted soft conformational parameters, proceed monotonically in $Cd(APP)_2NO_3{\cdot}NO_3{\cdot}2H_2O$ at 0.2 GPa. At 0.4 GPa, a strong discontinuous anomaly in the crystal compression (Figure 2) marks a first-order transition from the low-pressure phase I to the high-pressure phase II.

At this transition, the unit-cell parameter *a* lengthens by ca. 4%, the parameter *b* shrinks by ca. 6%, and the crystal volume is reduced by 4%, while the space-group symmetry $P2_1/c$ remains preserved, consistent with the isostructural type of phase transition. The strong strain caused by the transition in the crystal sample resulted in its fragmentation into the coexisting portions of the $Cd(APP)_2NO_3{\cdot}NO_3$ and $Cd(APP)_2(NO_3)_2$ phases. Their superimposed diffraction patterns in the recorded images were manifested as split reflections (see the insets in Figure 2). The split reflections occurred because of the strong strain between phases I and II, although their space-group symmetry remained unchanged. Because of the hysteresis of the transformation, both phases I and II (Table 1) coexisted at 0.4 GPa, and the unit-cell dimensions and structural model obtained at this pressure point are the averages of both contributing compounds $Cd(APP)_2NO_3{\cdot}NO_3$ and $Cd(APP)_2(NO_3)_2$, but not an intermediate stage of the reaction. In some of our experiments, particularly on small crystals, they became fully monocrystalline again after the phase transition above 0.5 GPa. Similar single-crystal-to-single-crystal isostructural transitions were previously observed also for other compounds.[35,36] However, some larger samples of $Cd(APP)_2NO_3{\cdot}NO_3$ above the transition broke into several smaller pieces of phase II, albeit with a very strong preferential orientation maintained during the compression, which allowed structural studies using the single-crystal diffraction technique. We have also observed visually that new elongated very thin crystals grew on the surface of the sample in phase II (cf. the Experimental Section); however, their diffraction could not be detected in the recorded images.

High-Pressure Association. At ambient pressure, the Cd-coordinated octahedron is distorted, mainly because of one bidentate nitrate ligand $N1O_3$ (Figure 1). Consequently, the corresponding edge O1–O2 of the octahedron is significantly shorter, of 2.159 Å, than others, between 3.238 Å (O3–N8) and 4.103 Å (N1–O1). The nitrate ligand can be either symmetrically bidentate, asymmetrically bidentate, or unidentate.[37,38] Cd cations display a strong preference for the symmetric bidentate coordination by the nitrate ligands, which is manifested in the exceptionally high stability of such complexes.[39]

In this context, the associative reaction induced by pressure in $Cd(APP)_2NO_3{\cdot}NO_3$ is quite surprising (Figures 3 and S3). When hydrostatic pressure reaches 0.4 GPa, the structure collapses because the associative reaction increases the 6-fold Cd^{2+} coordination in phase I to the 7-fold coordination in phase II (Scheme 1). The new Cd–O4 bond is formed when nitrate $N2O_3^-$ is pushed closer to Cd^{2+}. Thus, at the transition point, the compressibility increases,[40] and the crystal abruptly transforms into the more dense phase II.

The activation process of this association reaction requires that the associating group ($N2O_3^-$) be located near the metallic center. At ambient pressure, the anion $N2O_3^-$ lies in the vicinity of the octahedrally coordinated Cd^+ cation. With increased pressure, the Cd···O4 distance reduces from 3.884 Å at 0.1 MPa to 3.849 Å at 0.25 GPa (Figure 3a). At 0.4 GPa, this distance abruptly shortens to about 2.70 Å in phase II, which clearly marks the formation of the new coordination bond, Cd–O4. This associative reaction is accompanied by a lengthening of the bond Cd–O2, from 2.639 to 2.855 Å, and a somewhat smaller lengthening of Cd–O1, from 2.504 to 2.612 Å. Of all four Cd–N coordination bonds, only one, Cd–N1,

DOI: 10.1021/acs.inorgchem.8b00913
Inorg. Chem. 2018, 57, 8942–8950

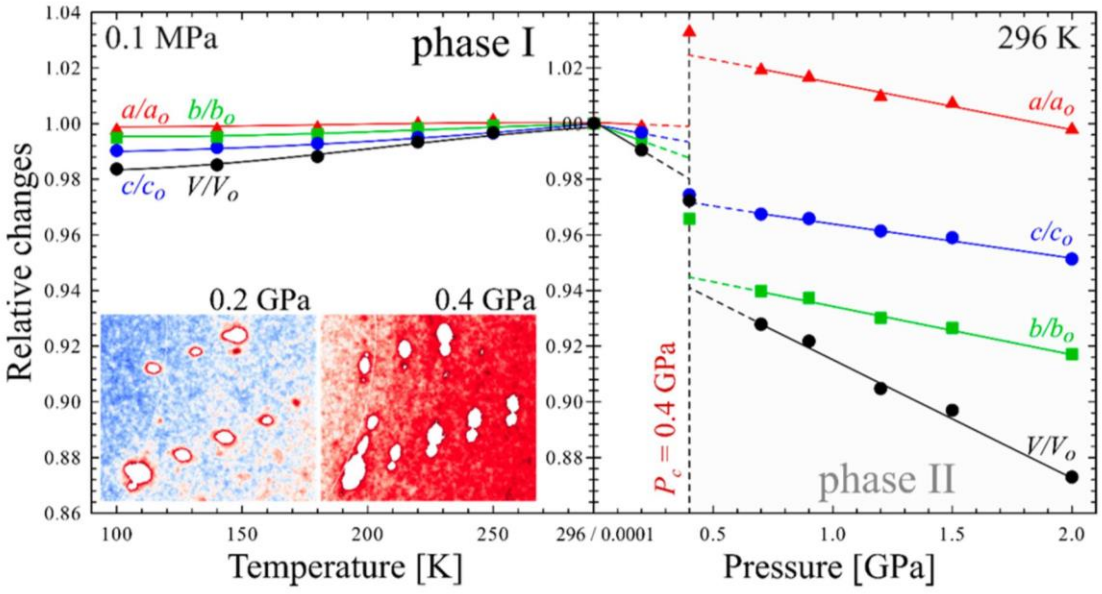

Figure 2. Relative changes of the unit-cell dimensions of crystal $Cd(APP)_2NO_3{\cdot}NO_3$: (left) cooled at 0.1 MPa; (right) compressed in isopropyl alcohol at 296 K. The vertical dashed line marks the reaction pressure. The insets illustrate the splitting of reflections in X-ray diffraction images due to the coexistence of phases I and II at 0.4 GPa (cf. Figure S2). The expansion and compression strains are graphically represented in Figures S9–S11.

Table 1. Selected Crystallographic Data of Dihydrates $Cd(APP)_2NO_3{\cdot}NO_3$ and $Cd(APP)_2(NO_3)_2$[a]

	phase I			phase I/II	phase II				
	0.0001 GPa	0.0001 GPa	0.20(3) GPa	0.40(3) GPa	0.70(3) GPa	0.90(3) GPa	1.20(3) GPa	1.50(3) GPa	2.00(3) GPa
temperature (K)	100	298	298	298	298	298	298	298	298
space group	$P2_1/c$	$P2_1/c$	$P2_1/c$	$P2_1/c$	$P2_1/c$	$P2_1/c$	$P2_1/c$	$P2_1/c$	$P2_1/c$
unit-cell parameters									
a (Å)	18.4776(15)	18.5224(1)	18.500(9)	19.130(2)	18.8771(14)	18.8295(6)	18.7012(11)	18.6563(9)	18.4820(11)
b (Å)	12.3500(10)	12.4128(9)	12.3460(9)	11.987(4)	11.6650(17)	11.6345(9)	11.5450(15)	11.5005(12)	11.3833(12)
c (Å)	13.3403(11)	13.4718(8)	13.4265(2)	13.126(6)	13.032(3)	13.0109(15)	12.951(3)	12.919(2)	12.815(3)
β (deg)	95.072(9)	95.580(6)	95.356(11)	95.263(19)	94.664(11)	94.543(5)	94.148(10)	94.078(7)	93.572(10)
volume (Å^3)	3032.3(4)	3082.7(4)	3053.3(16)	2997.1(17)	2860.2(9)	2841.4(4)	2788.8(7)	2764.8(6)	2690.8(7)
Z/Z'	4/1	4/1	4/1	4/1	4/1	4/1	4/1	4/1	4/1
D_x (g cm^{-3})	1.474	1.450	1.464	1.492	1.563	1.574	1.603	1.617	1.662

[a] D_x is calculated for the empirical formula $C_{20}H_{52}CdN_{10}O_8$ (M_r = 673.11), excluding the guest molecules (cf. Tables S4 and S5).

lengthens by ca. 0.1 Å. All coordination bonds hardly change in length at 0.20 GPa in phase I.

Our survey in the Cambridge Structural Database (Nov 2017 release)[41] shows that the distributions of the Cd–O/N distances in 6- and 7-fold-coordinated complexes with N and O donors are similar. In these complexes, the average Cd–N/O bond length is 2.4 Å and the longest bonds are 2.8–2.9 Å (Figure S8). According to these data, the associative reaction at 0.4 GPa increases the coordination number from 6 to 7. The changes of the APP conformations from 0.1 MPa to 2 GPa and of the lengths of the Cd–N and Cd–O bonds within phases I and II are very small (Figure S2 in SI), which testifies that the associative reaction is the main driving force of the transformation at 0.4 GPa.

The work contribution of the crystal compression $\int p\,dV$ to 0.4 GPa, when the reaction is triggered, is 1.9 kJ mol^{-1} (Figure 2), and the work performed at 0.4 GPa $p\Delta V$ is 7.4 kJ mol^{-1}. The summed energy of 9.3 kJ mol^{-1} is about 20 times smaller than the energy of Cd^{2+}–N/O bonds;[42] however, it does not include the entropy and chemical potential contributions or the significant energy changes of elongated Cd–N/O bonds.[43]

Compressed-Coordination Effects. The changes in coordination in compressed $Cd(APP)_2NO_3{\cdot}NO_3$ can be connected with a significant distortion of the CdN_4O_2 octahedron. Because of the bidentate bonds of nitrate $N1O_3$, the coordination octahedron O1···O2 edge is significantly shorter than the other edges N···N and N···O involving monodentate APP ligands (Figure 3). This significantly distorts the Cd-coordination sphere and opens a gap between O1 and N1: angle O1–Cd–N1 is close to 120° at ambient conditions, compared to O1–Cd–O2 of less than 50°(cf. Figure S5). At 0.4 GPa, atom O4 of nitrate $N2O_3$ is pushed into the gap between O1 and N1. This pressure-induced reaction can be rationalized in terms of the reduced radii of ligand atoms. Goldschmidt and Pauling's radius–ratio rule connects the coordination number with the radii of the ligands tightly arranged around the cation. It can be expected than the anionic and atomic radii are more affected by the pressure than the small cation at the center. In principle, the valence electrons in anions interact weaker with the nucleus, and they easier adjust to their environment than the outer electrons in the cations. This reasoning is consistent with our present result

DOI: 10.1021/acs.inorgchem.8b00913
Inorg. Chem. 2018, 57, 8942–8950

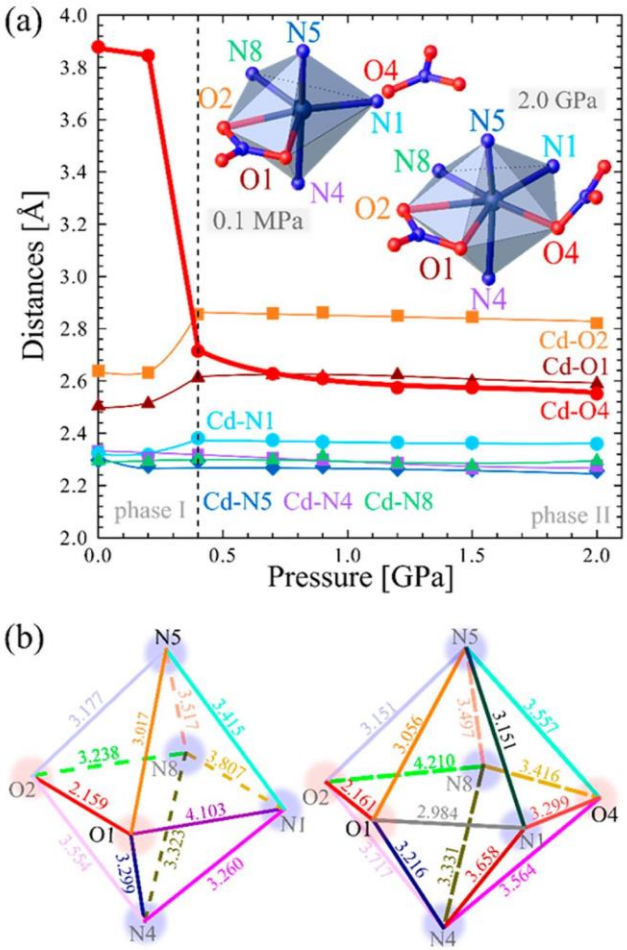

Figure 3. (a) Distances Cd−ligand. The insets show the coordination polyhedra in phases I (0.2 GPa) and II (2.0 GPa). The lines are for guiding the eye only. (b) Idealized coordination polyhedra and lengths of their edges in phases I (0.2 GPa) and II (0.75 GPa) (cf. their pressure dependences plotted in Figures S4−S7).

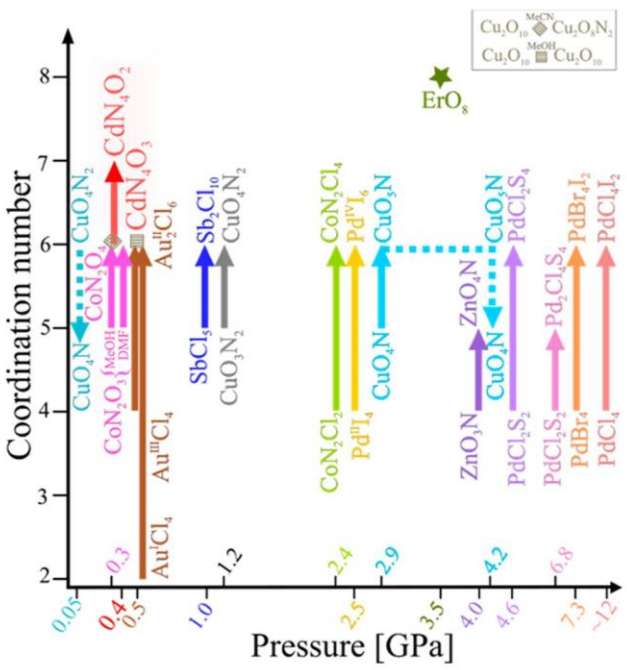

Figure 4. Coordination-number changes in CPs, MOFs, and complexes from the low-to-high-pressure structures indicated by arrows (see the text). The asterisk marks a rearrangement without the coordination-number change, and the dotted lines indicate that the coordination number decreases when the pressure increases.

that high pressure increases the coordination number in $Cd(APP)_2NO_3{\cdot}NO_3$. The compressed anionic radii result in increased R_{Ligand}/R_{Cation} ratios, consistent with the radius−ratio rule, and the number of ligands increases. Also, this reaction affects the electronic configuration of the cation, which is the response for its decreasing repulsion with ligands (Figure 3).[12,44−46]

In the literature, there is a number of structural reports on the pressure-induced changes of the coordination of metal cations. We have established that for most of these transformations the increasing pressure either increases the number of ligands or causes their exchange. The transformation of $Cd(APP)_2NO_3{\cdot}NO_3$ conforms to this rule that high pressure increases the coordination number. The literature and our results have been compiled and are illustrated in Figure 4.

For example, Cai et al.[33] showed that in $[Zn(L)_2(OH)_2]_n{\cdot}$Guest [where L is 4-(1*H*-naphtho[2,3-*d*]imidazol-1-yl)-benzoate and Guest is water or methanol (MeOH)] in pressure-induced phase II the tetrahedral coordination ZnO_3N changes to the 5-fold-coordinated ZnO_4N; Andrzejewski and Katrusiak[19] observed, along with the piezochromic phase transition in $CoCl_2bpp$, that the tetrahedral coordination $CoCl_2N_2$ increases to the octahedral coordination $CoCl_4N_2$; Lanza et al.[20] reported in $[Co_3(OH)_2btca_2]$ a transformation from 5-fold to octahedral coordination, involving a nucleophilic addition of MeOH/*N*,*N*-dimethylformamide (DMF) molecules to the Co^{2+} center; McKellar et al.[47] described a similar process that under hydrostatic pressure Cu-based metal−organic framework (MOF) STAM-1 (St. Andrews MOF-1) exchanges a water ligand at the axial metal site with MeOH and acetonitrile (MeCN); Spencer et al.[23] showed a rearrangement of bonds in the coordination sphere of $[tmenH_2][Er(HCOO)_4]_2$; Allan et al.[14] described a unique polymerization within $[PdCl_2([9]aneS_3)]$ ([9]aneS$_3$ = 1,4,7-trithiacyclononane), transforming a square-planar coordination to an octahedral coordination; Gould et al.[17] by compressing $[Cu(L\text{-}Asp)(H_2O)_2]$ (Asp = aspartate) increased the 5-fold coordination of Cu^{2+} to 6-fold coordination. Pressure-induced conversions of long contacts into primary bonds were observed also in the perovskite $CsHgCl_3$ (the octahedral coordination of Hg^+ becomes nearly ideal)[48] and in $CsGeBr_3$.[49] A pressure-induced solid-state reaction was observed in $Cs_2[PdX_4]\cdot I_2$ (X = Cl, Br, or I): the redox reaction converts $Cs_2[Pd^{2+}I_4]\cdot I_2$ to $Cs_2[Pd^{4+}I_6]$ at 2.5 GPa.[50] A closely related reaction $Au^I + Au^{III} = 2Au^{II}$ of 0.52 GPa in $CsAu^IAu^{III}Cl_6$, containing the chains of alternating square-planar $[AuCl_4]^-$ and linear $[AuCl_2]^-$ anions, transforms all of the 4-fold-coordinated Au^I to octahedrally coordinated Au^{II}.[51] Tidey et al.[52] reported for β-$[PdCl_2([9]aneS_2O)]$ the 4-to-5-fold coordination change, coupled with the dimeric complex formation. Bujak and Angel[53] postulated that above 1 GPa half of the Sb atoms in $[Me_2NHMe_2NH_3][SbCl_5]$ become 6-fold-coordinated and the other half retain their initial 5-fold coordination. Prescimone et al.[54] reported the pressure-induced elimination of one of the coordinating water molecules from half of the Cu^{2+} cations in

DOI: 10.1021/acs.inorgchem.8b00913
Inorg. Chem. 2018, 57, 8942−8950

$[Cu_2(OH)_2(H_2O)_2(tmen)_2](ClO_4)_2$ (tmen = tetramethylethylenediamine), leading to a change from 5-fold pyramidal coordination to a 6-fold distorted-octahedral coordination, where the sixth vertex is a perchlorate O atom. To our knowledge, the generally increased or rearranged coordination in compressed complexes has only two exceptions, which can be connected with competing compressed contacts, changing conformations, and other pressure-induced effects in the crystal structure (see the Supporting Information).[15,18]

It is noteworthy that MOFs and CPs are often classified as the intermediate compounds between the coordination and inorganic chemistry.[55] According to the IUPAC definition, MOFs constitute a subclass of CPs with organic ligands and voids accessible for guest molecules.[55] No such pores are present in CPs. The absence of pores in CPs is considered disadvantageous because they cannot be used as adsorbers of gases and other small-molecule compounds.[56] The associative reaction in $Cd(APP)_2NO_3{\cdot}NO_3$ at 0.4 GPa withdraws the NO_3^- anions from the voids, but they immediately collapse and no pores open up. However, it is possible that in other CPs high-pressure associative reaction can widen or open pores, which would allow the adsorption of some molecules from the environment, and then by the release of pressure, the pores would be closed and the guest molecules trapped inside. Such materials are sought for separating compounds, eliminating undesired components from air, and storing poisonous substances.[57−61]

Pressure-induced transformations are often compared to those induced by lowering of the temperature, and indeed the rule of inverse effects of temperature and pressure was formulated (abbreviated here as the "inverse p/T rule").[62] This relationship is associated with the reduction of thermal vibrations both at low temperature and under high pressure.[63] Compared to pressure-induced changes of the coordination number, there are relatively few reports on the coordination transformations resulting from temperature changes, particularly when one considers the much more frequent varied-temperature than varied-pressure studies.

All reports on temperature-induced associative reactions found by us in the literature have been scrutinized in the text below and are schematically illustrated in Figure 5. Zhang et al.[59] observed that in $[Ag_6Cl(atz)_4]OH{\cdot}6H_2O$ (atz = 3-amino-1,2,4-triazole anion) the coordination number of Ag cations is reduced from 4 to 2 above 293 K and it increases back to 4 below 103 K. Hu and Englert[64] showed that in $[ZnCl_2(bipy)]_n$ (bipy = 4,4′-bipyridine) the Zn ligancy decreases from 6 to 4 above 360 K and it increases back below 130 K. Xie et al.[65] reported that $UO_2(C_{18}H_{20}N_2O_4@CB6)_2Br_2$ [with a pseudorotaxane motif C6BPCA@CB6, where C6BPCA = 1,1′-(hexane-1,6-diyl)bis(4(carbonyl)pyridin-1-ium and CB6 = cucurbit[6]uril)] transforms between the 7-coordinated form in phase β-UP and the 6-coordinated one in phase α-UP respectively upon cooling and heating in the 170−320 K range. Zhu et al.[66] recorded a remarkable reversible association of free cations Eu^{3+} in $(H_3O^+)Eu_{0.5}[EuNa_{0.5}L(DMF)(H_2O)]\cdot(solvent)_x$ [L = 5,5′,5″-(1,3,5-triazine-2,4,6-triyltriimino)-triisophthalate hexaanion], below 193 K becoming $(H_3O^+)_2[Eu_3NaL_2(DMF)_5(H_2O)_2]\cdot(solvent)_y$ with 8-coordinated Eu^{3+}. Bernini et al.[67] changed the Yb^{3+} coordination in $[Yb(C_4H_4O_4)_{1.5}]$ between 8 and 7 by cooling it below 374 and heating it above 403 K, respectively (Figure 5).

All of the examples listed above agree with the inverse p/T rule. We have found only one exemption, the $[(Cl)Hg(m\text{-}Cl)_2(hep\text{-}H)]$ [hep-H = 2-(2-hydroxyethyl)pyridine] structure reported by Mobin et al.,[68] where the coordination number increases from 4 to 5 and the framework dimensionality increases also when heated to 383 K. The reaction reverses when the high-temperature compound $[(Cl)Hg(m\text{-}Cl)_2(hep\text{-}Cl)]$ is cooled and kept for 3 days at 298 K.

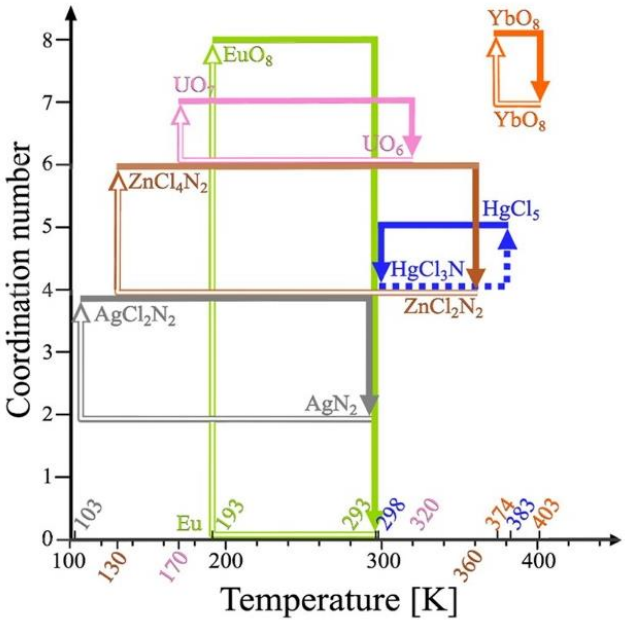

Figure 5. Coordination changes in CPs, MOFs, and complexes between the low- and high-temperature structures indicated by arrows (full and open lines refer to the heating and cooling runs; the dotted line marks the only exemption from the inverse p/T rule; cf. Figure 4).

It is apparent from Figure 5 that most of the structures (six compounds) comply with the inverse p/T rule, and at present, only one exemption supporting the direct p/T relationship is known. These systematic changes can be connected with the above-mentioned reduction of thermal vibrations. Indeed, it is known that the ionic radii are often established from the crystal structures determined at normal conditions.[69−73] Consequently, these experimentally determined radii incorporate the Debye−Waller factors,[74] which are both temperature- and pressure-dependent.

Fewer cases of temperature-induced changes in the coordination number compared to pressure-induced changes indicate that the effects of temperature are more subtle and susceptible to phase transformations, desorption, and other effects.[75,76] This conclusion is further supported by the considerable hysteresis of the transformations induced by temperature, of tens of Kelvin and even over 200 K. Therefore, the coordination changes at varied temperatures are less predictable compared to the systematic increase of the coordination number under high pressure, as described in this paper.

The changes in the magnitudes of atomic displacement parameters (ADPs) in $Cd(APP)_2NO_3{\cdot}NO_3$, plotted in Figure 6, show that, despite the stronger reduction in the ADP magnitudes at 100 K/0.1 MPa than those in phase II at 296 K/2.0 GPa, the temperature lowered at 0.1 MPa does not induce transformations of the crystal. However, the reaction is triggered by high pressure when the ADPs are hardly changed from their magnitudes at 296 K/0.1 MPa. It confirms that the

DOI: 10.1021/acs.inorgchem.8b00913
Inorg. Chem. 2018, 57, 8942−8950

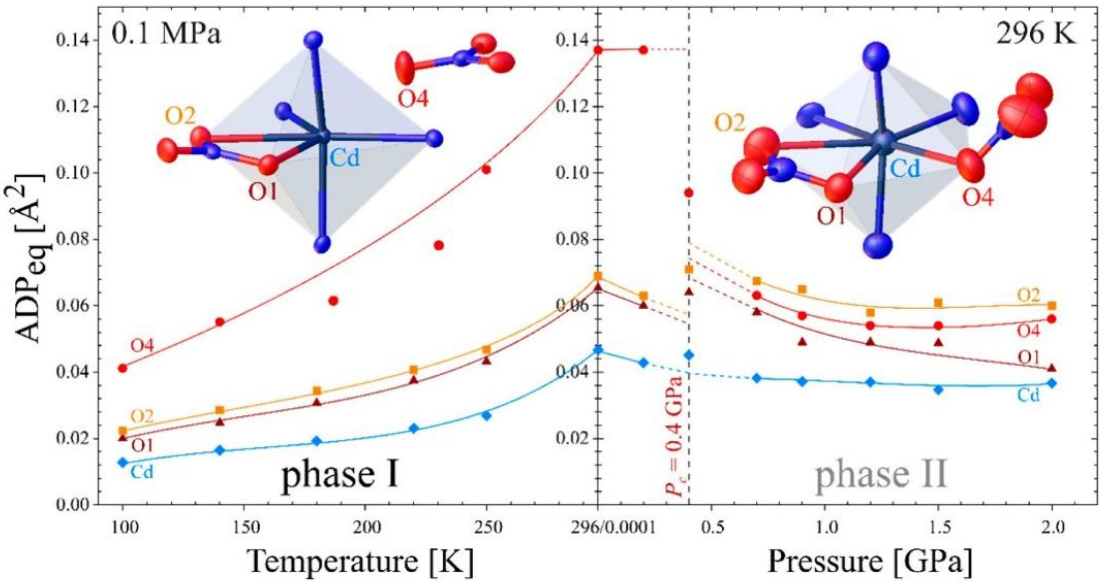

Figure 6. ADPs of atoms involved in the coordination sphere in $Cd(APP)_2NO_3{\cdot}NO_3$ plotted as a function of the temperature (left) and pressure (right). The insets show the relevant anisotropic thermal ellipsoids in the crystal, drawn at the 50% probability level.

high pressure is very efficient in inducing structural transformations and that the associated ADP changes play a minor role. It is characteristic that the considerable reduction of the ADP magnitude of the associatively bonded atom O4 is reduced after the reduction, and no pretransitional effect can be noted for this parameter.

■ CONCLUSIONS

Structural changes and chemical reactions induced by pressure in coordination complexes and polymers can be rationalized according to relatively simple rules describing (i) the effect of pressure on the radii of ligand atoms, (ii) the arrangement of ligands around the central cation, and (iii) the vicinity of other potential ligands. Rule i relies on the observation that the pressure reduces the radii of the ligand atoms and, hence, increases the R_{Cation}/R_{Ligand} ratio, which is favorable for the coordination number increase. The changes of the ligand-atom radii can originate from several effects, including the electronic structure and thermal vibrations of the atoms. Rule ii is based on the pressure effects eliminating gaps and voids around the central cation, which, in turn, favor even distributions of ligands and reduce the distortions of polyhedra in the compressed structures. Rule iii states that the reacting molecules or ions must be located in the vicinity of the cation. Most of pressure-induced reactions in coordination compounds reported so far conform to these rules (i–iii), as well as to the inverse p/T rule.

These coordination-compression rules complement the general knowledge on the microscopic changes of soft structural parameters in compressed compounds. It can be applied for employing the pressure techniques for obtaining new CPs by modifying specifically designed substrates.

■ EXPERIMENTAL SECTION

Synthesis. Single crystals of the coordination polymer $Cd(APP)_2NO_3{\cdot}NO_3$ were obtained using a diffusion method, similar to those described previously (Figure 7).[19,30,77−79] In our present study, the two layers containing the substrates, 0.075 g (1 mmol) of cadmium nitrate (Sigma-Aldrich) dissolved in 5 mL of MeCN and 0.1 mL (0.5 mmol) of 1,4-bis(3-aminopropyl)piperazine dissolved in 5 mL of xylene, were separated by the mixture of 1 mL of MeCN with 1 mL of xylene providing the diffusion environment. After 1 week, many transparent crystals appeared, a few of which were the desired product. Their block morphology was significantly distinct from other mainly needle-shaped crystals.

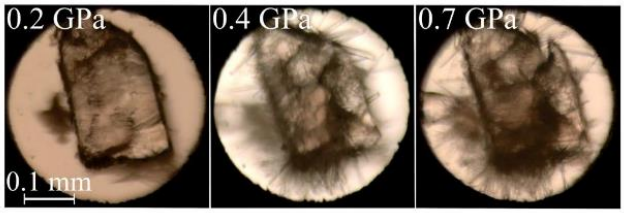

Figure 7. Single crystal of $Cd(APP)_2NO_3{\cdot}NO_3$ isothermally compressed in isopropyl alcohol in the DAC, as indicated at the top of the photographs. Several ruby chips for the pressure calibration lie by the left side of the crystal.

High-Pressure Measurements. High-pressure experiments on $Cd(APP)_2NO_3{\cdot}NO_3$ were performed in a Merrill-Bassett diamond-anvil cell (DAC),[80] modified by mounting the diamond anvils directly onto the steel supports with conical windows. The pressure in the DAC was calibrated by the ruby-fluorescence method with a photon control spectrometer, affording an accuracy of 0.03 GPa.[81,82] The gaskets were made of a 0.3-mm-thick tungsten foil with the spark-eroded holes 0.5 mm in diameter. Isopropyl alcohol was used as the hydrostatic medium. The X-ray diffraction data were measured on a KUMA4-CCD diffractometer with Mo Kα radiation (λ = 0.71073 Å). The DAC was centered by the gasket-shadow method.[83] The collected data were preliminarily reduced with the *CrysAlisPro* suite, version 171.38.46.[84] *OLEX2* was used.[85] The structure was solved by direct methods with *SHELXS* and least-squares refined with *SHELXL*.[86,87] The ambient-pressure structure was the starting model for the low-temperature and high-pressure structures below the reaction pressure. High-pressure absorption corrections were calculated by the program *REDSHABS*.[88,89] The final crystal data are summarized in Table 1 (cf. Tables S4 and S5) and have been deposited in the Cambridge Structural Database as supplementary publications CCDS 1549093, 1558178, 1558180, 1558181, 1558183, and 1830173−1830180. These deposits can be obtained free of

DOI: 10.1021/acs.inorgchem.8b00913
Inorg. Chem. 2018, 57, 8942−8950

charge from www.ccdc.cam.ac.uk and from the Crystallography Open Database (www.crystallography.net).

Low-Temperature X-ray Diffraction. The low-temperature data were measured on an Xcalibur EOS-CCD diffractometer equipped with a gas-flow Oxford Cryostream attachment, as a function of the temperature between 100 and 297 K in 40 K steps. All non-H atoms were refined with anisotropic thermal parameters. H atoms were located in the difference Fourier map and from the molecular geometry. Parameters U_{iso} of H atoms were set to 1.2 times U_{eq} of their carriers.

■ ASSOCIATED CONTENT

Supporting Information

The Supporting Information is available free of charge on the ACS Publications website at DOI: 10.1021/acs.inorgchem.8b00913.

Exceptional reduction of the coordination number under pressure, schematically presented layers in Cd(APP)$_2$NO$_3$·NO$_3$, an overlay of structures before and after reaction, full X-ray diffraction images for 0.2, 0.4, and 0.7 GPa, CCSD database analysis of Cd−O/N distances, pressure dependence of all Cd−ligand distances and angles between them, schematically illustrated idealized coordination polyhedra formed in phases I and II, thermal expansion, compressibility analysis, and detailed crystallographic data including ambient- and high-pressure measurements (DOCX)

Accession Codes

CCDC 1549093, 1558178, 1558180−1558181, 1558183, and 1830173−1830180 contain the supplementary crystallographic data for this paper. These data can be obtained free of charge via www.ccdc.cam.ac.uk/data_request/cif, or by emailing data_request@ccdc.cam.ac.uk, or by contacting The Cambridge Crystallographic Data Centre, 12 Union Road, Cambridge CB2 1EZ, UK; fax: +44 1223 336033.

■ AUTHOR INFORMATION

Corresponding Author

*E-mail: katran@amu.edu.pl. Phone: 48 61 8291590.

ORCID

Szymon Sobczak: 0000-0001-8234-2503

Andrzej Katrusiak: 0000-0002-1439-7278

Author Contributions

†These authors contributed equally.

Notes

The authors declare no competing financial interest.

■ ACKNOWLEDGMENTS

The authors are grateful to Dr. Michał Andrzejewski of Department of Chemistry and Biochemistry, University of Bern, for his advice and encouragement. This research was supported by funding from the Polish National Science Centre (OPUS 10 No. UMO-2015/19/B/ST5/00262).

■ REFERENCES

(1) Boldyreva, E.; Dera, P. *High-Pressure Crystallography: From Fundamental Phenomena to Technological Applications*; Springer Science & Business Media, 2010.

(2) Katrusiak, A.; McMillan, P. *High-Pressure Crystallography*; Springer Science & Business Media, 2004; Vol. *140*.

(3) McMillan, P. F. New Materials from High-Pressure Experiments. *Nat. Mater.* **2002**, *1*, 19−25.

(4) Wang, Y.; Wang, L.; Zheng, H.; Li, K.; Andrzejewski, M.; Hattori, T.; Sano-Furukawa, A.; Katrusiak, A.; Meng, Y.; Liao, F.; Hong, F.; Mao, H. Phase Transitions and Polymerization of C_6H_6−C_6F_6 Cocrystal under Extreme Conditions. *J. Phys. Chem. C* **2016**, *120*, 29510−29519.

(5) Blank, V. D.; Buga, S. G. B.; Dubitsky, G. A.; Serebryanaya, N. R.; Popov, M. Y.; Sundqvist, B. High-Pressure Polymerized Phases of C60. *Carbon* **1998**, *36*, 319−343.

(6) Sakashita, M.; Yamawaki, H.; Aoki, K. FT-IR Study of the Solid State Polymerization of Acetylene under Pressure. *J. Phys. Chem.* **1996**, *100* (23), 9943−9947.

(7) Eremets, M. I.; Popov, M. Y.; Trojan, I. A.; Denisov, V. N.; Boehler, R.; Hemley, R. J. Polymerization of Nitrogen in Sodium Azide. *J. Chem. Phys.* **2004**, *120*, 10618−10623.

(8) Aoki, K.; Usuba, S.; Yoshida, M.; Kakudate, Y.; Tanaka, K.; Fujiwara, S. Raman Study of the Solid-State Polymerization of Acetylene at High Pressure. *J. Chem. Phys.* **1988**, *89*, 529−534.

(9) Badding, J. V.; Parker, L. J.; Nesting, D. C. High Pressure Synthesis of Metastable Materials. *J. Solid State Chem.* **1995**, *117*, 229−235.

(10) Chelazzi, D.; Ceppatelli, M.; Santoro, M.; Bini, R.; Schettino, V. Pressure-Induced Polymerization in Solid Ethylene. *J. Phys. Chem. B* **2005**, *109*, 21658−21663.

(11) Nicol, M.; Yin, G. Organic chemistry at high pressure: can unsaturated bonds survive 10 GPa ? *J. Phys. Colloq* **1984**, *45*, C8-163−C8−172.

(12) Bastron, V. C.; Drickamer, H. G. Solid State Reactions in Organic Crystals at Very High Pressure. *J. Solid State Chem.* **1971**, *3*, 550−563.

(13) Yoo, C. S.; Nicol, M. Kinetics of a Pressure-Induced Polymerization Reaction of Cyanogen. *J. Phys. Chem.* **1986**, *90*, 6732−6736.

(14) Allan, D. R.; Blake, A. J.; Huang, D.; Prior, T. J.; Schröder, M. High Pressure Co-Ordination Chemistry of a Palladium Thioether Complex: Pressure versus Electrons. *Chem. Commun.* **2006**, *2*, 4081−4083.

(15) Moggach, S. A.; Galloway, K. W.; Lennie, A. R.; Parois, P.; Rowantree, N.; Brechin, E. K.; Warren, J. E.; Murrie, M.; Parsons, S. Polymerisation of a Cu(II) Dimer into 1D Chains Using High Pressure. *CrystEngComm* **2009**, *11*, 2601.

(16) Moggach, S. A.; Parsons, S. High Pressure Crystallography of Inorganic and Organometallic Complexes. *Spectroscopic Properties of Inorganic and Organometallic Compounds*; The Royal Society of Chemistry, 2009; Vol. *40*, pp 324−354.

(17) Gould, J. A.; Rosseinsky, M. J.; Moggach, S. A. Tuning the Coordination Chemistry of a Cu(Ii) Complex at High-Pressure. *Dalt. Trans.* **2012**, *41*, 5464.

(18) Clegg, J. K.; Brock, A. J.; Jolliffe, K. A.; Lindoy, L. F.; Parsons, S.; Tasker, P. A.; White, F. J. Reversible Pressure-Controlled Depolymerization of a Copper(II)-Containing Coordination Polymer. *Chem. - Eur. J.* **2017**, *23*, 12480−12483.

(19) Andrzejewski, M.; Katrusiak, A. Piezochromic Topology Switch in a Coordination Polymer. *J. Phys. Chem. Lett.* **2017**, *8*, 929−935.

(20) Lanza, A.; Germann, L. S.; Fisch, M.; Casati, N.; Macchi, P. Solid-State Reversible Nucleophilic Addition in a Highly Flexible MOF. *J. Am. Chem. Soc.* **2015**, *137*, 13072−13078.

(21) Li, M.; Liu, B.; Wang, B.; Wang, Z.; Gao, S.; Kurmoo, M. Erbium-Formate Frameworks Templated by Diammonium Cations: Syntheses, Structures, Structural Transition and Magnetic Properties. *Dalt. Trans.* **2011**, *40*, 6038.

(22) Spencer, E. C.; Angel, R. J.; Ross, N. L.; Hanson, B. E.; Howard, J. A. K. Pressure-Induced Cooperative Bond Rearrangement in a Zinc Imidazolate Framework: A High-Pressure Single-Crystal X-Ray Diffraction Study. *J. Am. Chem. Soc.* **2009**, *131*, 4022−4026.

(23) Spencer, E. C.; Kiran, M. S. R. N.; Li, W.; Ramamurty, U.; Ross, N. L.; Cheetham, A. K. Pressure-Induced Bond Rearrangement and Reversible Phase Transformation in a Metal-Organic Framework. *Angew. Chem., Int. Ed.* **2014**, *53*, 5583−5586.

(24) Ortiz, A. U.; Boutin, A.; Gagnon, K. J.; Clearfield, A.; Coudert, F. X. Remarkable Pressure Responses of Metal-Organic Frameworks: Proton Transfer and Linker Coiling in Zinc Alkyl Gates. *J. Am. Chem. Soc.* **2014**, *136*, 11540−11545.
(25) Im, J.; Seoung, D.; Hwang, G. C.; Jun, J. W.; Jhung, S. H.; Kao, C. C.; Vogt, T.; Lee, Y. Pressure-Dependent Structural and Chemical Changes in a Metal-Organic Framework with One-Dimensional Pore Structure. *Chem. Mater.* **2016**, *28*, 5336−5341.
(26) Coudert, F. X. Responsive Metal-Organic Frameworks and Framework Materials: Under Pressure, Taking the Heat, in the Spotlight, with Friends. *Chem. Mater.* **2015**, *27*, 1905−1916.
(27) McKellar, S. C.; Moggach, S. A. Structural Studies of Metal-Organic Frameworks under High Pressure. *Acta Crystallogr., Sect. B: Struct. Sci., Cryst. Eng. Mater.* **2015**, *71*, 587−607.
(28) Wang, Z.; Cohen, S. M. Postsynthetic Modification of Metal−organic Frameworks. *Chem. Soc. Rev.* **2009**, *38*, 1315.
(29) Su, Z.; Miao, Y.-R.; Zhang, G.; Miller, J. T.; Suslick, K. S. Bond Breakage under Pressure in a Metal Organic Framework. *Chem. Sci.* **2017**, *8*, 8004−8011.
(30) Andrzejewski, M.; Casati, N.; Katrusiak, A. Reversible Pressure-Preamorphization of a Piezochromic Metal-Organic Framework. *Dalt. Trans* **2017**, *46*, 14795−14803.
(31) Hu, Y. H.; Zhang, L. Amorphization of Metal-Organic Framework MOF-5 at Unusually Low Applied Pressure. *Phys. Rev. B: Condens. Matter Mater. Phys.* **2010**, *81*, 1−5.
(32) Bennett, T. D.; Simoncic, P.; Moggach, S. A.; Gozzo, F.; Macchi, P.; Keen, D. A.; Tan, J.-C.; Cheetham, A. K. Reversible Pressure-Induced Amorphization of a Zeolitic Imidazolate Framework (ZIF-4). *Chem. Commun.* **2011**, *47*, 7983.
(33) Cai, W.; Gładysiak, A.; Anioła, M.; Smith, V. J.; Barbour, L. J.; Katrusiak, A. Giant Negative Area Compressibility Tunable in a Soft Porous Framework Material. *J. Am. Chem. Soc.* **2015**, *137*, 9296−9301.
(34) Moggach, S. A.; Parsons, S. High Pressure Crystallography of Inorganic and Organometallic Complexes. *Spectroscopic Properties of Inorganic and Organometallic Compounds*; The Royal Society of Chemistry, 2009; Vol. *40*, pp 324−354.
(35) Patyk, E.; Jenczak, A.; Katrusiak, A. Giant Strain Geared to Transformable H-Bonded Network in Compressed *β*-*d*-Mannose. *Phys. Chem. Chem. Phys.* **2016**, *18*, 11474−11479.
(36) Katrusiak, A. High-Pressure X-Ray Diffraction Study on the Structure and Phase Transition of 1,3-Cyclohexanedione Crystals. *Acta Crystallogr., Sect. B: Struct. Sci.* **1990**, *46* (2), 246−256.
(37) Kleywegt, G. J.; Wiesmeijer, W. G. R.; Van Driel, G. J.; Driessen, W. L.; Reedijk, J.; Noordik, J. H. Unidentate versus Symmetrically and Unsymmetrically Bidentate Nitrate Co-Ordination in Pyrazole-Containing Chelates. The Crystal and Molecular Structures of (Nitrato-O)[tris(3,5-Dimethylpyrazol-1-Ylmethyl)-amine]copper(II) Nitrate, (Nitrato-O,O′)[tris(3,5-dimethylpyrazol-1-ylmethyl)amine]copper(II) nitrate, (nitrato-O,O′)[tris(3,5-dimethylpyrazol-1-ylmethyl)amine]nickel(II). *J. Chem. Soc., Dalton Trans.* **1985**, *10*, 2177−2184.
(38) Addison, C. C.; Logan, N.; Wallwork, S. C.; Garner, C. D. Structural Aspects of Co-Ordinated Nitrate Groups. *Q. Rev., Chem. Soc.* **1971**, *25*, 289.
(39) Parkin, G. Alkyl, Hydride, and Hydroxide Derivatives of the s- and p-Block Elements Supported by Poly(pyrazolyl)borato Ligation: Models for Carbonic Anhydrase, Receptors for Anions, and the Study of Controlled Crystallographic Disorder. In *Advances in Inorganic Chemistry*; Sykes, A. G., Ed.; Academic Press, 1995; Vol. *42*, pp 291−393.
(40) Papon, P.; Leblond, J.; Meijer, P. H. E. *The Physics of Phase Transition—Concepts and Applications*; Springer-Verlag: Berlin 2002; p 419.
(41) Groom, C. R.; Bruno, I. J.; Lightfoot, M. P.; Ward, S. C. The Cambridge Structural Database. *Acta Crystallogr., Sect. B: Struct. Sci., Cryst. Eng. Mater.* **2016**, *72*, 171−179.
(42) Glidewell, C. Metal-Ligand Coordinate Bond Energy Terms in Complexes of Ammonia and 1, 2-Diaminoethane. *J. Coord. Chem.* **1977**, *6*, 189−192.
(43) Nimmermark, A.; Öhrström, L.; Reedijk, J. Metal-Ligand Bond Lengths and Strengths: Are They Correlated? A Detailed CSD Analysis. *Z. Kristallogr. - Cryst. Mater.* **2013**, *228* (7), 311−317.
(44) Slichter, C. P.; Drickamer, H. G. Pressure-Induced Electronic Changes in Compounds of Iron. *J. Chem. Phys.* **1972**, *56*, 2142−2160.
(45) Drickamer, H. G.; Frank, C. W. *Electronic Structure, Electronic Transitions, and the High Pressure Chemistry and Physics of Solids*; Annual Reviews, 1972; Vol. *23*.
(46) Schettino, V.; Bini, R.; Ceppatelli, M.; Ciabini, L.; Citroni, M. Chemical Reactions at Very High Pressure. *Advances in Chemical Physics*; Wiley-Blackwell, 2005; Vol. *131*, pp 105−242.
(47) McKellar, S. C.; Graham, A. J.; Allan, D. R.; Mohideen, M. I. H.; Morris, R. E.; Moggach, S. A. The Effect of Pressure on the Post-Synthetic Modification of a Nanoporous Metal−organic Framework. *Nanoscale* **2014**, *6*, 4163−4173.
(48) Albarski, O.; Hillebrecht, H.; Rotter, H. W.; Thiele, G. Über Caesiumtrichloromercurat(II) CsHgCl3: Lösung Einer Komplexen Überstruktur Und Verhalten Unter Hohen Drücken. *Z. Anorg. Allg. Chem.* **2000**, *626*, 1296−1304.
(49) Schwarz, U.; Wagner, F.; Syassen, K.; Hillebrecht, H. Effect of Pressure on the Optical-Absorption Edges of And. *Phys. Rev. B: Condens. Matter Mater. Phys.* **1996**, *53*, 12545−12548.
(50) Heines, P.; Keller, H.-L.; Armbrüster, M.; Schwarz, U.; Tse, J. Pressure-Induced Internal Redox Reaction of $Cs_2[PdI_4]\cdot I_2$, $Cs_2[PdBr_4]\cdot I_2$, and $Cs_2[PdCl_4]\cdot I_2$. *Inorg. Chem.* **2006**, *45*, 9818−9825.
(51) Denner, W.; Schulz, H.; d'Amour, H. The Influence of High Hydrostatic Pressure on the Crystal Structure of Cesium Gold Chloride ($Cs_2Au^IAu^{III}Cl_6$) in the Pressure Range up to 52×10^8 Pa. *Acta Crystallogr., Sect. A: Cryst. Phys., Diffr., Theor. Gen. Crystallogr.* **1979**, *35*, 360−365.
(52) Tidey, J. P.; Wong, H. L. S.; McMaster, J.; Schroder, M.; Blake, A. J. High-Pressure Studies of Three Polymorphs of a Palladium(II) Oxathioether Macrocyclic Complex. *Acta Crystallogr., Sect. B: Struct. Sci., Cryst. Eng. Mater.* **2016**, *72*, 357−371.
(53) Bujak, M.; Angel, R. J. High-Pressure- and Low-Temperature-Induced Changes in $[(CH_3)_3NH(CH_3)_3NH_3][SbCl_5]$. *J. Phys. Chem. B* **2006**, *110*, 10322−10331.
(54) Prescimone, A.; Sanchez-Benitez, J.; Kamenev, K. K.; Moggach, S. A.; Warren, J. E.; Lennie, A. R.; Murrie, M.; Parsons, S.; Brechin, E. K. High Pressure Studies of Hydroxo-Bridged Cu(II) Dimers. *Dalt. Trans.* **2010**, *39*, 113−123.
(55) Batten, S. R.; Champness, N. R.; Chen, X.-M.; Garcia-Martinez, J.; Kitagawa, S.; Öhrström, L.; O'Keeffe, M.; Paik Suh, M.; Reedijk, J. Terminology of Metal−organic Frameworks and Coordination Polymers (IUPAC Recommendations 2013). *Pure Appl. Chem.* **2013**, *85*, 1715.
(56) Batten, S. R.; Champness, N. R.; Chen, X.-M.; Garcia-Martinez, J.; Kitagawa, S.; Öhrström, L.; O'Keeffe, M.; Suh, M. P.; Reedijk, J. Coordination Polymers, Metal−organic Frameworks and the Need for Terminology Guidelines. *CrystEngComm* **2012**, *14*, 3001.
(57) Zhang, J. P.; Chen, X. M. Exceptional Framework Flexibility and Sorption Behavior of a Multifunctional Porous Cuprous Triazolate Framework. *J. Am. Chem. Soc.* **2008**, *130*, 6010−6017.
(58) Mason, J. A.; Oktawiec, J.; Taylor, M. K.; Hudson, M. R.; Rodriguez, J.; Bachman, J. E.; Gonzalez, M. I.; Cervellino, A.; Guagliardi, A.; Brown, C. M.; Llewellyn, P. L.; Masciocchi, N.; Long, J. R. Methane Storage in Flexible Metal-Organic Frameworks with Intrinsic Thermal Management. *Nature* **2015**, *527*, 357−361.
(59) Zhang, J. P.; Lin, Y. Y.; Zhang, W. X.; Chen, X. M. Temperature- or Guest-Induced Drastic Single-Crystal-to-Single-Crystal Transformations of a Nanoporous Coordination Polymer. *J. Am. Chem. Soc.* **2005**, *127*, 14162−14163.
(60) Zhang, J.-P.; Zhou, H.-L.; Zhou, D.-D.; Liao, P.-Q.; Chen, X.-M. Controlling Flexibility of Metal−organic Frameworks. *Natl. Sci. Rev.* **2017**, *March*, 1−13.

DOI: 10.1021/acs.inorgchem.8b00913
Inorg. Chem. 2018, 57, 8942−8950

(61) Chapman, K. W.; Sava, D. F.; Halder, G. J.; Chupas, P. J.; Nenoff, T. M. Trapping Guests within a Nanoporous Metal-Organic Framework through Pressure-Induced Amorphization. *J. Am. Chem. Soc.* **2011**, *133*, 18583−18585.
(62) Hazen, R. M.; Finger, L. W. *Comparative Crystal Chemistry: Temperature, Pressure, Composition, and the Variation of Crystal Structure*; John Wiley, 1982.
(63) Katrusiak, A. High-Pressure x-Ray Diffraction Studies of Organic Crystals. *High Pressure Res.* **1990**, *4*, 496−498.
(64) Hu, C.; Englert, U. Crystal-to-Crystal Transformation from a Chain Polymer to a Two-Dimensional Network at Low Temperatures. *Angew. Chem., Int. Ed.* **2005**, *44*, 2281−2283.
(65) Xie, Z.; Mei, L.; Wu, Q.; Hu, K.; Xia, L.; Chai, Z.; Shi, W. Temperature-Induced Reversible Single-Crystal-to-Single-Crystal Isomerisation of Uranyl Polyrotaxanes: An Exquisite Case of Coordination Variability of the Uranyl Center. *Dalt. Trans* **2017**, *46*, 7392−7396.
(66) Zhu, M.; Song, X. Z.; Song, S. Y.; Zhao, S. N.; Meng, X.; Wu, L. L.; Wang, C.; Zhang, H. J. A Temperature-Responsive Smart Europium Metal-Organic Framework Switch for Reversible Capture and Release of Intrinsic Eu^{3+} Ions. *Adv. Sci.* **2015**, *2*, 1500012.
(67) Bernini, M. C.; Gandara, F.; Iglesias, M.; Snejko, N.; Gutierrez-Puebla, E.; Brusau, E. V.; Narda, G. E.; Monge, M. A. Reversible Breaking and Forming of Metal-Ligand Coordination Bonds: Temperature-Triggered Single-Crystal to Single-Crystal Transformation in a Metal-Organic Framework. *Chem. - Eur. J.* **2009**, *15*, 4896−4905.
(68) Mobin, S. M.; Srivastava, A. K.; Mathur, P.; Lahiri, G. K. Reversible Single-Crystal to Single-Crystal Transformations in a Hg(II) Derivative. 1D-Polymeric Chain ⇌ 2D-Networking as a Function of Temperature. *Dalt. Trans* **2010**, *39*, 8698.
(69) Slater, J. C. Atomic Radii in Crystals. *J. Chem. Phys.* **1964**, *41*, 3199−3204.
(70) Pauling, L. The Sizes of Ions and the Structure of Ionic Crystals. *J. Am. Chem. Soc.* **1927**, *49*, 765−790.
(71) Shannon, R. D. Revised Effective Ionic Radii and Systematic Studies of Interatomic Distances in Halides and Chalcogenides. *Acta Crystallogr., Sect. A: Cryst. Phys., Diffr., Theor. Gen. Crystallogr.* **1976**, *32*, 751−767.
(72) Pauling, L. Determination of Ionic Radii from Cation-Anion Distances in Crystal Structures; Discussion. *Am. Mineral.* **1987**, *72*, 1016.
(73) Shannon, R. D.; Prewitt, C. T. Effective Ionic Radii in Oxides and Fluorides. *Acta Crystallogr., Sect. B: Struct. Crystallogr. Cryst. Chem.* **1969**, *25*, 925−946.
(74) Miller, V. L.; Tidrow, S. C. Perovskites: Temperature and Coordination Dependent Ionic Radii. *Integr. Ferroelectr.* **2013**, *148*, 1−16.
(75) Kole, G. K.; Vittal, J. J. Solid-State Reactivity and Structural Transformations Involving Coordination Polymers. *Chem. Soc. Rev.* **2013**, *42*, 1755−1775.
(76) Vittal, J. J. Supramolecular Structural Transformations Involving Coordination Polymers in the Solid State. *Coord. Chem. Rev.* **2007**, *251*, 1781−1795.
(77) Sobczak, S.; Katrusiak, A. Zone-Collapse Amorphization Mimicking the Negative Compressibility of a Porous Compound. *Cryst. Growth Des.* **2018**, *18*, 1082−1089.
(78) Andrzejewski, M.; Katrusiak, A. Piezochromic Porous Metal−Organic Framework. *J. Phys. Chem. Lett.* **2017**, *8*, 279−284.
(79) Cai, W.; Katrusiak, A. Giant Negative Linear Compression Positively Coupled to Massive Thermal Expansion in a Metal-Organic Framework. *Nat. Commun.* **2014**, *5*, 4337.
(80) Merrill, L.; Bassett, W. A. Miniature Diamond Anvil Pressure Cell for Single Crystal X-Ray Diffraction Studies. *Rev. Sci. Instrum.* **1974**, *45*, 290−294.
(81) Mao, H. K.; Xu, J.; Bell, P. M. Calibration of the Ruby Pressure Gauge to 800 Kbar under Quasi-Hydrostatic Conditions. *J. Geophys. Res.* **1986**, *91*, 4673.
(82) Piermarini, G. J.; Block, S.; Barnett, J. D.; Forman, R. A. Calibration of the Pressure Dependence of the R1ruby Fluorescence Line to 195 Kbar. *J. Appl. Phys.* **1975**, *46*, 2774−2780.
(83) Budzianowski, A.; Katrusiak, A. High-Pressure Crystallographic Experiments With a CCD-Detector. *High Press. Crystallogr.* **2004**, *140*, 101−112.
(84) *Agilent CrysAlisPro Software System*; Technol. UK Ltd.: Yarnton, Oxford, U.K., 2014; Vol. *44*
(85) Dolomanov, O. V.; Bourhis, L. J.; Gildea, R. J.; Howard, J. A. K.; Puschmann, H. Olex2: A Complete Structure Solution, Refinement and Analysis Program. *J. Appl. Crystallogr.* **2009**, *42*, 339−341.
(86) Sheldrick, G. M. A Short History of SHELX. *Acta Crystallogr., Sect. A: Found. Crystallogr.* **2008**, *64*, 112−122.
(87) Sheldrick, G. M. Crystal Structure Refinement with SHELXL. *Acta Crystallogr., Sect. C: Struct. Chem.* **2015**, *71*, 3−8.
(88) Katrusiak, A. *REDSHABS—Program for Correcting Reflections Intensities for DAC Absorption, Gasket Shadowing and Sample Crystal Absorption*; Adam Mickiewicz University: Poznań, Poland, 2003.
(89) Katrusiak, A. Shadowing and Absorption Corrections of Single-Crystal High-Pressure Data. *Z. Kristallogr. - Cryst. Mater.* **2004**, *219*, 461−467.

DOI: 10.1021/acs.inorgchem.8b00913
Inorg. Chem. 2018, 57, 8942−8950

(R2) Sobczak, S.; Katrusiak, A. Environment-Controlled Postsynthetic Modifications of Iron Formate Frameworks. *Inorg. Chem*. **2019,** 58 (17), 11773–11781

Inorganic Chemistry
Cite This: Inorg. Chem. 2019, 58, 11773−11781
Article
pubs.acs.org/IC

Environment-Controlled Postsynthetic Modifications of Iron Formate Frameworks

Szymon Sobczak and Andrzej Katrusiak*

Faculty of Chemistry, Adam Mickiewicz University, Uniwersytetu Poznańskiego 8, 61-614 Poznań, Poland

Supporting Information

ABSTRACT: New, hybrid iron-formate perovskites have been obtained in high-pressure reactions. In addition to the pressure range, the liquid environment of the sample also regulates the course of transformations. Formate α-DmaFe^{2+}Fe^{3+}For$_6$ (Dma = $(CH_3)_2NH_2^+$, For = $HCOO^-$), when compressed in oil or in isopropanol at 1.40 GPa, transforms to a new phase γ, different than that obtained at low-temperature (phase β). In glycerol, phase α can be compressed to 1.40 GPa, but then it reacts to DmaFe^{2+}For$_3$, with all Fe(III) cations reduced, surrounded by amorphous iron formate devoid of Dma cations. Another mixed-valence framework Dma$_3$Fe$^{2+}_3$Fe^{3+}For$_{12}$·CO$_2$ can be produced from phase α incubated in methanol and ethanol at 1.15 GPa. These pressure-induced environment-sensitive modifications have been rationalized by the volume effects in transforming structures, their different chemical composition, voids, ligands, and cation oxidation states switching between Fe(II), Fe(III), their high- and low-spin states, as well as solubility, molecular size, and the chemical and physical properties of the pressure transmitting media. The topochemical redox paths controlled by pressure and the liquid environment offer new highly efficient, safe, and environment-friendly reactions leading to new advanced materials and their postsynthetic modifications.

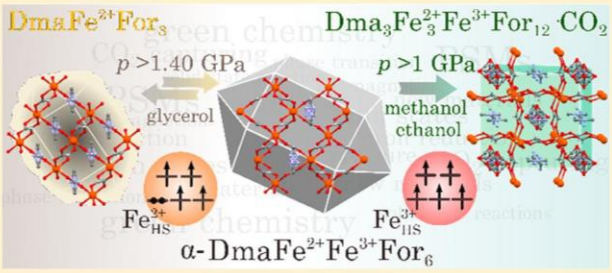

INTRODUCTION

The hybrid inorganic−organic frameworks display various attractive properties, which depend on the cations, linkers, their connectivity, topology, as well as the size and chemical character of surfaces in the voids.[1−13] In these multifunctional materials, the manifold functionalities lead to new cross-effects of higher order, both physical and chemical in nature. Particularly interesting are postsynthetic modifications (PSM) of metal−organic frameworks (MOFs).[14−30] The PSM can be used for fabricating in situ, under specific conditions, new materials with required properties. The PSM solid-state transitions and reactions are often initiated by physical stimuli. Because of the self-contained reaction space, requiring no additional substrates, the PSM can be invaluable for green technologies and for obtaining sophisticated advanced materials on requested sites. These topochemical reactions can be stimulated by light, temperature and pressure.[31−35] The typical high-pressure effects, such as tighter molecular packing, increased density, compressed coordination bonds, shorter distances to the ligands, and modified crystal field−all can destabilize material structure.[36−39]

Several rules were formulated for describing the pressure effects in various compounds, including elements and minerals by Prewitt and Downs.[40] Their Rule Number 4 states that the coordination number increases with pressure, and Rule 5 is that the nonmetal atoms (usually oxygen in minerals) are stronger compressed than cations.[40,41] Most recently, we showed that these rules also describe the effects of pressure on the coordination polymers (CPs) and porous MOFs: the increased coordination number in the high-pressure phases of CPs originates from the stronger compression of anions compared to central cations, and this rule can be extended to the temperature dependence of time-averaged volumes of central and ligand atoms.[42]

Hence, the inverse relationship between the pressure and temperature effects was observed in numerous reactions and transformations of CPs.[42−56] Presently, we further explore the pressure-induced PSMs. By choosing the mixed-valence perovskite-like iron-formate framework with dimethylamine cations (Dma), we have introduced into the system additional instabilities of low-spin and high-spin states, the oxidation changes between Fe^{2+} and Fe^{3+} cations and possible relocation, disproportionation, and reactions involving the formate and amine ions.

The strongly increased energy of interactions can result in electronic transitions, spin-state changes, and even in redox reactions. Spin crossover (SC) phenomena in transition-metal compounds under pressure were reviewed by Drickamer et al.[57,58] Since then, the SC transformations have been observed in many complexes of divalent and trivalent iron, cobalt, nickel, chromium, and manganese.[42] However, to our knowledge, no pressure-promoted SC transformations coupled to the redox reactions in MOFs have been reported. Here, we describe

Received: June 18, 2019
Published: August 22, 2019

DOI: 10.1021/acs.inorgchem.9b01817
Inorg. Chem. 2019, 58, 11773−11781

several high-pressure transformations involving electronic transformations for compound $[(CH_3)_2NH_2^+][Fe^{2+}Fe^{3+}(HCOO^-)_6]$, hereafter denoted as α-DmaFe^{2+}Fe^{3+}For$_6$ (Figure 1). Moreover, we have observed that the PSMs of iron formates strongly depend on their liquid environments.

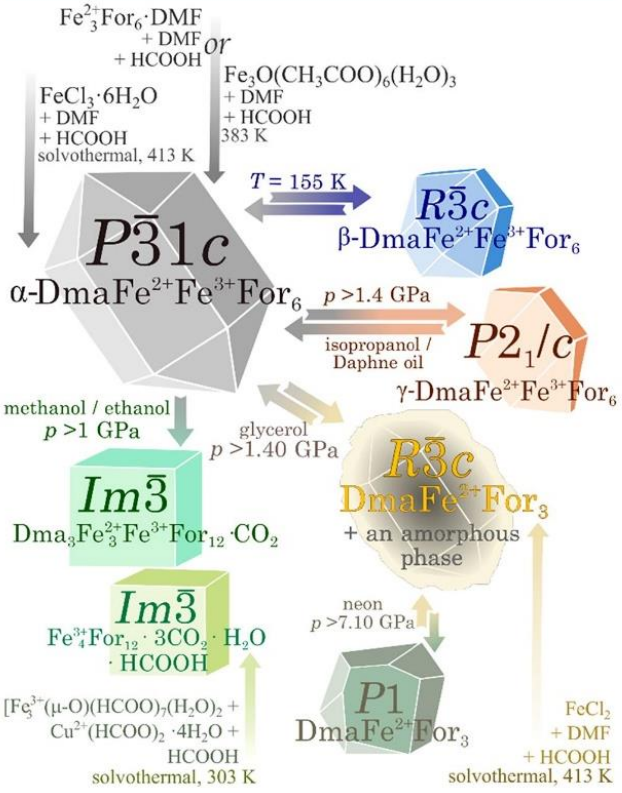

Figure 1. Schematic diagram of phase transformations and reactions of iron formates at various conditions. Double arrows mark the reversible transformations.

DISCUSSION

In the α-DmaFe^{2+}Fe^{3+}For$_6$ framework, each Fe(III) cation is surrounded by six octahedrally arranged Fe(II), each of which is likewise surrounded by six Fe(III) cations. Bonds Fe(II)−O and Fe(III)−O can be distinguished by their length, 2.12 and 2.01 Å, respectively, as the Fe(II) cation, is richer in one electron and hence larger than Fe(III). We have established for a series of iron formates the bond-length difference of about 0.1 Å between Fe(II)−O and Fe(III)−O is hardly affected by the pressure up to 1.2 GPa. Whereas the continuous compression reduces the Fe−O bond distance by less than 1% GPa^{-1}, the electronic transition between Fe(II) and Fe(III), as well as the SC transition, result in over 10% Fe−O distance changes.

Depending on the pressure range and solvent, α-DmaFe^{2+}Fe^{3+}For$_6$ transforms its framework and electronic states of the iron cations in three different ways (Figure 1). The different ionic radii in ferric and ferrous cations make the Fe−O distances highly responsive to the pressure changes. The observed changes in Fe−O bond distances, illustrated for selected iron formates in Figure 2, are the consequences of structural strains accumulated during the monotonic compression, as well as the electronic transitions and strains generated at anomalous transformations of the crystal.

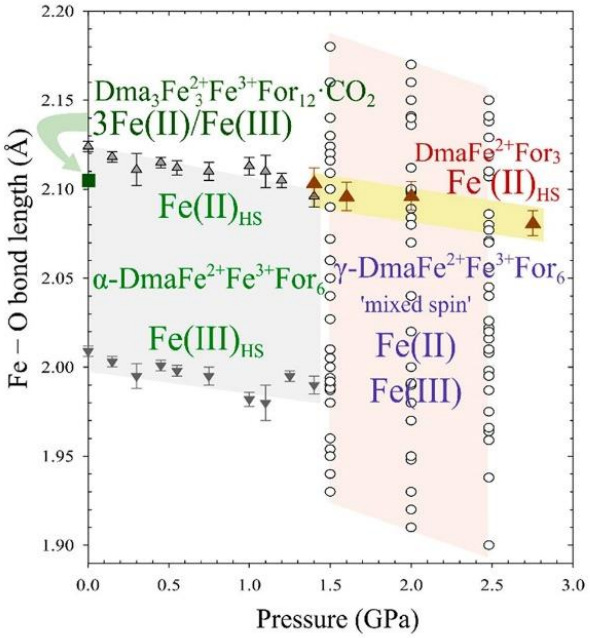

Figure 2. Bonds Fe−O in iron formates compressed in different media. The color code of highlights correspond to that in Figure 1; triangles up, down and circles indicate the Fe(II)$_{HS}$, Fe(III)$_{HS}$ and mixed, respectively. The iron oxidation state for Dma$_3$Fe$^{2+}_3$Fe^{3+}For$_{12}$·CO$_2$ is the average of 3:1 of Fe(II): Fe(III).

The structural features of the starting material are essential for understanding its PSMs. The ambient-pressure hybrid perovskite α-DmaFe^{2+}Fe^{3+}For$_6$, of trigonal space group $P\bar{3}1c$ (Table 1), is stable in different hydrostatic media nearly up to 1.40 GPa. As previously reported,[59,60] all iron cations in α-DmaFe^{2+}Fe^{3+}For$_6$ are octahedrally coordinated by formate anions in anti−anti configuration. Every second cavity of the framework is occupied by the Dma cation, and every other is empty. At ambient pressure, above 155 K,[59,60] the Dma cation is disordered in this way that the two methyls reside on the 3-fold axis and around the axis, the nitrogen atom is distributed between three equivalent sites. Below 155 K, the onset of the ordering of Dma cations breaks the symmetry and transforms the crystal to phase β of space group $R\bar{3}c$.[61,62]

Monotonic Compression of α-DmaFe^{2+}Fe^{3+}For$_6$. The high-pressure behavior of α-DmaFe^{2+}Fe^{3+}For$_6$ by itself is quite unique. Up to 1.0 GPa, phase α is hardly compressed along plane (001) and then, up to 1.40 GPa, it displays the extremely rare effect of negative area compressibility (NAC)[56,63−66] (Figure 3). On approaching the phase transition at 1.40 GPa both the NAC along plane (001) and the strong linear compression along [001] increase; between the ambient pressure and 1.40 GPa, parameter c of the hexagonal cell is reduced by about 1 Å. Despite this strong lattice strain, the structural changes are relatively small: the Fe···Fe distances are compressed from 5.889 Å at 0.1 MPa to 5.768 Å in 1.25 GPa; in this pressure range the O−C−O angle in formates increases by 1.38°, similarly as it was reported in compressed DmaNiFor$_3$, DmaCoFor$_3$,[67] DmaCuFor$_3$, DmaFeFor$_3$, and DmaMnFor$_3$.[68]

The magnetic properties of α-DmaFe^{3+}Fe^{2+}For$_6$ are consistent with high-spin configurations of the iron cations.[60]

DOI: 10.1021/acs.inorgchem.9b01817
Inorg. Chem. 2019, 58, 11773−11781

Table 1. Selected Crystallographic Data of α-DmaFe^{2+}Fe^{3+}For$_6$, γ-DmaFe^{2+}Fe^{3+}For$_6$, and DmaFe^{2+}For$_3$[a]

	α-DmaFe^{2+}Fe^{3+}For$_6$	α-DmaFe^{2+}Fe^{3+}For$_6$	γ-DmaFe^{2+}Fe^{3+}For$_6$	DmaFe^{2+}For$_3$
formula	$[(CH_3)_2NH_2^+]$ $[Fe^{3+}Fe^{2+}(HCOO^-)_6]$	$[(CH_3)_2NH_2^+]$ $[Fe^{3+}Fe^{2+}(HCOO^-)_6]$	$[(CH_3)_2NH_2^+]$ $[Fe^{3+}Fe^{2+}(HCOO^-)_6]$	$[(CH_3)_2NH_2^+]$ $[Fe^{2+}(HCOO^-)_3]$
medium	air	Daphne, isopropanol	Daphne, isopropanol	glycerol
pressure	0.1 MPa[59,60]	1.40 GPa	1.50 GPa	1.40 GPa
crystal system	trigonal	trigonal	monoclinic	trigonal
space group	$P\bar{3}1c$	$P\bar{3}1c$	$P2_1/c$	$R\bar{3}c$
a (Å)	8.2512(11)	8.2737(4)	8.353(3)	8.153(7)
b (Å)			14.119(3)	
c (Å)	13.846(3)	12.9287(4)	36.091(3)	21.913(3)
β (deg)			90.681(12)	
V (Å^3)	816.374(2)	766.45(5)	4256.0(18)	1262(2)

[a]See Tables S5–S8.

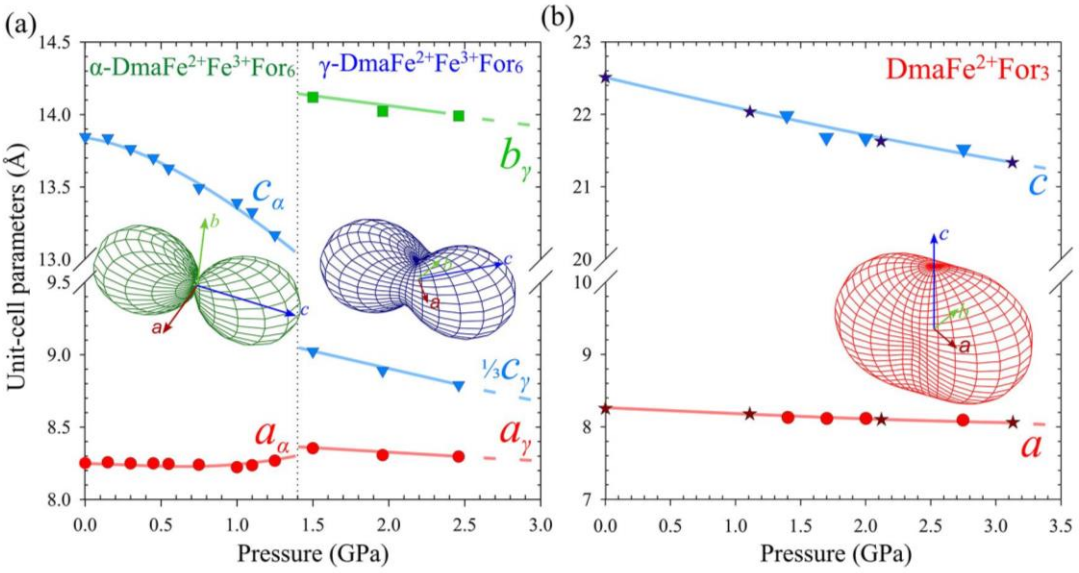

Figure 3. Changes in the unit-cell parameters of (a) α-DmaFe^{2+}Fe^{3+}For$_6$ compressed in Daphne 7474, isopropanol, methanol, and glycerol up to 1.40 GPa and then γ-DmaFe^{2+}Fe^{3+}For$_6$ compressed in Daphne 7474 and isopropanol; and (b) the compression of DmaFe^{2+}For$_3$ formed above 1.40 GPa in glycerol (full symbols) and of DmaFe^{2+}For$_3$ synthesized at ambient conditions (open symbols).[68,69] The insets graphically represent the strain tensors of the crystals at the low-pressure limit of their stability regions.[70]

The configuration of electrons in the partly filled 3*d* shell affects not only the potential energy and size of the cation, but also its reactivity. According to Hund's rule, the electronic configuration of maximum-multiplicity (highest-spin) is favored. Thus, the ferrous cation Fe(II) adopts the outer shell $3d^64s^\circ$, and it changes to $3d^54s^\circ$ for the cation reduced to ferric Fe(III). Both these cations can further differentiate into high-spin or low-spin states. The high-spin ferric state, with five orbitals, each containing one electron, is spherical ($^6A_1$). The high-spin ferrous state is in an asymmetric ($^5T_2$) ground state. On the other hand, the low-spin ferrous state is spherically symmetric ($^1A_1$), while the low-spin ferric state ($^2T_2$) is not.

In compressed high-spin α-DmaFe^{2+}Fe^{3+}For$_6$, the ligand field increases and the interelectronic repulsion (Racah parameter) decreases.[71] Thus, on one hand, the high-pressure increases the energy of all orbitals; and on the other, the interelectronic repulsion can be reduced by the spin-pairing energy. The lower energy of interelectronic interactions of the antiparallel spins, consistent with Pauling's principle, can also be associated with the reduction of the volume of electronic orbitals, with the reduction of ionic and atomic radii. These effects combine the high/low-spin transitions with the pressure stimuli. Other external stimuli, such as temperature and pH of the solvent, can further affect the ligand field. Such combined effects can cumulate for triggering phase transitions and topochemical reactions.

Generally, the coordinating electronegative atoms or anions are larger and stronger compressed than cations. Consequently, high-pressure usually favors the equilibrium of smaller anions and neutral structural units, even when achieved at the cost of a small increase of the cations volume (Figure 4). Moreover, the pressure can trigger a composition change reducing the overall volume of the crystals and its environment, treated as a whole system. The volume reduction can be achieved either by phase transitions or topochemical reactions.

For example, it was shown that high-pressure, through chemical reactions, promotes the reduced oxidation states in the series of oxides Fe_2O_3, Fe_3O_4, Fe_4O_5, Fe_5O_7, Fe_7O_9, and FeO.[57,58,71−75] For the iron formates under this study, the oxidation states of the Fe cations are the derivative of the crystal structure, ligands conformation, voids and of the compounds composition and its possible changes. Several types of pressure-induced transformations of iron formates reported in the literature,[76−79] and our present results,

DOI: 10.1021/acs.inorgchem.9b01817
Inorg. Chem. 2019, 58, 11773−11781

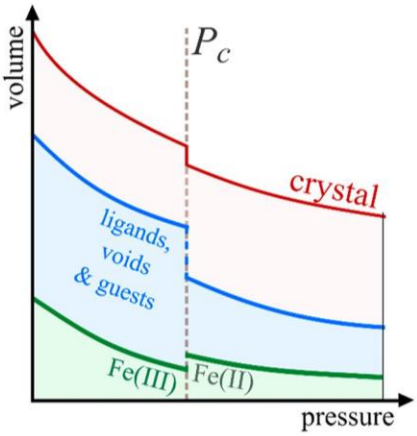

Figure 4. Monotonic and anomalous compression schematically illustrated for a crystal (the closed thermodynamic system), where at the transformation point, the overall volume drop of the crystal (red line) is mainly due to the ligands, voids, and dislocated guests. A subsystem of iron cations (green) can display a negative volume compression, fully compensated by the larger volume compression of the other subsystems. The dashed line marks critical pressure P_c.

illustrate the interplay of various structural components and their compressed environment.

Compression in Oil and in Isopropanol. At 1.40 GPa, α-DmaFe^{2+}Fe^{3+}For$_6$ reversibly transforms to phase γ, of monoclinic space group $P2_1/c$ (Figure 2, Table 1). In phase γ, the FeO$_6$ octahedra are distorted due to the Fe−O bonds and O···O distances significantly different in the strained structure (Figure 5). However, the structural dimensions, chemical composition and the distribution of Fe−O distances, all are consistent with the retained oxidation state Fe^{2+}Fe^{3+} in phase γ. The transition to phase γ has the character of both order−disorder (it halts the rotations of Dma cations) and reconstructive (every sixth formate anion changes its configuration from anti−anti to anti−syn) transformation. Figure 5 illustrates the main features of phases α and γ: the binding conformation of HCOO$^-$ linkers; disordered (phase α) and ordered (phase γ) Dma cations occupying every second cage of the perovskite structure (occupied cages are marked blue/gray; empty ones purple/yellow); and the presence of independent cages. The anti−syn configuration considerably reduces the volume of two-thirds of the empty cages in phase γ (Figures 5 and 6). In this way, 1/3 of all cages in the crystal in phase γ are empty and collapsed, while 1/6 of all cages are empty and remain open; the remaining 1/2 of all cages is filled by ordered Dma cations. This volume reduction effect is absent at ambient pressure and the transition between phases α and β (at 155 K) is purely of the order−disorder type.

Squeezing Dma off α-DmaFe^{2+}Fe^{3+}For$_6$ in Glycerol. In glycerol, α-DmaFe^{2+}Fe^{3+}For$_6$ is compressed like in Daphne oil and isopropanol up to 1.4 GPa (Figure 3), but then several spectacular macroscopic effects are clearly visible (Figure 7). The black single crystal of phase α gradually changes its shape and becomes transparent between the crystal surface and the dark central part. This color change of the outer part and its multigrain texture is clearly different from α-to-γ phase transition. On releasing pressure the transparent region is reduced until the sample is fully black again. This process could be repeated several times, after which the initial sharp edges of the sample become first rounded and next shattered.

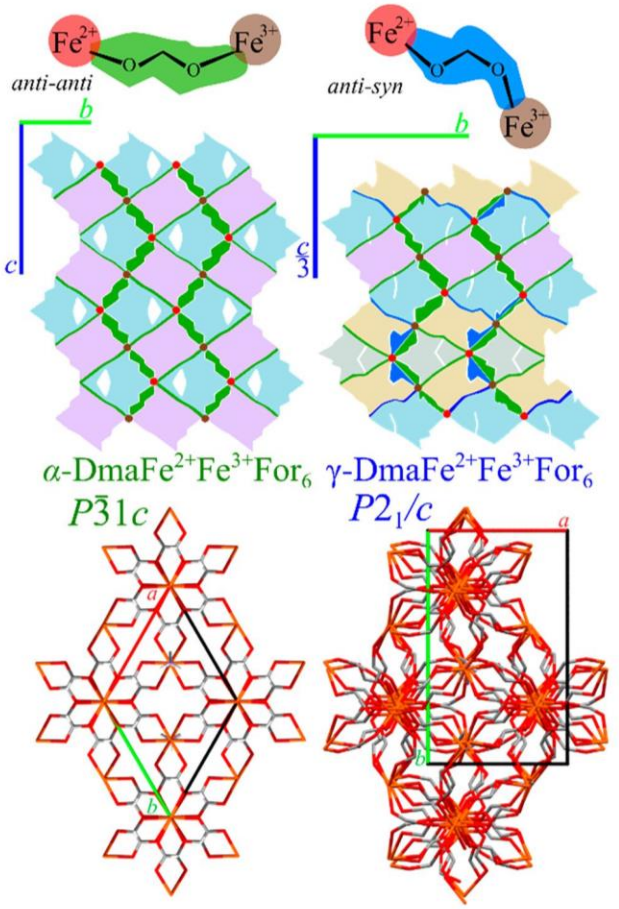

Figure 5. Structural features of DmaFe^{2+}Fe^{3+}For$_6$ phases. (Top) Schematic representations of the formate coordination configurations anti−anti (marked green) and in anti−syn (blue), as well as of phase α (left) projected down direction $[100]_\alpha$ and of phase γ (right) projected in corresponding direction $[100]_\gamma$. The cages occupied with Dma are colored blue and gray; the empty cages are purple and yellow. (Bottom) Capped-sticks models of the structures projected along the direction [001], collinear in phases α and γ.

The X-ray diffraction measurements confirmed that in glycerol phase α is compressed like in Daphne oil and isopropanol, but then a sudden transformation takes place to a new phase (Figure S1). Only one single-crystal diffraction pattern was present above 1.40 GPa, despite that, two different (transparent-outer and dark-internal) phases were clearly visible. By solving the crystal structure of the new diffraction pattern, we found that this is DmaFe^{2+}For$_3$ (Table 1), of trigonal space group $R\bar{3}c$. DmaFe^{2+}For$_3$ was synthesized before at ambient pressure and it forms transparent crystals,[80] and it could be an indication that the transparent-outer part of the sample corresponds to the new compound (Figure 7). The compression of DmaFe^{2+}For$_3$ was measured by Collings et al.,[69] and it is consistent with our measurements in glycerol in all the pressure range (Figure 2). However, in our experiment, the DmaFe^{2+}For$_3$ crystal disappears below 1.40 GPa and α-DmaFe^{2+}Fe^{3+}For$_6$ appears again.

It is apparent that the pressure-induced topochemical reaction in the single crystal of α-DmaFe^{2+}Fe^{3+}For$_6$ compressed in glycerol leads to at least two products, one of which we have identified by X-ray diffraction as DmaFe^{2+}For$_3$ and others are amorphous or in the form of fine powder, as no

DOI: 10.1021/acs.inorgchem.9b01817
Inorg. Chem. 2019, 58, 11773−11781

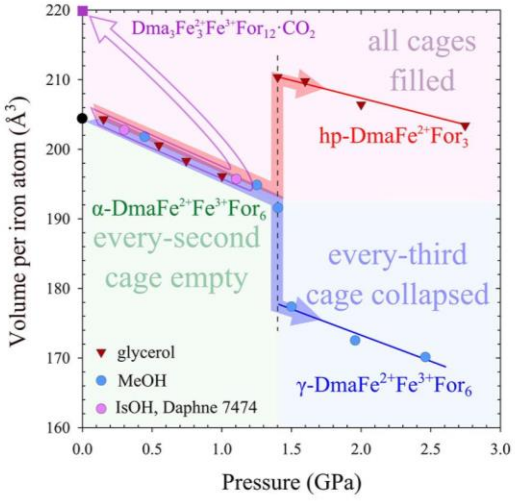

Figure 6. Compression of the unit-cell volume per one iron atom in iron-formates with half of the cages empty ($DmaFe^{2+}Fe^{3+}For_6$ phases α and γ) and all cages filled ($DmaFe^{2+}For_3$ and $Dma_3Fe^{2+}{}_3Fe^{3+}For_{12}\cdot CO_2$). Different pressure transmitting media are indicated by symbols described in the legend.

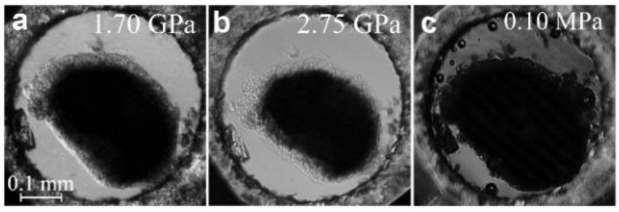

Figure 7. Single crystal of α-$DmaFe^{2+}Fe^{3+}For_6$ compressed in glycerol. It gradually becomes transparent above 1.40 GPa (a, b). The reverse reaction (c) after the pressure was released, as indicated by the presence of small air bubbles. Several small ruby chips lie close to the edge of the diamond anvil cell (DAC) chamber.

other diffraction pattern was observed. This reaction can be described by the equation

$$\alpha\text{-}DmaFe^{2+}Fe^{3+}For_6 \xleftrightarrow[\text{glycerol}]{1.40\ \text{GPa}} DmaFe^{2+}For_3 + X$$

where X can be either $Fe^{3+}For_3$ or $Fe^{2+}For_2\cdot For\cdot$ (For· stands for a radical form of formate ligand).

According to Drickamer et al.,[71] with increasing pressure the energy of 3d orbitals (placed against the ligand orbitals) lowers, at the same time increasing iron affinity for electrons. The formate anions possessing empty π orbitals can bond to the (filled) $t_{2g}(\pi)$ orbitals of the metal atom by the back-donation of metal electrons. The reduction of iron is accomplished at the point when the electron from a nonbonding ligand orbital is transferred to the metal 3d antibonding orbital. This reduction can lead either to a form of free radical formed at a ligand site or to an electron−hole circulating between the adjacent ligands.[71]

It is plausible that above 1.40 GPa on the crystal surface of α-$DmaFe^{2+}Fe^{3+}For_6$ all cages in framework collapse and the Dma cations are extruded toward the crystal center, where they fill in the empty (every second) cages, simultaneously with the reduction of adjacent cations Fe(III) to Fe(II). This mechanism implies that at the sample center, the single crystal of $DmaFe^{2+}For_3$ is surrounded by the transition zone of unidentified phase X, deprived of all Dma (most likely either $Fe^{3+}For_3$ or $Fe^{2+}For_2\cdot For\cdot$), which may further transform into the $Fe^{2+}For_2$ framework, where each For anion coordinates three Fe(II) cations. Such a structure of the collapsed $Fe^{2+}For_2$ framework at ambient conditions was determined by Wang et al.[81] Despite these strong changes in the structure and in properties, we observed that the reaction is reversible (Figure 7). It implies that the transforming regions are capable of transporting the Dma cations, resulting in the reconstruction of the original phase α-$DmaFe^{2+}Fe^{3+}For_6$ on the release of pressure.

Irreversible CO_2-Templated Reaction in MeOH and EtOH. We detected no signs of anomalous behavior for α-$DmaFe^{2+}Fe^{3+}For_6$ compressed in methanol and ethanol to about 1.10 GPa. However, at 1.15 GPa, the crystal slowly dissolved and small cubic prisms precipitated (Figure 8). We

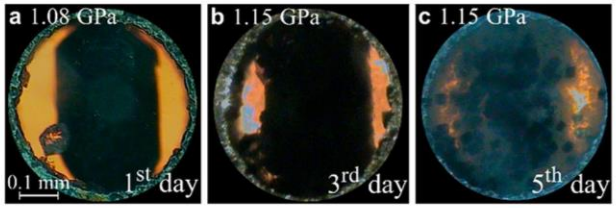

Figure 8. Chemical reaction of α-$DmaFe^{2+}Fe^{3+}For_6$ compressed in methanol: (left) the DAC chamber with one single crystal of phase α and a ruby chip for pressure calibration on its left edge, after increasing pressure to 1.08 GPa at 296 K; (middle) after 2 days of gradually increasing pressure to 1.15 GPa; and (right) incubated for another 5 days, the chamber filled by many small crystals of $Dma_3Fe^{2+}{}_3Fe^{3+}For_{12}\cdot CO_2$ (green in the transmitting light).

recovered them to ambient pressure and established by X-ray diffraction that they are formed of $Dma_3Fe^{2+}{}_3Fe^{3+}For_{12}\cdot CO_2$. Their cubic symmetry of space group $Im\bar{3}$, and the structure (Table 2) are analogous to a group of metal M(III) formates of

Table 2. New Iron Formate Obtained under High-Pressure (this work, see Table S9) Compared to the Analogous Crystal Synthesized in Hydrothermal Conditions by Tian et al.[83]

formula	$Dma_3Fe^{2+}{}_3Fe^{3+}For_{12}\cdot CO_2$	$Fe^{3+}{}_4(HCOO^-)_{12}\cdot 3CO_2\cdot H_2O\cdot HCOOH$
synthesis	0.9−1.2 GPa 269 K for 120 h	hydrothermal 423 K for 24 h[83]
cryst. system	cubic	cubic
space group	$Im\bar{3}$	$Im\bar{3}$
a (Å)	12.0752(4)	11.7697(11)
V (Å^3)	1760.68(10)	1630.4(3)
Z/Z'	8/0.166667	8/0.166667
D_x (g cm^{-3})	1.723	1.861

general formula $[M^{3+}(HCOO^-)_3\cdot 3/4CO_2\cdot 1/4H_2O\cdot 1/4HCOOH]$, where M = Mn, Fe, Al, Ga, and In.[82,83] They adopt the ReO_3-type structure, built of FeO_6 octahedra sharing formate anions at the vertices. The neutral CO_2 molecules and Dma cations trapped in the cages equilibrate the 3:1 ratio of Fe^{2+} and Fe^{3+} cations (Figure 9).

It appears that the main reason for the different effect of methanol and ethanol is that they better dissolve α-$DmaFe^{2+}Fe^{3+}For_6$ than isopropanol, Daphne oil, and glycerol.

DOI: 10.1021/acs.inorgchem.9b01817
Inorg. Chem. 2019, 58, 11773−11781

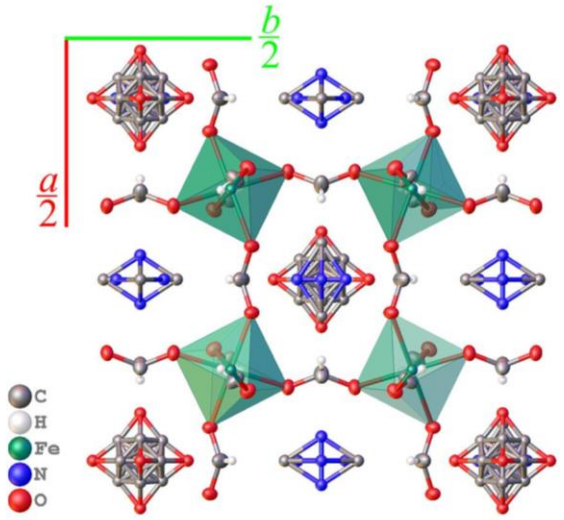

Figure 9. Cubic structure of $Dma_3Fe^{2+}{}_3Fe^{3+}For_{12}\cdot CO_2$ with Dma and CO_2 caged in the 3-dimensional framework. Two types of cages, one of site symmetry *mmm* and the other $m\bar{3}$, result in highly disordered Dma and CO_2, respectively. The Dma H-atoms are omitted for clarity.

Consequently, phase α dissolves and some formates decompose to CO_2 and H_2. This reaction involves an electron transfer from the formate nonbonding level to the metal d_π orbitals, according to

$$4\alpha\text{-}DmaFe^{2+}Fe^{3+}For_6 + 2For + 2Dma \xrightarrow[CH_3OH]{1.15\ GPa} 2Dma_3Fe_3{}^{2+}Fe^{3+}For_{12}\cdot CO_2 + H_2$$

The crystal structure of $Dma_3Fe^{2+}{}_3Fe^{3+}For_{12}\cdot CO_2$ is similar to that of $DmaFe^{2+}For_3$ in this respect that all cages are filled. However, in $Dma_3Fe^{2+}{}_3Fe^{3+}For_{12}\cdot CO_2$, every fourth cage are filled with the neutral CO_2 molecule. It is known that many formate salts of the general formula $MFor(H_2O)_x$ are prone to decarboxylation. For example, hydrated nickel formate decarboxylases at about 473 K, yielding the fine powder of pure metallic nickel.[84] Moreover, the catalytic effect of $Fe(BF_4)_2\cdot 6H_2O$ for the dehydrogenation of formic acid is highly efficient.[85]

Environment effects on α-$DmaFe^{3+}Fe^{2+}For_6$. Our experiments have revealed that α-$DmaFe^{2+}Fe^{3+}For_6$ is highly sensitive to the liquid medium used for the compression. Clearly, three different transformations of α-$DmaFe^{2+}Fe^{3+}For_6$ can be discriminated for the sample compressed in (a) Daphne oil 7474 and isopropanol, (b) glycerol, and (c) methanol and ethanol. These liquids are different in several respects, and it appears that their most significant properties are molecular volume, viscosity, and the hydrostatic limit.[86−88] The liquids also differ in the types of intermolecular interactions with the walls of cages and the crystal; surfaces. All these properties affect the penetration of molecules into the framework.[87] The highly viscous Daphne 7474 and isopropanol consist of large molecules, unlikely to penetrate the α-$DmaFe^{2+}Fe^{3+}For_6$ structure. It appears that glycerol is similar, but it is much more hydrophilic in interactions. Finally, small molecules of methanol and ethanol can penetrate the pores and, in this way, affect the compression.

CONCLUSIONS

When exposed to different external stimuli, the hybrid iron-formate perovskite α-$DmaFe^{2+}Fe^{3+}For_6$ displays a variety of transformations. Different phase transitions are induced by temperature and pressure. However, the most striking different chemical reactions are caused by the pressure in conjugation with different surrounding liquids. Three different types of transformations have been observed: classical order−disorder and displacive reversible thermodynamic transitions (between phases α, β, and γ); reversible chemical reaction (yielding $DmaFe^{2+}For_3$ and $Fe^{2+}For_2$); as well as irreversible reaction leading to $Dma_3Fe^{2+}{}_3Fe^{3+}For_{12}\cdot CO_2$ involving reduction of formates. The physical and chemical effects leading to these transformations include the work term of the Gibbs free energy ($\partial G/\partial p$) involving the volume changes between low/high-spin electron configurations, disorder and onsets of ordering of Dma cations, changes in oxidation state of iron, disproportionation of charges, configuration of coordination bonds, pressure-increased catalyst effect of iron, molecular size of liquid pressure transmitting media, their dissolving properties, etc. All these effects can be applied for planning the PSMs. Most importantly, this study on α-$DmaFe^{2+}Fe^{3+}For_6$ and its PSM products has revealed a variety of transformations and reactions that broaden the general understanding about the chemistry in extreme conditions, and in particular, the subtle effects most relevant to soft and highly sensitive hybrid metal−organic perovskites.

EXPERIMENTAL SECTION

Synthesis of α-$DmaFe^{2+}Fe^{3+}For_6$. Black single crystal of α-$DmaFe^{2+}Fe^{3+}For_6$ was synthesized according to the procedure reported by Zhao et al.[59] One gram of the $FeCl_3\cdot 6H_2O$ crystals were dissolved in a mixture of DMF and 88% formic acid and heated at 140 °C for several days in an autoclave.[89] After that, black crystals of $DmaFe^{2+}Fe^{3+}For_6$ were mechanically separated, washed, and dried. The Dma cations caged in the formate framework come from the hydrolysis of DMF used as the solvent for the reaction.

Synthesis of $Dma_3Fe^{2+}{}_3Fe^{3+}For_{12}\cdot CO_2$. $Dma_3Fe^{2+}{}_3Fe^{3+}For_{12}\cdot CO_2$ was synthesized from α-$DmaFe^{2+}Fe^{3+}For_6$ compressed to 1.15 GPa in methanol or ethanol. During 5 days, the phase α crystal gradually dissolved and the reaction yielded small green cubic crystals (Figure S4). Single-crystal X-ray measurements were performed on a SuperNova diffractometer with a microfocus source (Cu Kα = 1.54178 Å) revealed that the new product is $Dma_3Fe^{2+}{}_3Fe^{3+}For_{12}\cdot CO_2$ (detailed structural data from ambient and low-temperature structural measurements are located in Table S9). Crystallographic Information Files (including low-temperature measurements) have been deposited in the Cambridge Structural Database (CCDC, www.ccdc.cam.ac.uk) with numbers CCDC 1893002−1893006.

High-Pressure Structural Measurements. A black trigonal single crystal of the α-$DmaFe^{2+}Fe^{3+}For_6$ has been mounted in a Merrill-Bassett diamond anvil cell (DAC) chamber,[90] then filled with isopropanol, Daphne 7474 oil, glycerol, methanol, and ethanol and isothermally compressed. The pressure inside the DAC was calibrated by the ruby-fluorescence method.[91,92] The gaskets of 0.3 mm stainless steel foil with spark-eroded holes 0.5 mm in diameter were used. The DAC was centered by the gasket-shadow method.[93] The compression of crystals was measured by single-crystal X-ray diffraction on Xcalibur Eos-CCD and Kuma Eos-CCD 4-circle diffractometers (Mo Kα = 0.71073 Å). The optimum diffractometer settings for measuring the reflection intensities were applied.[94] Crystallographic data were collected and preliminarily reduced with the CrysAlisPro, version 1.171.33.[95] The structure was solved by direct methods in program Shelxs and refined with Shelxl using the Olex2 suite.[96−98] The final crystal data are summarized in Tables 1 and 2 (see Tables S5−S8) and obtained Crystallographic Information Files have been deposited

DOI: 10.1021/acs.inorgchem.9b01817
Inorg. Chem. 2019, 58, 11773−11781

in the CCDC with numbers 1892942−1892949, 1892963 (for α-$DmaFe^{2+}Fe^{3+}For_6$), 1892964−1892966 (for γ-$DmaFe^{2+}Fe^{3+}For_6$), and 1892970−1892973 (for $DmaFe^{2+}For_3$). The high-pressure experiments were repeated several times each to eliminate possible other reasons of different transitions and reactions.

■ ASSOCIATED CONTENT

Supporting Information

The Supporting Information is available free of charge on the ACS Publications website at DOI: 10.1021/acs.inorgchem.9b01817.

Selected X-ray diffraction layers *hkl* reconstructed for the experiments at 1.00 and 1.40 GPa in glycerol; a schematic representation of the hp-$DmaFe^{2+}For_3$ crystal; detailed compressibility data for α-$DmaFe^{3+}Fe^{2+}For_6$, γ-$DmaFe^{3+}Fe^{2+}For_6$, and hp-$DmaFe^{2+}For_3$; photographs of the products recovered after redox reactions in methanol; and tables with site symmetry of the Fe atoms for all phases and detailed crystallographic data (PDF)

Accession Codes

CCDC 1892942−1892949, 1892963, 1892970−1892973, and 1893002−1893006 contain the supplementary crystallographic data for this paper. These data can be obtained free of charge via www.ccdc.cam.ac.uk/data_request/cif, or by emailing data_request@ccdc.cam.ac.uk, or by contacting The Cambridge Crystallographic Data Centre, 12 Union Road, Cambridge CB2 1EZ, UK; fax: +44 1223 336033.

■ AUTHOR INFORMATION

Corresponding Author

*E-mail: katran@amu.edu.pl.

ORCID

Szymon Sobczak: 0000-0001-8234-2503

Andrzej Katrusiak: 0000-0002-1439-7278

Author Contributions

The manuscript was written through contributions of all authors.

Funding

This study was supported by project OPUS 10 UMO-2015/19/B/ST5/00262 from the Polish National Science Centre. S.S. also thanks to the EU European Social Fund, Operational Program Knowledge Education Development, for Grant POWR.03.02.00-00-I023/17.

Notes

The authors declare no competing financial interest.

■ ACKNOWLEDGMENTS

Authors are grateful to Ms. Dominika Czerwonka for valuable discussions.

■ REFERENCES

(1) Nakamura, T.; Fu, D.-W.; Ge, J.-Z.; Xiong, R.-G.; Zhang, W.; Cai, H.-L.; Huang, S. D.; Zhang, Y. A Multiferroic Perdeutero Metal-Organic Framework. *Angew. Chem., Int. Ed.* **2011**, *50*, 11947−11951.

(2) Zhou, B.; Kobayashi, A.; Cui, H. B.; Long, L. S.; Fujimori, H.; Kobayashi, H. Anomalous Dielectric Behavior and Thermal Motion of Water Molecules Confined in Channels of Porous Coordination Polymer Crystals. *J. Am. Chem. Soc.* **2011**, *133*, 5736−5739.

(3) Li, W.; Probert, M. R.; Kosa, M.; Bennett, T. D.; Thirumurugan, A.; Burwood, R. P.; Parinello, M.; Howard, J. A. K.; Cheetham, A. K. Negative Linear Compressibility of a Metal-Organic Framework. *J. Am. Chem. Soc.* **2012**, *134*, 11940−11943.

(4) Li, W.; Thirumurugan, A.; Barton, P. T.; Lin, Z.; Henke, S.; Yeung, H. H. M.; Wharmby, M. T.; Bithell, E. G.; Howard, C. J.; Cheetham, A. K. Mechanical Tunability via Hydrogen Bonding in Metal-Organic Frameworks with the Perovskite Architecture. *J. Am. Chem. Soc.* **2014**, *136*, 7801−7804.

(5) Di Sante, D.; Stroppa, A.; Jain, P.; Picozzi, S. Tuning the Ferroelectric Polarization in a Multiferroic Metal-Organic Framework. *J. Am. Chem. Soc.* **2013**, *135*, 18126−18130.

(6) Zhang, W.; Xiong, R. G. Ferroelectric Metal-Organic Frameworks. *Chem. Rev.* **2012**, *112*, 1163−1195.

(7) Shang, R.; Xu, G. C.; Wang, Z. M.; Gao, S. Phase Transitions, Prominent Dielectric Anomalies, and Negative Thermal Expansion in Three High Thermally Stable Ammonium Magnesium-Formate Frameworks. *Chem. - Eur. J.* **2014**, *20*, 1146−1158.

(8) Krishna, R.; Van Baten, J. M. A Molecular Simulation Study of Commensurate-Incommensurate Adsorption of n-Alkanes in Cobalt Formate Frameworks. *Mol. Simul.* **2009**, *35*, 1098−1104.

(9) Jain, P.; Stroppa, A.; Nabok, D.; Marino, A.; Rubano, A.; Paparo, D.; Matsubara, M.; Nakotte, H.; Fiebig, M.; Picozzi, S.; Choi, E. S.; Cheetham, A. K; Draxl, C.; Dalal, N. S; Zapf, V. S Switchable Electric Polarization and Ferroelectric Domains in a Metal-Organic-Framework. *Npj Quantum Mater.* **2016**, *1*, 16012.

(10) Rossin, A.; Ienco, A.; Costantino, F.; Montini, T.; Di Credico, B.; Caporali, M.; Gonsalvi, L.; Fornasiero, P.; Peruzzini, M. Phase Transitions and CO2 Adsorption Properties of Polymeric Magnesium Formate. *Cryst. Growth Des.* **2008**, *8*, 3302−3308.

(11) Dybtsev, D. N.; Chun, H.; Yoon, S. H.; Kim, D.; Kim, K. Microporous Manganese Formate: A Simple Metal-Organic Porous Material with High Framework Stability and Highly Selective Gas Sorption Properties. *J. Am. Chem. Soc.* **2004**, *126*, 32−33.

(12) Señarís-Rodríguez, M. A.; Castro-García, S.; Gracia-Fernández, C.; Pato-Doldán, B.; Sánchez-Andújar, M.; Haghighirad, A. A.; Yáñez-Vilar, S.; López-Beceiro, J.; Gómez-Aguirre, L. C.; Ritter, F. Near Room Temperature Dielectric Transition in the Perovskite Formate Framework $[(CH_3)_2NH_2][Mg(HCOO)_3]$. *Phys. Chem. Chem. Phys.* **2012**, *14*, 8498.

(13) Li, W.; Wang, Z.; Deschler, F.; Gao, S.; Friend, R. H.; Cheetham, A. K. Chemically Diverse and Multifunctional Hybrid Organic-inorganic Perovskites. *Nat. Rev. Mater.* **2017**, *2* (3), 16099.

(14) McKellar, S. C.; Graham, A. J.; Allan, D. R.; Mohideen, M. I. H.; Morris, R. E.; Moggach, S. A. The Effect of Pressure on the Post-Synthetic Modification of a Nanoporous Metal-Organic Framework. *Nanoscale* **2014**, *6*, 4163−4173.

(15) Burrows, A. D.; Frost, C. G.; Mahon, M. F.; Richardson, C. Post-Synthetic Modification of Tagged Metal-Organic Frameworks. *Angew. Chem., Int. Ed.* **2008**, *47*, 8482−8486.

(16) Tilset, M.; Lillerud, K. P.; Kandiah, M.; Svelle, S.; Usseglio, S.; Olsbye, U. Post-Synthetic Modification of the Metal-organic Framework Compound UiO-66. *J. Mater. Chem.* **2010**, *20*, 9848.

(17) Park, H. J.; Cheon, Y. E.; Suh, M. P. Post-Synthetic Reversible Incorporation of Organic Linkers into Porous Metal-Organic Frameworks through Single-Crystal-to-Single-Crystal Transformations and Modification of Gas-Sorption Properties. *Chem. - Eur. J.* **2010**, *16*, 11662−11669.

(18) Evans, J. D.; Sumby, C. J.; Doonan, C. J. Post-Synthetic Metalation of Metal-Organic Frameworks. *Chem. Soc. Rev.* **2014**, *43*, 5933−5951.

(19) Farrusseng, D.; Canivet, J.; Quadrelli, A. Design of Functional Metal−Organic Frameworks by Post-Synthetic Modification. In *Metal−Organic Frameworks: Applications from Catalysis to Gas Storage*; Wiley-VCH Verlag GmbH & Co. KGaA: Weinheim, Germany, 2011; pp 23−48.

(20) Song, X.; Kim, T. K.; Kim, H.; Kim, D.; Jeong, S.; Moon, H. R.; Lah, M. S. Post-Synthetic Modifications of Framework Metal Ions in Isostructural Metal-Organic Frameworks: Core-Shell Heterostructures via Selective Transmetalations. *Chem. Mater.* **2012**, *24*, 3065−3073.

DOI: 10.1021/acs.inorgchem.9b01817
Inorg. Chem. 2019, 58, 11773−11781

(21) Zhou, T.; Du, Y.; Borgna, A.; Hong, J.; Wang, Y.; Han, J.; Zhang, W.; Xu, R. Post-Synthesis Modification of a Metal-Organic Framework to Construct a Bifunctional Photocatalyst for Hydrogen Production. *Energy Environ. Sci.* **2013**, *6*, 3229−3234.
(22) Zhang, Z.; Gao, W. Y.; Wojtas, L.; Ma, S.; Eddaoudi, M.; Zaworotko, M. J. Post-Synthetic Modification of Porphyrin-Encapsulating Metal-Organic Materials by Cooperative Addition of Inorganic Salts to Enhance CO_2/CH_4 Selectivity. *Angew. Chem., Int. Ed.* **2012**, *51*, 9330−9334.
(23) Servalli, M.; Ranocchiari, M.; Van Bokhoven, J. A. Fast and High Yield Post-Synthetic Modification of Metal-Organic Frameworks by Vapor Diffusion. *Chem. Commun.* **2012**, *48*, 1904−1906.
(24) Mulfort, K. L.; Farha, O. K.; Stern, C. L.; Sarjeant, A. A.; Hupp, J. T. Post-Synthesis Alkoxide Formation within Metal-Organic Framework Materials: A Strategy for Incorporating Highly Coordinatively Unsaturated Metal Ions. *J. Am. Chem. Soc.* **2009**, *131*, 3866−3868.
(25) Haneda, T.; Kawano, M.; Kawamichi, T.; Fujita, M. Direct Observation of the Labile Imine Formation through Single-Crystal-to-Single-Crystal Reactions in the Pores of a Porous Coordination Network. *J. Am. Chem. Soc.* **2008**, *130*, 1578−1579.
(26) Wang, Z.; Cohen, S. M. Postsynthetic Covalent Modification of a Neutral Metal-Organic Framework. *J. Am. Chem. Soc.* **2007**, *129*, 12368−12369.
(27) Tanabe, K. K.; Cohen, S. M. Postsynthetic Modification of Metal-Organic Frameworks - A Progress Report. *Chem. Soc. Rev.* **2011**, *40*, 498−519.
(28) Bloch, E. D.; Britt, D.; Lee, C.; Doonan, C. J.; Uribe-Romo, F. J.; Furukawa, H.; Long, J. R.; Yaghi, O. M. Metal Insertion in a Microporous Metal-Organic Framework Lined with 2,2′-Bipyridine. *J. Am. Chem. Soc.* **2010**, *132*, 14382−14384.
(29) Das, S.; Kim, H.; Kim, O. Metathesis in Single Crystal: Complete and Reversible Exchange of Metal Ions Constituting the Frameworks of Metal-Organic Frameworks. *J. Am. Chem. Soc.* **2009**, *131*, 3814−3815.
(30) Mukherjee, G.; Biradha, K. Post-Synthetic Modification of Isomorphic Coordination Layers: Exchange Dynamics of Metal Ions in a Single Crystal to Single Crystal Fashion. *Chem. Commun.* **2012**, *48*, 4293−4295.
(31) Ramamurthy, V.; Venkatesan, K. Photochemical Reactions of Organic Crystals. *Chem. Rev.* **1987**, *87*, 433−481.
(32) Hopf, H.; Greiving, H.; Jones, P. G.; Bubenitschek, P. Topochemical Reaction Control in Solution. *Angew. Chem., Int. Ed. Engl.* **1995**, *34*, 685−687.
(33) Boldyrev, V. V. Control of the Reactivity of Solids. *Annu. Rev. Mater. Sci.* **1979**, *9*, 455−469.
(34) Biradha, K.; Santra, R. Crystal Engineering of Topochemical Solid State Reactions. *Chem. Soc. Rev.* **2013**, *42*, 950−967.
(35) Kaiser, J.; Wegner, G.; Fischer, E. W. Topochemical Reactions of Monomers with Conjugated Triple-Bonds VII Mechanism of Transition from Monomer to Polymer Phase During Solid-State Polymerisation. *Isr. J. Chem.* **1972**, *10*, 157−171.
(36) van Eldik, R.; Klärner, F. G. *High Pressure Chemistry: Synthetic, Mechanistic, and Supercritical Applications*; Wiley-VCH, 2007.
(37) Bastron, V. C.; Drickamer, H. G. Solid State Reactions in Organic Crystals at Very High Pressure. *J. Solid State Chem.* **1971**, *3*, 550−563.
(38) Ciabini, L.; Bini, R.; Ceppatelli, M.; Citroni, M.; Schettino, V. Chemical Reactions at Very High Pressure. In *Advances in Chemical Physics*; Wiley-Blackwell, 2005; Vol. *131*, pp 105−242.
(39) Boldyreva, E. Mechanochemistry of Inorganic and Organic Systems: What Is Similar, What Is Different? *Chem. Soc. Rev.* **2013**, *42*, 7719.
(40) Prewitt, C. T.; Downs, R. T. High-Pressure Crystal Chemistry. *Reviews in Mineralogy & Geochemistry* **1998**, *37*, 283−318.
(41) Grochala, W.; Hoffmann, R.; Feng, J.; Ashcroft, N. W. The Chemical Imagination at Work in Very Tight Places. *Angew. Chem., Int. Ed.* **2007**, *46*, 3620−3642.
(42) Półrolniczak, A.; Sobczak, S.; Katrusiak, A. Solid-State Associative Reactions and the Coordination Compression Mechanism. *Inorg. Chem.* **2018**, *57*, 8942−8950.
(43) Warren, J. E.; Murrie, M.; Moggach, S. A.; Parois, P.; Lennie, A. R.; Rowantree, N.; Parsons, S.; Brechin, E. K.; Galloway, K. W. Polymerisation of a Cu(II) Dimer into 1D Chains Using High Pressure. *CrystEngComm* **2009**, *11*, 2601.
(44) Andrzejewski, M.; Katrusiak, A. Piezochromic Topology Switch in a Coordination Polymer. *J. Phys. Chem. Lett.* **2017**, *8*, 929−935.
(45) Allan, D. R.; Blake, A. J.; Huang, D.; Prior, T. J.; Schröder, M. High Pressure Co-Ordination Chemistry of a Palladium Thioether Complex: Pressure versus Electrons. *Chem. Commun.* **2006**, *2*, 4081−4083.
(46) Moggach, S. A.; Parsons, S. High Pressure Crystallography of Inorganic and Organometallic Complexes. In *Spectroscopic Properties of Inorganic and Organometallic Compounds*; The Royal Society of Chemistry, 2009; Vol. *40*, pp 324−354.
(47) Bujak, M.; Angel, R. J. High-Pressure- and Low-Temperature-Induced Changes in $[(CH_3)_3NH(CH_3)_3NH_3][SbCl_5]$. *J. Phys. Chem. B* **2006**, *110*, 10322−10331.
(48) Denner, W.; Schulz, H.; D'Amour, H. The Influence of High Hydrostatic Pressure on the Crystal Structure of Cesium Gold Chloride ($Cs_2Au^IAu^{III}Cl_6$) in the Pressure Range up to 52×10^8 Pa. *Acta Crystallogr., Sect. A: Cryst. Phys., Diffr., Theor. Gen. Crystallogr.* **1979**, *35*, 360−365.
(49) Ortiz, A. U.; Boutin, A.; Gagnon, K. J.; Clearfield, A.; Coudert, F. X. Remarkable Pressure Responses of Metal-Organic Frameworks: Proton Transfer and Linker Coiling in Zinc Alkyl Gates. *J. Am. Chem. Soc.* **2014**, *136*, 11540−11545.
(50) Clegg, J. K.; Brock, A. J.; Jolliffe, K. A.; Lindoy, L. F.; Parsons, S.; Tasker, P. A.; White, F. J. Reversible Pressure-Controlled Depolymerization of a Copper(II)-Containing Coordination Polymer. *Chem. - Eur. J.* **2017**, *23*, 12480−12483.
(51) Armbrüster, M.; Tse, J.; Heines, P.; Schwarz, U.; Keller, H.-L. Pressure-Induced Internal Redox Reaction of $Cs_2[PdI_4]\cdot I_2$, $Cs_2[PdBr_4]\cdot I_2$, and $Cs_2[PdCl_4]\cdot I_2$. *Inorg. Chem.* **2006**, *45*, 9818−9825.
(52) Zhang, J. P.; Lin, Y. Y.; Zhang, W. X.; Chen, X. M. Temperature- or Guest-Induced Drastic Single-Crystal-to-Single-Crystal Transformations of a Nanoporous Coordination Polymer. *J. Am. Chem. Soc.* **2005**, *127*, 14162−14163.
(53) Hu, C.; Englert, U. Crystal-to-Crystal Transformation from a Chain Polymer to a Two-Dimensional Network at Low Temperatures. *Angew. Chem., Int. Ed.* **2005**, *44*, 2281−2283.
(54) Lanza, A.; Germann, L. S.; Fisch, M.; Casati, N.; Macchi, P. Solid-State Reversible Nucleophilic Addition in a Highly Flexible MOF. *J. Am. Chem. Soc.* **2015**, *137*, 13072−13078.
(55) Mobin, S. M.; Srivastava, A. K.; Mathur, P.; Lahiri, G. K. Reversible Single-Crystal to Single-Crystal Transformations in a Hg(Ii) Derivative. 1D-Polymeric Chain 2D-Networking as a Function of Temperature. *Dalt. Trans.* **2010**, *39*, 8698−8705.
(56) Cai, W.; Gładysiak, A.; Anioła, M.; Smith, V. J.; Barbour, L. J.; Katrusiak, A. Giant Negative Area Compressibility Tunable in a Soft Porous Framework Material. *J. Am. Chem. Soc.* **2015**, *137*, 9296−9301.
(57) Edwards, D. M. *Electronic Transitions and the High Pressure Chemistry and Physics of Solids*; Springer Netherlands: Dordrecht, 2015; Vol. *24*.
(58) Slichter, C. P.; Drickamer, H. G. Pressure-Induced Electronic Changes in Compounds of Iron. *J. Chem. Phys.* **1972**, *56*, 2142−2160.
(59) Zhao, J.-P.; Hu, B.-W.; Lloret, F.; Tao, J.; Yang, Q.; Zhang, X.-F.; Bu, X.-H. Magnetic Behavior Control in Niccolite Structural Metal Formate Frameworks $[(CH_3)_2NH_2][Fe^{III}M^{II}(HCOO)_6]$ (M = Fe, Mn, and Co) by Varying the Divalent Metal Ions. *Inorg. Chem.* **2010**, *49*, 10390−10399.
(60) Hagen, K. S.; Naik, S. G.; Huynh, B. H.; Masello, A.; Christou, G. Intensely Colored Mixed-Valence Iron(II) Iron(III) Formate Analogue of Prussian Blue Exhibits Néel N-Type Ferrimagnetism. *J. Am. Chem. Soc.* **2009**, *131*, 7516−7517.

DOI: 10.1021/acs.inorgchem.9b01817
Inorg. Chem. 2019, 58, 11773−11781

(61) Cañadillas-Delgado, L.; Fabelo, O.; Rodríguez-Velamazán, J. A.; Lemée-Cailleau, M. H.; Mason, S. A.; Pardo, E.; Lloret, F.; Zhao, J. P.; Bu, X. H.; Simonet, V.; Colin, C. V.; Rodríguez-Carvajal, J. The Role of Order-Disorder Transitions in the Quest for Molecular Multiferroics: Structural and Magnetic Neutron Studies of a Mixed Valence Iron(II)-Iron(III) Formate Framework. *J. Am. Chem. Soc.* **2012**, *134*, 19772−19781.
(62) Sieradzki, A.; Pawlus, S.; Tripathy, S. N.; Gagor, A.; Ciupa, A.; Maczka, M.; Paluch, M. Dielectric Relaxation Behavior in Antiferroelectric Metal Organic Framework $[(CH_3)_2NH_2][Fe^{III}Fe^{II}(HCOO)_6]$ Single Crystals. *Phys. Chem. Chem. Phys.* **2016**, *18*, 8462−8467.
(63) Cairns, A. B.; Goodwin, A. L. Negative Linear Compressibility. *Phys. Chem. Chem. Phys.* **2015**, *17*, 20449−20465.
(64) Baughman, R. H.; Stafström, S.; Cui, C.; Dantas, S. O. Materials with Negative Compressibilities in One or More Dimensions. *Science* **1998**, *279*, 1522−1524.
(65) Cai, W.; Katrusiak, A. Conformationally Assisted Negative Area Compression in Methyl Benzoate. *J. Phys. Chem. C* **2013**, *117*, 21460−21465.
(66) Lim, T. C. 2D Structures Exhibiting Negative Area Compressibility. *Phys. Status Solidi B* **2017**, *254*, 1600682.
(67) Sobczak, S.; Chitnis, A.; Andrzejewski, M.; Maczka, M.; Gohil, S.; Garg, N.; Katrusiak, A. Framework and Coordination Strain in Two Isostructural Hybrid Metal-Organic Perovskites. *CrystEngComm* **2018**, *20*, 5348−5355.
(68) Collings, I. E.; Bykov, M.; Bykova, E.; Hanfland, M.; Van Smaalen, S.; Dubrovinsky, L.; Dubrovinskaia, N. Disorder-Order Transitions in the Perovskite Metal-Organic Frameworks $[(CH_3)_2NH_2][M(HCOO)_3]$ at High Pressure. *CrystEngComm* **2018**, *20*, 3512−3521.
(69) Wang, X. Y.; Gan, L.; Zhang, S. W.; Gao, S. Perovskite-like Metal Formates with Weak Ferromagnetism and as Precursors to Amorphous Materials. *Inorg. Chem.* **2004**, *43*, 4615−4625.
(70) Cliffe, M. J.; Goodwin, A. L. PASCal: A Principal-Axis Strain Calculator for Thermal Expansion and Compressibility Determination. *J. Appl. Crystallogr.* **2012**, *45*, 1321−1329.
(71) Drickamer, H. G.; Bastron, V. C.; Fisher, D. C.; Grenoble, D. C. The High-Pressure Chemistry of Iron. *J. Solid State Chem.* **1970**, *2*, 94−104.
(72) Hu, Q.; Kim, D. Y.; Yang, W.; Yang, L.; Meng, Y.; Zhang, L.; Mao, H. K. FeO2 and FeOOH under Deep Lower-Mantle Conditions and Earth's Oxygen-Hydrogen Cycles. *Nature* **2016**, *534*, 241−244.
(73) Mao, H. K.; Hu, Q.; Yang, L.; Liu, J.; Kim, D. Y.; Meng, Y.; Zhang, L.; Prakapenka, V. B.; Yang, W.; Mao, W. L. When Water Meets Iron at Earth's Core-Mantle Boundary. *Natl. Sci. Rev.* **2017**, *4*, 870−878.
(74) Nishi, M.; Kuwayama, Y.; Tsuchiya, J.; Tsuchiya, T. The Pyrite-Type High-Pressure Form of FeOOH. *Nature* **2017**, *547*, 205−208.
(75) Sinmyo, R.; Bykova, E.; Ovsyannikov, S. V.; McCammon, C.; Kupenko, I.; Ismailova, L.; Dubrovinsky, L. Discovery of Fe_7O_9: A New Iron Oxide with a Complex Monoclinic Structure. *Sci. Rep.* **2016**, *6*, 32852.
(76) Mączka, M.; Pasińska, K.; Ptak, M.; Paraguassu, W.; da Silva, T. A.; Sieradzki, A.; Pikul, A. Effect of Solvent, Temperature and Pressure on the Stability of Chiral and Perovskite Metal Formate Frameworks of $[NH_2NH_3][M(HCOO)_3]$ (M = Mn, Fe, Zn). *Phys. Chem. Chem. Phys.* **2016**, *18*, 31653−31663.
(77) Collings, I. E.; Dubrovinskaia, N.; van Smaalen, S.; Glazyrin, K.; Dubrovinsky, L.; Bykova, E.; Bykov, M.; Petitgirard, S.; Goodwin, A. L.; Hanfland, M.; Tucker, M. G. Structural Distortions in the High-Pressure Polar Phases of Ammonium Metal Formates. *CrystEngComm* **2016**, *18*, 8849−8857.
(78) Maczka, M.; Ptak, M.; Pawlus, S.; Paraguassu, W.; Sieradzki, A.; Balciunas, S.; Simenas, M.; Banys, J. Temperature- and Pressure-Dependent Studies of Niccolite-Type Formate Frameworks of $[NH_3(CH_2)_4NH_3][M_2(HCOO)_6]$ (M = Zn, Co, Fe). *Phys. Chem. Chem. Phys.* **2016**, *18*, 27613−27622.
(79) Collings, I. E.; Bykova, E.; Bykov, M.; Petitgirard, S.; Hanfland, M.; Paliwoda, D.; Dubrovinsky, L.; Dubrovinskaia, N. Neon-Bearing Ammonium Metal Formates: Formation and Behaviour under Pressure. *ChemPhysChem* **2016**, *17*, 3369−3372.
(80) Cheetham, A. K.; Zhou, H. D.; Jain, P.; Toby, B. H.; Kroto, H. W.; Ramachandran, V.; Dalal, N. S.; Clark, R. J. Multiferroic Behavior Associated with an Order-Disorder Hydrogen Bonding Transition in Metal-Organic Frameworks (MOFs) with the Perovskite ABX 3 Architecture. *J. Am. Chem. Soc.* **2009**, *131*, 13625−13627.
(81) Wang, Z.-M.; Zhang, Y.-J.; Liu, T.; Kurmoo, M.; Gao, S. $[Fe_3(HCOO)_6]$: A Permanent Porous Diamond Framework Displaying H2/N2 Adsorption, Guest Inclusion, and Guest-Dependent Magnetism. *Adv. Funct. Mater.* **2007**, *17*, 1523−1536.
(82) Cornia, A.; Caneschi, A.; Dapporto, P.; Fabretti, A. C.; Gatteschi, D.; Malavasi, W.; Sangregorio, C.; Sessoli, R. Manganese-(III) Formate: A Three-Dimensional Framework That Traps Carbon Dioxide Molecules. *Angew. Chem., Int. Ed.* **1999**, *38*, 1780−1782.
(83) Tian, Y.-Q.; Zhao, Y.-M.; Xu, H.-J.; Chi, C.-Y. CO 2 Template Synthesis of Metal Formates with a ReO 3 Net. *Inorg. Chem.* **2007**, *46*, 1612−1616.
(84) Reutemann, W.; Kieczka, H. Formic Acid. In *Ullmann's Encyclopedia of Industrial Chemistry*; Wiley-VCH Verlag GmbH & Co. KGaA: Weinheim, Germany, 2000.
(85) Boddien, A.; Mellmann, D.; Gartner, F.; Jackstell, R.; Junge, H.; Dyson, P. J.; Laurenczy, G.; Ludwig, R.; Beller, M. Efficient Dehydrogenation of Formic Acid Using an Iron Catalyst. *Science* **2011**, *333*, 1733−1736.
(86) Zakharov, B. A.; Goryainov, S. V.; Boldyreva, E. V. Unusual Seeding Effect in the Liquid-Assisted High-Pressure Polymorphism of Chlorpropamide. *CrystEngComm* **2016**, *18*, 5423−5428.
(87) Boldyreva, E. V.; Hanfland, M.; Kurnosov, A. V.; Zakharov, B. A.; Seryotkin, Y. V.; Paliwoda, D.; Tumanov, N. A. The Role of Fluids in High-Pressure Polymorphism of Drugs: Different Behaviour of β-Chlorpropamide in Different Inert Gas and Liquid Media. *RSC Adv.* **2016**, *6*, 92629−92637.
(88) Zakharov, B. A.; Tumanov, N. A.; Boldyreva, E. V. β-Alanine under Pressure: Towards Understanding the Nature of Phase Transitions. *CrystEngComm* **2015**, *17*, 2074−2079.
(89) Tan, J. C.; Jain, P.; Cheetham, A. K. Influence of Ligand Field Stabilization Energy on the Elastic Properties of Multiferroic MOFs with the Perovskite Architecture. *Dalt. Trans.* **2012**, *41*, 3949−3952.
(90) Merrill, L.; Bassett, W. A. Miniature Diamond Anvil Pressure Cell for Single Crystal X-Ray Diffraction Studies. *Rev. Sci. Instrum.* **1974**, *45*, 290−294.
(91) Piermarini, G. J.; Block, S.; Barnett, J. D.; Forman, R. A. Calibration of the Pressure Dependence of the R1ruby Fluorescence Line to 195 Kbar. *J. Appl. Phys.* **1975**, *46*, 2774−2780.
(92) Mao, H. K.; Xu, J.; Bell, P. M. Calibration of the Ruby Pressure Gauge to 800 Kbar under Quasi-Hydrostatic Conditions. *Journal of Geophysical Research* **1986**, *91*, 4673.
(93) Dera, P.; Katrusiak, A. Diffractometric Crystal Centering. *J. Appl. Crystallogr.* **1999**, *32*, 510−515.
(94) Budzianowski, A.; Katrusiak, A. High-Pressure Crystallographic Experiments with a CCD-Detector. In *High-Pressure Crystallography*; Springer Netherlands: Dordrecht, 2013; Vol. *140*, pp 101−112.
(95) Rigaku Corporation; Agilent Technologies. *Xcalibur CCD System, Crys Alis Pro Software System*, version 1.171.37.31; 2014.
(96) Sheldrick, G. M. A Short History of *SHELX*. *Acta Crystallogr., Sect. A: Found. Crystallogr.* **2008**, *64*, 112−122.
(97) Sheldrick, G. M. Crystal Structure Refinement with SHELXL. *Acta Crystallogr., Sect. C: Struct. Chem.* **2015**, *71*, 3−8.
(98) Dolomanov, O. V.; Bourhis, L. J.; Gildea, R. J.; Howard, J. A. K.; Puschmann, H. OLEX2: A Complete Structure Solution, Refinement and Analysis Program. *J. Appl. Crystallogr.* **2009**, *42*, 339−341.

■ NOTE ADDED AFTER ASAP PUBLICATION

This paper was published ASAP on August 22, 2019 with an incorrect entry in Table 2. The corrected version was reposted on September 2, 2019.

DOI: 10.1021/acs.inorgchem.9b01817
Inorg. Chem. 2019, 58, 11773−11781

(**R3**) Sobczak, S.; Fidelli, A.; Do, J.-L. Demopoulos, G.; Moores, A.; Friščić, T.; Katrusiak A. Toward elusive iodoplumbic acid '$HPbI_3$': first observation of hydronium salts of the PbI_3^- anion through high-energy isochoric synthesis at elevated temperature and pressure *ChemRxiv – archived* **2021**.

Toward elusive iodoplumbic acid 'HPbI$_3$': high-energy isochoric synthesis of hydronium salts of the PbI$_3^-$ anion at elevated temperature and pressure

Szymon Sobczak†,[a] Athena M. Fidelli†,[b] Jean-Louis Do,[b] George Demopoulos*,[c] Audrey Moores*,[b] Tomislav Friščić*[b] and Andrzej Katrusiak*[a]

[a] S. Sobczak, Prof. A. Katrusiak
Departament of Chemistry, Adam Mickiewicz University, Poznan
Uniwersytetu Poznanskiego 8, 61-619 Poznan, Poland
[b] Dr. Athena Fidelli, Prof. Tomislav Friščić
Department of Chemistry, McGill University
801 Sherbrooke St. W., H3A 0B8 Montreal, Canada
† contributed equally

Abstract: High-pressure and -temperature crystallization and X-ray diffraction crystallography have revealed hydronium salts of the proposed but never demonstrated iodoplumbic acid HPbI$_3$. Depending on the pressure range, the reaction of PbI$_2$ and aqueous concentrated hydriodic acid under isochoric conditions in a diamond anvil cell (DAC) held between 0.11 and 1.20 GPa produces two hydrated hydronium salts with compositions [H$_3$O][PbI$_3$]·nH$_2$O (n = 3, 4). Comprised of polymeric one-dimensional PbI$_3^-$ anions, these hydronium salts represent the so far best match for the elusive HPbI$_3$ progenitor of hybrid lead perovskites. We also reveal a new three-dimensional polymorph of lead iodide (PbI$_2$), so far known only as a layered structure.

The emergence of photovoltaic lead halide perovskites of the general formula APbI$_3$ (where A = alkaline metal, ammonium or organoammonium cation)[1] and composed of polymeric PbI$_3^-$ anions, such as NH$_4$PbI$_3$,[2] [CH$_3$NH$_3$]PbI$_3$[3–8] or CsPbI$_3$,[9–11] conducted via traditional[12] as well as unconventional methods,[13–16] has inspired extensive studies on the existence of iodoplumbic(II) acid. The proposed iodoplumbic acid HPbI$_3$ is anticipated to be the simplest member of this class of compounds and the formally fully inorganic progenitor of hybrid as well as inorganic lead(II) perovskites. Whereas iodoplumbic acid was first proposed as a solid-state precursor for the synthesis of hybrid perovskites in 2015 by Zhao *et al.*,[17] the existence of an acid with composition HPbI$_3$ has remained controversial. The proposed HPbI$_3$ material, which results from precipitation of solutions containing PbI$_2$ and HI from N,N-dimethylformamide (DMF), as shown by several groups, including Kanatzidis and Hillebrecht,[18,19] proved to be the dimethylammonium hybrid perovskite precursor [N(CH$_3$)$_2$H$_2$]PbI$_3$. Moreover, in another study Daub and Hillebrecht demonstrated that, while HPbI$_3$ is not accessible from the DMF solutions, the direct reaction of PbI$_2$ with concentrated (57% by weight) aqueous hydroiodic acid (HI) can produce two forms of hydrated iodoplumbic acids.[19] One exhibits the composition [H$_3$O]$_{2x}$[Pb$_{1-x}$I$_2$]·(2–2x)H$_2$O (**1**) ($x \approx 0.23$), and is based on two-dimensional (2-D) anionic CdI$_2$-type sheets with approximate composition [Pb$_3$I$_8^{2-}$]$_n$. The second one exhibits the composition (H$_3$O)$_2$Pb$_3$I$_8$·6H$_2$O (**2**) (Figure 1),

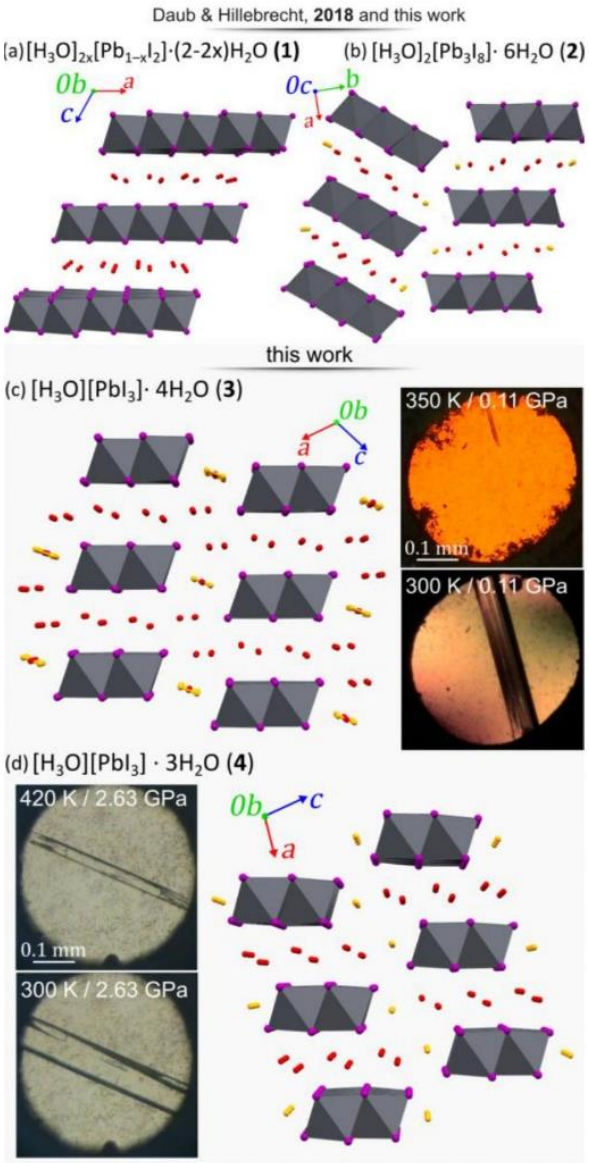

Figure 1. Four forms of hydrated iodoplumbic acid obtained in the reaction of PbI$_2$ with concentrated HI aqueous solution: (a) [H$_3$O]$_{2x}$[Pb$_{1-x}$I$_2$]·(2–2x)H$_2$O (compound **1**); (b) (H$_3$O)$_2$Pb$_3$I$_8$·6H$_2$O (**2**);[19] and those synthesized under high-p high-T: (c) (H$_3$O)PbI$_3$·4H$_2$O (**3**) and (d) (H$_3$O)PbI$_3$·3H$_2$O (**4**). The proposed sites of H$_3$O$^+$ cations are marked in orange. Photographs show crystals **3** and **4** *in situ* grown under pressure.

and is based on one-dimensional (1-D) polyanionic tapes of $[Pb_3I_8^{2-}]_n$. Compound **2** was reported to be the first product of either crystallization of PbI_2 from concentrated aqueous HI, or of the gas-solid reaction between PbI_2 and HI vapors. Upon standing in air, **2** quickly transforms into **1**. Anions in both **1** and **2** are separated by layers of water molecules containing hydronium ions. Overall, these prior studies indicate that an inorganic acid based on the PbI_3^- anion does not exist, and that the only accessible forms of iodoplumbic acid are hydronium salts of the $Pb_3I_8^{2-}$ anion.

We now show that the crystallization of PbI_2 from concentrated aqueous HI provides, at pressure above 0.11 GPa, access to hydronium salts of 1-D polyanions with composition PbI_3^-. Based on the chemical composition of the anion, and the absence of any ammonium or metal cations, the herein reported structures are the so far closest match for the elusive $HPbI_3$.

With $HPbI_3$ apparently inaccessible by solution techniques, our study has focused on less conventional reaction environments based on introduction of mechanical energy in the form of either ball milling (mechanochemistry) or by high-pressure chemistry. Our first exploration of reactivity between PbI_2 and concentrated aqueous hydroiodic acid HI(aq) was done mechanochemically, by milling of the two components in the stoichiometric ratio of PbI_2/HI = 1.5:1 (corresponding to the 3:8 stoichiometric ratio of Pb to I, respectively). Milling produced a bright yellow powder that, upon powder X-ray diffraction (PXRD) analysis, was found to match the previously reported **1** (Figure S4 in ESI). Increasing the amount of HI(aq) for the milling stoichiometric reaction of PbI_2/HI= 1:3 leads to the formation of compound **2** in a pure form (Figure S5 in ESI). Consistent with previous report, [18] upon standing in air **2** slowly transforms to **1** and, subsequently, to solid orange PbI_2. Having established that both reported hydrated iodoplumbic acids (**1** and **2**) are also accessible mechanochemically, but no new phases have been observed by milling, we turned to investigate the PbI_2/HI(aq) system under elevated pressures.

A different approach to introduce mechanical energy to a reaction system is high-pressure chemistry in a diamond anvil cell (DAC), where the application of force to the chemical-reaction system is in the form of static, hydrostatic pressure, allows for otherwise inaccessible thermodynamic coordinates.[20] As a reactor, the DAC represents an almost perfect closed system confining the reaction to the volume of ~0.02 mm^3 between two diamond culets and a steel gasket.[21] The introduction of energy to the chemical reaction in the DAC is achieved by compression, typically leading to the formation of new products.[22]

For each of the high-pressure reactions, a saturated solution of PbI_2 in HI(aq) was loaded in the DAC, and isothermally compressed. At 0.11 GPa, a polycrystalline mass precipitated that, upon subsequent recrystallization by cycles of gentle heating and cooling, led to a colorless, prism-shaped crystal suitable for structure determination by single-crystal X-ray diffraction (SCXRD). Structural analysis revealed for the crystal at 0.5 GPa a structure of formula $(H_3O)PbI_3 \cdot 4H_2O$ (**3**), comprising 1-D anionic PbI_3^- tapes composed of edge-sharing PbI_6-octahedra running along the crystallographic *b*-axis (Figure 1). Crystallographic parameters for **3** are distinct from those of previously reported[18] **1** or **2** (Figure 1, Table 1). The PbI_6 octahedra in the polyanion are slightly distorted, exhibiting four different lengths of Pb–I bonds around each metal ion: 3.046(2), 3.174(6) (twice), 3.250(6) (twice), and 3.3663(19) Å.

Table 1. Selected crystallographic data for compounds **1**-**4** and β-PbI_2 The structure of **1** was measured at ambient conditions on a crystal recovered from the DAC.

Compound	1[a]	2[19]	3	4	β-PbI_2
p	0.1 MPa	0.1 MPa	0.5 GPa	2.63 GPa	2.05 GPa
T	300 K	300 K	300 K	300 K	320 K
Space group	*C*2/*m*	*Pbam*	*I*2/*m*	$P2_1/m$	*C*2/*m*
a (Å)	7.8946(10)	10.033(3)	16.205(2)	9.57(3)	14.06(4)
b (Å)	4.5598(3)	30.126(7)	4.5170(1)	4.513(3)	4.4560(12
c (Å)	11.1985(18)	4.5610(10)	17.184(14	12.98(11)	10.540(6)
β (°)	118.023(19)	-	111.50(4)	95.9(6)	93.08(12)
V (Å^3)	355.859	1378.66(6)	1170.3(10	558(5)	654.9(17)
D_{calc} (g/cm^3)	4.638	4.290	3.666	3.883	7.013
Z / *Z'*	4/0.5	2/0.25	4/0.5	2/0.5	2/0.25

[a] The herein determined structure is analogous that previously reported $[H_3O]_{2x}[Pb_{1-x}I_2]\cdot(2-2x)H_2O$ (x=0.23), but with x = 0.20.

The polymeric anions are counterbalanced by hydronium cations. Although the presence of heavy atoms in **3** hinders the location of hydrogen atoms and distinguishing water molecules from H_3O^+ cations, the latter ones are likely to form the shortest contacts with the lead-based anions. The anions are separated by tapes of hydrogen-bonded water molecules (Figure 2) O-H···O hydrogen-bonded into an extended honeycomb-like structure, O···O distances of 2.63(4) Å, 2.68(6) Å, 2.79(7) Å, periodically interrupted by short contacts with the iodoplumbate(II) anions. These contacts are consistent with O–H···I hydrogen bonding of 3.2(2) Å, which is significantly shorter than the O···I non-bonding distance of about 3.5 Å expected from the van der Waals radii of O (1.50 Å) and I (2.04 Å) atoms.[23] In addition to oxygen atoms in these extended hydrogen-bonded nets of water molecules, the structure of **3** also exhibits 1-D arrays of oxygen atoms that are located between pairs of PbI_3^- anions (Figure 2b). The anionic framework of **3** is analogous to that in NH_4CdCl_3,[24] NH_4PbI_3,[25] $CsPbI_3$[26] and $RbPbI_3$.[27,28] Consequently, **3** can be seen as the acidic, hydronium-based analogue of these perovskite solids.

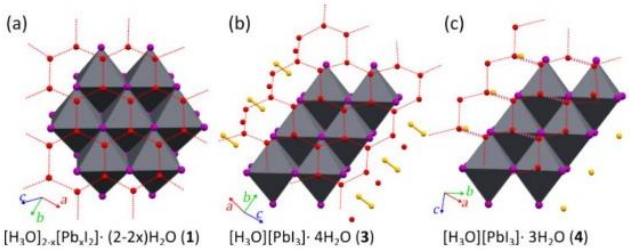

Figure 2. Crystal structures of (a) **1**; (b) **3**; and (c) **4** viewed perpendicular to the honeycomb water networks, with the longer O···O distances shown lighter. The oxygen atom sites suggested for H_3O^+ ions are shown in orange.

While increasing the pressure up to 1.20 GPa does not affect the crystals of **3**, releasing the pressure to 0.1 MPa quickly leads to their transformation into **1** (Figure 3). The transformation takes place in a single-crystal-to-single-crystal (SCSC) manner, as shown by X-ray diffraction on the crystal recovered from the DAC (see ESI), which revealed a clear matrix relationship between the lattices for the starting crystal of $H_3OPbI_3{\cdot}4H_2O$ (**3**) and the daughter phase **1**:

$$\begin{pmatrix} -1/3 & 0 & 1/3 \\ 0 & -1 & 0 \\ 2/3 & 0 & 1/3 \end{pmatrix} \begin{pmatrix} \boldsymbol{a_3} \\ \boldsymbol{b_3} \\ \boldsymbol{c_3} \end{pmatrix} = \begin{pmatrix} \boldsymbol{a_1} \\ \boldsymbol{b_1} \\ \boldsymbol{c_1} \end{pmatrix},$$

where a_1, b_1, c_1 and a_3, b_3, c_3 are sets of unit-cell parameters for **1** and **3**, respectively (Table 1).

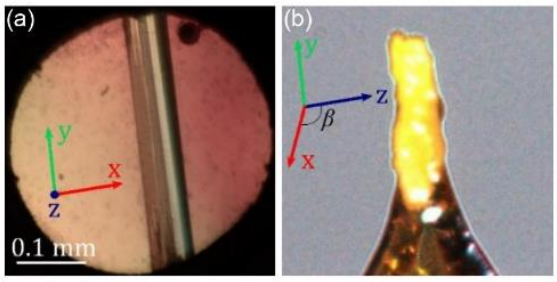

Figure 3. A crystal of **3**: as grown in the DAC (a) and (b) then recovered to ambient conditions and transformed to **1**, on a nylon loop. Crystal axes are indicated.

The quality of the crystal recovered to 0.1 MPa permitted the SCXRD measurement of lattice dimensions and structure refinement, which revealed monoclinic symmetry (Table 1, also SI). It is highly pseudo-symmetric (see the SI) and similar to the trigonal structure previously reported for **1**.[19] The two determinations of this layered structure of $[H_3O]_{2x}[Pb_{1-x}I_2]\cdot(2-2x)H_2O$ are consistent, except for somewhat lower x value resulting from our SCXRD measurement (0.20 compared to 0.23). The difference, we believe, indicates the possibility of **1** to adopt a wide range of compositions. The highly topotactic transformation from **3** to **1** requires a transition from 1-D to 2-D polyanions, in which some of the water and HI molecules leave the structure, probably by diffusion, while the edge-sharing connectivity of PbI_6 octahedra is preserved in both materials.

Above 1.2 GPa and at temperature above 420 K we obtained a pink-colored crystalline material (Figure 4a), different from **3**. Subsequent SCXRD was conducted at 320 K and above 2.05 GPa, revealing a high-pressure polymorph of PbI_2, herein termed β-PbI_2. The β-PbI_2 displays a reverse solubility, as we observed the growth of β-PbI_2 crystals on increasing the temperature, and their dissolution on cooling of the DAC. This new form of β-PbI_2 crystallizes in the monoclinic space group *C*2/*m* with unit-cell parameters *a* =14.10(3) Å, *b* = 4.4548(9) Å, *c* = 10.610(5) Å, and β = 92.89(11)° and it has a 3-D framework of alternating six- and seven- coordinated Pb^{2+} cations bridged by iodide ions (Table 1, Figure 4d,e, also see ESI). In this respect, it contrasts with the well-known 2-D layered structure with six-coordinated Pb^{2+} cations in α-PbI_2. To the best of our knowledge, this is the first observation of polymorphism in PbI_2. The formation of β-PbI_2 is consistent with higher pressure leading to increased coordination numbers due to stronger compression of anions than cations.[29]

We obtained a yet another crystalline phase by two different methods, either by recrystallizing **3** above 1.2 GPa or by a spontaneous recrystallization of β-PbI_2 crystals in the DAC below 350 K (Fig 3a-c). Below 1.2 GPa, at 320 K, pink β-PbI_2 dissolves and colorless needle-like crystals of another new phase (**4**) appear. Recrystallization by mild temperature oscillation produced a diffraction-quality single crystal of **4**, revealing another structure based on PbI_3^- polyanions (Table 1). Compound **4** was found to exhibit the formula $(H_3O)PbI_3{\cdot}3H_2O$, based on identical polymeric anions with edge-sharing PbI_6-octahedra, as those in **3**, but with a lower content of water of crystallization (Figure 3). The lower content of water in **4** compared to **3** is consistent with shorter I···I contacts at higher pressure. In this case also, four distinct lengths of Pb–I bonds are present in the anions: 2.81(4), 3.186(12) (twice), 3.232(11) (twice), and 3.34(4) Å. In **4**, oxygen atoms of water molecules form ribbons (about 10 Å wide). Within the ribbons shorter hydrogen bonds [O···O distances of 2.73(9) Å] are arranged into three 1-D zigzag chains, interconnected by weaker bonds [O···O distance of 3.1(2) Å] into a strongly distorted honeycomb motif. The ribbons separate the adjacent pairs of PbI_3^- polyanions . Additionally, there are also oxygen atoms not involved in any O···O contacts commensurate with hydrogen bonds, but they are each close to three iodine atoms of PbI_3^- anions, with O···I distances of 3.187(12) (twice), 3.232(11) (twice), 2.80(4) (once) and 3.33(4) (once) Å at (at 2.63 GPa, 300 K). According to the criterion of close vicinity to the anions, it is tempting to identify these oxygen atoms as belonging to hydronium species, although the location of protons by X-ray diffraction currently is not possible.

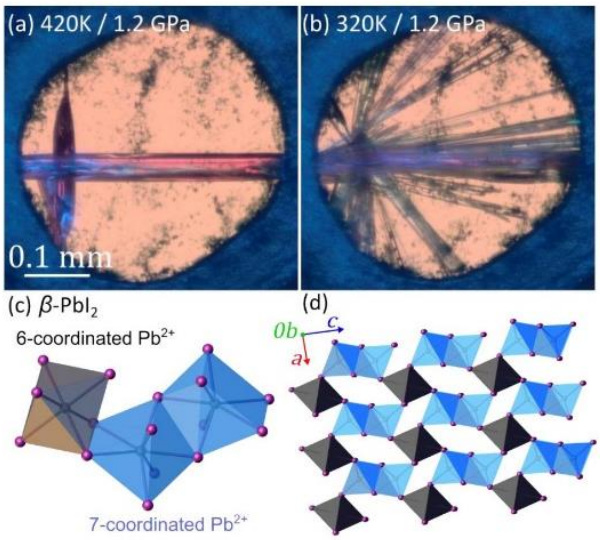

Figure 4. Pink single crystals of β-PbI_2 at 1.2 GPa and: (a) 420K and (b) 320 K covered by a bundle of needle crystals of **3**. Views of the *β*-PbI_2.structure: (c) six- and seven-coordinated Pb^{2+} cations and (d) the 3-dimensional network viewed along the crystallographic *b*-axis.

The series of structures of α- and β-forms of PbI_2, as well as its hydronium derivatives **1** – **4** exhibit polymeric Pb–I bonded 2D sheets or 1D ribbons, with a common motif of edge-sharing PbI_6 octahedra (cf. Figs. 1 and 2). They are by far and large the least compressed bonds constituting the scaffolds of the structures (Table 1), as clearly indicated by the structural relations between the members of this series of analogues, i.e. see the matrix relation between **1** and **3**. The cohesion forces between the polyanions are considerably weaker due to the contacts of the electronegative iodine atoms. These I···I contacts are most affected by high pressure. They are also most sensitive to the temperature and to the sample environment. The PbI_2 polymorphs and compounds **1** – **4** display stability regions mapped in the preference *p*-*T* diagram in Figure 5. The low-pressure end-member of this series is *α*-PbI_2 of clearly layer structure of 2D-sheets. The high-pressure end-member is *β*-PbI_2, where the Pb^{2+} cations become 7-coordinated and the additional Pb–I bonds bind the sheets into a 3D network. In structures **1** – **4** the vicinity of electronegative iodine atoms is filled by water and hydronium units that form $OH\cdots I^-$ and $OH^+\cdots I^-$ hydrogen bonds and compensate the electrostatically unfavored close locations of $I^{\delta-}$ atoms. The presence of four such compounds revealed for the pressure region up to 2.63 GPa is consistent with the high-sensitivity of the system to the external stimuli.

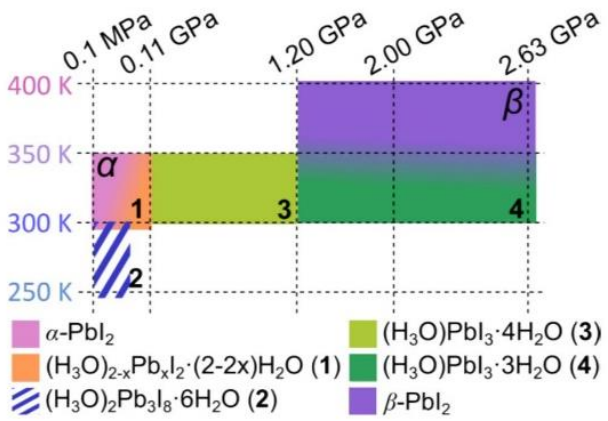

Figure 5. The *p*/*T* preference diagram of PbI_2 and HI(aq) system, with their end members of 2D-polymorph *α*-PbI_2 and 3D-polymorph β-PbI_2. Hydronium salt **1** and **2** were obtained by milling and vapor deposition, whereas **1**, **3**, **4** and *β*-PbI_2 through high-pressure synthesis in the DAC.

It is reasonable to expect that in the highly acidic environment of HI(aq), ionic pairs H_3O^+/I^- are intercalated, too. Their presence between the $(PbI_2)_n$ layers have the consequences consistent with the observed transformations between *α*-PbI_2 → **1** – **4** → *β*-PbI_2 compounds, where the increasing presence of acidic protons leads to the incorporation of the counteranions into the $(PbI_3^-)_n$. It is characteristic that we observed a desorption of water molecule above 1.2 GPa, because pressure above 1 GPa often destabilizes hydrates.[30,31] It is plausible that an analogues mechanism reduces the contents of intercalated water molecules and hydronium cations for the crystals in the environment of HI(aq), which leads to the *β*-PbI_2 polymorph as the end member of the series on the high-pressure side.

In summary, high-energy isochoric syntheses in a DAC revealed the existence of two new hydrated iodoplumbic acid solids, based on one-dimensional polyanions of composition PbI_3^-. The anion composition makes the herein observed high-pressure hydronium salts the so far best match to the elusive iodoplumbic acid $HPbI_3$, which is of fundamental importance as the progenitor of the highly popular class of hybrid perovskite materials. High-energy crystallization in the DAC also gave rise to the so far first known polymorph of PbI_2 which, unlike the commonly known form based on 2-dimensional sheets, presents an unprecedented PbI_2 structure based on Pb-I polyhedra connected into a three-dimensional structure. This work highlights the potential of crystallization from the high-energy environment as a simple and straightforward means to discover new phases, even in systems that have been extensively studied, over a long time. The herein observed hydrated iodoplumbic acids and a new form of PbI_2, together with previously reported structures, represent a closely related family of structures, in which the electrostatic repulsion between electronegative atoms is reduced by the intercalation of water molecules and hydronium cations, and is overcome completely at high pressure (>2 GPa) and

temperature (>350K), when a new 3D polymorph β-PbI_2 appears.

Keywords: high-pressure chemistry • led halide perovskites • iodoplumbic acid • lead(II) iodide polymorphism • mechanochemistry

[1] Y. Zheng, H. Sato, P. Wu, H. J. Jeon, R. Matsuda, S. Kitagawa, *Nat. Commun.* **2017**, *8*, 100.
[2] L.-Q. Fan, J.-H. Wu, *Acta Crystallogr. Sect. E* **2007**, *63*, i189–i189.
[3] J. Burschka, N. Pellet, S. J. Moon, R. Humphry-Baker, P. Gao, M. K. Nazeeruddin, M. Grätzel, *Nature* **2013**, *499*, 316–319.
[4] N. J. Jeon, J. H. Noh, Y. C. Kim, W. S. Yang, S. Ryu, S. Il Seok, *Nat. Mater.* **2014**, *13*, 897–903.
[5] H. Z. Sheng Huang, Peng Huang, Lei Wang, Junbo Han, Yu Chen, *Adv. Mater.* **2019**, *31* , 1903830.
[6] M. Szafrański, A. Katrusiak, *J. Phys. Chem. Lett.* **2016**, *7*, 3458–3466.
[7] M. Szafrański, A. Katrusiak, *J. Phys. Chem. Lett.* **2017**, *8*, 2496–2506.
[8] M. Shirayama, H. Kadowaki, T. Miyadera, T. Sugita, M. Tamakoshi, M. Kato, T. Fujiseki, D. Murata, S. Hara, T. N. Murakami, S. Fujimoto, M. Chikamatsu, H. Fujiwara, *Phys. Rev. Appl.* **2016**, *5*, 1–25.
[9] D. Prochowicz, R. Runjhun, M. M. Tavakoli, P. Yadav, M. Saski, A. Q. Alanazi, D. J. Kubicki, Z. Kaszkur, S. M. Zakeeruddin, J. Lewiński, M. Grätzel, *Chem. Mater.* **2019**, *31*, 1620–1627.
[10] Y. Wang, M. Ibrahim Dar, L. K. Ono, T. Zhang, M. Kan, Y. Li, L. Zhang, X. Wang, Y. Yang, X. Gao, Y. Qi, M. Grätzel, Y. Zhao, *Science,* **2019**, *365*, 591–595.
[11] W. Ahmad, J. Khan, G. Niu, J. Tang, *Sol. RRL* **2017**, *1*, 1–9.
[12] T. Baikie, Y. Fang, J. M. Kadro, M. Schreyer, F. Wei, S. G. Mhaisalkar, M. Graetzel, T. J. White, *J. Mater. Chem. A* **2013**, *1*, 5628–5641.
[13] D. Prochowicz, M. Franckevičius, A. M. Cieślak, S. M. Zakeeruddin, M. Grätzel, J. Lewiński, *J. Mater. Chem. A* **2015**, *3*, 20772–20777.
[14] D. Prochowicz, P. Yadav, M. Saliba, M. Saski, S. M. Zakeeruddin, J. Lewiński, M. Grätzel, *Sustain. Energy Fuels* **2017**, *1*, 689–693.
[15] W. Huang, J. S. Manser, S. Sadhu, P. V. Kamat, S. Ptasinska, *J. Phys. Chem. Lett.* **2016**, *7*, 5068–5073.
[16] Y. Zong, Y. Zhou, M. Ju, H. F. Garces, A. R. Krause, F. Ji, G. Cui, X. C. Zeng, N. P. Padture, S. Pang, *Angew. Chem. Int. Ed.* **2016**, *55*, 14723–14727.
[17] F. Wang, H. Yu, H. Xu, N. Zhao, *Adv. Funct. Mater.* **2015**, *25*, 1120–1126.
[18] W. Ke, I. Spanopoulos, C. C. Stoumpos, M. G. Kanatzidis, *Nat. Commun.* **2018**, *9*:4785.
[19] M. Daub, H. Hillebrecht, *Zeit. Anorg. Allg. Chemie* **2018**, *644*, 1393–1400.
[20] A. Katrusiak, *Acta Cryst.* **2019**, *B75*, 918–926.
[21] A. Katrusiak, in *Int. Tables Crystallogr. (2019). Vol. H.*, **2019**, pp. 156–173.
[22] S. Sobczak, A. Katrusiak, *Inorg. Chem.* **2019**, *58*, 11773–11781.
[23] S. Alvarez, *Dalt. Trans.* **2013**, *42*, 8617–8636.
[24] H. Brasseur, L. Pauling, *J. Am. Chem. Soc.* **1938**, *60*, 2886–2890.
[25] D. Bedlivy, K. Mereiter, *Acta Cryst.* **1980**, *B36*, 782–785.
[26] C. K. Møller, *Nature* **1958**, *182*, 1436–1436.
[27] H. J. Haupt, F. Huber, C. Krüger, H. Preut, D. Thierbach, *Zeit. Anorg. Allg. Chemie* **1977**, *436*, 229–236.
[28] D. M. Trots, S. V. Myagkota, *J. Phys. Chem. Solids* **2008**, *69*, 2520–2526.
[29] A. Półrolniczak, S. Sobczak, A. Katrusiak, *Inorg. Chem.* **2018**, *57*, 8942–8950.
[30] H. Tomkowiak, A. Olejniczak, A. Katrusiak, *Cryst. Growth Des.* **2013**, *13*, 121–125.
[31] F. Safari, A. Olejniczak, A. Katrusiak, *Cryst. Growth Des.* **2020**, *20*, 3112–3118.

(**R4**) Sobczak, S.; Drożdż, W.; Lampronti, G. I.; Belenguer, A. M. A.; Katrusiak, A.; Stefankiewicz, A. R. Dynamic Covalent Chemistry under High-Pressure: A New Route to Disulfide Metathesis. *Chem. - A Eur. J.* **2018**, *24* (35), 8769–8773

ChemPubSoc Europe

DOI: 10.1002/chem.201801740

CHEMISTRY A European Journal Communication

High-Pressure Chemistry

Dynamic Covalent Chemistry under High-Pressure:A New Route to Disulfide Metathesis

Szymon Sobczak,[a] Wojciech Drożdż,[a, b] Giulio I. Lampronti,[c, d] Ana M. Belenguer,[d] Andrzej Katrusiak,*[a] and Artur R. Stefankiewicz*[a, b]

Abstract: This work describes, for the first time, the application of combined pressure and temperature stimuli in disulfide metathesis reactions. In the system studied, above a pressure of 0.2 GPa, equimolar amounts of symmetric disulfides bis 4-chlorophenyl disulfide [$(4\text{-ClPhS})_2$] and bis 2-nitrophenyl disulfide [$(2\text{-NO}_2\text{PhS})_2$] react to give the heterodimeric product 4-Cl-PhSSPh-2-NO_2. In contrast to experiments conducted in solution at atmospheric pressure or in mechanochemical experiments under ball-mill grinding conditions, there is no necessity to use a base or thiolate anion as a catalyst for the exchange reaction under investigated conditions. Single-crystal and powder X-ray diffraction revealed also that, despite the high-pressure conditions of this reaction, the heterodimeric-disulfide product unexpectedly crystallizes into the low-density polymorph A. This counterintuitive result contrasts with the high-pressure stability of the higher-density polymorph B, confirmed by its compression up to 2.8 GPa with no signs of a phase transition.

There is ongoing demand for the development of stimuli-responsive materials, and a great deal of work has been dedicated to the generation of molecular and supramolecular systems that can be crafted into functional smart materials.[1] Investigation of stimuli-responsive molecular behavior can facilitate better understanding of biological systems but also accelerate the development of artificial "intelligent" materials capable of reversible structural, electronic, and chemical modification in response to an external stimulus, such as temperature, pH, or light.[2] In this context, the emergence of dynamic covalent chemistry (DCC) has substantially influenced chemical synthesis, with the concept relying on the formation/breakage of reversible covalent bonds in response to the external environment.[3] Among various dynamic covalent bonds, those of disulfides are important due to their pivotal roles in biology, for example in stabilization of the secondary structures of proteins.[4] Although disulfides are relatively stable, the kinetics of their production, reduction, isomerization, and interconversion reactions are highly pH-sensitive, commonly attaining maximum rates in the pH range 7–9. In biological systems, many disulfide exchange processes are controlled and catalyzed by delicate enzyme machineries, providing elegant examples of one form of DCC. In the usual solution state, thiol/disulfide exchange involves nucleophilic displacement (S_N2) of the thiolate anion from the disulfide (cleavage of the original S–S bond), through attack by another thiolate anion and, finally, protonation of the liberated thiolate moiety.[5] Another exchange mechanism involving homolytic cleavage to give radicals, followed by the recombination of the disulfide bond, is also possible.[6]

The reversibility of disulfide bonds has been exploited in the construction of many complex functional architectures, for example, macrocycles, catenanes, knots, cages, and self-replicating systems.[4,7] The synthesis of functional disulfide molecular systems displays great sensitivity to external stimuli (physical or chemical), which can significantly alter the position of the reaction equilibrium.[8] The most widely used chemical stimuli involve the use of template molecules or pH.[9] The Ramström group showed that disulfide exchange is possible by application of phosphine,[10] whereas the group of Pittelkow discovered exchange between diselenides and disulfides at neutral pH.[11] On the other hand, Alfonso et al. showed the effect of DMSO on the thiol-disulfide exchange.[12] Physical stimuli include, light, temperature, ultrasound, or pressure and, though the first three have been previously employed,[13] to the best of our knowledge, no investigation into exchange of disulfides under high-pressure conditions has been published.

The application of pressure as a variable in chemical studies can lead to the discovery of new materials with unique properties and can provide an efficient means of modifying the structure of crystals.[14] Within a relatively low pressure range of a few GPa the volume of molecular crystals can be compressed by as much as 80% and molecular conformations and intermo-

[a] S. Sobczak, W. Drożdż, Prof. A. Katrusiak, Dr. A. R. Stefankiewicz
Faculty of Chemistry, Adam Mickiewicz University
Umultowska 89b, 61-614 Poznań (Poland)
E-mail: katran@amu.edu.pl
ars@amu.edu.pl

[b] W. Drożdż, Dr. A. R. Stefankiewicz
Centre for Advanced Technologies
Adam Mickiewicz University
Umultowska 89c, 61-614 Poznań (Poland)

[c] G. I. Lampronti
Department of Earth Sciences
University of Cambridge
Downing St, Cambridge, CB2 3EQ (UK)

[d] G. I. Lampronti, A. M. Belenguer
Department of Chemistry, University of Cambridge
Lensfield Road, Cambridge, CB2 1EW (UK)

Supporting information and the ORCID identification number(s) for the author(s) of this article can be found under:
https://doi.org/10.1002/chem.201801740.

lecular interactions can be markedly changed. Consequently, pressure has been used for generating new polymorphs,[15] new solvates,[16] and new reaction pathways when activation volumes differ.[17] In particular, diamond-anvil cell high-pressure experiments have been employed in the transformations of intramolecular contacts,[18] formation of new coordinate bonds,[19] or conformational conversions in disulfide compounds.[20] This indicates that exchange reactions of weakly bound species could be triggered by the application of pressure only, leading to a new, unexplored, catalyst-free, high-pressure DCC field.

Here, we report a new approach to the disulfide-exchange reaction, in which high pressure was used as a physical stimulus in the reconfiguration process within DCC. We have shown that, above the pressure of 0.2 GPa equimolar amounts of symmetric disulfide homodimers, [(4-ClPhS)$_2$] and [(2-NO$_2$PhS)$_2$], react in the absence of base catalyst to give the heterodimeric product 4-Cl-PhSSPh-2-NO$_2$. To the best of our knowledge, this is the first example where high pressure imposed at a mildly elevated temperature has been used to promote a disulfide exchange reaction under non-basic and non-reducing conditions. The use of the diamond-anvil cell (DAC) chamber in the conducted experiments made it possible not only to work under high pressure conditions but also to control the temperature of the reaction, which proved to be necessary to dissolve the reaction substrates.

The formation of heterodimeric product 4-Cl-PhSSPh-2-NO$_2$ was investigated by means of four distinct synthetic methodologies (Figure 1). In general, the metathesis of aromatic disulfides is not spontaneous and requires a base catalyst (DBU, 1,8-diazabicycloundec-7-ene was used in the present studies). In solution state, the reaction between equimolar amounts of two homodimers [(4-ClPhS)$_2$] and [(2-NO$_2$PhS)$_2$], in the presence of base (DBU) led to a mixture of the initial substrates and the heterodimeric product 4-Cl-PhSSPh-2-NO$_2$ in the statistical 1:1:2 ratio (Figure 1a).[21] The same reaction was further explored under liquid-assisted grinding (LAG) and neat grinding (NG) conditions (Figure 1b and c). It has been shown that

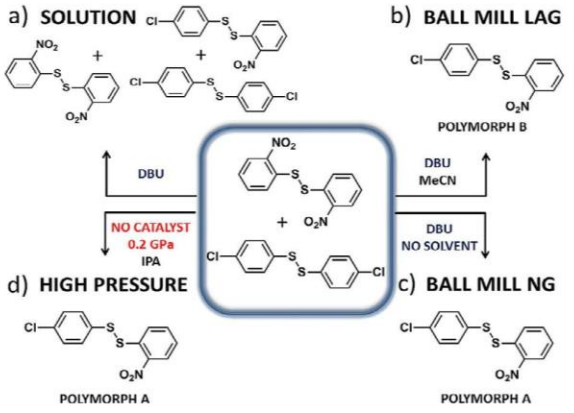

Figure 1. Generation of disulfide structures via four different synthetic methodologies: a) in solution; b) under liquid-assisted grinding (LAG) conditions; c) under neat grinding (NG) conditions; d) under high-pressure conditions.

in the solid suspension in slurry at 0.1 MPa/300 K and in the solid state under milling conditions, the thermodynamic equilibrium DCC shown below in Equation (1):

$$(4\text{-Cl-PhS})_2 + (2\text{-NO}_2\text{PhS})_2 = 2\,(4\text{-Cl-PhSSPh-2-NO}_2) \qquad (1)$$

lies very much to the right, with the mole fraction often exceeding 95% of heterodimer in the reported experiments.[21,25] The results that we present here suggest that this holds also at high pressure. Due to experimental constraints, we were not able to determine for certain whether this reaction achieved thermodynamic equilibrium DCC composition in the solid precipitate in any of the experiments presented. However, the fact that the homodimers react to give the heterodimer shows that under high pressure conditions such thermodynamic equilibrium DCC composition can, in principle, be achieved even in the absence of a catalyst.

Mechanochemistry using manual or ball-mill grinding equipment is emerging as an attractive and sustainable synthetic tool.[22] LAG, a technique which consists of grinding solid materials in the presence of a few drops of solvent, has dramatically broadened the applications of mechanochemistry;[23] LAG often accelerates reaction kinetics and indeed sometimes yields different outcomes to NG techniques.[21,24] We extensively investigated the exchange reaction of two homodimers under LAG and NG conditions, which resulted in the generation of two different polymorphs of the heterodimeric product 4-Cl-PhSSPh-2-NO$_2$, namely, low density polymorph A (CSD refcode FUQLIM01, space group $P2_1/n$) and high density polymorph B (CSD refcode FUQLIM, space group $P\bar{1}$). The former was generated under ball-mill NG conditions, whereas polymorph B was formed under ball-mill LAG conditions where a few drops of MeCN (>23 μL per 200 mg) were added to the powder.[21,25] The reaction yield is 50% in solution, whereas it is over 97% under mechanochemical conditions. These studies have also demonstrated a thermodynamic control of the product distribution: the relative stabilities of the two polymorphs have been shown to be affected by crystal surface solvation coupled with the nanosize nature of the milled powder. These thermodynamic concepts are general and apply to all systems.[25b]

For the purpose of investigating the disulfide exchange reaction under high pressure conditions several solvents were tested, of which 2-propanol (IPA) proved to give the best results both in terms of single-crystal quality of the product and reaction yield quantification, as explained below (Figure 2 and the Supporting Information, section 4.2). Because of the small quantities of substrates contained in the DAC chamber, we used the methods of powder and single-crystal diffraction for identifying the products recovered after the reactions. In a typical experiment, an equimolar mixture of homodimers [(4-ClPhS)$_2$] and [(2-NO$_2$PhS)$_2$] was added at room temperature to an appropriate solvent and loaded into a DAC chamber at appropriate concentrations, where disulfide exchange under high-pressure conditions was investigated (Figure 2a, for detailed experimental procedures, see chapter 4 in the Supporting Information). The lowest pressure at which reaction be-

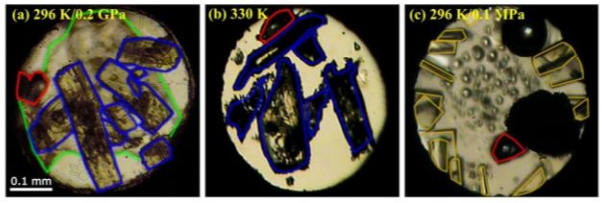

Figure 2. The DAC high-pressure chamber in three stages of the disulfide-exchange reaction: (a) mixture of crystals of both homodimers ([(4-ClPhS)$_2$] and [(2-NO$_2$PhS)$_2$], encircled in green and blue, respectively) and a ruby chip for pressure calibration (encircled red) in IPA at 0.2 GPa/296 K; (b) reaction mixture at 330 K showing completely dissolved [(4-ClPhS)$_2$]; (c) crystals of generated heterodimer 4-Cl-PhSSPh-2-NO$_2$ (encircled yellow) at 0.1 MPa/296 K (an air bubble testifies to the released pressure); photos from taken in experiment No. 3 (Supporting Information, section 4.2.3).

tween two homodimers occurred was 0.2 GPa. The solubility of both homodimers, ([(2-NO$_2$PhS)$_2$] being generally significantly less soluble than [(4-ClPhS)$_2$]), under these conditions was found to be several times lower than that under ambient conditions. Initially, the reaction mixture was heated to 330 K causing dissolution of homodimer [(4-ClPhS)$_2$] (Figure 2b), whereas the second component [(2-NO$_2$PhS)$_2$] dissolved at 349 K. The reaction mixture thus prepared was heated at 323 K for 5 h after which it was gradually cooled to room temperature and the pressure was released to 0.1 MPa. This led to precipitation of a crystalline material (Figure 2c), which was recovered from the DAC and characterized by single-crystal X-ray diffraction measurements. The unit-cell dimensions and space-group symmetry unequivocally showed the exclusive formation of the heterodimeric disulfide product 4-Cl-PhSSPh-2-NO$_2$. Furthermore, the product was obtained solely in the form of low density polymorph A. In order to eliminate the possibility of the presence of any ingredients acting as the catalyst promoting the heterodimer, all high-pressure reactions were repeated on super-clean substrates and consistent results have been obtained.

The high-pressure synthesis experiments were performed at various pressures (from 0.18 to 0.85 GPa), temperatures (from 296 to 495 K, increased till almost all of the substrates were dissolved) and in three different solvents: 2-propanol (IPA), methanol, and acetonitrile. Experiments carried out under various reaction conditions were aimed at investigating their effect on the form of the product obtained as well as generation of the best quality material possible for X-ray analysis. We established that the solvent used for the high-pressure reactions significantly affects the final form of the product. When IPA was employed the product precipitated in the form of single crystals of heterodimer 4-Cl-PhSSPh-2-NO$_2$ solely as polymorph A (see the Supporting Information, section 4.2). On the other hand, the reaction in acetonitrile yielded only very small crystals of 4-Cl-PhSSPh-2-NO$_2$, however in this case, a mixture of both polymorphs A and B were identified in a series of single-crystal diffraction measurements. Unfortunately, despite a number of attempts (various reaction conditions were tested, namely distinct concentrations, pressures, temperatures, and incubation times) to grow single crystals from the material generated in the reaction in methanol, only fine powders were obtained (see the Supporting Information, section 4.3).

To confirm the results obtained by means of single-crystal X-ray crystallography, an additional experiment was performed in which we collected the polycrystalline material obtained in the DAC chamber with IPA as a solvent and gathered it with immersion oil on a nylon loop. A 1D powder pattern (see Figure S22a in the Supporting Information) was obtained by integrating the frames collected over 2θ. A Rietveld refinement performed on this pattern after a background subtraction (see Figure S22b) showed that the polycrystalline material was predominantly polymorph A. The so obtained PXRD pattern is also here compared to those of polymorph A (blue) and B (red) (Figure 3). It is clear that polymorph B does not match the experimental pattern.

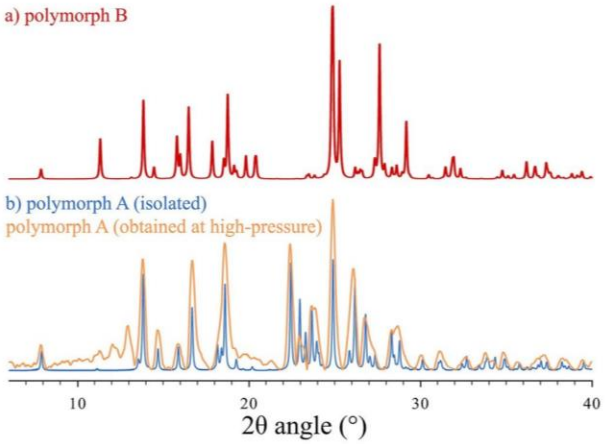

Figure 3. X-ray diffraction patterns of heterodimer 4-Cl-PhSSPh-2-NO$_2$ a) in the form of polymorph B (marked as red); b) in the form of polymorph A (marked as blue) superimposed with the data obtained from the material collected from the experiment at high pressure (marked as orange).

To further characterize the nature of the reactions, we investigated the possibility of phase transition between low-density polymorph A and high-density polymorph B of heterodimer 4-Cl-PhSSPh-2-NO$_2$ under high pressure conditions. For the high-pressure in situ experiments, crystals of heterodimer 4-Cl-PhSSPh-2-NO$_2$ in the polymorph B form were used. We employed a Merrill-Bassett DAC, modified by mounting the diamond anvil directly on steel supports with conical windows.[26] The gaskets were made of steel foil, 0.3 mm thick, with spark-eroded 0.4 mm holes. Pressure was calibrated by the R1 ruby-line shift, measured by a photon control spectrometer affording 0.02 GPa accuracy.[27] The structure of polymorph B was refined starting from its ambient-pressure structure[28] by full-matrix least squares fitting with SHELXL;[29] the Olex2 interface was used.[30] The unit-cell parameters of polymorph B decreased monotonically up to 2.8 GPa (Figure 4, see the Supporting Information for details) and no phase transitions were observed.

Heterodimeric polymorphs A and B display a significant density difference of 1.554 and 1.619 g cm^{-3} at 0.1 MPa (cf. Sup-

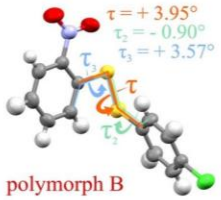

Figure 4. Heterodimer in polymorph B with indicated changes of torsion angles between 0.1 MPa and 2.8 GPa.

porting Information Table S4, see also ref. [28]), respectively, suggesting that polymorph B should be more stable at high pressure than polymorph A.[31] In terms of the average compression of molecular crystals, this difference of 0.020 g cm^{-3} is usually generated by about 0.15 GPa. Nonetheless, despite the high-pressure conditions, we obtained the heterodimer in the form of low-density polymorph A. In addition, our experimental data show that polymorph B does not convert into polymorph A at high pressure. Therefore, it is plausible that the reaction product nucleated in the form of low-density polymorph A, in accordance with Ostwald's rule of stages and despite that it is in the metastable state under the high-pressure conditions.

At the present stage of the study, two explanations of these results are possible. In the first scenario, at 150 MPa and above 400 K polymorph A becomes more stable than polymorph B. Under these conditions, the heterodimer product precipitates in the form of the more stable polymorph A. When the temperature is lowered at isochoric conditions polymorph B becomes more stable, but the heterodimer crystals continue to grow in the form of nucleated form A, in the absence of any seeds of polymorph B. Consequently, despite the high-pressure preference of polymorph B at 20 °C, polymorph A is obtained instead.

Alternatively, polymorph B is more stable than polymorph A throughout the high-pressure high-temperature range. Then the nucleation of the low-density polymorph A occurs according to Ostwald's rule of stages.[32] Polymorph A has been shown to be more stable than polymorph B when the crystal size is in the range of tens of nm at ambient pressure.[22b] When the DAC is cooled, the crystals grow in this nucleated form in isochoric conditions down to room temperature and the heterodimer product is recovered in the form of the metastable polymorph A.

We have successfully applied a new approach to disulfide exchange reactions by using the effect of pressure instead of catalytic/reducing agents. Particular conditions of pressure and temperature allow an equimolar mixture of the symmetrical disulfides [(4-ClPhS)$_2$] and [(2-NO$_2$PhS)$_2$] to react to form exclusively the heterodimer 4-Cl-PhSSPh-2-NO$_2$ in the absence of any base catalyst in a range of solvents. The purchased homodimers were purified by recrystallization (see the Supporting Information, section 1.1) for the experiments here discussed. Therefore, we exclude that the phenomena observed could possibly be explained by some contaminant acting as a catalyst at high temperature and/or pressure. The absence of a catalyst is remarkable, as it proves that the reaction proceeds under the influence of physical stimuli only. Therefore, the experimental results here presented show that supercritical or close to supercritical conditions are particularly attractive as they provide alternative catalyst-free high-pressure and high-temperature routes for DCC processes requiring a catalytic agent.

Acknowledgements

We thank National Centre for Research and Development (grant LIDER/024/391/L-5/13/NCBR/2014) and Polish National Science Centre (grant PRELUDIUM 2017/27/N/ST5/00693) for financial support. We are grateful to the EPSRC (A.M.B.) and Prof. Simon Redfern and the Department of Earth Sciences and the University of Cambridge for general support (G.I.L.). We are grateful to Prof Jeremy K. M. Sanders and Prof. Jack Harrowfield for important discussions on this topic (A.R.S.).

Conflict of interest

The authors declare no conflict of interest.

Keywords: disulfides · dynamic covalent chemistry · high pressure · mechanochemistry · reversible chemistry

[1] a) P. Theato, B. S. Sumerlin, R. K. O'Reilly, T. H. Epps III, *Chem. Soc. Rev.* **2013**, *42*, 7055 – 7056; b) A. Gorczyński, J. M. Harrowfield, V. Patroniak, A. R. Stefankiewicz, *Chem. Rev.* **2016**, *116*, 14620 – 14674.
[2] A. J. McConnell, C. S. Wood, P. P. Neelakandan, J. R. Nitschke, *Chem. Rev.* **2015**, *115*, 7729 – 7793.
[3] Y. Jin, C. Yu, R. J. Denman, W. Zhang, *Chem. Soc. Rev.* **2013**, *42*, 6634 – 6654.
[4] S. P. Black, J. K. M. Sanders, A. R. Stefankiewicz, *Chem. Soc. Rev.* **2014**, *43*, 1861 – 1872.
[5] P. A. Fernandes, M. J. Ramos, *Chem. Eur. J.* **2004**, *10*, 257 – 266.
[6] C. H. Sohn, J. Gao, D. A. Thomas, T.-Y. Kim, W. A. Goddard III, J. L. Beauchamp, *Chem. Sci.* **2015**, *6*, 4550 – 4560.
[7] a) W. Drożdż, C. Bouillon, C. Kotras, S. Richeter, M. Barboiu, S. Clément, A. R. Stefankiewicz, S. Ulrich, *Chem. Eur. J.* **2017**, *23*, 18010 – 18018; b) W. Drożdż, M. Kołodziejski, G. Markiewicz, A. Jenczak, A. Stefankiewicz, *Int. J. Mol. Sci.* **2015**, *16*, 16300 – 16312.
[8] a) A. R. Stefankiewicz, J. K. M. Sanders, *Chem. Commun.* **2013**, *49*, 5820 – 5822; b) P. J. Bygrave, D. H. Case, G. M. Day, *Faraday Discuss.* **2014**, *170*, 41 – 57.
[9] A. R. Stefankiewicz, M. R. Sambrook, J. K. M. Sanders, *Chem. Sci.* **2012**, *3*, 2326 – 2329.
[10] R. Caraballo, M. Rahm, P. Vongvilai, T. Brinck, O. Ramstrom, *Chem. Commun.* **2008**, 6603 – 6605.
[11] B. Rasmussen, A. Sorensen, H. Gotfredsen, M. Pittelkow, *Chem. Commun.* **2014**, *50*, 3716 – 3718.
[12] J. Atcher, I. Alfonso, *RSC Adv.* **2013**, *3*, 25605 – 25608.
[13] a) F. Dénès, M. Pichowicz, G. Povie, P. Renaud, *Chem. Rev.* **2014**, *114*, 2587 – 2693; b) U. F. Fritze, M. von Delius, *Chem. Commun.* **2016**, *52*, 6363 – 6366; c) S. Ji, W. Cao, Y. Yu, H. Xu, *Angew. Chem. Int. Ed.* **2014**, *53*, 6781 – 6785; *Angew. Chem.* **2014**, *126*, 6899 – 6903.
[14] a) A. Katrusiak, *Acta Crystallogr. Sect. A* **2008**, *64*, 135 – 148; b) E. Boldyreva, *Cryst. Growth Des.* **2007**, *7*, 1662 – 1668.
[15] a) Y. Tsuchida, T. Yagi, *Nature* **1990**, *347*, 267; b) T. Yagi, T. Suzuki, S.-I. Akimoto, *J. Phys. Chem. Solids* **1983**, *44*, 135 – 140; c) N. A. Dubrovinskaia, L. S. Dubrovinsky, R. Ahuja, V. B. Prokopenko, V. Dmitriev, H. P. Weber, J. M. Osorio-Guillen, B. Johansson, *Phys. Rev. Lett.* **2001**, *87*, 275501; d) E. V. Boldyreva, *Cryst. Eng.* **2003**, *6*, 235 – 254; e) E. Patyk, J.

Skumiel, M. Podsiadło, A. Katrusiak, *Angew. Chem. Int. Ed.* **2012**, *51*, 2146 – 2150; *Angew. Chem.* **2012**, *124*, 2188 – 2192.
[16] a) F. P. A. Fabbiani, D. C. Levendis, G. Buth, W. F. Kuhs, N. Shankland, H. Sowa, *CrystEngComm* **2010**, *12*, 2354 – 2360; b) W. Zielinski, A. Katrusiak, *CrystEngComm* **2015**, *17*, 5468 – 5473; c) A. Olejniczak, A. Katrusiak, *Cryst. Growth Des.* **2011**, *11*, 2250 – 2256.
[17] a) J. Bąkowicz, I. Turowska-Tyrk, *J. Photochem. Photobiol. A* **2012**, *232*, 41 – 43; b) V. V. Brazhkin, A. G. Lyapin, R. J. Hemley, *Philos. Mag. A* **2002**, *82*, 231 – 253.
[18] G. Kaupp, *CrystEngComm* **2009**, *11*, 388 – 403.
[19] W. Cai, A. Gładysiak, M. Anioła, V. J. Smith, L. J. Barbour, A. Katrusiak, *J. Am. Chem. Soc.* **2015**, *137*, 9296 – 9301.
[20] S. Sobczak, A. Katrusiak, *J. Phys. Chem. C* **2017**, *121*, 2539 – 2545.
[21] A. M. Belenguer, T. Friscic, G. M. Day, J. K. M. Sanders, *Chem. Sci.* **2011**, *2*, 696 – 700.
[22] P. Baláž, M. Achimovičová, M. Baláž, P. Billik, Z. Cherkezova-Zheleva, J. M. Criado, F. Delogu, E. Dutková, E. Gaffet, F. J. Gotor, R. Kumar, I. Mitov, T. Rojac, M. Senna, A. Streletskii, K. Wieczorek-Ciurowa, *Chem. Soc. Rev.* **2013**, *42*, 7571 – 7637.
[23] S. L. James, C. J. Adams, C. Bolm, D. Braga, P. Collier, T. Friscic, F. Grepioni, K. D. M. Harris, G. Hyett, W. Jones, A. Krebs, J. Mack, L. Maini, A. G. Orpen, I. P. Parkin, W. C. Shearouse, J. W. Steed, D. C. Waddell, *Chem. Soc. Rev.* **2012**, *41*, 413 – 447.
[24] a) D. Braga, S. L. Giaffreda, F. Grepioni, M. R. Chierotti, R. Gobetto, G. Palladino, M. Polito, *CrystEngComm* **2007**, *9*, 879 – 881; b) G. A. Bowmaker, *Chem. Commun.* **2013**, *49*, 334 – 348.
[25] a) A. M. Belenguer, G. I. Lampronti, D. J. Wales, J. K. M. Sanders, *J. Am. Chem. Soc.* **2014**, *136*, 16156 – 16166; b) A. M. Belenguer, G. I. Lampronti, A. J. Cruz-Cabeza, C. A. Hunter, J. K. M. Sanders, *Chem. Sci.* **2016**, *7*, 6617 – 6627.
[26] S. A. Moggach, D. R. Allan, S. Parsons, J. E. Warren, *J. Appl. Crystallogr.* **2008**, *41*, 249 – 251.
[27] H. K. Mao, J. Xu, P. M. Bell, *J. Geophys. Res.: Solid Earth* **1986**, *91*, 4673 – 4676.
[28] C. Glidewell, J. N. Low, J. L. Wardell, *Acta Crystallogr. Sect. B* **2000**, *56*, 893 – 905.
[29] G. Sheldrick, *Acta Crystallogr. Sect. C* **2015**, *71*, 3 – 8.
[30] O. V. Dolomanov, L. J. Bourhis, R. J. Gildea, J. A. K. Howard, H. Puschmann, *J. Appl. Crystallogr.* **2009**, *42*, 339 – 341.
[31] a) P. F. McMillan, *Nat. Mater.* **2002**, *1*, 19; b) M. A. Neumann, J. van de Streek, F. P. A. Fabbiani, P. Hidber, O. Grassmann, *Nat. Commun.* **2015**, *6*, 7793; c) F. P. A. Fabbiani, C. R. Pulham, *Chem. Soc. Rev.* **2006**, *35*, 932 – 942; d) E. Boldyreva, *Acta Crystallogr. Sect. A* **2008**, *64*, 218 – 231.
[32] a) W. Ostwald, *Z. Phys. Chem.* **1897**, *22*, 289 – 330; b) A. R. Verma, P. Krishna, *Polymorphism and polytypism in crystals*, Wiley, New York, **1966**; c) J. Bernstein, *Polymorphism in molecular crystals, Vol. 14*, Oxford University Press, Oxford, **2002**; d) H. G. Brittain, *Polymorphism in pharmaceutical solids*, CRC, Boca Raton, **2016**.

Manuscript received: April 6, 2018
Accepted manuscript online: April 20, 2018
Version of record online: May 30, 2018

(**R5**) Sobczak, S.; Ratajczyk, P.; Katrusiak, A.; Squeezing out the catalysts: the disulphide bond exchange in aryl disulphides at high hydrostatic pressure *ChemRxiv – archived* **2020**, doi.org/10.26434/chemrxiv.13160996.v2

Squeezing out the catalysts: disulfide bond exchange in aryl disulfides under high pressure

Szymon Sobczak, Paulina Ratajczyk and Andrzej Katrusiak**

Faculty of Chemistry, Adam Mickiewicz University, Uniwersytetu Poznańskiego 8, 61-614 Poznań, Poland

KEYWORDS high-pressure chemistry, disulfide exchange reaction, green chemistry, catalyst-free process

ABSTRACT: High pressure is capable of eliminating the catalysts or stimuli, such as reducing agents, strong bases, ultraviolet light, or ultrasound, required by equilibrium reactions of disulfide bond exchange at normal conditions. The exchange of aryl disulfides in the absence of catalysts or other stimuli has been systematically studied. The effects of pressure in the range between 100 and 400 MPa, accessible in large-scale technological installations, have been tested for promoting exchange reactions between various homodimeric aryl disulfides. For the optimized conditions, 100% yields of the heterodimer in pure single-crystal form were obtained. The reactions were performed in a diamond-anvil cell, as well as in a hydraulic piston-and-cylinder press, and the products were characterized by X-ray diffraction, mass spectrometry and nuclear magnetic resonance (NMR) spectroscopy. A prominent role of high-entropy states, not attainable under ambient conditions, as well as the high-entropy nucleation, kinetic crystallization and other effects associated with the high-pressure environment, is apparent. These entropy-driven reactions represent an efficient, environmentally friendly, one-pot method for obtaining pure crystalline heterodimeric disulfides.

INTRODUCTION

High-pressure methods constantly gain interest due to practical applications in various fields of science and industry.[1,2] For example, the high-pressure food preservation is the least damaging for the products and therefore it witnesses a steady grows in the market worth billions of dollars.[2–4] The successful applications of pressure methods in food, polymers, petrochemical, fertilizers and other processes prompts further research in other fields, too.[1] The apparent advantages of high-pressure technologies are low-energy consumption, confined space of the process, reducing the emissions, amounts of needed solvents etc., whereas disadvantages are connected with variable costs (labor, area, energy, utilities, maintenance and others) as well as the capital invested in the high-pressure equipment. However, these expenses gradually reduce as the demand and market for pressure technologies grows. But most importantly, the profits of high-pressure processed materials can far exceed these disadvantages.[5,6] In this report we have investigated the possibilities emerging from the high-pressure environments for the aryl disulfide exchange reactions.

Aryl disulfides have versatile applications owing to the properties of the C−S bond. These compounds have found use in the coatings of metal surfaces, anticorrosive agents, paints, oils, and lubricants[7–9] as well as in active pharmaceutical ingredients (e.g., lansoprazole, sulindac, esomeprazole, and quetiapine) used to treat cancer, inflammation, asthma, Alzheimer's disease, Parkinson's disease, HIV-AIDS and other diseases.[10–16] Reversible exchange of disulfide bonds underlies living functions, contributing to the stability of the native conformations of proteins.[17,18] The sensitivity of disulfide metathesis to environmental stimuli has been employed in dynamic covalent chemistry (DCC).[19–22] In contrast to traditional organic synthesis performed under the kinetic regime, DCC involves thermodynamic control of reactions, which results in the spontaneous elimination of less stable products. Conversely, in kinetically controlled reactions, the form of substrates and catalysts, as well as reaction conditions, must be carefully chosen to favor the target products over the substrates and possible intermediates.[19] In most reversible disulfide systems, the exchange reactions proceed by nucleophilic attack of a free thiolate at the disulfide bond and often require long equilibration times, even in the presence of catalysts, which limits their applications.[22] Some significant progress toward cleaner and more efficient methods of disulfide metathesis has only recently been reported.[23–28] A Brønsted base-free method requiring a phosphine to facilitate the reaction was described by Ramstrom *et al.*[24] Belenguer, Friščić and Sanders used mechanochemistry for high-conversion disulfide metathesis in the presence of 1,8-diazabicyclo[5.4.0]undec-7-ene.[23,26] Pittelkow's group found that diselenides spontaneously exchange in water and can be used to catalyze disulfide exchange.[27] Fritze and Delius showed that ultrasound supports the exchange of disulfides in CH_3Cl.[25] Most recently, we have shown that high pressure can promote the metathesis between homodimeric bis(4-chloroophenyl)disulfide with bis(2-nitrophenyl)disulfide without any catalyst or reducing agents, obtaining the heterodimeric product in several solvents.[29]

Presently, we have explored the mechanism of pressure-induced disulfide metathesis. For this purpose, we performed 35 reactions in a diamond-anvil cell (DAC) between 15 homodimeric disulfides that differ in the

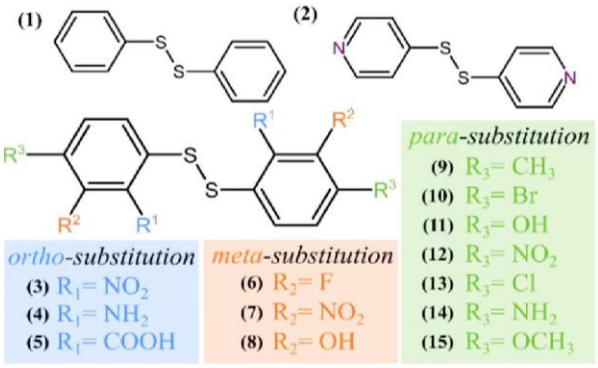

Figure 1. Aryl disulfides investigated under high pressure. The color code indicates the (blue) *ortho*-; (red) *meta*-; and (green) *para*-substituents.

character, size and position of their substituents. The effects of strongly electron-withdrawing groups (EWGs) COOH and NO_2, electron-donating groups (EDGs) NH_2, OCH_3, CH_3, and OH, and halogens displaying dual positive-mesomeric and negative-induction features (Cl, Br and F) were studied and compared. Reactions were conducted in three different solvents: polar protic isopropanol and methanol, as well as polar aprotic acetonitrile. These solvents remain liquid within the range of our high-pressure experiments and secure hydrostatic conditions.[30,31] Due to their low freezing pressure, nonpolar solvents were not considered for these experiments. Under pressure and without catalyst, we obtained 21 different heterodimeric aryl disulfides. In six cases, after optimizing the reaction conditions, the products precipitated as single crystals, and their structures could be determined by X-ray diffraction. The formation of 15 other products was confirmed by mass spectrometry. Our results reveal the role of high-pressure reactions and their advantages for DCC.

RESULTS AND DISCUSSION

It was established that high pressure increases the rate of reaction, allowing the process to run at lower temperatures.[32–35] Among the most prominent reactions accelerated by high pressure are Diels-Alder reactions, 1,3-dipolar cycloadditions, [2+2] cycloadditions, sigmatropic rearrangements and radical polymerizations. Although the impact of pressure on the reaction equilibrium is intuitive, it must be considered on several levels. At the molecular scale, when new bonds are formed, the reaction is accelerated by pressure due to reduced intermolecular distances and molecular volume. The reverse reaction, homolytic bond cleavage, increases the volume and shifts the equilibrium toward the reactants.[36] Compression, however, does not affect only the molecules themselves but changes all thermodynamic properties of the reaction system.

Under pressure, the void spaces and distances between molecules are reduced, as is the space necessary for thermally induced motion and collisions. Additionally, the physical properties of the liquid environment are altered, resulting in a higher boiling point, increased density, viscosity and reduced solubility of most compounds.

Reaction procedure and optimization

We performed a series of high-pressure reactions in a DAC used as the high-pressure reactor. The DAC was modified by mounting the diamonds directly on the steel supports.[37] All reactions were conducted according to the same procedure (Figure 2). Two homodimeric substrates in the form of a single crystal were inspected through a microscope, and grains of equal $V_{si}\,d_i/M_{si}$ (V_{si}, d_i and M_{si} are the grain volume, density and molecular weight of the substrate, respectively) were selected to obtain a 1:1 molar ratio. Then, the grains were loaded into the DAC chamber, together with small ruby spheres for pressure calibration.[38,39] Next, the DAC chamber was filled with a solvent, sealed and compressed. The solvent volume (V_{sol}) is:

$$V_{sol} = V_{DAC} - [(V_{si} + V_{sii}) + V_r],$$

where V_{DAC} is the DAC chamber volume, V_r is the volume of the ruby sphere, and the molar concentration (c_i) of substrates is

$$c_i = (V_{si} \times d_{si}/M_{si})/V_{sol}.$$

Then, the DAC was heated until both reactants dissolved. Depending on the experiment—the substrates, their concentration, the solvent and pressure—the dissolution required increasing the temperature from 323 K to 400 K.

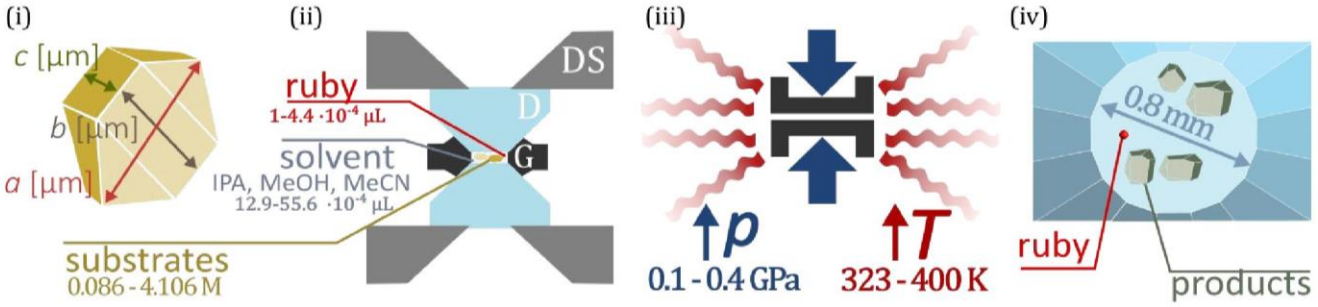

Figure 2. Schematic illustration of the high-pressure reaction procedure: (i) single-crystal measurements; (ii) loading the DAC chamber with two homodimeric substrates, together with ruby spheres, and filling the remaining volume with the solvent, 2-propanol (IPA), methanol (MeOH) or acetonitrile (MeCN), where the DAC consists of two parallel diamonds (D) supported by steel disks (DSs) and a squeezed metal

gasket (G); (iii) compression and heating of the DAC reactor until the substrates dissolve; and (iv) recovery and analysis of the solid precipitate.

After dissolving the substrates, the DAC was cooled, and when the DAC chamber was unsealed, the solvent evaporated. The crude solid precipitate was analyzed by direct insertion probe–mass spectrometry (DIP-MS) and X-ray diffraction. DIP-MS does not require gas chromatographic separation, which eliminates the possibility of the reverse reaction in the analyzed product. High temperatures used for sample ionization in the DIP-MS technique could be responsible for the fragmentation of product/substrate molecules in the analyzed the sample; therefore, DIP-MS was used mainly for quick yield evaluation.The conditions were optimized by varying the concentrations, solvents, pressures and temperatures. For 6 out of 21 reactions (Section 3 in the Supporting Information [SI]), the yields approached 100%, and the products precipitated in the form of single crystals of sufficiently high quality for X-ray structural study. The crystals of the heterodimeric products were recovered from the DAC chamber and analyzed on a SuperNova (*Rigaku* Oxford Diffraction) diffractometer equipped with a microfocus X-ray tube, detailed crystallographic data are summarized in Table S39, in Section 7 of the SI. To establish the reaction

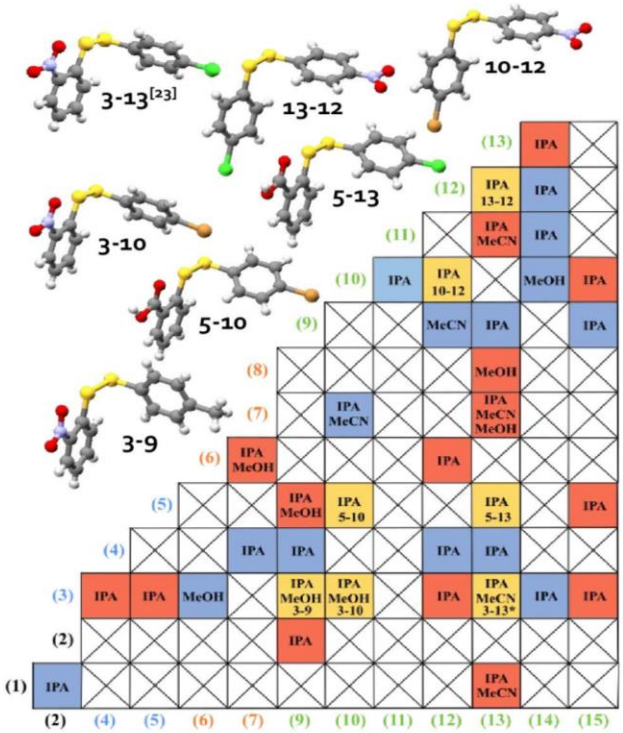

Figure 3. Compilation of all high-pressure reactions presently investigated; the numbers in brackets label to the substrates in Figure 1. Yellow represents the high-yield heterodimer products characterized by X-ray diffraction; blue represents products detected by DIP-MS spectra; and red represents no heterodimer traces. Crosses indicate that no reactions were performed. The solvents are indicated: MeOH, methanol; IPA, 2-propanol; and MeCN, acetonitrile. The insets show heterodimers obtained in the form of single crystals.

equilibria in the solution for successfully exchanged systems (**11/14**, **3/14**, **9/13**, **4/13**, **4/12**, **4/9**, **4/7**, **1/2**, **10/12**, **3/9** and **3/10**, see Figure 1), at ambient and high pressure, we collected carbon nuclear magnetic resonance (^{13}C-NMR) spectra of homodimeric mixtures in 2-propanol-d8 and CD_3CN before and after compression to 0.4 GPa, for the experimental procedure and spectra, see Section 1.2.1 and Section 5 of the SI, respectively. Interestingly, the solubility of **3, 12** and **5** in 2-propanol-d8 and CD_3CN under ambient conditions was extremely poor (spectra 5.1.4 and 5.1.10 of Section 5 in the SI).

Additionally, the effect of high temperature on the homodimeric mixture during its slow heating to 673 K was investigated by thermogravimetry–differential scanning calorimetry (TG-DSC). No thermal effects associated with chemical reactions were detected (Section 6.1 in the SI). The influence of anisotropic pressure on the mixtures of solid homodimers with and without a few drops (4-5 μL) of 2-isopropanol (IPA), investigated by powder X-ray diffraction, showed no traces of heterodimeric products (Section 6.2 in the SI).

High-pressure chemistry

Control over high-pressure reactions, as under ambient conditions, can be achieved by two different basic approaches. In a kinetically controlled reaction, differences between the volume of activation $\Delta V^{\neq}$ (which, according to transition state theory, is a difference between the partial molar volumes of the transition state and the sums of the partial volumes of the reactants at the same temperature and pressure) leading to different product molecules must be achieved. Alteration of $\Delta V^{\neq}$ can be achieved either by a pressure-induced change in the reaction mechanism or by the difference between the volumes of the transition structures within the same, or at least similar, mechanism. In a thermodynamically controlled reaction, the reaction rate increases when the reaction volume ΔV^{o} decreases. Recently, it was shown both theoretically and experimentally that instead of being proposed to occur before [2 + 2] metathesis, S–S reversible bond cleavage and formation is a radical-mediated process (Scheme 1).[40–44]

Scheme 1. Mechanisms of [2+1] radical-mediated disulfide exchange

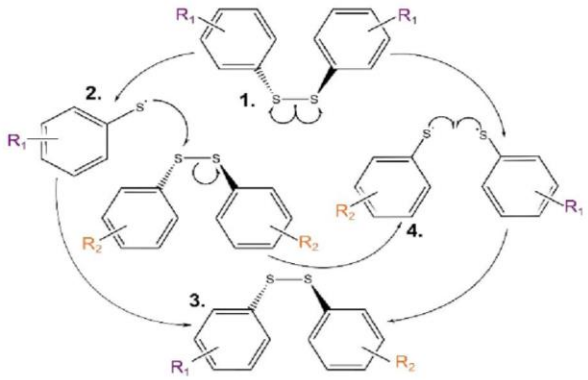

According to this mechanism, the reaction initiates when sulfenyl radicals are formed (step 1). Bond dissociation is a process associated with volume expansion, and at high pressure, it is a rate-determining step that could possibly even lead to reaction inhibition. Thus, it is apparent that at high pressure, this process does not resemble the ultraviolet (UV) or ultrasound generation of radicals but rather a chain reaction where positive feedback leads to a self-amplifying chain of events.

The formation of sulfenyl radicals strongly depends on the S–S bond energy. Theoretical studies on disulfide-based polymers connect the S–S length with bond energy in an inverse correlation.[43] Our survey of the molecular structures of homodimeric aryl disulfides reported in this work and those deposited in the Cambridge Structural Database (CSD Version 5.41, ConQuest Version 2.05, Figure S1) shows that the substitution of an EDG in the *para*- or *ortho*-position or an EWG in the *ortho*-position, as well as the presence of a heteroatom in the aromatic ring, results in longer S–S distances. It appears that substitution by an EDG adds electron density to a conjugated π-system *via* resonance or inductive effects. This increase in electron density into the antibonding σ_{SS}^* bond, followed by elongation of the S–S bond, lowers its dissociation energy. Similarly, the *ortho*-position EWG, due to the resonance effect, creates an electron-deficient (δ+) region at the S atom and weakens the S–S bond. In contrast, the *para*-substituted EWG had the opposite effect, shortening the S–S bond. At high pressures, the energy necessary for bond dissociation can be achieved at lower temperatures, as shown for **9**.[45] Its recrystallization at 0.45 GPa results in S–S bond elongation from 2.024 Å under ambient conditions to 2.058 Å, accompanied by a phase transition.[45] Once free radicals are generated, they attack other homodimers and produce new free radicals (step **2**), along with a product molecule (step **3**). At this stage, reverse recombination is also possible. However, at high pressure, the reverse reaction can only

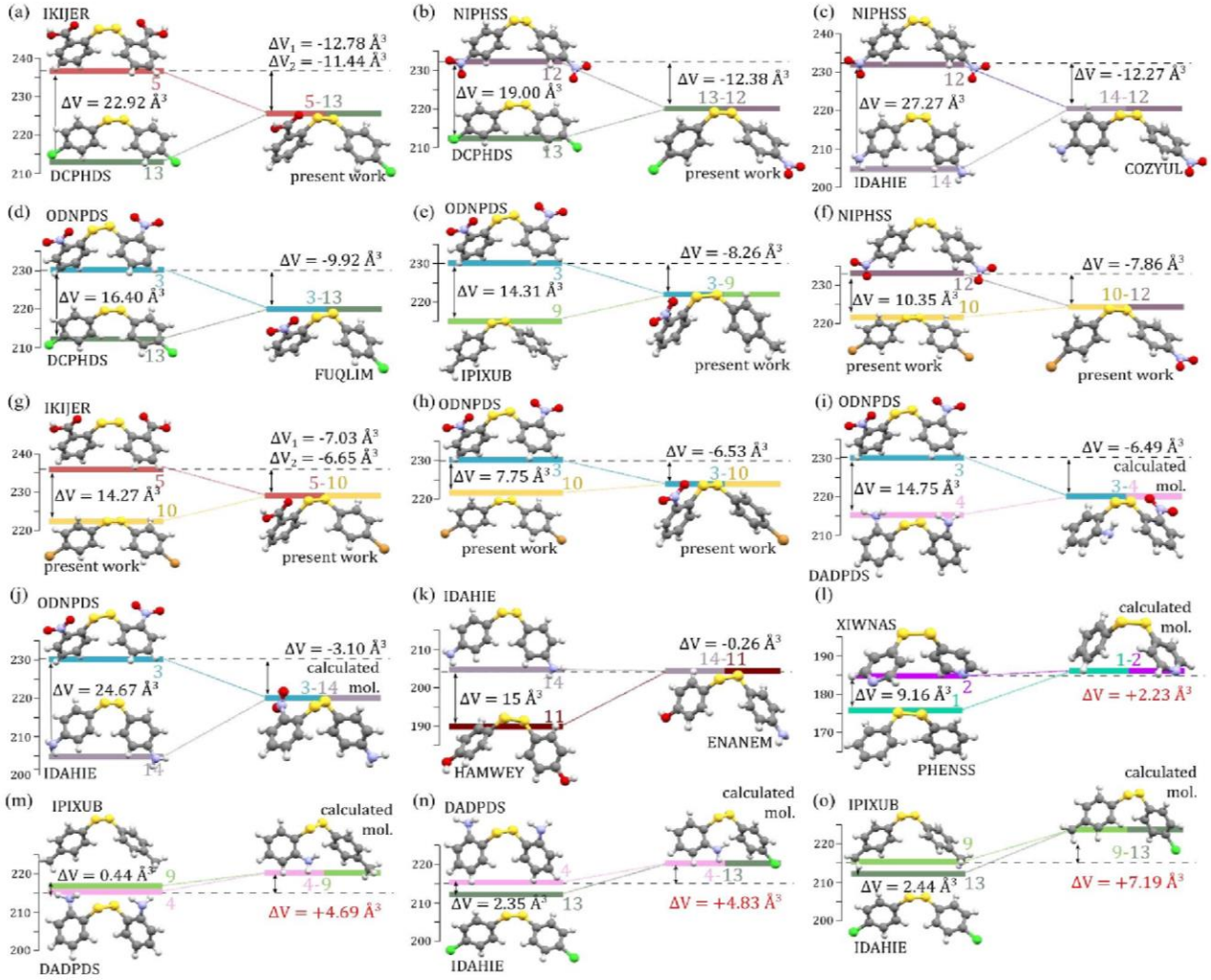

Figure 4. Van der Waals volumes profile calculated for the exchange reaction. Compound labels refer to Figures 1 and 3. The structures were determined in this work or retrieved from the CSD (where six-letter refcodes are given). For reactions **3/4**, **1/2**, **4/13, 4/9** and **9/13**, the molecular conformation of the product molecules has been calculated in Gaussian16 with the B3LYP/6–311+ G (2d, 2p) level of theory4

occur if the formation of the product leads to a negligible reduction in ΔV^{o}. The reaction terminates when two different radical species react with each other to form a heterodimeric adduct (step **4**).

To resolve whether the pressure reactions in the DAC chamber (conducted in the solid-solute-solid sequence, cf. section: *Reaction procedure and optimization*) proceed under thermodynamic or kinetic regime, i.e., the reactions are generally characterized by negative ΔV^{o} or there is some kinetic aspect involved, we compared the results with the pressure effect on compressed mixtures of homodimers dissolved in 2-propanol-d8 and CD_3CN. For equilibrium reactions with large negative ΔV^{o}, the application of high pressure would lead to a significant yield increase. This relationship comes from the fact that a small change in free Gibbs energy (ΔG) leads to a logarithmically amplified change in the equilibrium position, according to

$$\Delta G = \partial \ln K / \partial pT = -\Delta V^{o}/RT,$$

where R is the gas constant, T is the temperature and K is the equilibrium constant.

A kinetic study was performed for 11 different systems, corresponding to reactions successfully conducted in the DAC. Homodimers were first dissolved in 2-propanol-d8 and CD_3CN and then mixed, and after 12 h under ambient conditions, their ^{13}C-NMR spectra were collected. In seven systems (**11/14**, **3/14**, **10/12**, **3/9**, **3/10** and **4/12**), no product was observed, while in five other reactions (**4/9**, **4/7**, **1/2**, **9/13** and **4/13**), an equilibrium was established below 50% conversion to the product. In reactions **10/12** and **3/10,** due to the extremely poor solubility of the substrates, compression experiments were not performed. Subsequently, four systems, **11/14**, **3/14**, **3/9**, and **4/12**, were compressed isothermally at 0.4 GPa, and their spectra were collected within 0.5 h after the pressure was released. Surprisingly, compression of the dissolved homodimers in reactions **11/14**, **3/14**, **3/9**, and **4/12** still did not result in the formation of the heterodimeric product (cf. the SI). The amount of formed product for **11/14**, **3/14**, **9/13**, **4/13** and **3/9** was additionally confirmed by DIP-MS (Section 5.5 of the SI). Surprisingly, four systems, **1/2**, **4/9**, **4/13**, and **9/13** (with positive ΔV^{o} values of +2.23 Å^3, +4.69 Å^3, +4.83 Å^3 and +7.19 Å^3, respectively, Figure 4), were mixtures equilibrated with an approx. 1:1 product-to-substrate ratio under ambient conditions, while in **3/9**, **11/14** and **3/14** with negative ΔV^{o} values, no products, even after compression, were generated. It is apparent that compression of **1/2**, **4/9**, **4/13**, **9/13** would not, and indeed did not, result in reaction acceleration. On the other hand, the compression mixtures of **3/9**, **11/14** and **3/14** should lead to reaction initiation; however, the ^{13}C-NMR spectra did not show any trace amounts of homodimers. Most likely, the reduction in ΔV^{o} of approximately -8 Å^3 is not enough to compensate for the ΔV^{o} gained while radicals are formed; thus, these reactions are inhibited.

We have connected these results with the intrinsic volume profiles of the reactions (Figure 4) based on the van der Waals models of the substrate and product molecules. Owing to the significantly different volumes of substituents R_i in the substrates (Figure 1), the molecular volume of the heterodimer is close to the intermediate of the volumes of homodimers. Subtle departures from the mean value (ΔV_m) are mainly due to the S–S bond length changes (ΔL), according to the approximate formula $\Delta V_m \approx 18.3\Delta L$ [Å^3]. The S–S length change of 0.07 Å, e.g., between 2.01 and 2.07 Å, corresponds to ΔV_m = 1.0 Å^3, comparable to the accuracy of our volume calculations. The molecular conformation is yet another variable capable of stimulating heterodimer formation at high pressure.[46,47] The intermolecular interactions can considerably change soft conformational parameters and may be relevant for improving the reactivity of disulfides.[28,48] It was suggested for free radical polymerization of ethylene that the formation of various supramolecular intermediate forms can be unique for high-pressure conditions and thus essential for increasing the conversion rate to the product form.[46] In all the heterodimeric disulfides, the C–S–S–C torsional angles are within ±(85° ± 3°). The value of this torsion angle is dominated by 3p lone pairs on the two S atoms, which minimize their mutual overlap and repulsion integrals for the orthogonal position.[49]

High-entropy nucleation

The synthesis of heterodimers (AB) from homodimers (A_2 and B_2) can be achieved, even with 100% yield, in the entropy-driven kinetic process. The process consists of several stages, schematically depicted in Figure 5. Initially, the system entropy (S) is maximized and then the nucleation and kinetic crystallization of the heterodimer induce non-equilibrium conditions in the solution due to the deficiency of the heterodimer, which promotes its production.

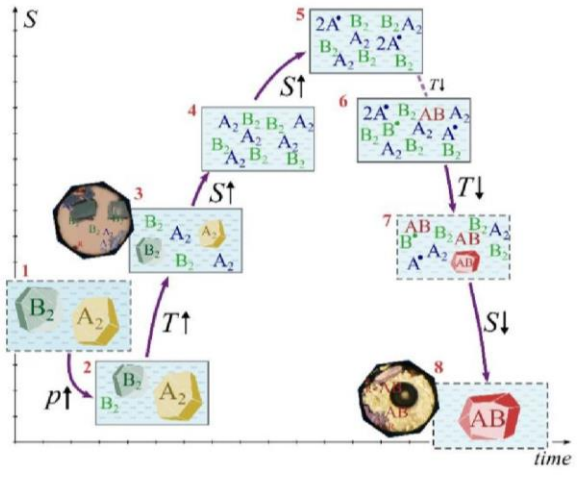

Figure 5. Schematic illustration of the entropy-driven synthesis of heterodimers AB from homodimers A_2 and B_2 dissolved in solvent (gray dashes). The stages of the process (red numbers) are described in the text. The open and closed systems have been indicated by the dashed and solid edges of boxes, respectively.

High pressure plays an essential role, allowing the entropy to increase beyond that attainable at atmospheric pressure. Thus, at stage **1,** this system consisting of equimolar amounts of homodimers A_2 and B_2 and some solvent (F) is closed in a DAC chamber. The chamber is sealed and pressurized to approximately 200 MPa (2000 bar). These conditions add the compression work component to the Gibbs free energy (G), and most homodimers A_2 and B_2 remain in the crystalline state. The solubility usually decreases with increasing pressure, so apart from the work contribution (pV), the entropy (S) decreases due to a smaller portion of the crystals dissolved at stage **2** than at stage **1**. In stage **3**, the sample is heated until stage **4**, when crystals A_2 and B_2 dissolve. At this point, the system assumes the maximum entropy when molecules A_2, B_2 and F are randomly mixed. At this stage, the dimers still increase the entropy through their conformational variation. According to experiments and theoretical calculations, under mechanical stress the S–S distance significantly increases, facilitating bond cleavage; additionally, the disulfide conformation affects the micro-environment around the molecules, as they become more 'open' to be attacked by sulfenyl radicals.[28,45,48] Then, the entropy can be further increased at still higher temperatures when the homodimers start to dissociate into radicals at stage **5**. The increased number of radicals intensifies the chain reactions, leading to heterodimer AB, whereas some recombinations occur in A_2 and B_2 when the product and substrate are both comparable in volume. Upon lowering the temperature, the system (stage **6**) tends to reduce the entropy, while the ratio between the homo- and heterodimers depends on the equilibrium in the solution under the given thermodynamic conditions. For the exchange reaction A_2+B_2=2AB the equilibrium constant $K = x/(1 - x)$, of the hetero- and homodimers ratio, is the function of one variable x, which is the fraction of reacted homodimers. Constant K generally depends on the thermodynamic conditions, which in our experiments include temperature, pressure, solvent type and concertation. In particular, the saturation of reactants strongly depends on the solvent, temperature and pressure. It is apparent that the solubility of AB, compared to that of A_2 and B_2, is important for nucleation and its further crystallization. It is reasonable to assume that relative to that of homodimers, the polarity of heterodimeric molecules significantly increases, which in turn increases the electrostatic cohesion forces and reduces the crystal solubility. This interdependence offers an effective control on the precipitation of the product, leading to a non-equilibrium state occurring at stage **7**. During this process a significant reduction in entropy is achieved by the nucleation and subsequent kinetic crystallization of the product. Consequently, the product concentration in the solution drops by dx, to $(x - dx)$, and the ratio of heterodimers to homodimers ratio drops too, which offsets the equilibrium by $dK = -dx/(1 - x)$, as indicated on Figure 6. This kinetic crystallization of AB results in a deficiency of the product in the solution again and fuels the synthesis of heterodimers. At the final stage **8**, at 296 K, most of the homodimers have reacted into the heterodimer, present in the solid form of one or more crystal grains, while there are still small amounts of A_2, B_2 and AB dimers (hence low entropy, S) remaining dissolved in solution. At this stage the solubility of the compounds is reduced, due to the low-temperature and high-pressure conditions. However, there is still the same volume of the solvent inside the sealed DAC chamber. The complete reaction of homodimers requires that the DAC chamber be unsealed and all solvent evaporates. Then the heterodimer crystallizes further and its 100% yield can be obtained.

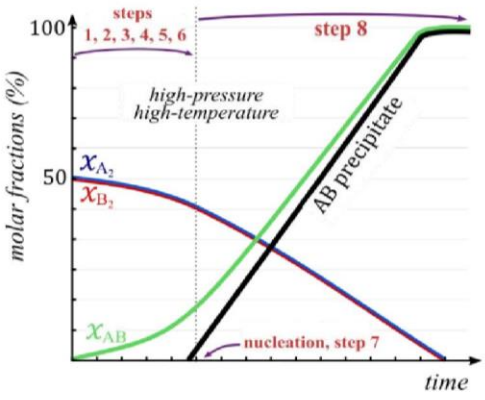

Figure 6. The time dependence of the molar ratios of homodimers x_{A_2} (blue) and x_{B_2}(green) and the heterodimeric product x_{AB} corresponding to the equilibrium constant $K = x/(1 - x)$ equal to 0.2.

In the presented process the high-pressure conditions have been used as an efficient method of sealing the system in order to dissolve and excite the reactants by increasing temperature. For a closed system, the entropy can be increased to the required level (stage **5**) of strongly mixed molecules and radicals. After stage **7**, the confining role of the DAC chamber is continued, irrespective of the pressure value, which can be kept high or released.

CONCLUSIONS

Disulfide exchange reactions have been systematically investigated for a series of representative, and in some cases unique, aryl disulfides with distinct chemical features in different environments and under extreme conditions of high pressure and high temperature. These results provide microscopic insight into noncatalytic disulfide exchange reactions. The application of high pressure extends the thermodynamic conditions to high temperatures not attainable in open systems. Owing to the confined reaction space, the entropy of the system can be increased in a controlled manner to a stage when the substrates are dissolved at high concentrations and well mixed and in which their molecules are excited into high E_p conformers and high vibrational states and are at least partly dissociated. Then, by lowering the temperature, the high-entropy

nucleation and subsequent kinetic crystallization can offset the thermodynamic equilibrium, resulting in high yields of exchanged disulfides for catalyst-free, ambient-pressure reactions. The comprehensive experiments performed to characterize the substrates and products, involving DIP-MS, NMR spectroscopy, TG-DSC, single-crystal and powder X-ray diffraction, and theoretical calculations, corroborate this mechanism and the understanding of the disulfide exchange reactions. The application of high pressure is essential for high-entropy effects (including excited conformational states and S–S bond cleavage), nucleation and subsequent kinetic crystallization, which are the key elements leading to noncatalytic disulfide exchange. These results indicate that such high-pressure techniques are most suited for tailoring one-pot, high-yield reaction systems leading to high-quality single crystalline products. Notably, the pressure of approximately 0.2 GPa proved sufficient for sealing the reaction space, which technologically is readily accessible in various types of equipment, for example, in the lower range of operation of many piston-and-cylinder devices and in many autoclaves. At the same time, these high-entropy methods eliminate the need for a catalyst, which apart from environmental issues, including further purification of the obtained product, makes these approaches financially competitive.

ASSOCIATED CONTENT

A detailed description of all experimental data, including high-pressure equipment, analytic methods, volume calculations, and summarized results, with all NMR and DIP-MS spectra, of all conducted high-pressure reactions in the DAC and in compressed-mixture reactions, a description regarding deconvolution of the accompanying effect of temperature and nonhydrostatic pressure acting alone, details about molecular volume calculations and tabularized results, detailed crystallographic data of novel substrates and products and synthetic procedure for **10**, is available free of charge via the Internet at http://pubs.acs.org."

The CIF files have been deposited in the Cambridge Structural Database (CCDC, www.ccdc.cam.ac.uk) as supplementary publications with reference numbers 2033598, 2033599, 2033600, 2033601, 2033602 and 2033603 for synthesized heterodimers **3-10**, **10-12**, **13-12**, **3-9**, **5-13** and **5-10**, respectively, and 2033604, 2033605 and 2033606 for **15**, **6** and **10**, respectively.

AUTHOR INFORMATION

Corresponding Author

*szymon.sobczak@amu.edu.pl
*katran@amu.edu.pl

Author Contributions

All authors have given approval to the final version of the manuscript.

Funding Sources

We thank the Polish National Science Centre (grant PRELUDIUM 2017/27/N/ST5/00693)

ACKNOWLEDGMENT

The authors are grateful to Dominika Czerwonka of the Department of Chemistry, Adam Mickiewicz University, Poznan; Jean-Louis Do of the Department of Chemistry, McGill University; Michal Andrzejewski of the Department of Chemistry and Biochemistry, University of Bern; and Tomasz Poręba of ESRF for valuable suggestions and fruitful discussions.

ABBREVIATIONS

DCC, dynamic covalent chemistry; DAC, diamond-anvil cell; EWG, electron-withdrawing group; EDG, electron-donating group; DIP-MS, direct insertion probe – mass spectrometry.

REFERENCES

(1) Eggers, R. *Industrial High Pressure Applications*; 2012. https://doi.org/10.1002/9783527652655.

(2) Elamin, W. M.; Endan, J. B.; Yosuf, Y. A.; Shamsudin, R.; Ahmedov, A. High Pressure Processing Technology and Equipment Evolution: A Review. *J. Eng. Sci. Technol. Rev.* **2015**, *8* (5), 75–83. https://doi.org/10.25103/jestr.085.11.

(3) Huang, H. W.; Wu, S. J.; Lu, J. K.; Shyu, Y. T.; Wang, C. Y. Current Status and Future Trends of High-Pressure Processing in Food Industry. *Food Control* **2017**, *72* (12), 1–8. https://doi.org/10.1016/j.foodcont.2016.07.019.

(4) Mújica-Paz, H.; Valdez-Fragoso, A.; Samson, C. T.; Welti-Chanes, J.; Torres, A. High-Pressure Processing Technologies for the Pasteurization and Sterilization of Foods. *Food Bioprocess Technol.* **2011**, *4* (6), 969–985. https://doi.org/10.1007/s11947-011-0543-5.

(5) Bermúdez-Aguirre, D.; Barbosa-Cánovas, G. V. An Update on High Hydrostatic Pressure, from the Laboratory to Industrial Applications. *Food Eng. Rev.* **2011**, *3* (1), 44–61. https://doi.org/10.1007/s12393-010-9030-4.

(6) Sampedro, F.; McAloon, A.; Yee, W.; Fan, X.; Geveke, D. J. Cost Analysis and Environmental Impact of Pulsed Electric Fields and High Pressure Processing in Comparison with Thermal Pasteurization. *Food Bioprocess Technol.* **2014**, *7* (7), 1928–1937. https://doi.org/10.1007/s11947-014-1298-6.

(7) Forbes, E. S. The Load-Carrying Action of Organo-Sulphur Compounds-A Review. *Wear* **1970**, *15* (2), 87–96. https://doi.org/10.1016/0043-1648(70)90002-5.

(8) ALLUM, K. G.; Forbes, E. S. The Load-Carrying Properties of Organic Sulpher Compounds. Part II. The Influence of Chemical Structure on the Anti-Wear Properties of Organic Disulphides. *J. Inst. Pet.* **1967**, *53* (521), 174.

(9) Yanez, C. O.; Andrade, C. D.; Belfield, K. D. Characterization of Novel Sulfonium Photoacid Generators and Their Microwave-Assisted Synthesis. *Chem. Commun.* **2009**, No. 7, 827–829. https://doi.org/10.1039/b815831b.

(10) Labelle, M.; Belley, M.; Gareau, Y.; Gauthier, J. Y.; Guay, D.; Gordon, R.; Grossman, S. G.; Jones, T. R.; Leblanc, Y.; McAuliffe, M.; et al. Discovery of MK-0476, a Potent and Orally Active Leukotriene D4 Receptor Antagonist Devoid of Peroxisomal Enxyme Induction. *Bioorganic Med. Chem. Lett.* **1995**. https://doi.org/10.1016/0960-894X(95)00023-M.

(11) Wang, Y.; Chackalamannil, S.; Hu, Z.; Clader, J. W.; Greenlee, W.; Billard, W.; Binch, H.; Crosby, G.; Ruperto, V.; Duffy, R. A.; et al. Design and Synthesis of Piperidinyl

Piperidine Analogues as Potent and Selective M2 Muscarinic Receptor Antagonists. *Bioorganic Med. Chem. Lett.* **2000**, *10* (20), 2247–2250. https://doi.org/10.1016/S0960-894X(00)00457-1.

(12) Ram, V. J.; Vlietinck, A. J. Chemotherapeutical Agents. VII. Synthesis and Pesticidal Activities of Sulphides and Sulphones Derived from Bis[4-Aryl-1,2,4-Triazoline-5-Thione-3-Yl]Alkane and 5-Phenyl-1,3,4-Oxadiazole-2-Thione. *J. Heterocycl. Chem.* **1988**, *25* (1), 253–256. https://doi.org/10.1002/jhet.5570250141.

(13) Otzen, T.; Wempe, E. G.; Kunz, B.; Bartels, R.; Lehwark-Yvetot, G.; Hänsel, W.; Schaper, K. J.; Seydel, J. K. Folate-Synthesizing Enzyme System as Target for Development of Inhibitors and Inhibitor Combinations against Candida Albicans - Synthesis and Biological Activity of New 2,4-Diaminopyrimidines and 4′-Substituted 4-Aminodiphenyl Sulfones. *J. Med. Chem.* **2004**, *47* (1), 240–253. https://doi.org/10.1021/jm030931w.

(14) Alcaraz, M. L.; Atkinson, S.; Cornwall, P.; Foster, A. C.; Gill, D. M.; Humphries, L. A.; Keegan, P. S.; Kemp, R.; Merifield, E.; Nixon, R. A.; et al. Efficient Syntheses of AZD4407 via Thioether Formation by Nucleophilic Attack of Organometallic Species on Sulphur. *Org. Process Res. Dev.* **2005**, *9* (5), 555–569. https://doi.org/10.1021/op0500483.

(15) Llauger, L.; He, H.; Kim, J.; Aguirre, J.; Rosen, N.; Peters, U.; Davies, P.; Chiosis, G. Evaluation of 8-Arylsulfanyl, 8-Arylsulfoxyl, and 8-Arylsulfonyl Adenine Derivatives as Inhibitors of the Heat Shock Protein 90. *J. Med. Chem.* **2005**, *48* (8), 2892–2905. https://doi.org/10.1021/jm049012b.

(16) Pasquini, S.; Mugnaini, C.; Tintori, C.; Botta, M.; Trejos, A.; Arvela, R. K.; Larhed, M.; Witvrouw, M.; Michiels, M.; Christ, F.; et al. Investigations on the 4-Quinolone-3-Carboxylic Acid Motif. 1. Synthesis and Structure-Activity Relationship of a Class of Human Immunodeficiency Virus Type 1 Integrase Inhibitors. *J. Med. Chem.* **2008**, *51* (16), 5125–5129. https://doi.org/10.1021/jm8003784.

(17) Ladenstein, R.; Ren, B. Reconsideration of an Early Dogma, Saying "There Is No Evidence for Disulfide Bonds in Proteins from Archaea." *Extremophiles* **2008**, *12* (1), 29–38. https://doi.org/10.1007/s00792-007-0076-z.

(18) Sevier, C. S.; Kaiser, C. A. Formation and Transfer of Disulphide Bonds in Living Cells. *Nat. Rev. Mol. Cell Biol.* **2002**, *3* (11), 836–847. https://doi.org/10.1038/nrm954.

(19) Gasparini, G.; Dal Molin, M.; Lovato, A.; Prins, L. J. Dynamic Covalent Chemistry. *Supramol. Chem.* **2012**, No. Dcc. https://doi.org/10.1002/9780470661345.smc161.

(20) Jin, Y.; Yu, C.; Denman, R. J.; Zhang, W. Recent Advances in Dynamic Covalent Chemistry. *Chem. Soc. Rev.* **2013**, *42* (16), 6634–6654. https://doi.org/10.1039/c3cs60044k.

(21) Corbett, P. T.; Leclaire, J.; Vial, L.; West, K. R.; Wietor, J. L.; Sanders, J. K. M.; Otto, S. Dynamic Combinatorial Chemistry. *Chem. Rev.* **2006**, *106* (9), 3652–3711. https://doi.org/10.1021/cr020452p.

(22) Black, S. P.; Sanders, J. K. M.; Stefankiewicz, A. R. Disulfide Exchange: Exposing Supramolecular Reactivity through Dynamic Covalent Chemistry. *Chem. Soc. Rev.* **2014**, *43* (6), 1861–1872. https://doi.org/10.1039/c3cs60326a.

(23) Belenguer, A. M.; Lampronti, G. I.; Wales, D. J.; Sanders, J. K. M. Direct Observation of Intermediates in a Thermodynamically Controlled Solid-State Dynamic Covalent Reaction. *J. Am. Chem. Soc.* **2014**, *136* (46), 16156–16166. https://doi.org/10.1021/ja500707z.

(24) Caraballo, R.; Rahm, M.; Vongvilai, P.; Brinck, T.; Ramström, O. Phosphine-Catalyzed Disulfide Metathesis. *Chem. Commun.* **2008**, No. 48, 6603–6605. https://doi.org/10.1039/b815710c.

(25) Fritze, U. F.; Von Delius, M. Dynamic Disulfide Metathesis Induced by Ultrasound. *Chem. Commun.* **2016**, *52* (38), 6363–6366. https://doi.org/10.1039/c6cc02034h.

(26) Belenguer, A. M.; Friščić, T.; Day, G. M.; Sanders, J. K. M. Solid-State Dynamic Combinatorial Chemistry: Reversibility and Thermodynamic Product Selection in Covalent Mechanosynthesis. *Chem. Sci.* **2011**, *2* (4), 696. https://doi.org/10.1039/c0sc00533a.

(27) Rasmussen, B.; Sørensen, A.; Gotfredsen, H.; Pittelkow, M. Dynamic Combinatorial Chemistry with Diselenides and Disulfides in Water. *Chem. Commun.* **2014**, *50* (28), 3716–3718. https://doi.org/10.1039/c4cc00523f.

(28) Dopieralski, P.; Ribas-Arino, J.; Anjukandi, P.; Krupicka, M.; Kiss, J.; Marx, D. The Janus-Faced Role of External Forces in Mechanochemical Disulfide Bond Cleavage. *Nat. Chem.* **2013**, *5* (8), 685–691. https://doi.org/10.1038/nchem.1676.

(29) Sobczak, S.; Drożdż, W.; Lampronti, G. I.; Belenguer, A. M. A.; Katrusiak, A.; Stefankiewicz, A. R. Dynamic Covalent Chemistry under High-Pressure:A New Route to Disulfide Metathesis. *Chem. - A Eur. J.* **2018**, *24* (35), 8769–8773. https://doi.org/10.1002/chem.201801740.

(30) Klotz, S.; Chervin, J. C.; Munsch, P.; Le Marchand, G. Hydrostatic Limits of 11 Pressure Transmitting Media. *J. Phys. D. Appl. Phys.* **2009**, *42* (7). https://doi.org/10.1088/0022-3727/42/7/075413.

(31) Olejniczak, A.; Katrusiak, A. Supramolecular Reaction between Pressure-Frozen Acetonitrile Phases α and β. *J. Phys. Chem. B* **2008**, *112* (24), 7183–7190. https://doi.org/10.1021/jp800753n.

(32) van Eldik, R.; Klärner, F. G. *High Pressure Chemistry: Synthetic, Mechanistic, and Supercritical Applications*; van Eldik, R., Klärner, F., Eds.; Wiley, 2007. https://doi.org/10.1002/9783527612628.

(33) Benson, S. W.; Berson, J. A. The Effect of Pressure on the Rate and Equilibrium Constants of Chemical Reactions. The Calculation of Activation Volumes by Application of the Tait Equation. *J. Am. Chem. Soc.* **1962**, *84* (2), 152–158. https://doi.org/10.1021/ja00861a005.

(34) Asano, T.; Noble, W. J. L. Activation and Reaction Volumes in Solution. *Chem. Rev.* **1978**, *78* (4), 407–489. https://doi.org/10.1021/cr60314a004.

(35) Noble, W. J. Organic Synthesis at High Pressure. In *High Pressure Chemistry and Biochemistry*; 1987. https://doi.org/10.1007/978-94-009-3827-4_12.

(36) van Eldik, R.; Klärner, F. G. *High Pressure Chemistry: Synthetic, Mechanistic, and Supercritical Applications*; Wiley-VCH, 2007. https://doi.org/10.1002/9783527612628.

(37) Merrill, L.; Bassett, W. A. Miniature Diamond Anvil Pressure Cell for Single Crystal X-Ray Diffraction Studies. *Rev. Sci. Instrum.* **1974**, *45* (2), 290–294. https://doi.org/10.1063/1.1686607.

(38) Piermarini, G. J.; Block, S.; Barnett, J. D.; Forman, R. A.

Calibration of the Pressure Dependence of the R1ruby Fluorescence Line to 195 Kbar. *J. Appl. Phys.* **1975**, *46* (6), 2774–2780. https://doi.org/10.1063/1.321957.

(39) Mao, H. K.; Xu, J.; Bell, P. M. Calibration of the Ruby Pressure Gauge to 800 Kbar under Quasi-Hydrostatic Conditions. *Journal of Geophysical Research*. 1986, pp 4673–4676. https://doi.org/10.1029/jb091ib05p04673.

(40) Azcune, I.; Odriozola, I. Aromatic Disulfide Crosslinks in Polymer Systems: Self-Healing, Reprocessability, Recyclability and More. *Eur. Polym. J.* **2016**, *84*, 147–160. https://doi.org/10.1016/j.eurpolymj.2016.09.023.

(41) Nevejans, S.; Ballard, N.; Miranda, J. I.; Reck, B.; Asua, J. M. The Underlying Mechanisms for Self-Healing of Poly(Disulfide)S. *Phys. Chem. Chem. Phys.* **2016**, *18* (39), 27577–27583. https://doi.org/10.1039/c6cp04028d.

(42) Formoso, E.; Asua, J. M.; Matxain, J. M.; Ruipérez, F. The Role of Non-Covalent Interactions in the Self-Healing Mechanism of Disulfide-Based Polymers. *Phys. Chem. Chem. Phys.* **2017**, *19* (28), 18461–18470. https://doi.org/10.1039/c7cp03570e.

(43) Matxain, J. M.; Asua, J. M.; Ruipérez, F. Design of New Disulfide-Based Organic Compounds for the Improvement of Self-Healing Materials. *Phys. Chem. Chem. Phys.* **2016**, *18* (3), 1758–1770. https://doi.org/10.1039/c5cp06660c.

(44) Irigoyen, M.; Matxain, J. M.; Ruipérez, F. Effect of Molecular Structure in the Chain Mobility of Dichalcogenide-Based Polymers with Self-Healing Capacity. *Polymers (Basel).* **2019**, *11* (12). https://doi.org/10.3390/polym11121960.

(45) Sobczak, S.; Katrusiak, A. Colossal Strain Release by Conformational Energy Up-Conversion in a Compressed Molecular Crystal. *J. Phys. Chem. C* **2017**, *121* (5), 2539–2545. https://doi.org/10.1021/acs.jpcc.6b11030.

(46) Stoiljkovich, D.; Jovanovich, S. Mechanism of the High-Pressure Free Radical Polymerization of Ethylene. *J. Polym. Sci. A1.* **1981**, *19* (3), 741–747.

(47) Stoiljković, D.; Jovanović, S. Compression, Supramolecular Organization and Free Radical Polymerization of Ethylene Gas. *Polyolefins J.* **2019**, *6* (1), 23–41. https://doi.org/10.22063/poj.2018.2252.1117.

(48) Dopieralski, P.; Ribas-Arino, J.; Anjukandi, P.; Krupicka, M.; Marx, D. Unexpected Mechanochemical Complexity in the Mechanistic Scenarios of Disulfide Bond Reduction in Alkaline Solution. *Nat. Chem.* **2017**, *9* (2), 164–170. https://doi.org/10.1038/NCHEM.2632.

(49) Glidewell, C.; Low, J. N.; Wardell, J. L. Conformational Preferences and Supramolecular Aggregation in 2-Nitrophenylthiolates: Disulfides and Thiosulfonates. *Acta Crystallogr. Sect. B Struct. Sci.* **2000**, *56* (5), 893–905. https://doi.org/10.1107/S0108768100007114.

Insert Table of Contents artwork here

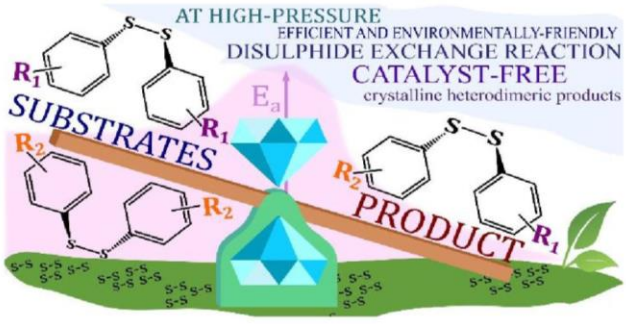

(**R6**) Sobczak, S.; Katrusiak, A. Colossal Strain Release by Conformational Energy Up-Conversion in a Compressed Molecular Crystal. *J. Phys. Chem. C* **2017**, 121 (5), 2539–2545

THE JOURNAL OF PHYSICAL CHEMISTRY C

Article

pubs.acs.org/JPCC

Colossal Strain Release by Conformational Energy Up-Conversion in a Compressed Molecular Crystal

Szymon Sobczak and Andrzej Katrusiak*

Department of Materials Chemistry, Faculty of Chemistry, Adam Mickiewicz University, Umultowska 89b, 61-614 Poznań, Poland

Supporting Information

ABSTRACT: External stimuli trigger conformational up-conversion in the molecules of di-*p*-tolyl disulfide ($CH_3-C_6H_4-S-)_2$, compensating the stress and absorbing its energy. These mechanochemical transformations explain at the molecular level the lubricating performance of di-*p*-tolyl disulfide and suggest new applications for storing energy. High pressure induces the conversion either in the solid state, as a phase transition, or at the nucleation stage on the solution-solid interphase as a detour of crystallization preference. The discontinuous transition at 1.6 GPa reduces the symmetry of ambient-pressure monoclinic phase α (space group $P2_1$) to triclinic phase β (space group $P1$). The recrystallizations above 0.45 GPa yield a new polymorph γ (space group $P2_1/c$), most spectacular in the conformational up-conversion absorbing 6 kJmol^{-1}.

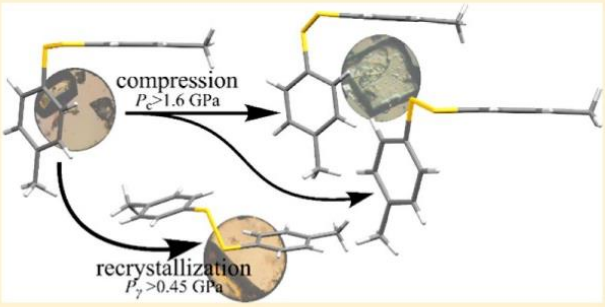

INTRODUCTION

Disulfides for decades have been applied as additives in lubricants,[1] significantly increasing their bearing properties under extreme loads. Allum and Forbes[2] demonstrated that the high-pressure performance of organic disulfides increases from phenyl, across *n*-butyl, *s*-butyl, and *t*-butyl to benzyl. The antiwear properties of organic disulfides increase from *n*-butyl, allyl, and benzyl to phenyl,[3] suggesting that the load-bearing properties are associated with conformational changes and also that they depend on the strength of the S−S bonds. All these features at the macroscopic and microscopic levels are relevant to the technical applications of organic disulfides. The molecule of di-*p*-tolyl disulfide is prototypic for a large group of diphenyl disulfides. Their common features are the exceptional conformational flexibility of the C−S−S−C bridge between the phenyls and low melting temperature. Of diphenyl-disulfide derivatives studied by X-ray diffraction and deposited in the Cambridge Structural Database (CSD Version 5.37,[4] ConQuest Version 1.18,[5] Figure S1 in the Supporting Information), there are 44 crystals with half of the molecule in the asymmetric unit ($Z' = 1/2$), 122 structures with one independent molecule ($Z' = 1$), 5 structures with 1.5 molecules independent ($Z' = 1.5$), 10 structures with $Z' = 2$, and 1 structure with $Z' = 4$ (Table S1). There are no molecules with symmetry C_i, while 45 molecules are C_2-symmetric and 147 asymmetric. Thus, in all these crystals, a conformational chirality of individual molecules is associated with the torsion angles around tether bonds C−S−S−C. This can be connected to a considerable part of the deposited noncentrosymmetric crystal structures (7%). The distribution of flexible torsion angles C−C−S−S and S−S−C−C as a function of angle C−S−S−C suggests that the asymmetric conformation of diphenyl-sulfide is energetically favored (Figure 1, Figure S2).

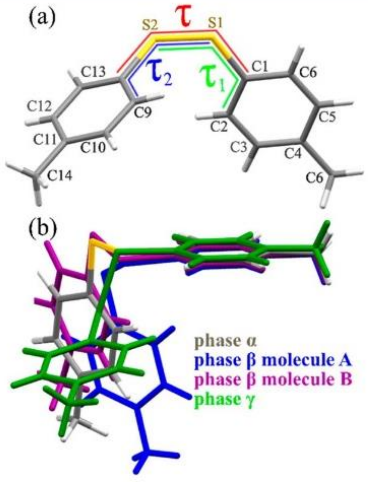

Figure 1. (a) The molecule of di-*p*-tolyl disulfide (*p*-Tol_2S_2) with soft torsion angles indicated by red, blue, and green lines drawn along the involved tether bonds; (b) the conformers present in phases α, β (two symmetry-independent molecules present in phase β are labeled with letters A and B), and γ superimposed on one of the tolyl rings minimizing the differences of the other ring position.

Received: November 2, 2016
Revised: January 4, 2017
Published: January 4, 2017

DOI: 10.1021/acs.jpcc.6b11030
J. Phys. Chem. C 2017, 121, 2539−2545

It is well-known that high pressure strongly affects molecular arrangement in crystals, as demonstrated by obtaining new polymorphs of several common compounds,[6−11] active pharmaceutical ingredients,[12−21] explosives,[22,23] ferroelectrics,[24−28] relaxors,[29−33] semiconductors,[34,35] and other types of materials.[36−44] Apart from new forms induced by compressing solid compounds, also other neat polymorphs and solvates were obtained by in-situ high-pressure recrystallizations at varied temperatures and of different solutions. Finally, new compounds can be synthesized at extreme conditions.[45−47] The mechanisms of high-pressure crystallization and reactions involve the compressed molecular environments and new types of intermolecular interactions as well as the changes in the molecular structure, such as conformational transformations. High pressure efficiently reduces the volume of organic compounds and often modifies conformation of molecules,[48] which adjust to the steric hindrances,[49] aggregation type,[50] and intermolecular interactions in a confined volume of compressed crystal.[51] However, the energy partition of these transformations is not fully understood. Presently, we have investigated the effect of pressure on conformational properties of di-*p*-totyl disulfide (*p*-Tol_2S_2, Figure 1) and its molecular aggregation in the crystalline state.

■ EXPERIMENTAL SECTION

High-pressure experiments of *p*-Tol_2S_2 have been performed in a Merrill−Bassett diamond-anvil cell (DAC), modified by mounting the diamond anvils directly on the steel supports with conical windows.[52] Pressure in the DAC was calibrated by the ruby-fluorescence method[53] with a photon control spectrometer of enhanced resolution, affording the accuracy of 0.02 GPa. The gaskets of 0.3 mm tungsten foil with spark-eroded holes 0.4 mm in diameter were used. High-pressure experiments were carried out in two different ways (Figure 2).

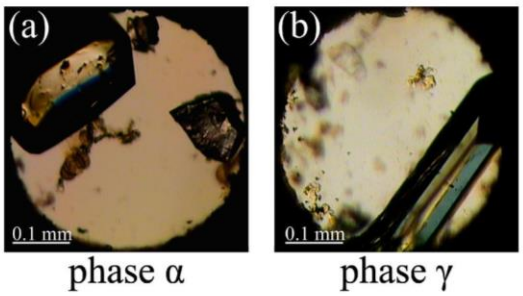

Figure 2. Single crystals of di-*p*-tolyl disulfide recrystallized in situ in isochoric conditions from the isopropanol solution: (a) phase α at 0.15 GPa; (b) phase γ at 0.45 GPa (cf. Figures S4 and S5). Several small ruby chips are scattered in the chamber for pressure calibration.

Initially, the isothermal compression of a single crystal of *p*-Tol_2S_2 was measured in the DAC in glycerin as the hydrostatic medium.[54] Glycerin was used in order to avoid dissolution of the sample, so the crystals grown at ambient conditions could be compressed. The ambient-pressure phase α was compressed monotonically to 1.6 GPa, when a transition to a new phase β took place. The transition did not significantly affect the quality of the crystal sample, and the compression of phase β was studied to 2.8 GPa. On releasing pressure, the β phase of *p*-Tol_2S_2 transformed back to phase α below 1.6 GPa. In another series of experiments, we explored the thermodynamic landscape of *p*-Tol_2S_2 by recrystallizing it in situ in the DAC at elevated pressure. In these experiments, methanol, ethanol, and isopropanol were used as the solvents and hydrostatic fluids for isochoric crystallizations. The best quality single crystals could be grown from the isopropanol solutions. The DAC chamber was loaded with a few crystal grains of *p*-Tol_2S_2 and was filled up with the solvent, and after sealing the DAC and generating the required pressure, the whole DAC was heated by a heat gun until all the *p*-Tol_2S_2 sample inside dissolved. Then, the DAC was slowly cooled while the progress in the single-crystal growth was controlled through a microscope (Figures S4−S5). Above 0.45 GPa, the isochoric recrystallizations[55] yielded a new phase, labeled γ (Figure 2). Their crystal symmetry and structure were determined by X-ray diffraction. We attempted to recover the samples in phase γ from the DAC; however, they all failed, suggesting that phase γ is unstable at ambient pressure.

The X-ray diffraction data were measured on a KUMA4-CCD diffractometer (MoKα radiation from a sealed tube). The DAC was centered by the gasket-shadow method.[56] The data were collected and were preliminarily reduced with the CrysAlisPro suite version 1.171.33.[57] The structures were solved by direct methods (Shelxs) and were refined with SHELXL;[58,59] the Olex2 interface was used.[60] H-Atoms were located from molecular geometry at the ideal positions, with U_{iso} equal to 1.2 U_{eq} of their carriers. The final crystal data are summarized in Table 1 (cf. Table S1) and have been deposited in the Cambridge Structural Database (CCDC, www.ccdc.cam.ac.uk) as supplementary publications with reference numbers CCDS 1509319−1509333; these deposits can be obtained free of charge from the CCDC and Crystallography Open Database (COD, www.crystallography.net).

To calculate the potential energy (E_p) of *p*-Tol_2S_2 conformers, we have applied several levels of theory[61] which have been described in the Supporting Information (Figure S6). The atomic coordinates determined by the diffraction measurements were used as the starting models. Full optimizations, except soft torsion angles $\tau/\tau_1/\tau_2$ fixed at the values present in phases $\alpha/\beta/\gamma$, were performed. For all the quantum mechanical calculations, the program Gaussian09e was applied.[62]

■ DISCUSSION

The ambient-pressure phase α of *p*-Tol_2S_2 is monotonically compressed to P_c at 1.6 GPa, when the crystal discontinuously transforms to a new high-pressure phase β. The phase transition is clearly marked by the molecular-volume drop δV_m of −2.5 Å^3, as well as by a slight lengthening of the unit-cell parameter *a*, strong lengthening of *b*, and strong shortening of *c* (Figure 3). The transition proceeds between monoclinic phase α and triclinic phase β, with the unit-cell shape approximately preserved (as described earlier). Above P_c, angles α and γ divert by about 5° from 90° and angle β increases by 2.3° (Figure S3), so these shear strains of the crystal considerably contribute to the volume drop at the phase transition. It is remarkable that the relatively large samples transformed to phase β in one piece, without splitting of reflection, allowing the continuation of single-crystal diffractometric measurements. This could be a sign of purely enantiomorphic crystals of phases α and β and also of the strain-compensating role of conformational transformations of molecules.

The recrystallizations below 0.45 GPa of phase α yielded parallelepiped crystals, clearly different from elongated plates of phase γ grown above 0.45 GPa (Figure 2, recrystallization

DOI: 10.1021/acs.jpcc.6b11030
J. Phys. Chem. C 2017, 121, 2539−2545

Table 1. Selected Crystal Data of di-*p*-Tolyl Disulfide (p-Tol_2S_2) Polymorphs α, β, and γ at the Pressure Limits of Their Stability Regions and at 2.8 GPa

phase	α	α	β	β	γ	γ
pressure	0.1 MPa	1.52 GPa	1.72 GPa	2.8 GPa	0.45 MPa	2.8 GPa
crystal system	monoclinic	monoclinic	triclinic	triclinic	monoclinic	monoclinic
space group	$P2_1$	$P2_1$	$P1$	$P1$	$P2_1/c$	$P2_1/c$
a (Å)	7.59270(11)	7.3193(19)	7.3057(5)	7.1934(6)	15.26(2)	14.09(6)
b (Å)	5.71318(10)	5.4277(18)	5.5093(12)	5.4685(3)	5.9620(4)	5.7029(14)
c (Å)	14.7220(2)	14.37(3)	14.038 (8)	13.814(4)	14.615(10)	14.18(2)
α (deg)	90	90	95.14(3)	95.915(14)	90	90
β (deg)	94.7615(13)	94.93(8)	97.23(2)	98.142(17)	115.56(14)	114.8(4)
γ (deg)	90	90	85.358(14)	84.699(6)	90	90
volume (Å^3)	636.414(17)	568.6(13)	556.9(3)	533.39(15)	1099(2)	1035(6)
Z/Z'	2/1	2/1	2/2	2/2	4/1	4/1

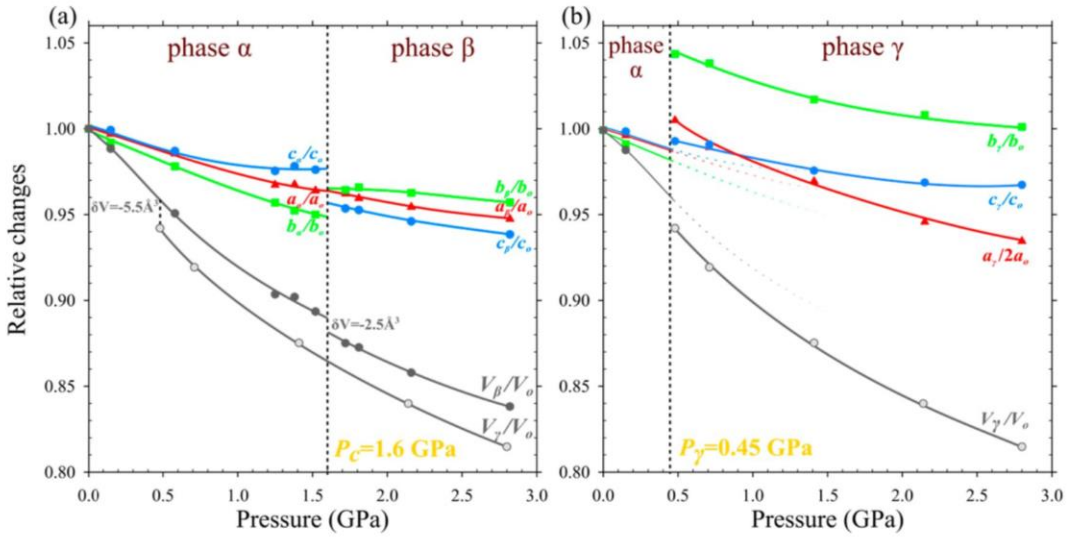

Figure 3. Compression of the unit-cell parameters in p-Tol_2S_2 phases: (a) in phases α and β related to the unit-cell parameters of phase α at 0.1 MPa: a_o, b_o, and c_o; as well as (b) in phases α and γ related to $2a_o$, b_o, and c_o. The vertical dotted line in a marks critical pressure P_c of solid−solid phase transition between phases α and β and in b it marks pressure P_γ reversing the crystallization preference between phases α and γ. The magnitudes of corresponding discontinuous molecular volume changes δV are indicated in plot a.

details are shown in Figures S4 and S5). The unit cell of phase γ is surprisingly similar to those of phases α and β (except for the doubling of parameter a_γ, cf. Figures 3 and 4), despite that molecules assume significantly different conformations. This correlation of the unit-cell dimensions is due to analogous interactions of tolyl rings, and it is discussed further later.

In phase α, there is one independent molecule ($Z' = 1$), and its conformation is asymmetric, with C−C−S−S angles τ_1 and τ_2 significantly different, of 2° and −22°, respectively (Figure 5). Their values and the difference $(\tau_1 - \tau_2)$ of about 24° are hardly affected by the pressure within phase α up to P_c at 1.6 GPa. Above P_c in phase β, the symmetry of p-Tol_2S_2 is reduced to space group $P1$, and the independent part of the structure doubles and contains two molecules ($Z' = 2$) denoted by letters A and B (Figures 1 and 4 and Figure S7). The difference $(\tau_1 - \tau_2)$ is reduced to nearly 0° in molecule B, which becomes nearly symmetric with respect to the 2-fold axis (pseudo-C_2) perpendicular to the S−S bond. In molecule A, the $(\tau_1 - \tau_2)$ difference increases to over 60°, indicating a considerably more asymmetric conformer than that in phase α. Thus, the onset of structural phase transformation at 1.6 GPa discriminates the molecules into two distinct conformers in phase β. According to our theoretical calculations, conformers A and B present in phase β have their potential energy (E_p) higher than that in ambient phase α by 2 and 0.5 kJmol^{-1}, respectively (Figure 6).

The differentiation of molecular shape in two conformers at P_c improves their crystal packing[64] (Figure 4) by adjusting the strains of intermolecular interactions to short contacts hampering the compression of the structure. In centrosymmetric phase γ, the molecules in one conformation can pack even denser (Table 1, Figure 3). Figure 7 shows that in phase α all short intermolecular contacts are compressed, except the initial lengthening of the shortest H···H contact to about 0.5 GPa. The strongest compression occurs for the H···H and S···H contacts, although the transition to phase β at P_c reverses these trends to about 2.2 GPa and also slows down the compression of other contacts.

The formation of phase γ clearly releases the shortest contacts. The most significant elongation is observed for distances S···H and C···C. The elimination of these short contacts in the compressed phase γ is achieved at the cost of conformational up-conversion. Above 1.5 GPa, the compression of contacts H···H and S···H is much weaker, and these contacts are fewer and much longer compared to those in phases α and β. These structural dimensions are consistent with the stability of phase γ above 0.45 GPa and with its

DOI: 10.1021/acs.jpcc.6b11030
J. Phys. Chem. C 2017, 121, 2539−2545

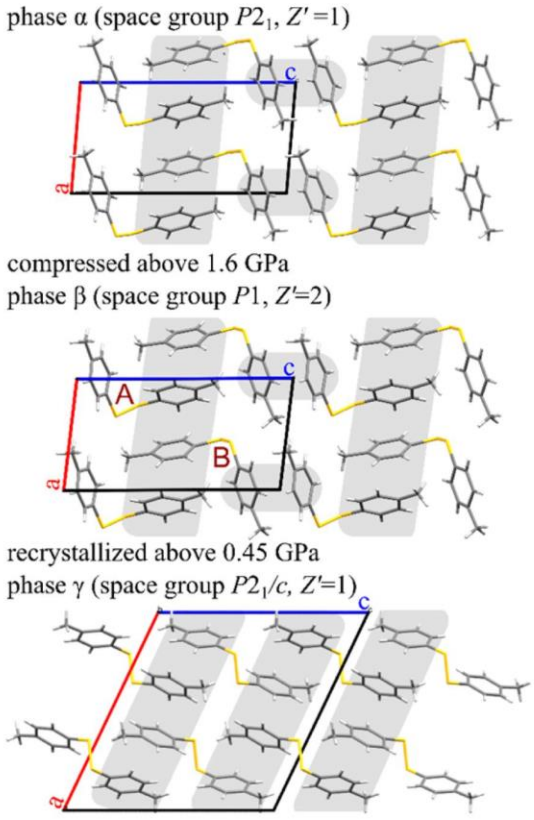

Figure 4. Crystal structure of *p*-Tol_2S_2 in phases α (top), β (middle), and γ (bottom). Capital letters A and B label independent molecules in phase β. Similar row and pair motifs of *p*-tolyl-sulfide moieties are highlighted.

compression stronger than that of phases α and β. However, the formation of phase γ stable above 0.45 GPa requires the sample recrystallization. Similarly, the formation of high-pressure phases of imidazole[65] and of 1,4-diazabicyclo[2.2.2]-octane hydrobromide monohydrate[66] required recrystallization, and therefore they were called "hidden phases". The formation of phase γ of *p*-Tol_2S_2 requires that molecules assume a considerably different conformation energetically disadvantaged by about 6.0 kJmol^{-1} compared to that in phase α and similarly by about 6.0 and 5.5 kJmol^{-1} compared to molecules A and B in phase β, respectively (Figure 7). It is characteristic that despite considerable differences in torsion angles τ, τ_1, and τ_2 the dihedral angle between tolyl rings in one molecule remains within the 70−90° range. This dihedral angle is equal to 86.56° in phase α, to 89.44° in phase β, to 73.39° in molecules A and B, and to 80.99° in phase γ.

The high E_p value of the γ-phase conformer indicates that the main energetic gain of phase γ is in the intermolecular interactions. The formation of phase γ requires considerable rearrangements of molecules (compared to phases α and β). For these reasons, it is likely that phase γ can be accessed only through the recrystallization, when at the liquid−solid interphase the molecules adjust their conformation to the energetic wells associated with the most efficient packing.

The molecular aggregation in phase γ is distinct from those in phases α and β in that the toluene rings are differently arranged into rows, as illustrated in Figure 4. It is a common feature of all three *p*-Tol_2S_2 phases that the rows of rings along

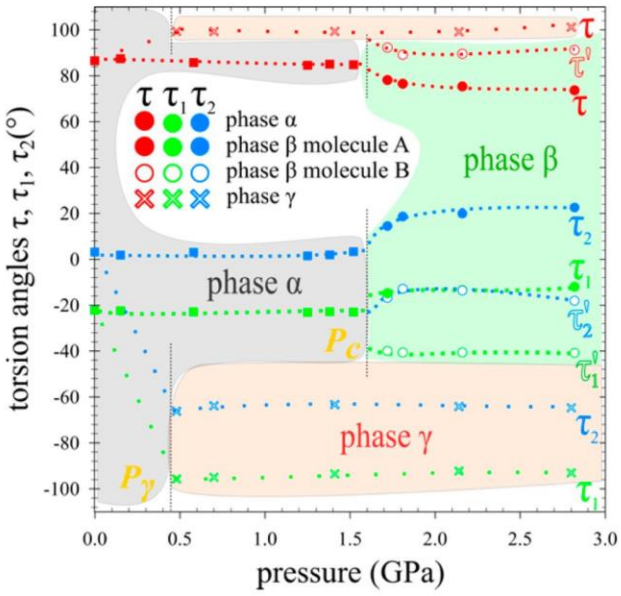

Figure 5. Molecular conformation described by torsion angles τ (C4−S1−S2−C11), τ_1 (C3−C4−S1−S2), and τ_2 (C12−C11−S2−S1), as well as the analogous primed values referring to molecule B, plotted vs pressure for experimentally determined *p*-Tol_2S_2 structures of phases α, β, and γ. The vertical dashed lines indicate the phase transition between phases α and β at P_c = 1.6 GPa and the change of preferential crystallization between phases α and γ at P_γ = 0.45 GPa. The regions of τ changes in *p*-Tol_2S_2 phases α, β and γ are highlighed in gray, green and red, respectively. The legend of symbols used for the τ angles is presented on the white background (cf. Figure 1). The dotted lines joining the points are for guiding the eye only.

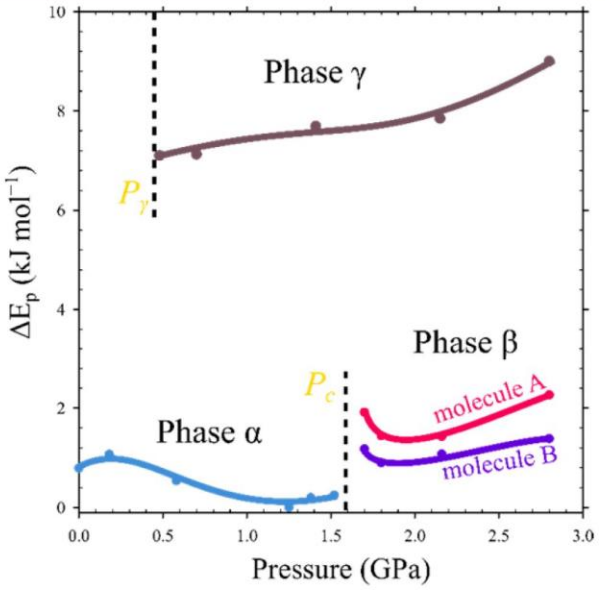

Figure 6. Potential energy changes (ΔE_p) calculated by Gaussian (cf. Experimental Section) for the isolated molecule in its conformation experimentally determined in the *p*-Tol_2S_2 structures of phases α, β, and γ. Two independent conformers A and B, present in phase β, were each treated separately in the calculations.

the direction [100] are due to CH···π bonds, analogues to the motifs described as αHα for toluene polymorphs. In this notation, the first letter describes the H atom location in the

DOI: 10.1021/acs.jpcc.6b11030
J. Phys. Chem. C 2017, 121, 2539−2545

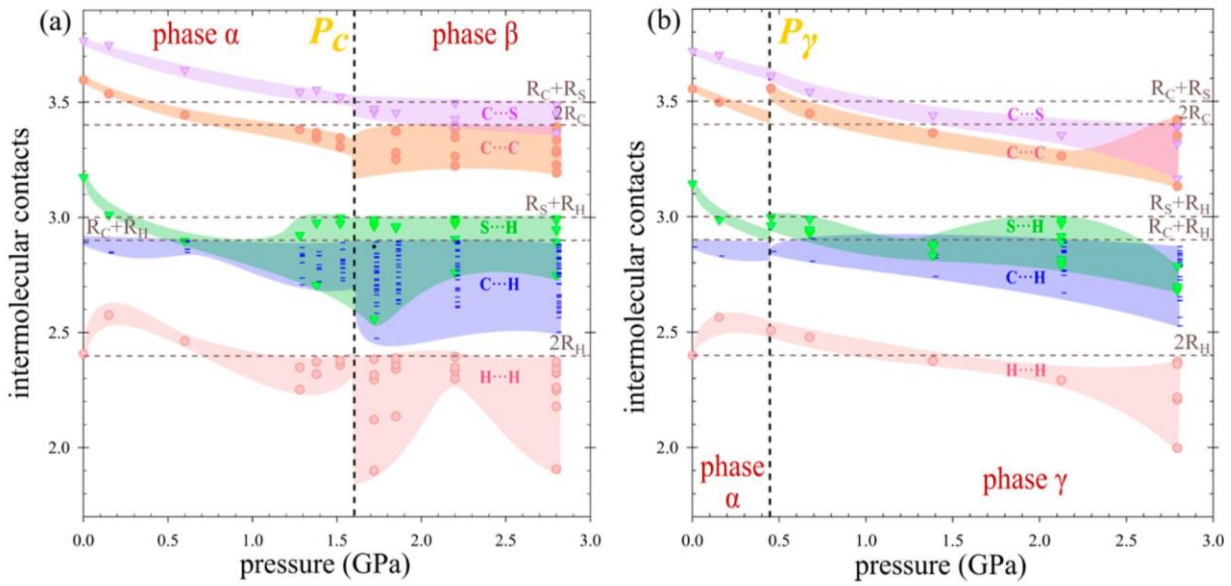

Figure 7. Intermolecular contacts H···H, H···C, H···S, C···C, and C···S shorter than the sum of van der Waals radii of interacting atoms in experimentally determined structures of p-Tol_2S_2 in (a) phases α and β as well as in (b) phases α and γ. The horizontal dashed lines mark the sums of van der Waals radii according to Bondi,[63] while the vertical dashed lines indicate the critical P_c and preference P_γ pressure separating the phases. The short contacts of the same type (H···H, H···C, H···S, C···C, and C···S) are highlighted in different colors for guiding the eye. See Figure S12 for the magnified versions of these plots.

tolyl ring (α-orto, β-meta, and γ-para, with respect to the methyl substituent, and m for the methyl H atoms), and the last letter indicates the location of the interacting C atom in the other molecule (here m indicated the methyl-substituted arene C-atom).[67] In p-Tol_2S_2 phases α and β, these rows are separated by detached pairs of rings interacting approximately along the direction [001] by motif αHαm, (with approximately equal intermolecular distances from H12 to C11 and C12). In toluene phase I the interactions of αHα and αHm motifs combine molecules into a 2-dimensional pattern.[67]

In p-Tol_2S_2 phase γ, all toluene rings are arranged into rows along [100], according to motifs αHα and βHm.[67] The rows along direction [x], common for all phases, are responsible for a similar length of the unit-cells dimensions $2a_\alpha$, $2a_\beta$, and a_γ (corresponding to quadrupoled CH···π distance of ca. 3.2 Å); parameters b correspond to the phenyl ring dimension along its plane and perpendicular to C−C bonds (ca. 5.5 Å); and similar dimensions of parameters c in phases α, β, and γ result in the molecular-volume (V_m) constrain.

It is remarkable that the work contribution to the Gibbs' energy calculated as $\int V(p)\mathrm{d}P$ between ambient pressure and the smallest pressure of phase γ is equal to 6.6 kJmol^{-1}, which agrees well with the conformational energy of molecules in this phase (Figure 6). It is consistent with a small contribution of intermolecular interactions and relatively long intermolecular distances at 0.45 GPa. The work contribution to Gibbs' energy of phases α and β compressed between 0.1 MPa and 1.72 GPa is 18 kJmol^{-1}, which is mainly associated with compressed interactions, and only about 1.5 kJmol^{-1} comes from the conformational conversion. Figure 8 illustrates the thermodynamic relations between the p-Tol_2S_2 phases. Phase α is thermodynamically stable at ambient pressure, but above 0.45 GPa, it becomes metastable with respect to phase γ. At 1.6 GPa, phase β becomes more stable than phase α, and the α–β phase transition occurs. Phase γ, the stable phase above 0.45 GPa,

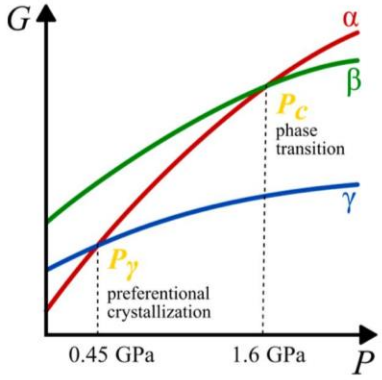

Figure 8. Schematically shown relations between free Gibbs' energy (G) of phases α, β, and γ as a function of pressure for p-Tol_2S_2.

requires high-pressure recrystallization to be formed; up to 2.8 GPa, it was not formed by a solid−solid transformation.

■ CONCLUSIONS

It has been shown that the interplay of conformational transformation of p-Tol_2S_2 molecules and their interactions control the thermodynamic stability of this compound. There is an apparent conformation−volume relation for the crystal, as the molecules absorb the stress of compressed intermolecular contacts. Much stronger conformational conversion in the liquid or at the liquid−solid interface can be connected with the lubricating properties of p-Tol_2S_2. The molecules can absorb and store considerable amounts of energy, of about 6 kJmol^{-1}, and possibly even more in the liquid state, which reduces the thermal effect of friction. The up-conversion between conformers efficiently relaxes the strain. It appears that the conformational and energetic response of p-Tol_2S_2 molecules to the pressure stimuli can now be applied for smart liquid and

DOI: 10.1021/acs.jpcc.6b11030
J. Phys. Chem. C 2017, 121, 2539−2545

solid materials and can be further optimized for analogous[68,69] as well as new types of conformationally flexible compounds.

■ ASSOCIATED CONTENT

Supporting Information

The Supporting Information is available free of charge on the ACS Publications website at DOI: 10.1021/acs.jpcc.6b11030.

Detailed crystallographic data including ambient and high-pressure measurements of *p*-Tol_2S_2, CCSD database analysis, changes of cell angles, illustrations showing growth of the crystal phases α and γ, electrostatic potential mapped on Hirshfeld surfaces, potential energy chart, analysis of the volume and arrangement of voids (PDF)

■ AUTHOR INFORMATION

Corresponding Author

*E-mail: katran@amu.edu.pl. Phone: +48618291590.

ORCID

Andrzej Katrusiak: 0000-0002-1439-7278

Notes

The authors declare no competing financial interest.

■ ACKNOWLEDGMENTS

PL-Grid Infrastructure is acknowledged for providing access to computational resources.

■ REFERENCES

(1) Forbes, E. S. The load-carrying action of organo-sulphur compounds-A review. *Wear* **1970**, *15*, 87−96.

(2) Allum, K. G.; Forbes, E. S. The load-carrying properties of organic sulphur compounds. Pt. II. The influence of chemical structure on the anti-wear properties of organic disulphides. *J. Inst. Petrol.* **1967**, *53*, 521.

(3) Allum, K. G.; Ford, J. F. Load-carrying properties of organic sulphur compounds. 2. Influence of chemical structure on anti-wear properties of organic disulphides. *J. Inst. Petrol.* **1965**, *51*, 497.

(4) Allen, F. H. The Cambridge Structural Database: A quarter of a million crystal structures and rising. *Acta Crystallogr., Sect. B: Struct. Sci.* **2002**, *58*, 380−388.

(5) Bruno, I. J.; Cole, J. C.; Edgington, P. R.; Kessler, M.; Macrae, C. F.; McCabe, P.; Pearson, J.; Taylor, R. New software for searching the Cambridge Structural Database and visualizing crystal structures. *Acta Crystallogr., Sect. B: Struct. Sci.* **2002**, *58*, 389−397.

(6) Allan, D.; Clark, S.; Brugmans, M.; Ackland, G.; Vos, W. Structure of crystalline methanol at high pressure. *Phys. Rev. B: Condens. Matter Mater. Phys.* **1998**, *58*, R11809−R11812.

(7) Boldyreva, E. V.; Ivashevskaya, S. N.; Sowa, H.; Ahsbahs, H.; Weber, H. P. Effect of high pressure on crystalline glycine: A new high-pressure polymorph. *Dokl. Phys. Chem.* **2004**, *396*, 111−114.

(8) Chen, C.; Xu, Y.; Sun, X.; Wang, S. Novel superconducting phases of HCl and HBr under high pressure: An ab initio study. *J. Phys. Chem. C* **2015**, *119*, 17039−17043.

(9) Andrzejewski, M.; Olejniczak, A.; Katrusiak, A. Humidity control of isostructural dehydration and pressure-induced polymorphism in 1,4-diazabicyclo[2.2.2]octane dihydrobromide monohydrate. *Cryst. Growth Des.* **2011**, *11*, 4892−4899.

(10) Patyk, E.; Skumiel, J.; Podsiadło, M.; Katrusiak, A. High-pressure (+)-sucrose polymorph. *Angew. Chem., Int. Ed.* **2012**, *51*, 2146−2150.

(11) Patyk, E.; Katrusiak, A. Transformable H-bonds and conformation in compressed glucose. *Chem. Sci.* **2015**, *6*, 1991−1995.

(12) Shakhtshneider, T. P.; Boldyreva, E. V.; Vasilchenko, M. A.; Ahsbahs, H.; Uchtmann, H. Anisotropy of crystal structure distortion in organic molecular crystals of drugs induced by hydrostatic compression. *J. Struct. Chem.* **1999**, *40*, 892−898.

(13) Boldyreva, E. V.; Shakhtshneider, T. P.; Vasilchenko, M. A.; Ahsbahsc, H.; Uchtmann, H. Anisotropic crystal structure distortion of the monoclinic polymorph of acetaminophen at high hydrostatic pressures. *Acta Crystallogr., Sect. B: Struct. Sci.* **2000**, *56*, 299−309.

(14) Boldyreva, E. V.; Shakhtshneider, T. P.; Ahsbahs, H.; Sowa, H.; Uchtmann, H. Effect of high pressure on the polymorphs of paracetamol. *J. Therm. Anal. Calorim.* **2002**, *68*, 437−452.

(15) Tan, X.; Wang, K.; Li, S.; Yuan, H.; Yan, T.; Liu, J.; Yang, K.; Liu, B.; Zou, G.; Zou, B. Exploration of the pyrazinamide polymorphism at high pressure. *J. Phys. Chem. B* **2012**, *116*, 14441−14450.

(16) Fabbiani, F. P. A; Buth, G.; Levendis, D. C.; Cruz-Cabeza, A. J. Pharmaceutical Hydrates under ambient conditions from high-pressure seeds: a case study of GABA monohydrate. *Chem. Commun. (Cambridge, U. K.)* **2014**, *50*, 1817−1819.

(17) Ostrowska, K.; Kropidłowska, M.; Katrusiak, A. High-pressure crystallization and structural transformations in compressed R,S-ibuprofen. *Cryst. Growth Des.* **2015**, *15*, 1512−1517.

(18) Neumann, M. A.; van de Streek, J.; Fabbiani, F. P. A.; Hidber, P.; Grassmann, O. Combined crystal structure prediction and high-pressure crystallization in rational pharmaceutical polymorph screening. *Nat. Commun.* **2015**, *6*, 7793.

(19) Zakharov, B.; Seryotkin, Y.; Tumanov, N.; Paliwoda, D.; Hanfland, M.; Kurnosov, A. V.; Boldyreva, E. V. The role of fluids in high-pressure polymorphism of drugs: different behaviour of β-chlorpropamide in different inert gas and liquid media. *RSC Adv.* **2016**, *6*, 92629−92637.

(20) Seryotkin, Y. V.; Drebushchak, T. N.; Boldyreva, E. V. A high-pressure polymorph of chlorpropamide formed on hydrostatic compression of the α-form in saturated ethanol solution. *Acta Crystallogr., Sect. B: Struct. Sci., Cryst. Eng. Mater.* **2013**, *69*, 77−85.

(21) Zakharov, B. A.; Goryainov, S. V.; Boldyreva, E. V. Unusual seeding effect in the liquid-assisted high-pressure polymorphism of chlorpropamide. *CrystEngComm* **2016**, *18*, 5423−5428.

(22) Davidson, A. J.; Oswald, I. D. H.; Francis, D. J.; Lennie, A. R.; Marshall, W. G.; Millar, D. I. A.; Pulham, C. R.; Warren, J. E.; Cumming, A. S. Explosives under pressure—the crystal structure of gamma-RDX as determined by high-pressure X-ray and neutron diffraction. *CrystEngComm* **2008**, *10*, 162−165.

(23) Fabbiani, F. P. A.; Pulham, C. R. High-pressure studies of pharmaceutical compounds and energetic materials. *Chem. Soc. Rev.* **2006**, *35*, 932−942.

(24) Szafrański, M. Low-temperature and high-pressure phase transitions in ferroelectric dabcoHBF4. *J. Phys.: Condens. Matter* **2004**, *16*, 6053−6062.

(25) Szafrański, M.; Szafraniak, I. Phase transitions and pressure effects in simple pyridinium salts. *J. Phys.: Condens. Matter* **2003**, *15* (35), 5933−5944.

(26) Gesi, K. Effect of hydrostatic pressure on ferroelectric and related phase transitions. *Phase Transitions* **1992**, *40* (1−4), 187−215.

(27) Sikora, M.; Pojawis, P.; Katrusiak, A. Damping and resonance correlations in OH···O bonded ferroelectrics. *J. Phys. Chem. C* **2013**, *117*, 14213−14217.

(28) Zieliński, W.; Katrusiak, A. Colossal monotonic response to hydrostatic pressure in molecular crystal induced by a chemical modification. *Cryst. Growth Des.* **2014**, *14*, 4247−4253.

(29) Kreisel, J.; Glazer, A.; Bouvier, P.; Lucazeau, G. High-pressure Raman study of a relaxor ferroelectric: The $Na_{0.5}Bi_{0.5}TiO_3$ perovskite. *Phys. Rev. B: Condens. Matter Mater. Phys.* **2001**, *63*, 1−10.

(30) Kreisel, J.; Dkhil, B.; Bouvier, P.; Kiat, J.-M. Effect of high pressure on relaxor ferroelectrics. *Phys. Rev. B: Condens. Matter Mater. Phys.* **2002**, *65*, 1−4.

(31) Chaabane, B.; Kreisel, J.; Dkhil, B.; Bouvier, P.; Mezouar, M. Pressure-induced suppression of the diffuse scattering in the model relaxor ferroelectric $PbMg_{(1/3)}Nb_{(2/3)}O_3$. *Phys. Rev. Lett.* **2003**, *90*, 257601.

(32) Kreisel, J.; Bouvier, P.; Maglione, M.; Dkhil, B.; Simon, A. High-pressure Raman investigation of the Pb-free relaxor $BaTi_{0.65}Zr_{0.35}O_3$. *Phys. Rev. B: Condens. Matter Mater. Phys.* **2004**, *69*, 092104.

(33) Nowicki, W.; Olejniczak, A.; Andrzejewski, M.; Katrusiak, A. reverse sequence of transitions in prototypic relaxor 1,4-diazabicyclo[2.2.2]octane. *CrystEngComm* **2012**, *14*, 6428.
(34) Tolbert, S. H.; Alivisatos, A. P. High-pressure structural transformations in semiconductor nanocrystals. *Annu. Rev. Phys. Chem.* **1995**, *46*, 595−625.
(35) Bergantin, S.; Moret, M.; Buth, G.; Fabbiani, F. P. A. Pressure-induced conformational change in organic semiconductors: triggering a reversible phase transition in rubrene. *J. Phys. Chem. C* **2014**, *118*, 13476−13483.
(36) Boldyreva, E. V. High-pressure-induced structural changes in molecular crystals preserving the space group symmetry: anisotropic distortion/isosymmetric polymorphism. *Cryst. Eng.* **2003**, *6*, 235−254.
(37) Mirebeau, I.; Goncharenko, I. N.; Cadavez-Peres, P.; Bramwell, S. T.; Gingras, M. J. P.; Gardner, J. S. Pressure-induced crystallization of a spin liquid. *Nature* **2002**, *420*, 54−57.
(38) Gauzzi, A.; Takashima, S.; Takeshita, N.; Terakura, C.; Takagi, H.; Emery, N.; Hérold, C.; Lagrange, P.; Loupias, G. Enhancement of superconductivity and evidence of structural instability in intercalated graphite CaC_6 under high pressure. *Phys. Rev. Lett.* **2007**, *98*, 15−18.
(39) Bujak, M.; Podsiadło, M.; Katrusiak, A. Energetics of conformational conversion between 1,1,2-trichloroethane polymorphs. *Chem. Commun. (Cambridge, U. K.)* **2008**, *37*, 4439−4441.
(40) Lemée-Cailleau, M.; Le Cointe, M.; Cailleau, H.; Luty, T.; Moussa, F.; Roos, J.; Brinkmann, D.; Toudic, B.; Ayache, C.; Karl, N. Thermodynamics of the neutral-to-ionic transition as condensation and crystallization of charge-transfer excitations. *Phys. Rev. Lett.* **1997**, *79*, 1690−1693.
(41) Minkov, V. S.; Tumanov, N. A.; Cabrera, R. Q.; Boldyreva, E. V. Low temperature/high pressure polymorphism in DL-cysteine. *CrystEngComm* **2010**, *12*, 2551−2560.
(42) Dziubek, K. F.; Katrusiak, A. Pressure-induced pseudorotation in crystalline pyrrolidine. *Phys. Chem. Chem. Phys.* **2011**, *13*, 15428−15431.
(43) Ridout, J.; Probert, M. R. High-pressure and low-temperature polymorphism in C−H···F−C hydrogen bonded monofluorotoluenes. *Cryst. Growth Des.* **2013**, *13*, 1943−1948.
(44) Cai, W.; Katrusiak, A. Conformationally assisted negative area compression in methyl benzoate. *J. Phys. Chem. C* **2013**, *117*, 21460−21465.
(45) Jurczak, J.; Baranowski, B. *High Pressure Chemical Synthesis*; Elsevier: Amsterdam, 1989.
(46) Olejniczak, A.; Katrusiak, A. Pressure induced transformations of 1,4 diazabicyclo[2.2.2]octane (DABCO) hydroiodide: diprotonation of dabco, its n-methylation and co-crystallization with methanol. *CrystEngComm* **2010**, *12*, 2528−2532.
(47) Zielinski, W.; Katrusiak, A. Hydrate smaller than the anhydrate. *CrystEngComm* **2015**, *17*, 5468−5473.
(48) Woodall, C. H.; Beavers, C. M.; Christensen, J.; Hatcher, L. E.; Intissar, M.; Parlett, A.; Teat, S. J.; Reber, C.; Raithby, P. R. Hingeless negative linear compression in the mechanochromic gold complex [(C6F5Au)2(μ-1,4-diisocyanobenzene)]. *Angew. Chem., Int. Ed.* **2013**, *52*, 9691−9694.
(49) Patyk, E.; Podsiadło, M.; Katrusiak, A. CH···N bonds and dynamics in isostructural pyrimidine polymorphs. *Cryst. Growth Des.* **2015**, *15*, 4039−4044.
(50) Gajda, R.; Katrusiak, A.; Crassous, J. Pressure-controlled aggregation in carboxylic acids. a case study on the polymorphism of bromochlorofluoroacetic acid. *CrystEngComm* **2009**, *11*, 2668−2676.
(51) Marciniak, J.; Andrzejewski, M.; Cai, W.; Katrusiak, A. Wallach's rule enforced by pressure in mandelic acid. *J. Phys. Chem. C* **2014**, *118* (8), 4309−4313.
(52) Merrill, L. miniature diamond anvil pressure cell for single crystal X-Ray diffraction studies. *Rev. Sci. Instrum.* **1974**, *45*, 290.
(53) Mao, H. K.; Xu, J.; Bell, P. M. calibration of the ruby pressure gauge to 800 Kbar under quasi-hydrostatic conditions. *J. Geophys. Res.* **1986**, *91*, 4673.
(54) Osakabe, T.; Kakurai, K. Feasibility tests on pressure-transmitting media for single-crystal magnetic neutron diffraction under high pressure. *Jpn. J. Appl. Phys.* **2008**, *47*, 6544.
(55) Podsiadlo, M.; Olejniczak, A.; Katrusiak, A. Halogen···halogen contra C−H···halogen interactions. *CrystEngComm* **2014**, *16*, 8279−8285.
(56) Budzianowski, A.; Katrusiak, A. High-pressure crystallographic experiments with a CCD detector. In *High-Pressure Crystallography*; Katrusiak, A., McMillan, P. F., Eds.; Kluwer Academic Publisher: Dordrecht, The Netherlands, 2004; pp 101−113.
(57) Xcalibur CCD System. *CrysAlisPro Software System*, version 1.171.33; Oxford Diffraction Ltd.: Wrocław, Poland, 2009.
(58) Sheldrick, G. M. Crystal structure refinement with SHELXL. *Acta Crystallogr., Sect. C: Struct. Chem.* **2015**, *C71*, 3−8.
(59) Sheldrick, G. M. A short history Of SHELX. *Acta Crystallogr., Sect. A: Found. Crystallogr.* **2008**, *64*, 112−122.
(60) Dolomanov, O. V.; Bourhis, L. J.; Gildea, R. J.; Howard, J. A. K.; Puschmann, H. OLEX2: a complete structure solution, refinement and analysis program. *J. Appl. Crystallogr.* **2009**, *42*, 339−341.
(61) Wiberg, K. B. Basis set effects on calculated geometries: 6-311++G** vs. aug-cc-pVDZ. *J. Comput. Chem.* **2004**, *25*, 1342−1346.
(62) Frisch, M. J.; Trucks, G. W.; Schlegel, H. B.; Scuseria, G. E.; Robb, M. A.; Cheeseman, J. R.; Scalmani, G.; Barone, V.; Mennucci, B.; Petersson, G. A.; et al. *Gaussian 09*, revision E.01; Gaussian, Inc.: Wallingford, CT, 2009.
(63) Bondi, A. Van der Waals volumes and radii. *J. Phys. Chem.* **1964**, *68*, 441−451.
(64) Kitaigorodskii, A. I. The principle of close packing and the condition of thermodynamic stability of organic crystals. *Acta Crystallogr.* **1965**, *18*, 585−590.
(65) Paliwoda, D.; Dziubek, K. F.; Katrusiak, A. Imidazole hidden polar phase. *Cryst. Growth Des.* **2012**, *12*, 4302−4305.
(66) Anioła, M.; Katrusiak, A. Conformational conversion of 4,4′-bipyridinium in a hidden high-pressure Phase. *Cryst. Growth Des.* **2015**, *15*, 764−770.
(67) Marciniak, J.; Bąkowicz, J.; Dobrowolski, M.; Dziubek, K. F.; Kaźmierczak, M.; Paliwoda, D.; Rajewski, K. W.; Sobczak, S.; Stachowicz, M.; Katrusiak, A. Most frequent organic interactions compressed in toluene. *Cryst. Growth Des.* **2016**, *16*, 1435−1441.
(68) Fuller, A. L.; Scott-Hayward, L. a S.; Li, Y.; Bühl, M.; Slawin, A. M. Z.; Woollins, J. D. Automated chemical crystallography. *J. Am. Chem. Soc.* **2010**, *132*, 5799−5802.
(69) Glidewell, C.; Low, J. N.; Wardell, J. L. Conformational preferences and supramolecular aggregation in 2-nitrophenylthiolates: disulfides and thiosulfonates. *Acta Crystallogr., Sect. B: Struct. Sci.* **2000**, *56*, 893−905.

DOI: 10.1021/acs.jpcc.6b11030
J. Phys. Chem. C 2017, 121, 2539−2545

(**R7**) Sobczak, S.; Ratajczyk, P.; Katrusiak, A.; High-pressure nucleation of low-density polymorphs *Chem. – A Eur. J*. **2021**, 10.1002/chem.202005121

Chemistry–A European Journal
Communication
doi.org/10.1002/chem.202005121

Crystal Engineering |Hot Paper|

High-pressure Nucleation of Low-Density Polymorphs**

Szymon Sobczak, Paulina Ratajczyk, and Andrzej Katrusiak*[a]

Abstract: New polymorphs β and γ of bis-3-nitrophenyl disulphide, crystallized above 0.3 GPa, are less dense than the ambient-pressure polymorph α. This counterintuitive density relation results from the high-entropy nucleation and subsequent kinetic crystallization. The work performed by pressure compensates the high entropy and temperature product, substantiated in varied conformers and increased chemical potential. Pressure-increased viscosity promotes the kinetic polymorphs, in accordance with empirical Ostwald's rule of stages. It contrasts to mechanochemical techniques, favouring high-density polymorphs.

The rational control over polymorphic forms of organic compounds is one of the challenges of materials sciences, modern chemistry, and related technologies.[1–3] Apart from the environment (solvent, pressure, temperature, composition, evaporation rate, etc.) also the intrinsic features (intra- and intermolecular interactions of conformers, mesmeric forms, tautomers, solvates etc.) need to be taken into account for designing the robust process aimed at the desired specific polymorph.[2,4–6] Such precise technologies are applied for obtaining required forms of pharmaceuticals, pesticides, food, plastics, dyes and various other products. Despite a considerable progress in the crystal-structure prediction,[7–10] in most cases the experimental screening provides the most reliable information about polymorphs of compounds. Generally, the crystal form results from the initial aggregation of molecules, either primary or secondary nucleation, and from the time-dependent crystal growth, either dynamic or kinetic.[1,2,5,11] The dynamic crystallizations proceed slowly, in the nearly equilibrated systems, whereas the kinetic crystallizations take place off the thermodynamic equilibrium, for example in quickly cooled molten or dissolved compounds. The dynamic and kinetic crystallizations often lead to different polymorphs. Some compounds, irrespective of thermodynamic conditions of their nucleation, have been obtained in only one crystalline form, for example naphthalene and CS_2.[12,13] An interesting example of high-pressure crystallization controlled by the seeds obtained at normal conditions for promoting the growth of low-density polymorphs was described for chlorpropamide;[14] a reverse approach of controlling the ambient-pressure crystallization by the seeds obtained in the 0.4–0.8 GPa range was demonstrated for GABA monohydrate.[6]

Presently we report a simple method of high-entropy nucleation, capable of generating new polymorphs, in this case study on bis-3-nitrophenyl disulphide (3-NO_2-PhS)$_2$, shown on Fig. 1. The thermodynamic conditions of such a nucleation process are extended by subjecting a compound (or its solution) to high-pressure. It increases the range of accessible temperature beyond the ambient-pressure boiling point of the compound (or the solvent), where strongly excited states of rota-vibrations, high-energy conformations, tautomers or other forms not accessible at normal conditions are activated.

The family of biphenyl disulphides is important due to their applications as drugs,[15] sensors,[16] lubricants,[17] polymers;[18–21] source of PhS substituents in organic reactions[22,23] and precursors for supramolecular systems.[24–26] Recently we showed that di-*p*-tolyl disulphide (4-CH_3-PhS)$_2$ absorbs the energy of compression by phase transitions and conformational transformations.[27] We also observed that exchange reaction between aryl homodimeric disulphides can be achieved at high-pressure without an addition of catalyst. Particularly the reaction between bis-4-chlorophenyl disulphide (4-Cl-PhS)$_2$ and bis-2-nitrophenyl disulphide (2-NO_2-PhS)$_2$ yields a low-density polymorph A of 4-Cl-PhSSPh-2-NO_2 at high-pressure conditions (refcode ROVWUX),[28] whereas the catalyst-promoted ball mill liquid-assisted grinding (LAG) at ambient pressure leads to the high-density polymorph (FUQLIM).[29–30] The 3-NO_2 analogue, of those disulphides is known, and commercially available in the centrosymmetric form of monoclinic space group *C*2/*c*, with molecules located on the 2-fold axes (FUGQUT, hereafter referred to as polymorph α).[31] Our systematic study on (3-NO_2-PhS)$_2$ combines the effects of primary nucleation with dynamic and kinetic crystallization attainable and conveniently controlled under high pressure. We found that the high-entropy nucleation yields two new polymorphs, labelled β and γ, both of lower density as compared to that of polymorph α obtained at the ambient conditions. The counterintuitive result sheds new light on empirical Ostwald's rule of stages

[a] S. Sobczak, P. Ratajczyk, Prof. A. Katrusiak
Department of Materials Chemistry
Faculty of Chemistry
Adam Mickiewicz University
Uniwersytetu Poznańskiego 8, 61-614 Poznań (Poland)
E-mail: katran@amuedu.pl

[**] A previous version of this manuscript has been deposited on a preprint server (https://doi.org/10.26434/chemrxiv.13161956.v1).

Supporting information and the ORCID identification number(s) for the author(s) of this article can be found under: https://doi.org/10.1002/chem.202005121.

and Wallach's rule relating the densities of enantiomers and racemates.

The protocol for obtaining kinetic polymorphs β and γ resulting from the high-pressure nucleation, described in detail in Supporting Information, was developed in the course of reiterated experiments for different solvents and concentrations. The diamond anvil cell (DAC) chamber was loaded with controlled amounts of α-(3-NO_2-PhS)$_2$ and a solvent. After sealing the DAC, the sample was compressed, and heated until all crystals dissolved. The high-temperature high-pressure nucleation in the DAC was followed by its cooling and opening, aimed at growing the crystals. The quality and size of the crystals recovered from the DAC chamber (of about 0.02 mm^3 in volume) were just sufficient for the single-crystal X-ray diffraction experiments, solution and refinement of the structures, although due to the small size of the samples the reflections were weak, which affected the range of 2θ angle for observed reflections and the accuracy of refined parameters (see the Supporting Information).

Well known are the structural features usually valid for the polymorphs obtained under kinetic regime: (i) their symmetry is lower;[32] (ii) their Z' number is higher;[3,32–34] and (iii) they are less dense, when compared to the dynamic-regime polymorphs.[35] It is also characteristic of conformational polymorphs that (iv) the kinetic polymorphs are built of conformers of the potential energy (E_p) higher than those of the dynamic polymorphs.[5,9,36,37]

Both polymorphs β and γ of (3-NO_2-PhS)$_2$ could be textbook examples of kinetic polymorphs, with all their characteristic features (i–iv). Both forms crystallize in the chiral space group $P2_1$, which is a subgroup of space group $C2/c$, and their density is significantly lower than that of polymorph α (Table 1). It is remarkable that the structures of both polymorphs β and γ are composed of layers displaying a pseudo-symmetry involving local inversion centres and glide planes perpendicular to [y]. In polymorph β the pseudo-inversion lies at [0.195, 0.13, 0.24]; in polymorph γ the pseudo-inversion is at [0.38, 0.11, 0.23] and the pseudo-glide planes are perpendicular to [y] and parallel to the layers (cf. Figure S4 in Supporting Information).

As illustrated in Figure 1, the disulphide molecules are conformationally flexible and their 'soft' torsion angles about bonds S–S (τ) and C–S (τ_2 and τ_3) can be modified by momentary environment changes in the liquid and by crystal field in the solid state. The Z' number is 0.5 in dynamic polymorph α, hence its torsion angles τ_2 and τ_3 are identical, while in kinetic polymorphs β and γ the Z' number is 4. In polymorph β four independent conformers, labelled A, B, C and D, are located at general positions, in pseudo-centrosymmetric relations between conformers A to C, and B to D. This relation is most prominent for torsion angles τ, τ_2 and τ_3 (Table 2). Similar pseudo-symmetry relations are also apparent in the structure of polymorph γ.

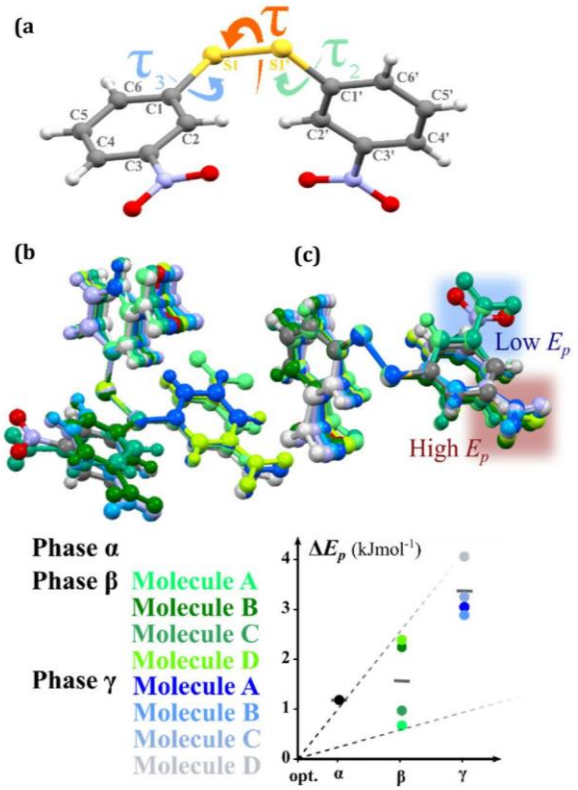

Figure 1. Conformers in (3-NO_2-PhS)$_2$ (a) polymorph α with torsion angles τ, τ_2 and τ_3 indicated; (b) all molecules of polymorphs α, β, and γ superimposed on the C1-S1-S1′ fragment; (c) these rotational enantiomers adjusted to torsion angle τ positive in order to visualise the presence of low-E_p and high-E_p conformers. The plot shows the E_p differences and bars indicate their average values.

The (3-NO_2-PhS)$_2$ molecule has two favoured conformations. In the low-E_p (LE) conformer angels τ, τ_2 and τ_3 are close to 90°, 0° and 0°, whereas in the high-E_p (HE) conformer these angels are close to 90°, 0° and 165°, respectively. Polymorph α is built of LE conformers (Figure 1 and Table 2), in polymorph β there are equal numbers of LE and HE conformers; in polymorph γ only HE conformers are present. The average conformational energies of polymorph α, β, and γ are 1.18, 1.57 and 3.42 kJ mol^{-1} (referred to the fully optimized low-energy conformer) as shown in the inset in Figure 1. Polymorphs β and γ (Figure 2) contain equal numbers of rotational enantiomers and in this respect they are conformational kryptoracemates.[38]

Table 1. Selected crystal data of (3-NO_2-PhS) polymorphs α, β and γ at ambient conditions (296 K, 0.1 MPa).

Polymorph		α[31]	β	γ
space group		$C2/c$	$P2_1$	$P2_1$
unit cell	a [Å]	13.6731(9)	8.1262(17)	8.1069(10)
	b [Å]	8.9078(6)	26.952(4)	22.406(3)
	c [Å]	12.4539(8)	12.6335(19)	14.7478(16)
	β (°)	120.070(1)	105.214(19)	94.087(12)
V (Å^3)		1312.70(15)	2669.9(8)	2672.0(6)
Z/Z'		4/0.5	8/4	8/4
V/Z		328.18	333.74	334.01
D_x (g/cm^3)		1.573	1.534	1.533

Table 2. Torsion angles τ, τ_2 and τ_3 (Figure 1) in conformers present in (3-NO_2-PhS)$_2$ polymorphs α (half molecule independent), β and γ (4 independent molecules labelled A, B, C and D), as well as their potential energy ΔE_p related to the fully optimized isolated conformer. LE denotes low E_p and HE high E_p conformers.

Torsion angle		τ [°]	τ_2 [°]	τ_3 [°]	ΔE_p [kJ mol^{-1}]	E_p state
optimized mol.		84.78	4.13	4.13	0	LE
phase α		97.63	−8.55	−8.55	1.18	LE
phase β	A	−88.07	−22.32	12.06	0.67	LE
	B	87.08	−1.24	171.13	2.28	HE
	C	91.21	−14.30	21.27	0.97	LE
	D	−87.01	1.46	−169.62	2.35	HE
phase γ	A	−84.77	−5.30	−162.45	2.98	HE
	B	91.05	8.26	163.13	2.95	HE
	C	89.39	16.49	165.05	3.29	HE
	D	−91.05	−22.65	−165.42	4.06	HE

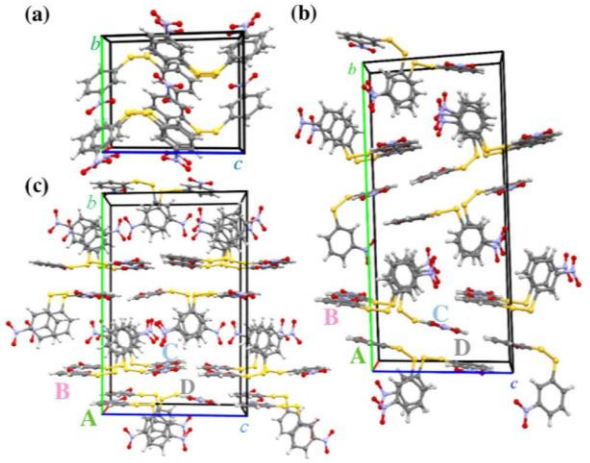

Figure 2. Structure of (3-NO_2-PhS)$_2$ polymorphs **(a)** α; **(b)** β; and **(c)** γ. Capital letters A, B, C and D label independent conformers in polymorphs γ and β.

Apart from the molecular conformation, the crystal structure and packing motifs in polymorph α of (3-NO_2-PhS)$_2$ strongly differ from those in isomers (2-NO_2-PhS)$_2$ (ODNPDS)[39] and (4-NO_2-PhS)$_2$ (NIPHSS).[40] In their crystals, molecules are linked into chains by C–H···O hydrogen bond, absent in α-(3-NO_2-PhS)$_2$, where sheets are formed through π–π stacking of aromatic rings.[31,41] On the other hand, in (3-NO_2-PhS)$_2$ polymorphs β and γ various types of intermolecular contacts (Figure S2) and cohesion forces are present, such as CH··O, π–π stacking and S···S.

It is apparent that the conditions of nucleation affect the hierarchy of interactions in the crystal structure. It was demonstrated that the intermolecular hydrogen bonds are strongly modified under pressure,[42–44] when they have to compromise with the increased role of close packing. Most importantly, ambient-pressure molecular crystals easily sublimate, melt and evaporate, but under high-pressure the temperature of the system can be increased to higher values, which increases the kinetic energy of molecular motion. According to Boltzmann's statistics for the ideal gas, the average kinetic energy of its molecules increases linearly with temperature and is equal $k_BT/2$ (k_B is Boltzmann's constant) per each degree of freedom. This rough assessment, when applied to molecules of (3-NO_2-PhS)$_2$, shows that high temperature can easily destabilize their interactions (mainly C–H···O, Figure S2) and excite the conformers to the HE states, then observed in polymorphs β and γ. The increased E_p values of conformers in these high-T/p polymorphs (Table 2) increase their chemical potential, compared to that of polymorph α.[45,46]

Thus, the internal energies (U) of polymorphs β and γ are higher compared to that of polymorph α. This U-energy relation is essential for the most surprising high average volume of molecules in polymorphs β and γ, as their crystal fields stabilize the HE conformers (Tables 1 and 2). At first glance, this result seems to contradict numerous high-pressure crystallizations and syntheses leading to high-density polymorphs. In fact, high-pressure techniques are generally aimed at obtaining hard, high-density forms of crystals.[47] However, such crystallizations are performed slowly under the dynamic regime, allowing the system to equilibrate. All characteristic features (i–iv) of kinetic polymorphs can be rationalized in terms of the thermodynamic conditions of the crystallization process: (i) the low symmetry is a consequence of the conformational and orientational variety consistent with the high entropy of the system at high-temperature, which is also connected with (ii) the high Z' number; the high T also explains the high E_p states of excited molecules (compared to lower E_p conformer in the dynamic polymorph α). The quick crystallization leaves no sufficient time for the molecules to reorient or change the positions of substituents. Finally, the low density (iii) despite the high-pressure conditions can be attributed to: (a) higher internal energy, in part associated with the HE conformers and the cohesion forces partly used for their stabilization; (b) higher compressibility of the low-density polymorphs than that of the high-density polymorph, hence their density difference diminishes with pressure; (c) the nucleation taking place at high temperature implies high entropy and strong rota-vibrations requiring an additional space; and (d) the high-temperature nucleation directs the crystallization leaving no space for other polymorphs, particularly that the crystallization is the fastest close to the melting curve.

It is convenient to heat sample under pressure, which increases the freezing point and hence moves the nucleation to the high-entropy region. Furthermore, under high-pressure the viscosity of the solution or melt significantly increases,[48] which hampers the rigid-molecule motions and internal reorientations of molecular moieties. These effects of viscosity are thus consistent with varied conformations and high Z' number. Moreover, the increased viscosity expands the time scale for the kinetic crystallization. In other words, the kinetic process at high-pressure is considerably slower than at 0.1 MPa. This 'extended' kinematic regime increases the likelihood of the nucleation of kinetic polymorphs. Then the growth of their seeds is favourably continued on lowering the temperature, which reduces the concertation of the solution to below the saturation and prevents the nucleation of other polymorphs, even when the process is slowed down to the dynamic regime.

Interestingly, all our attempts to obtain the kinetic polymorphs β and γ by mechanochemical methods, liquid-assisted grinding (LAG) with acetonitrile and isopropanol, as well as neat ball milling, failed (*cf.* Supporting Information). This contrasts with the successful production of heterodimeric low-density polymorph A of 4-Cl-PhSSPh-2-NO_2 during the neat grinding.[28,29] Later, we obtained this polymorph by high-entropy nucleation, too.[27]

To conclude, the high-pressure crystallization of low-density polymorphs β and γ of (3-NO_2-PhS)$_2$ reveals the background of this counterintuitive phenomenon. The increased pressure expands the thermodynamic space of temperature and concertation, where high-entropy nucleation is the source of kinetic polymorphs. The molecular-level mechanism of Ostwald's rule of stages appears as a natural consequence of the kinetic effects fueled by the considerably increased accessible temperature range under high pressure. Noteworthy, (3-NO_2-PhS)$_2$ low-density polymorphs β and γ are non-centrosymmetric, unlike the centrosymmetric polymorph α. Centrosymmetric crystals are usually more dense than non-centrosymmetric ones, but rare exceptions from this rule[49,50] can be regarded as an indication that more experimental results and studies are needed for the rigorous description of the crystallization process, which still today is often considered to be more 'art' than 'science'.[1]

Supporting Information

Detailed experimental data including protocol for obtaining high-pressure nucleated polymorphs, single-crystals of polymorphs β and γ, the shortest intermolecular contacts plotted for all polymorphic forms, A, B, C and D conformers present in form β and γ together with their pseudo-symmetry relations, as well as the results of ball-mill experiments can be found in Supporting Information. Deposition Number(s) 2040892 and 2040891 contain(s) the supplementary crystallographic data for this paper. These data are provided free of charge by the joint Cambridge Crystallographic Data Centre and Fachinformationszentrum Karlsruhe Access Structures service www.ccdc.cam.ac.uk/structures.

Acknowledgements

We thank the Polish National Science Centre (grant PRELUDIUM 2017/27/N/ST5/00693) for financial support. This research was supported in part by PLGrid Infrastructure.

Conflict of interest

The authors declare no conflict of interest.

Keywords: crystal growth · high-pressure chemistry · kinetic crystallization · nucleation · polymorphism

[1] J. Bernstein, *Polymorphism in Molecular Crystals*, Oxford University Press, **2007**.
[2] J. Bernstein, *J. Phys. D* **1993**, *26*, B66–B76.
[3] J. Bernstein, J. D. Dunitz, A. Gavezzotti, *Cryst. Growth Des.* **2008**, *8*, 2011–2018.
[4] R. J. Davey, N. Blagden, G. D. Potts, R. Docherty, *J. Am. Chem. Soc.* **1997**, *119*, 1767–1772.
[5] A. Nangia, *Acc. Chem. Res.* **2008**, *41*, 595–604.
[6] F. P. A. Fabbiani, G. Buth, D. C. Levendis, A. J. Cruz-Cabeza, *Chem. Commun.* **2014**, *50*, 1817–1819.
[7] S. M. Woodley, R. Catlow, *Nat. Mater.* **2008**, *7*, 937–946.
[8] A. R. Oganov, *Modern Methods of Crystal Structure Prediction*, **2010**.
[9] S. L. Price, *Phys. Chem. Chem. Phys.* **2008**, *10*, 1996–2009.
[10] A. Gavezzotti, *Acc. Chem. Res.* **1994**, *27*, 309–314.
[11] J. Haleblian, W. McCrone, *J. Pharm. Sci.* **1969**, *58*, 911–929.
[12] F. P. A. Fabbiani, D. R. Allan, S. Parsons, C. R. Pulham, *Acta Crystallogr. Sect. B* **2006**, *62*, 826–842.
[13] K. F. Dziubek, A. Katrusiak, *J. Phys. Chem. B* **2004**, *108*, 19089–19092.
[14] B. A. Zakharov, S. V. Goryainov, E. V. Boldyreva, *CrystEngComm* **2016**, *18*, 5423–5428.
[15] J. M. Young, A. J. Tomolonis, *Agents Actions* **1987**, *21*, 314–315.
[16] M. B. Gholivand, Y. Mozaffari, *Talanta* **2003**, *59*, 399–407.
[17] E. S. Forbes, *Wear* **1970**, *15*, 87–96.
[18] S. Nevejans, N. Ballard, J. I. Miranda, B. Reck, J. M. Asua, *Phys. Chem. Chem. Phys.* **2016**, *18*, 27577–27583.
[19] J. M. Matxain, J. M. Asua, F. Ruipérez, *Phys. Chem. Chem. Phys.* **2016**, *18*, 1758–1770.
[20] E. Formoso, J. M. Asua, J. M. Matxain, F. Ruipérez, *Phys. Chem. Chem. Phys.* **2017**, *19*, 18461–18470.
[21] M. Irigoyen, J. M. Matxain, F. Ruipérez, *Polymers (Basel)* **2019**, *11*, 1960.
[22] J. H. Byers, *Encycl. Reagents Org. Synth.*, American Cancer Society **2001**.
[23] T.-L. Ho, M. Fieser, L. Fieser, *Fieser Fieser's Reagents Org. Synth.*, John Wiley & Sons, Inc., Hoboken, NJ, USA **2006**.
[24] S. P. Black, J. K. M. Sanders, A. R. Stefankiewicz, *Chem. Soc. Rev.* **2014**, *43*, 1861–1872.
[25] T. Friščić, *Chem. Soc. Rev.* **2012**, *41*, 3493–3510.
[26] N. M. Phan, E. G. Percástegui, D. W. Johnson, *Chempluschem* **2020**, *85*, 1270–1282.
[27] S. Sobczak, A. Katrusiak, *J. Phys. Chem. C* **2017**, *121*, 2539–2545.
[28] S. Sobczak, W. Drożdż, G. I. Lampronti, A. M. A. Belenguer, A. Katrusiak, A. R. Stefankiewicz, *Chem. Eur. J.* **2018**, *24*, 8769–8773.
[29] A. M. Belenguer, G. I. Lampronti, D. J. Wales, J. K. M. Sanders, *J. Am. Chem. Soc.* **2014**, *136*, 16156–16166.
[30] A. M. Belenguer, T. Friščić, G. M. Day, J. K. M. M. Sanders, *Chem. Sci.* **2011**, *2*, 696.
[31] D. Cannon, C. Glidewell, J. N. Low, J. L. Wardell, *Acta Crystallogr. Sect. C* **2000**, *56*, 1267–1268.
[32] J. W. Steed, *CrystEngComm* **2003**, *5*, 169–179.
[33] C. P. Brock, *Acta Crystallogr. Sect. B* **2016**, *72*, 807–821.
[34] K. M. Steed, J. W. Steed, *Chem. Rev.* **2015**, *115*, 2895–2933.
[35] E. H. Lee, *Asian J. Pharm. Sci.* **2014**, *9*, 163–175.
[36] S. L. Price, *Acta Crystallogr. Sect. B* **2013**, *69*, 313–328.
[37] A. J. Cruz-Cabeza, S. M. Reutzel-Edens, J. Bernstein, *Chem. Soc. Rev.* **2015**, *44*, 8619–8635.
[38] L. Fábián, C. P. Brock, *Acta Crystallogr. Sect. B* **2010**, *66*, 94–103.
[39] C. Glidewell, J. N. Low, J. L. Wardell, *Acta Crystallogr. Sect. B* **2000**, *56*, 893–905.
[40] J. S. Ricci, I. Bernal, J. S. Ricci, I. Bernal, *J. Am. Chem. Soc.* **1969**, *91*, 4078–4082.
[41] C. Glidewell, J. N. Low, J. M. S. Skakle, J. L. Wardell, *Acta Crystallogr. Sect. C* **2002**, *58*, o485–o486.
[42] E. Patyk, J. Skumiel, M. Podsiadło, A. Katrusiak, *Angew. Chem. Int. Ed.* **2012**, *51*, 2146–2150; *Angew. Chem.* **2012**, *124*, 2188–2192.
[43] M. Podsiadło, A. Olejniczak, A. Katrusiak, *CrystEngComm* **2014**, *16*, 8279–8285.
[44] K. W. Rajewski, M. Andrzejewski, A. Katrusiak, *Cryst. Growth Des.* **2016**, *16*, 3869–3874.
[45] P. Dopieralski, J. Ribas-Arino, P. Anjukandi, M. Krupicka, J. Kiss, D. Marx, *Nat. Chem.* **2013**, *5*, 685–691.
[46] P. Dopieralski, J. Ribas-Arino, P. Anjukandi, M. Krupicka, D. Marx, *Nat. Chem.* **2017**, *9*, 164–170.
[47] E. Boldyreva, *Cryst. Growth Des.* **2007**, *7*, 1662–1668.

[48] E. U. Franck, *Experimental Studies of Compressed Fluids in High Press. Chem. Biochem.*, Springer Netherlands, Dordrecht, **1987**, pp. 93–116.
[49] W. Cai, J. Marciniak, M. Andrzejewski, A. Katrusiak, *J. Phys. Chem. C* **2013**, *117*, 7279–7285.
[50] J. Marciniak, M. Andrzejewski, W. Cai, A. Katrusiak, *J. Phys. Chem. C* **2014**, *118*, 4309–4313.

Manuscript received: November 26, 2020
Revised manuscript received: January 18, 2021
Accepted manuscript online: January 28, 2021
Version of record online: ■■ ■■, 0000

COMMUNICATION

Crystal Engineering

S. Sobczak, P. Ratajczyk, A. Katrusiak*

■■ – ■■

High-pressure Nucleation of Low-Density Polymorphs

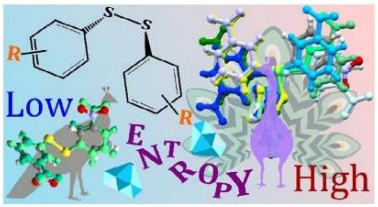

High-entropy nucleation and subsequent crystallization performed under high-pressure and high-temperature conditions lead to kinetic polymorphs of aryl disulfides, characterized by lower symmetry, higher Z′ number and lower density than the ambient-pressure polymorphs.